University of South Bohemia in České Budějovice

Faculty of Science

Carotenoid Excited State Processes by Femtosecond Time-Resolved Pump-Probe and Multi-Pulse Spectroscopies

Ph.D. Thesis

Robert G. West

Supervisor: **prof. RNDr. Tomáš Polívka**

Annotation

This Ph.D. thesis is an exploration of carotenoids by ultrafast, time-resolved absorption spectroscopy to investigate their complicated relaxation processes, means of energy transfer, and dependence on structure. The introduction begins with an overview of carotenoids, intended for the reader to appreciate their importance and their complexity as revealed by decades of research in carotenoid photophysics. To understand the primary concerns of this research field, the reader is guided through basic theory of energetic processes, the experimental method, and methods of analysis. The main body of the text is the Research Chapter, containing four sections, each describing research using varied ultrafast transient absorption spectroscopies on carotenoids in solution and when bound to a host protein. Section 2.1 concerns an equilibration phenomenon in the lower energetic structure of the carotenoid fucoxanthin in various solutions and temperatures by a multipulse transient absorption method. The same method is applied to fucoxanthin in a host antennae protein of the pennate diatom *Phaeodactylum tricornutum* to investigate the function of the equilibration in energy transfer to Chlorophyll *a* in Section 2.2. The next two sections regard the effect of carotenoid structure on its relaxation dynamics. Section 2.3 investigates the effect of the non-conjugated acyloxy group of two fucoxanthin derivatives in various solvents. Here, one of the energetic states involved in the equilibrium mentioned above is seen drastically affected. Lastly, Section 2.4 investigates alloxanthin, a carotenoid with an unusual pair of carbon-carbon triple bonds. Their effect on the conjugation is evaluated based upon the molecules' decay dynamics. A general summary and conclusion is provided at the end.

Declaration [in Czech]

Prohlašuji, že svoji disertační práci jsem vypracoval samostatně pouze s použitím pramenů a literatury uvedených v seznamu citované literatury.

Prohlašuji, že v souladu s § 47b zákona č. 111/1998 Sb. v platném znění souhlasím se zveřejněním své disertační práce, a to v úpravě vzniklé vypuštěním vyznačených částí archivovaných Přírodovědeckou fakultou elektronickou cestou ve veřejně přístupné části databáze STAG provozované Jihočeskou univerzitou v Českých Budějovicích na jejích internetových stránkách, a to se zachováním mého autorského práva k odevzdanému textu této kvalifikační práce. Souhlasím dále s tím, aby toutéž elektronickou cestou byly v souladu s uvedeným ustanovením zákona č. 111/1998 Sb. zveřejněny posudky školitele a oponentů práce i záznam o průběhu a výsledku obhajoby kvalifikační práce. Rovněž souhlasím s porovnáním textu mé kvalifikační práce s databází kvalifikačních prací Theses.cz provozovanou Národním registrem vysokoškolských kvalifikačních prací a systémem na odhalování plagiátů.

České Budějovice, 30. dubna 2018   ....
                                                                          Robert G. West

Přírodovědecká fakulta
Faculty of Science

Acknowledgements

Due to the limitations in paper binding and financial resources, unfortunately I have had to reduce this most important section of my thesis to a few pages.

First I must mention Dr. Seyed Sadeghi, of the University of Alabama in Huntsville. Though the contents of this thesis are not directly related to his work, our griping research in non-radiative energy transfer in quantum dots certainly boosted my confidence in my ability as a scientist early on and unmistakably led me away on the path of spectroscopy and photosynthesis. Thank you.

I can hardly dare to be so concise in my thanks to my supervisor, Prof. Tomáš Polívka, nor can I begin to express my profound respect for his knowledge and work which has guided my way through tangly light harvesting proteins and successfully converted me to carotenoids, to appreciating the wonders of carotenoids and the joys of working in the field of ultrafast spectroscopy. Thanks for the super-interesting and fruitful project work of pump-dump and sending me all over the world.

Thanks Drs. Allen and Laurie Diles of Harding University whose general lovingness, dedication, scholarship, and deep interest all things Czech gave me such confidence to do something as crazy as I just did.

Thanks to the Sides family for their continual support and interest in my work and general life which helped me persevere. Ashley, I'll miss our Friday morning refreshment the most.

I must have the most supportive parents in the world. Mom and dad, whose unparalleled taste for beauty in their craft, contagious industriousness, and unrelenting diligence, formed my world view of working folk and instilled the concept of working for the Lord and not for men.

No one could be credited with keeping me sane and on the right path as my brother, Chris. Though across the world, you've always been there for me. I'm always looking up to you even when you're not flying.

I want to thank my good friends and colleagues without whom, I would never had had such a rich life. I would never had enjoyed dancing with

spoons so much, among a million other great and ridiculously awesome memories without my homie Gürkan Keşan. I wouldn't know about the wonders of Chicken Kiev or of rigorous sportsmanship if it weren't for my buddy Denys Biriukov. Valentyna Kuznetsova, you were like my "overseas exchange sister". I really do hope we'll land at another conference to have a good time again someday. Vašek Šlouf, life in the Czech Republic would not have been possible without you, you know. I'm glad to have met one of the selfless men I've ever known. Every day life will truly be extremely boring without my friend Vaclav Šebelík, III. Thanks for sacrificing your wedding anniversaries with me for the cause of science and economic accomodation, sorry Lenka. Certainly, I must thank my colleague and friend Hristina Staleva-Musto for endless help in the lab and contagious enthusiasm and curiosity which was a major factor driving me forward in my own research.

To my good friend Brent Smith, that was super-awesome you found it so important to spend a bunch of bucks in the midst of your own wedding planning to come and visit me.

Marcel, thanks for helping everyone get to the root of the equilibration issue with more than a few etymological escapades. Milan, you were a key factor in making me feel very much at home in the Czech Republic. Franta, thanks for always being kind and saying, "Ahoj." Prof. Mikas Vengris, who spent unrequited amounts of time with me in the lab and over coffee. I really enjoyed my time in Lithuania.

To my sweetheart fiancé Jana: suddenly all of the hours in the dark lab or frustrated at the computer while fitting the data were worth it when I met you. Thanks for your sweet nature and support. I'm looking forward to life together.

List of Papers and Author's Contribution

This thesis is based on the following papers (listed in order of their appearance in the Research Chapter):

PAPER I. **R. G. West**, M. Fuciman, H. Staleva-Musto, V. Šebelík, D. Bína, M. Durchan, V. Kuznetsova, T. Polívka. Equilibration dependence of fucoxanthin S_1 and ICT signatures on polarity, proticity, and temperature by multi-pulse femtosecond absorption spectroscopy. Submitted: Journal of Physical Chemistry B, May, 2018.

RW performed multi-pulse time-resolved transient absorption measurements; analyzed the data; assisted in developing the population dynamic model, applying the model in various computational scripts; wrote the main body of the text and revised it.

PAPER II. **R. G. West**, D. Bína, M. Fuciman, V. Kuznetsova, R. Litvín, T. Polívka. Ultrafast multi-pulse transient absorption spectroscopy of fucoxanthin chlorophyll *a* protein from *Phaeodactylum tricornutum*. BBA Bioenergetics, 2018, 1859 (5), 357-365.

RW performed multi-pulse time-resolved transient absorption measurements; analyzed the data; assisted in developing the population dynamic model, applying the model in various computational scripts; assisted in writing and revision of the text.

PAPER III. H. Staleva-Musto, V. Kuznetsova, **R. G. West**, G. Keşan, B. Minofar, M. Fuciman, D. Bína, R. Litvín, T. Polívka. Nonconjugated Acyloxy Group Deactivates the Intamolecular Charge-Transfer State in the Carotenoid Fucoxanthin. Journal of Physical Chemistry B, 2018, 122 (11), 2922-2930.

RW participated intime-resolved transient absorption measurements.

PAPER IV. **R. G. West**, G. Keşan, E. Trsková, R. Sobotka, R. Kaňa, M. Fuciman, T. Polívka. Spectroscopic properties of the triple bond carotenoid alloxanthin. Chemical Physics Letters, 2016, 653, 167-172.

RW performed time-resolved transient absorption measurements and assisted in writing and revision of text.

Foreword

Though science is celebrated as the study of what we observe or could observe, the quality and reliability which all scientists are expected to uphold are ultimately based upon immeasurable, unquantifiable, invisible qualities such as diligence, critical reasoning, and most important of all, honesty.

The faith we have that men possess these qualities should not be taken for granted. We must reason that these qualities can and should be valued in order for any scientific endeavor to succeed in coming closer to the truths of the natural world.

To the same degree, I cannot provide a measure by which the reader may evaluate the soundness of my own research as with the great scientists on whose hard labor and whit we all stand. So, the reader must take me at my word and hopefully, the honest investigation and the strains to which I attempt to explain in a clear manner what I have learned, in spite of my limited knowledge, will be a testament to the reliability of the results enclosed.

Robert G. West

"What we observe is not nature itself but nature exposed to our method of questioning."

Werner Heisenberg

Contents

Dedicated to Mom and Dad

In memory of

Andrej Okonkwo
husband, father, friend, my brother-in-law

1 Introduction

1.1   Overview

To understand where this study of carotenoids falls within the grand scheme of photosynthetic research, one must also appreciate some of the history of carotenoids and why biologists and biophysicists have concentrated much of their work on carotenoids in recent years. The oldest geological record of carotenoids have been found in chloroplasts of the unicellular algae *Prochloron*, which is cyanobacteria.[1] Due to its anti-oxidative qualities observed in such complex organelles as chloroplasts (See Fig. 1.1), it is assumed that the presence of carotenoids dates back to the appearance of oxygenic photosynthesis for the mechanism to have survived over-exposure to sunlight. Carotenoids, thereafter, are found in a host of organisms serving photosynthetic and non-photosynthetic roles such as pigmentation in crustaceans, parrot feathers, or even grasshoppers, to name a few.[2–4] Ingested carotenoids are even found concentrated in the human eye,[5] and studies indicating the relation between ingestion of carotenoid-rich foods and eye health seem to point towards its oxidation or excess energy suppressing qualities are preferred also in the animal kingdom.[6,7]

From the time humans themselves had first laid their eyes on carotenoids, their bright, light-tuning properties were also preferred as a medium for artistry and dyes.[8,9] It was not until the early 19th century that carotenoids were first isolated and became known as lipochromes: fat-soluble hydrocarbon pigments often giving color to fat.[10] In 1907, Willstätter and Mieg determined the molecular formula for β-carotene is $C_{40}H_{56}$,[11] then Paul Karrer determined xanthophylls contained oxygen as hydroxy groups. At last, precise carotenoid structures were discovered by the application of chromatography in the 1930s.[12] Since then, the structure of more than 700 carotenoids have been determined, about 200 of these being carbonyl carotenoids, meaning they posses a carbonyl, or keto,* group (contains $C = O$).[1]

Fucoxanthin, being one of these keto-carotenoids, is the primary carotenoid featured in this thesis. Fucoxanthin was first extracted in 1867,

---

*For more info: www.chemguide.co.uk/organicprops/carbonyls/background.html

though the name "xanthin" was not given until 1878, and thoroughly studied as a component of brown algae by Willstätter and Page in 1914,[13] and its structure was determined in 1969 by B. C. L. Weedon and his group.[14] The carotenoid's prevelance was unique: even in the most diverse conditions, fucoxanthin was found to be uniformly the primary carotenoid pigment in the algae. In regard to its world-wide photosynthetic impact, T. W. Goodwin said in his book, *The Comparative Biochemistry of the Carotenoids*:[15] "When the algal distribution over the world's surface is considered, fucoxanthin is probably the most abundant naturally-occurring carotenoid."

The reason for fucoxanthin's success as a ubiquitous sensitizer must be its structure, and a carotenoid's structure determines its function within the light harvesting antenna protein. Specifically, its carbonyl group has been determined to induce a charge transfer state in polar environments, which enhances energy transfer to chlorophyll within the antenna. This is also observed for peridinin in its native protein of dinoflagellates (a component of phytoplankton).[21] Therefore, as Polívka et. al. describes it: "the light-harvesting strategy employing a charge transfer state is likely to play a significant role in the total photosynthetic production on Earth."[22]

The goal of this thesis, in part, is to describe and quantify the nature of this charge transfer character of fucoxanthin in various solution environments (Section 2.1) and in its native protein, fucoxanthin chlorophyll protein (Section 2.2). These studies showcase the multipulse, femtosecond transient absorption (TA) technique, a technique which successfully reveals the nature of coupled first excited and charge transfer states and gives insight into the energy transfer pathways of carotenoid-chlorophyll antenna proteins. Additionally, by pump-probe TA spectroscopy, the electron distribution dependence of the charge transfer state is investigated with two fucoxanthin derivatives having acyloxy groups attached to the carbon-carbon backbone yet apart from the electron conjugation (Section 2.3). These derivatives are found in *Aureococcus anophagefferens*, an algae which produces brown tide blooms harmful
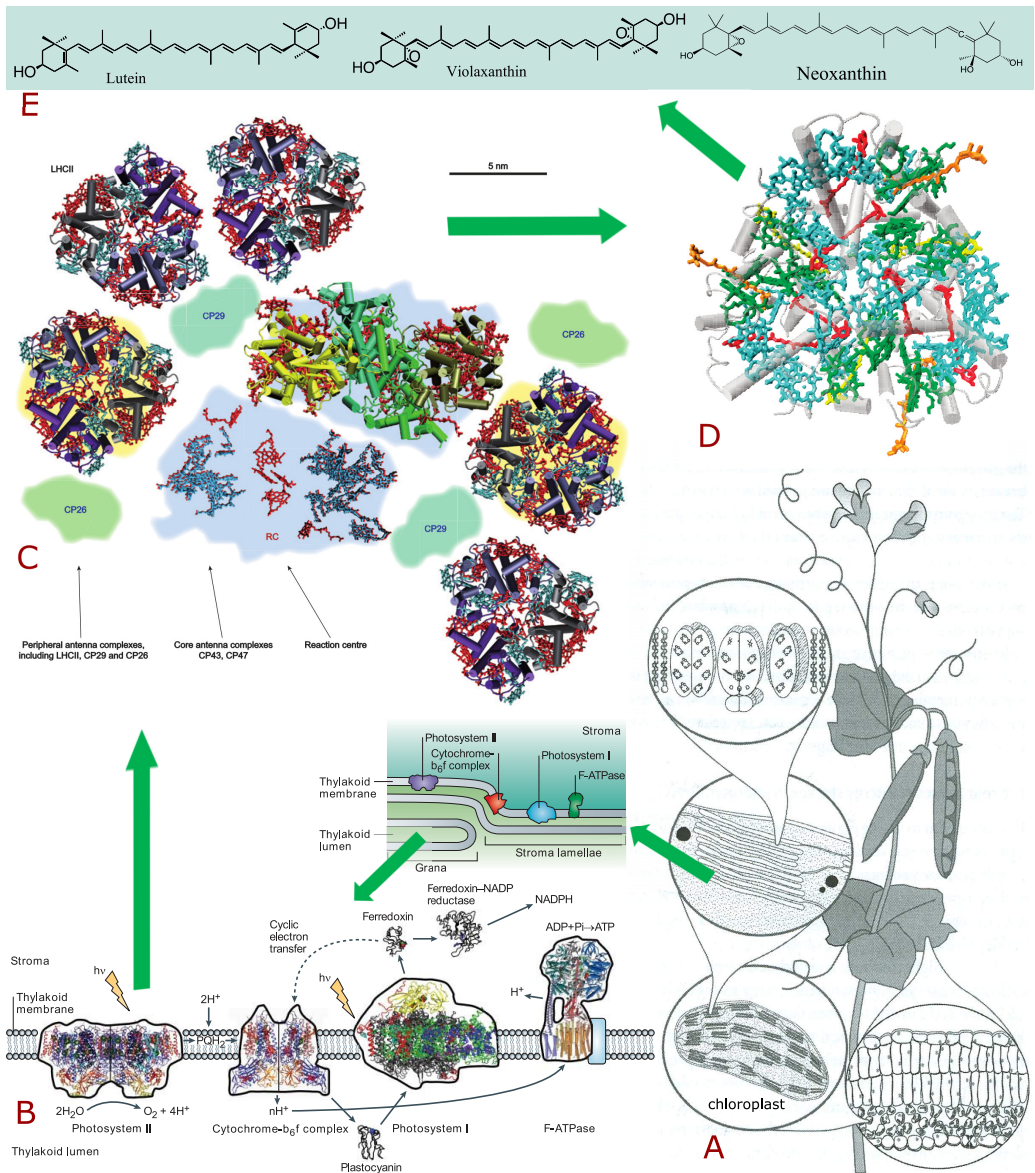
FIGURE 1.1: An exploding diagram indicating the location of carotenoids in LHCII of plants. The three types of carotenoids (E) found in LHCII (D) of PSII (C) located on the thylakoid membrane (B) of chloroplasts as found in the leaves of plants (A). Figures obtained from refs. 16, 17, 18, 19, and 20, respectively.

to suspension feeders and some aquatic vegetation.[23] Lastly, a brief investigation of the non-carbonyl carotenoid alloxanthin is presented. Alloxanthin is a unique carotenoid with two carbon-carbon triple bonds in its backbone found in the Cryptophyte algae *Rhodomonas salina*, which demonstrates unique non-photochemical quenching properties when overexposed to light (Section 2.4).[24]

1.1.1 Carotenoid Biosynthesis

A proper appreciation for the role of carotenoids would be amiss without some understanding of its synthesis. There are various pathways by which carotenoids are synthesized in unicellular organisms as well as higher plants, but not in animals. In higher plants, carotenoid synthesis falls within the same synthetic pathway as other isopreniods such as cholesterol, a process which absorbs water and produces CO_2 to make the ten-carbon molecule, geranyl phosphate. Geranyl-geranyl pyrophosphate is then synthesized as a precursor to the 40-carbon phytoene, a precursor of lycopene which is celebrated by epidemiologists for prostate cancer prevention.[25,26] From lycopene, a carotenoid which aside from its methyl groups mimics a linear polyene, stems more complex structures: α-carotene and β-carotene, the predecessor of xanthophylls.[27]

The fucoxanthin-chlorophyll *a* complex of the diatom *Phaeodactylum tricornutum*, featured in this thesis, has an antenna complex similar to that of plants; and the pathway to fucoxanthin synthesis traverses the analogous β-carotene synthesis in plants. According to a recent study,[28] from β-carotene hydroxy groups are added to make zeaxanthin, violaxanthin by addition of two epoxy groups, neoxanthin, and finally, allenic double bonds are formed to produce the carbonyl carotenoid fucoxanthin.

The type and concentration of carotenoids synthesized in particular systems is dependent on the light condition in which the host organism thrives. In fact, carotenoids may be synthesized between a quenching and a sensitizing carotenoid in fluctuating light conditions.[29,30] and they may perform a photoprotective in addition to a light harvesting role in their native proteins.[31,32] Therefore, it is expected that their synthesized structure is related

a polyene
(*N*=7)

lycopene

spirilloxanthin

β-carotene

alloxanthin

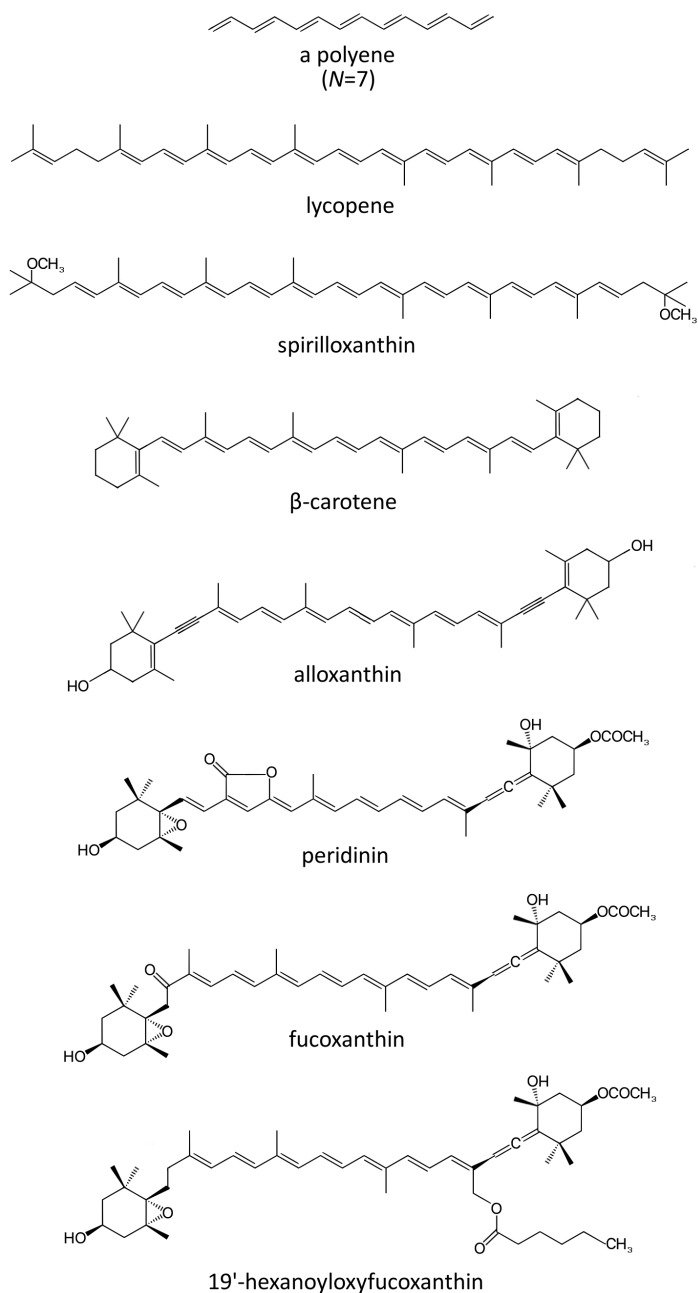peridinin

fucoxanthin

19'-hexanoyloxyfucoxanthin

FIGURE 1.2: All carotenoids contain a polyene backbone. Lycopene and spirilloxanthin are linear carotenoids. *β*-carotene is the predecessor of xanthophylls such as alloxanthin, peridinin, and fucoxanthin. 19'-hexanyloxyfucoxanthin is a fucoxanthin derivative addressed in Section 2.3.

to their function. Consequently, minute changes in their physical structure affects their energetic transfer and spectroscopic properties.

1.1.2 Carotenoid Function as Revealed by Spectroscopy

Three types of pigments are found in natural light harvesting (LH) antenna: open-chain bilin, chlorophylls, and carotenoids. The purpose of antenna systems is, firstly, to funnel energy to the reaction center (RC) where stable energy products for cellular processes are manufactured. Antenna systems also sensitize other proteins to the spectra of incident light, or light quality. Lastly, the antenna system also enacts photoprotection by various means depending on the organism in the case of high-light conditions which could damage the LH system.[20] Specifically, carotenoid molecules perform these roles locally, and their diversity within LH systems implies their vital role in the adaptation of systems under numerous light conditions. Therefore, determining the role of specific carotenoids in their host proteins is necessary for the initiation and function of all photosynthetic processes. The primary factor governing the utility of LH systems, natural or synthetic, even for inorganic systems, is the electron yield per photon. Carotenoids exhibit efficient energy transfer upon excitation[33] due to the fact that their energy transfer (ET) rate is faster than their deactivation rate.[20]

Carotenoids are also distinguished by their multiple roles in light harvesting:[34]

- sensitization: collection and absorption of light and energy transfer to chlorophylls (Chls) or bacteriochlorophylls (BChls);
- photoprotection: chlorophyll triplet quenching and singlet oxygen scavenging;
- regulation: dissipation of excess energy by, for example, the xanthophyll cycle; and
- stabilization: reinforcement of the antenna protein structure.

Carotenoids have even been found to take roles unrelated to light-harvesting but photoactivation, such as light-activation of the Orange-Carotenoid Protein in cyanobacteria.[35]

The hundreds of naturally occurring carotenoids (as in Fig. 1.2) locally serve one or more of these functions in their systems according to the host organism's habitat. For example, green sulfur bacteria, found in the lowest light conditions of all photosynthetic organisms,[20] contains isorenieratone, whose structure is similar to β-carotene but whose terminal aryl rings have been found to significantly tune its absorption properties to be advantageous for sensitizing its host chlorosome.[36] On the other hand, under high-light conditions, the photoprotective function of β-carotene in high-light induced proteins (Hlips) from cyanobacteria is observed due to the position of its lowest singlet-state energy, which is strictly dependent upon the structure and conformation of its backbone.[37]

These are just a few examples of how a carotenoid's structure invariably determines its function. Due to their shared relation to phytoene, all carotenoids have alternating single-double, carbon-carbon backbones. This is why the ideal physical model for the carotenoid is a finite polyene, and deciphering the energetic structure of carotenoids begins with a C_{2h} point group model for determination of its energetic structure, though this assignment has been debated.[38] The polyene model provides a basis for expected states, state symmetries, and allowed transitions which all depend upon the length of the backbone over which the electrons can be delocalized, or conjugated.[39] However, addition of end groups and other complications of carotenoids' structures can break this symmetry. The addition of various terminal rings, keto groups, symmetry of the arrangement of keto groups, and lactone rings, not to mention the conformation of the entire molecule, affect the energetic structure, introduce new environmental dependencies, intermediate energy levels, and intermolecular energetic pathways.

Beyond computational analysis of these structures, the ever-developing field of spectroscopy has led the expedition to unwravel the complexities of carotenoid photophysics. Carotenoids are tested for their general behavior and response to the polarity of the environment in solution; then, their functions are explored when bound to proteins isolated from photosynthetic organisms or in mutated proteins. Peridinin, for example, absorbs strongly in

the green spectral band and has the strongest dipole moment among investigated carotenoids.[40] Therefore, it is vastly present in oceanic photosynthetic organisms as green light penetrates deeper into the water.[20] In solution, peridinin's lowest singlet excited state exhibits lifetimes ranging from 160 fs to 9 ps depending on the polarity, from non-polar to polar, respectively.[41,42] Such a variation in lifetime has been attributed to a much-debated intermolecular charge transfer (ICT) state. In the environment of the well-studied peridinin-Chlorophyll-Protein (PCP) complex, peridinin is utilized as its main LH pigment where peridinin and Chls are in Van der Waals contact (within 4-11 Å) and maintain a concentration 4:1 predinin:Chl-a (see Fig. 1.7).[20,22,43] This is just one example of how carotenoids are situated in LH proteins.

Numerous other LH complexes and carotenoids have been investigated. This thesis mostly focuses on carbonyl carotenoids and their function in light harvesting antennae such as FCP. Even though a high-resolution detail of the structure of FCP is yet to be resolved and the exact nature of the coupling between the S_1 and ICT states of fucoxanthin is still in question, the energetic structure, excited state decay processes, and energy transfer tendencies may be investigated by manipulation of its energetic manifold.

1.1.3   Observations of Carotenoid Excited States

The excited states of carotenoids have either positive or negative parity, each with its own unique symmetry that, in part, governs its behavior and allowed transitions. In brief, the singlet electronic states are classified not only by the energy level (1, 2, 3...) but by symmetry and pseudoparity. The symmetry of a state is either g (gerade, or "straight") or u (ungerade, or "odd"), which concerns the π-electron bonding and anti-bonding orbitals. Likewise, Pariser labels are applied to the state as with either $+$ (positive) pseudoparity or $-$ (negative).[44] Pariser's labels indicate whether an optical transition is allowed; whereby, the transition is forbidden among states of similar parity (discussed in more detail in Section 1.2).[45,46] Generally, it has been observed that the states with positive parity depend more on solvent polarity.[47]

The carotenoid's environment influences its spectroscopic behavior. For this reason, to understand the effect of the protein environment on
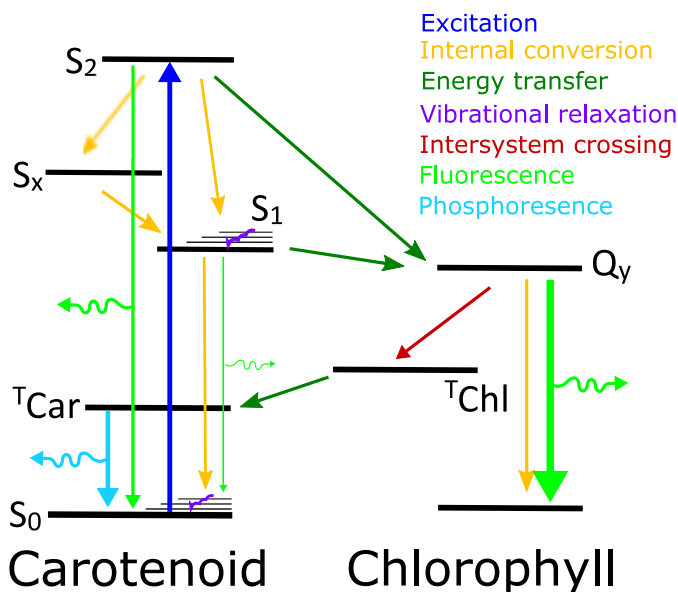
FIGURE 1.3: Energy level diagram representing excited state processes in carotenoid systems. S_X represents an intermediate state. Not all states are shown, and not all processes occur nor are they limited to the transitions shown. Adapted from ref. [48] in addition to ref. [49].

carotenoids, its is useful to test them in a controlled solution environment in order to judge their dependencies on polarity, proticity, temperature, and conformation. Though spectroscopic time-resolved studies on carotenoids in solution have also provided insight into the effect of the structure on their excited states and studies of proteins have revealed much about energy transfer processes with these states as well as conformational dependecies, in the protein environment, spectral features become more crowded and intuitive analysis of carotenoids' excited states is required to discriminate between pathways within the carotenoid and between the carotenoid and chlorophyll (Chl), as shown in Fig. 1.3.

Below is a general overview of the characteristics of each of the known, debated, and suspected excited states of carotenoids in various solution and protein environments. Of course, it must be mentioned that the principal origin of all excitations (excluding excited state absorptions) is the ground

state, often labeled S_0, posessing $1^1A_g^-$ symmetry. It represents the unexcited, relaxed carotenoid. Its only spectral properties observed are ground state bleaching and, indirectly, ground state vibrational relaxation. Upon excitation, the ground state is immediately partially depopulated, and as the excited molecule relaxes, the ground state is repopulated and the bleaching signature amplitude decreases. When the S_0 vibrational levels are populated, hot ground state species may be formed, but generally, their relaxation occurs within 5-15 ps.[22]

The S_1 State ($2^1A_g^-$) and the Intramolecular Charge Transfer (ICT) State

In Solution

   The lowest singlet excited state of carotenoids, named the S_1 state, has symmetry $2A_g^-$ and its similar parity with the ground state forbids direct single photon excitation. In light harvesting systems, the state has been suspected to play a crucial role in energy flow regulation whose energy transfer to neighboring Chls is critically dependent on the structure of the carotenoid as well as its immediate environment. However, due to its forbidden nature, this state remained elusive for a time since its prediction.[18]

   From the inception of spectroscopy of the S_1 state, it was determined partly by means of the Energy Gap Law (Eqn. 1.10) that the energy of the state decreases with increase in conjugation length (see Fig. 1.4), yet spectroscopic measurements of the weak emission from this state precluded the exact placement of the energy level. Further experiments established that for longer carotenoids the region of interest is covered by the S_2 state emission.[22] Later, when transient absorption measurements were made, there was hope that the S_1 energy could be determined by the $S_0 \rightarrow S_n$ and $S_1 \rightarrow S_n$ transition spectra (see Fig. 1.5), but the ground state bleaching signal overlays the high energy side of the latter. Moreover, the vibrational structure of the S_n state is unclear from the $S_1 \rightarrow S_n$ transient absorption spectrum. Nonetheless, it was determined that the S_1 state is far less sensitive to the polarizability of the solvent than S_2, the strongly absorbing carotenoid excited state.[51]

   Later on, transient absorption studies looked to the near infrared region, monitoring the $S_1 \rightarrow S_2$ transition in order to determine the energy of

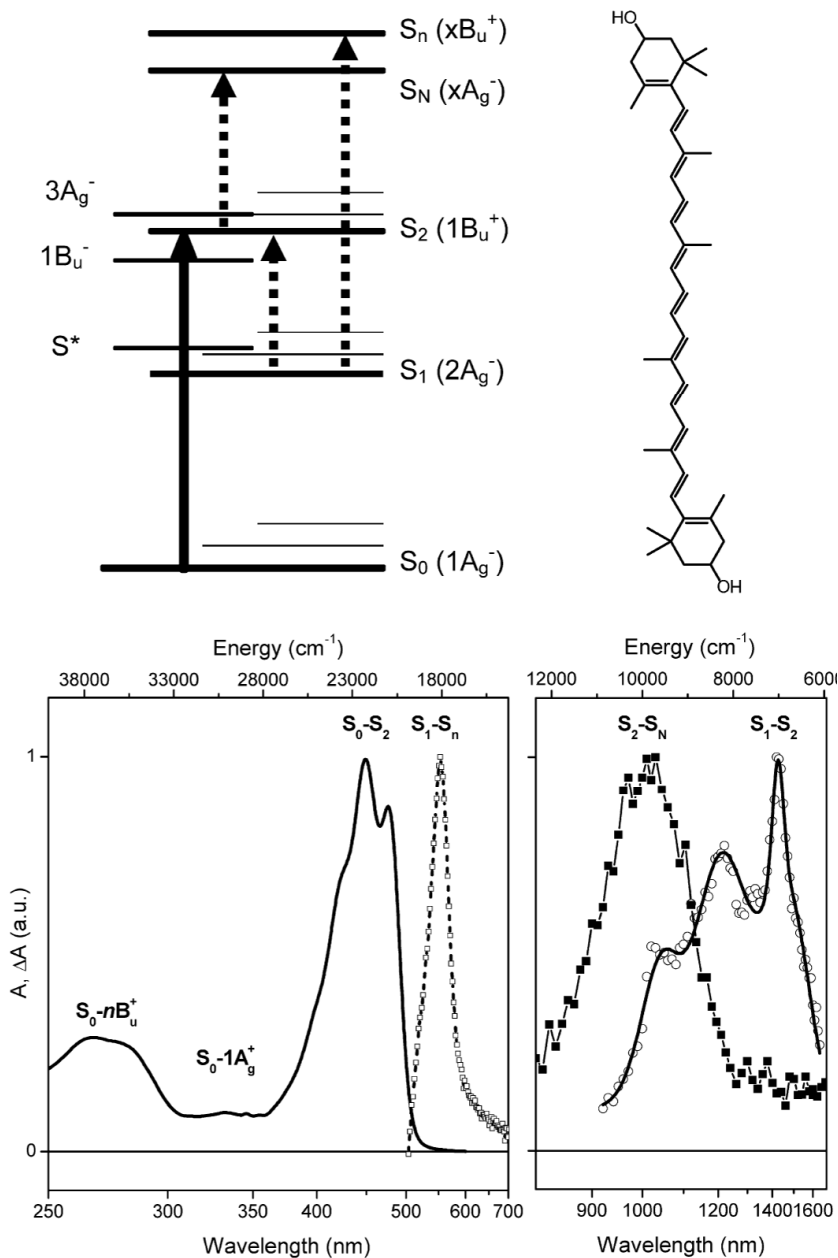FIGURE 1.5: (top) Simplified energy level scheme of a carotenoid molecule. The solid arrow represents the $S_0 \rightarrow S_2$ transition, the dotted arrows are transitions corresponding to transient signals occurring after excitation. (bottom) Spectral bands corresponding to various transitions in the carotenoid zeaxanthin whose molecular structure is also shown. Figures and caption taken from ref. [52].

the S_1 state. This technique is reliable for longer carotenoids; whereas, for shorter carotenoids, Raman and fluorescence spectroscopies are more reliable.[22] These studies revealed that the S_1 properties of carotenoids are considerably dependent on the molecular structure, leading to what has been called the conformational hypothesis: exceptions to the S_1 state's energetic dependence on conjugation length (N) are due to variability in the carotenoid's structure.
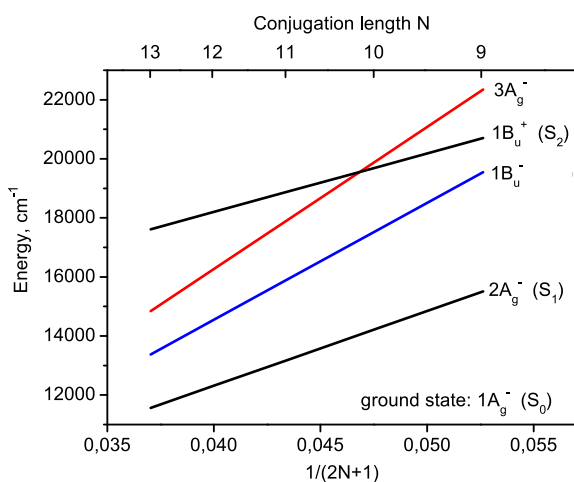
FIGURE 1.4: The theoretically determined dependence of the excited state energies on conjugation length N. Obtained from ref. [50]

Another notable spectroscopic method for determining the S_1 state energy is two-photon absorption spectroscopy. With a high flux of photons at roughly half the energy gap between the S_0 and S_1 states strikes an allowed transition via virtual states. This method can probe carotenoids whose S_1 state emission is relatively weak but also carotenoids with carbonyl groups (carbonyl carotenoids) whose absorption spectra demonstrate the presence of the mutual ICT state.[*]

Carbonyl carotenoids act like carotenoids without a carbonyl group in nonpolar solvents; however, in polar solvents the S_1 signatures have been found to decay much faster. Generally, it was found that increase in polarity generally shortens the lifetime.[42,54] According to one model,[16] this behavior had been attributed to the decay of the S_1 state to an immediate state below it, called the Intramolecular Charge Transfer (ICT) state. It is named for its

---

[*]A technique using resonance-Raman excitation profiles has also been successful in probing this state directly.[53]
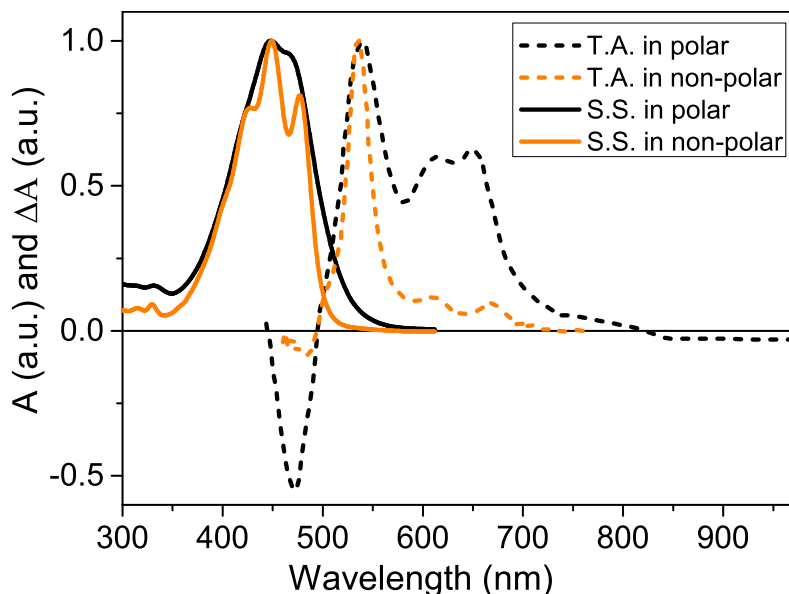
FIGURE 1.6: Normalized steady-state (S.S.) and maximum transient absorption (T.A.) spectra of fucoxanthin in non-polar (n-hexane for S.S. and cyclohexane[55] for T.A.) and polar solvents (in methanol for S.S. and T.A.[56]). The broadening of the S_2 absorption, the red shoulder on the S_1 state signature, and the stimulated emission in the near-IR are all signatures of carbonyl carotenoids in polar solvent. The latter two properties are signatures of the ICT state.

conventional charge transfer character, which was later assigned to the presence of the carbonyl group.[41] Likewise, in the absorption spectrum, the state's presence is recognized by a broad, red-shifted form in the transient absorption spectra decaying with the S_1 band and stimulated emission in the near-IR region (see Fig. 1.6).[22,55] Despite its universally recognized spectral features, the ICT state's relation to the S_1 state has long been debated.

The existence of the ICT state has been found to be strictly dependent on the presence of a carbonyl group (keto group) attached to the conjugated backbone. What was originally considered the effect of an electron density shift in the lactone ring of peridinin[54] was later attributed to the carbonyl group on that ring.[57] Also, it was found that the effects of solvent polarity is indifferent to whether the carbonyl group is located on the ring if the conjugation

extends to the ring or on the backbone.[41,58,59] However, if there are two carbonyl groups in symmetric positions on the molecule, such as in crocetindial, the polarity-induced behavior of the ICT state is entirely mitigated, even obtaining an excited state decay lifetime similar in hexane and acetonitrile.[60]

Though multifaceted time-resolved single- and two-photon absorption studies have indicated that the S_1 and ICT dynamics are strongly coupled,[54,59,61] there still remained diverse experimental and computational studies with varied conclusions. In the most basic sense, the question was whether the S_1 and ICT states are the same excited state species, or whether they are entirely different; though the signatures of ICT arise in certain conditions, it's evolution is entirely indistinguishable from the S_1 state by global analysis. In summary, the two states have been described as:

- the same state with a large dipole moment,[61]
- in equilibrium with each other[62] or strongly coupled and thus forming a collective state with its own potential energy surface,[54,59,63] or
- distinct and behaving independently.[64,65]

The enhancement of the charge transfer (CT) character of a carotenoid and its carbonyl group as an electron acceptor is considered to be due to its ability to form hydrogen bonds with a polar, protic solution, and a change in the carotenoid structure is thought to be the cause of the ICT state stabilization, at least within 1 ps in peridinin.[66] Stabilization refers to how the charge transfer characteristics subside after 1 or 2 ps and its dynamics coincides with the S_1 decay. Considering the S_1 and ICT states to be part of the same potential energy surface, stabilization is consistent with the ICT state being a potential minimum through which part of the excited state population relaxes.

Recently, however, Redeckas et. al.[56] demonstrated in a multi-pulse transient absorption study of fucoxanthin in methanol, the states are strongly coupled yet independently affected by stimulated emission pumping (or dumping), by an ultrafast spectropic method described in Section 1.3, the showcase method of this thesis. By prematurely dumping (or removing) the population of the ICT by a pulse resonant with its characteristic stimulated emission. This study revealed that the S_1 and ICT states, are in an equilibrium

which is restored after dumping. Section 2.1 features an in-depth study of the dependence of S_1/ICT equilibration by dumping as well as repumping both states individually. By this study, we revealed that lower polarity, proticity, and temperature delays S_1/ICT equilibration; and we reaffirmed the concept of a single potential energy surface.

In Antenna Proteins

The S_1 state of some carotenoids is modified in the protein environment of light harvesting systems which may affect the transfer of energy to or quenching of local chlorophylls, as found recently.[37] For example, zeaxanthin and violaxanthin have lifetimes of 11 and 24 ps, but in the binding pockets of LHCII, violaxanthin's lifetime shortens to near that of zeaxanthin. Spectrally, the $S_1 \rightarrow S_N$ transition band of carotenoids is redshifted in the protein environment.[17] The lifetime shortening in violaxanthin was considered to be due to its ability to conform to the binding pocket; whereas, zeaxanthin's rigidity was considered to actually affect the protein's conformation such that the Chl *a* could be quenched.[67,68] In photosystems, the energy quenching and donating ability of a carotenoid's S_1 state is largely dependent upon its energetic level relative to the Chl's Q_y state, it's lowest singlet excited state.

The S_1 state may act as an energy quencher, lying below a Chl's Q_y state, and it has been considered to be an energy transfer pathway for non-photochemical quenching (NPQ), some process by which excessive light energy is controlled and dissipated to avoid reactive oxygen species.[32,37,69]

Primarily, the S_1 state acts as an energy donor. Even if the state is not promoted above the Q_y state, the carotenoid may still transfer energy from a vibrationally hot S_1 state; that is, from the vibrational levels of the state. In the unique environment of PCP (see Fig. 1.7), energy transfer from the S_1 state is by far the dominant pathway, and peridinin exceeds the light harvesting capacity of Chls in the protein. The tight packing of pigments makes the system ideal for energy transfer, and there is a significant charge transfer characteristic due to peridinin's carbonyl group.[22] In fact, efficiency of peridinin-Chl energy transfer was found to be almost 100%, of which 88% has been attributed to the combined S_1/ICT state, decaying at 2.5 ps and a vibrational decay of

700 fs.[54,70] It was determined the charge transfer character of the carotenoid enhanced the energy transfer to chlorophyll.[71] The recent pump-dump-probe study has revealed that the S_1 and ICT states of peridinin are independent in PCP, the states equilibrate in less than a picosecond, and that the ICT state is the primary donor in carotenoid-Chl *a* energy transfer.[72]
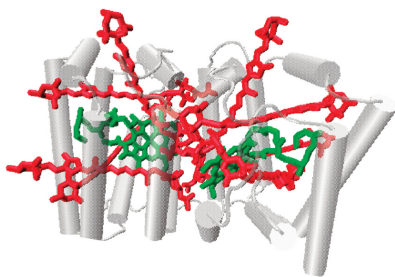
FIGURE 1.7: A simplified structure of PCP from ref. [17]. Peridinin carotenoids are in red and chlorophyll *a* are in green.

Much attention has also been given to fucoxanthin-chlorophyll protein (FCP), whose structure has not yet been resolved. This complex, found in the membrane of diatoms in varied forms, shares a very similar sequence homology with LHCII antenna from plants.[73] Two forms of fucoxanthin exist in FCP proteins studied so far and two energy transfer channels from the S_1/ICT state, particularly, transferring within a few picoseconds.[74–77] The total efficiency of carotenoid-Chl energy transfer has been observed near 90%, and the S_1/ICT state energy transfer has demonstrated efficiencies from 30% to 40%. In their two-dimensional transient absorption spectroscopy study of FCPa from *Cyclotella meneghiniana*, Gelzinis et. al.,[78] determined the a "red" form of fucoxanthin, the slightly slower decaying form (15-28 ps), demonstrated more efficient energy transfer to Chl.* In Section 2.2 is featured a pump-dump-probe study on FCP from the diatom *Phaeodactylum tricornutum*. By prematurely dumping the slowly decaying fucoxanthin species, we determined the S_1 portion of the S_1/ICT potential energy surface is the primary donor of the slow-form fucoxanthins with a net equilibration time of approximately 7 ps.[79]

Due to the sensitivity of the ICT state on the environment, in order for the combined S_1/ICT state to efficiently transfer energy, proper orientation, polarity, and hydrogen bonding may all be key factors in light harvesting antennae. In seeking to understand this state and how it functions in light

---

*The red form is considered more efficient because the magnitude of the signal associated with the carotenoid is reduced compared to the blue form.

harvesting systems, we come to understand more the primary process of all antennae systems containing carbonyl carotenoids which are the most prolific known light harvesting structures on the earth.[22]

The S_2 ($1^1B_u^+$) State

As mentioned before (Section 1.2), the S_2 state is highly absorbing due to the strongly allowed $S_0 \rightarrow S_2$ transition and is assigned an odd $1B_u^+$ symmetry.[80] This transition is responsible for much of the color we see when leaves change color, even in some birds[†] and crustaceans. In spectroscopy, this transition is often recognizwed by its three strong, vibrational peaks separated by about 1300 cm^{-1};[52] the redmost indicates the 0-0 transition found in the range 475-525 nm.[22] The energy gaps between these peaks are indicative of the C-C and C=C vibrational modes, and their resolution is dependent on the nature of the conjugation as well as the polarity of the environment.[22] For example, if the conjugation extends to the rings of the carotenoid, as in β-carotene, the vibrational structure is less prominent due to varied conformations in solution caused by the twisting of rings whose methyl groups are repelled by hydrogen atoms on the backbone.[6,82,83] As already mentioned, the resolution of the vibrational structure in carbonyl carotenoids is less (see Fig. 1.6), and the whole S_2 spectrum is assymetrically biased toward the red, often sensitizing photosynthetic organisms to green wavelengths. This loss of vibrational structure in polar solvents is due to the charge transfer character of the ground state where a stabilized negative charge on the oxygen of the keto group causes several ground-state conformations.[41,59,66] In fact, the broadening to the red demonstrates close association with protic solvents where oxygen forms hydrogen bonds and further stabilizes the charge transfer character.[59]

In solution, the properties of the S_2 state demonstrate some unusual dependencies on conjugation length, and its decay diverges from the Energy Gap Law (Eqn. 1.10). The general trend observed is a decrease in S_2 energy with increase in conjugation length (N) (see Fig. 1.4) closely following the

---

[†]In fact, birds' eyes have light-absorbing sacks filled with carotenoids which act as filters in order for them to distinguish some colors.[81]

inverse relation $E = A + B/N$, where A and B are parameters.[84–86] The S_2 state, however, defies Kasha's Rule[*][87] and begins to fluoresce for carotenoids $N \geq 8$.[86] For carotenoids $9 \leq N \leq 13$, the S_2 state is the primary emitter instead of the lowest singlet state, producing a mirror-image spectrum of its absorption, a Stokes shift of 150-300 cm^{-1}.[82,85,86,88,89] Likewise, as opposed to values expected by the Strickler-Berg equation (see ref. [90]), the state has been found to decay two orders of magnitude faster, in the range of 100-300 fs, for varied carotenoids and synthetic analogues.[91–94] Though the conjugation length has been found to affect the $S_1 - S_2$ energy gap, there is no lifetime dependence on conjugation length for non-carbonyl carotenoids, and of course, this violates the Energy Gap Law (EGL) (Eqn. 1.10). In fact, internal conversion between the states has been found incompatible with EGL in that some studies indicate the internal conversion rate increases as N gets larger.[91,93]

The S_2 states is also affected by the presence of a carbonyl group on the conjugated backbone. With a keto group, the $S_2 - S_1$ energy gap is decreased,[43] the state does not emit as much.[95,96] The short lifetime of the S_2 state in carbonyl carotenoids has been attributed, in part, to mixing with the S_1 state.[61,97,98]

In the light-harvesting antennae, a bound carotenoid is more often restricted and, therefore, less free to adopt varied conformation. As a result of a restricted distribution of conformations, the vibrational structure of the S_2 steady-state absorption spectrum becomes more refined.[22] Varied studies indicate that the S_2 state of many carotenoids are capable of transferring energy not only to the (B)Chl Q_x state but even to the Q_y state.[75,77,99] Such energy transfer is possible for when there is sufficient overlap of donor emission and acceptor absorption spectra as the FRET mechanism has been found to dominate over the Dexter mechanism for S_2 energy transfer in these systems.[22]

Other Singlet States

In addition to the states mentioned already, other dark states have been predicted in calculations of polyene energetic structures.[39] However,

---

[*]According to Kasha's Rule, only the lowest singlet excited states fluoresce.

their forbidden nature precludes their direct observation, and spectral and dynamic features are often convoluted with vibrational decays and suspected conformational changes. Nonetheless, these states can be involved in energy transfer[100,101] and are, at times, indicators of structural changes within the carotenoid.[19,101] Though these states may not be mentioned in the research section (Section 2), the transient absorption methods and analyses presented in this thesis can provide a means to investigate dark states in the future.

The S^* State

Upon discovery of an independent, long-decaying, high-energy shoulder on the $S_1 \rightarrow S_N$ transient absorption signature in spirilloxanthin, it was determined that a dark state, called the S^* state, might lie between the S_1 and S_2 states.[102] In spirilloxanthin, the S^*-associated feature was four times as long as the S_1 signal decay. These characteristics have since been identified in many other carotenoids (S^* in rhodoxanthin in Fig. 1.8), generally for those which are longer than 9 conjugate double bonds ($N \geq 9$).[102,103] Otherwise, the state has been found to have no obvious dependence on the conjugation length.[100,102,104] Though $S^* \rightarrow Chl$ energy transfer has been reported for some bacterial light harvesting complexes,[100,102,105] its origin and energy transfer properties have been debated.[52]

Due to the fact that the S^* lifetime is comparable to common ground state vibrational relaxation rates, it has been considered that the S^* state is actually a vibrationally hot ground state,[102] but the observed signal lacks the expected shift, narrowing, and correspondence to the rates determined by the Energy Gap Law.[22,52] Nonetheless, pump-dump-probe measurements seemed to indicate the S^* state is a hot ground state, not an intermediate populated from the S_2 state, because it was not affected when the S_2 state was dumped.[103] On the other hand, some studies have strongly supported the idea that the S^* exists due to the carotenoids having a twisted conformation,[19] and the state may, in fact, be the S_1 state itself. In this case, deviating, twisted conformations promote the S_1 state; then, the molecules relax to their ground state conformations.[19,106,107] The observed $S^* \rightarrow S_1$ relaxation pathway[48,106] would thus indicate conformational relaxation to the S_1 state.
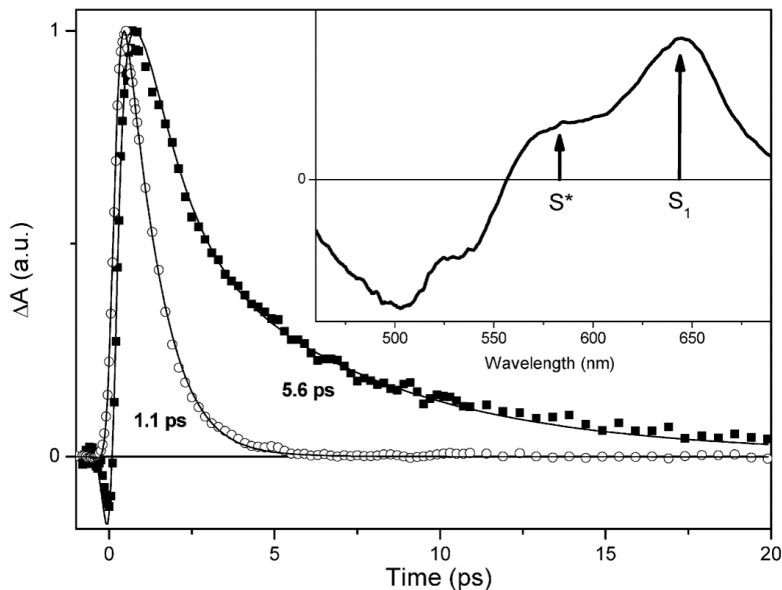
FIGURE 1.8: Kinetics of rhodoxanthin at maxima of the S^* (571 nm, full squares) and S_1 (642 nm, open circles) bands. The inset figure shows a transient absorption spectrum at 1 ps. The figure and caption obtained from Ref. [52].

Recently, however, a unified interpretation of the S^* state for all carotenoids has been proposed.[108] Taking into account vibrational energy relaxation, S^* transient absorption signatures are manifestations of vibronic transitions from either the S_1 state or vibrationally excited levels of the ground state. Therefore, the pump-dump-probe observations mentioned above are the result of populating a ground state intermediate (GSI), in this case, a vibrationally hot ground state.

The $1B_u^-$ and $3A_g^-$ States

The theory of finite polyenes, which predicted the S_1 and S_2 states, also predicted two dark states: $1B_u^-$ and $3A_g^-$. Raman studies agree with the theory, the $1B_u^-$ state was determined to lie between the S_2 and S_1 states for carotenoids $N \leq 10$, about 16550 cm^{-1} for β-carotene.[52,109,110] Nonetheless, the state remains absent from direct absorption from the ground state because it is both one- and two-photon forbidden.[39]

Over the years, different excited state absorption features have been attributed to the $1B_u^-$ state. Claims for evidence of this state's spectral signatures were observed in the near-IR in β-carotene and neurosporene; whereas, in the visible region, any spectral signatures are complicated by the sub-picosecond S_2 stimulated emission features.[111,112] Some visible features have been attributed to the state, but the features are not found to blueshift with increasing conjugation length in accordance with the theory of polyenes.[113] Nonetheless, the $1B_u^-$ has been suspected as an intermediate in internal conversion from the S_2 to S_1 states as well as energy transfer to Bacteriochlorophylls (BChls).

Internal conversion to the $3A_g^-$ state from S_2, however, is forbidden due to symmetry breaking.[38,46] It had been predicted to lie above the S_2 state, but from Raman excitation profiles, the state appeared to be more likely between the S_2 and $1B_u^-$ states. The exceptions were carotenoids of $N \approx 10$, like spheroidene for which the S_2 state overlaps.[110]

Triplet States

At last, the properties and function of the carotenoid triplet state will be mentioned briefly. The state has never been diretly observed for carotenoids in solution.[52] The state, however, finds its function in light harvesting systems as the carotenoid prevents the formation of oxygen radicals by rapidly quenching the triplet state of (B)Chls, which sensitizes the damaging singlet oxygen, or reactive oxygen species (ROS), formation:

$$^TChla^* + O_2 \rightarrow Chla + {}^1O_2^*.$$
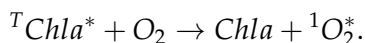
Nearby carotenoids can mitigate this problem by triplet-triplet energy transfer, based upon the Dexter exchange mechanism (Section 1.2),:[40,114]

$$^TChla^* + Car \rightarrow Chla + {}^TCar^*.$$
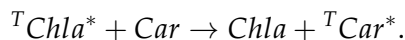
The yield of triplet quenching by carotenoids has been found to increase with N.[43] The triplet state of carotenoids are also capable of directly quenching singlet oxygen, called singlet oxygen scavenging; whereby, the carotenoid triplet

state functions as the direct quencher:[40]

$$^1O_2^* + Car \rightarrow O_2 + {}^TCar.$$
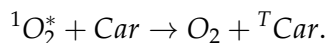
1.1.4   Carotenoid Structure as Revealed by Spectroscopy

The carotenoid excited state dynamics and spectral features are inextricably related to its structure, including its conformation, which also determines its interaction with the environment and its function in the light harvesting system. Though there are numerous structural factors controlling a carotenoid's temporal-spectral response, the focus here will be primarily on the conjugation length and the presence of carbonyl groups on the carotenoid. The variability of the colors of leaves in the fall is a demonstration of the conjugation length: the length of the carbon-carbon, alternating double-bonded backbone of the carotenoid over which electrons are delocalized from their parent atoms. This is widely quantified by the letter N, representing the number of carbon-carbon double bonds in the alternating pattern of the backbone. The band of wavelengths to which the carotenoid is sensitive depends upon N. As the S_2 state is a strongly absorbing state, its energy dependence on the conjugation length is an inverse relationship: a carotenoid with shorter conjugation length has a promoted S_2 state and, therefore, a bluer absorption band than the structurally longer, red-absorbing carotenoids.[22,115] Specifically, the conjugation length dependence of energy of the S_2 state may be approximated as $E = A + B/N$, with A and B as scaling parameters.[85,86] This general behavior is the same for all predicted excited states of polyenes, except for the S^* state of linear polyenes,[115] following the trend shown in Fig. 1.4. For the lowest singlet excited state, including the ICT state, shorter conjugation results in longer relaxation lifetime.[22] This is not always the case, however, for the S_2 state as in peridinin, for example, where the decay lifetime can decrease with smaller N, more closely related to the predictions of the theory of conical intersections (Section 1.2.2).[116]

Though the conjugated orbitals in carotenoids require the alternating single-double, carbon-carbon bonds of the backbone, it is possible that the conjugation may extend into the rings. The twisting of the rings of β-carotene,

for example, causes preferential population of the S^* state and bring forth a larger distribution of ground state conformers.[115] It was also determined that twisting of the rings can effectively increase the energy of the first excited state; whereby, the conjugation length is effectively shortened.[117,118] When the conjugation extends into the rings with a C=C bond, s-*cis* conformers exhibit for this bond an effective conjugation $N_{eff} = 0.5$ and s-*trans*, $N_{eff} = 1.0$. For various carotenoids, such as presented in this work with alloxanthin (Section 2.4) where there are triple bonds at either end of the backbone, the concept of effective conjugation length (N_{eff}) has been useful in determining various structural properties of carotenoids.[118,119] The conjugation may also extend to groups such as a keto group, for which, despite its position on the conjugation, an effective N_{eff} of 0.5 is observed.

Though the ICT character is strictly dependent upon the presence of a conjugated carbonyl group, the number and position of carbonyl groups on the carotenoid are important. For example, various studies of peridinin analogues have demonstrated that the greater assymmetry in the positioning of the lactone ring, the greater the charge transfer character.[120] Whereas, with greater symmetry in the positioning of the keto groups, the weaker the ICT signatures are. Theoretically, this is because the ICT state has a strong dipole moment; thus, the more assymmetric the distribution of the reducing carbonyl groups, the stronger the state wil be.[97]

In our study of fucoxanthin derivatives in Section 2.3, we sought to determine the effect of a non-conjugated acyloxy group on the ICT state properties. The decrease of the transient ICT excited state spectral signatures, the lengthened their decay lifetime, and the broadening of steady-state features of the steady-state spectrum all indicated that the assymetry dependence of the ICT state is not limited to groups which are a part of the conjugation.

1.2 Foundational Theory for Spectroscopy of Carotenoids

Since the late 1980s,[121] ultrafast spectroscopy has allowed us to observe real-time, the behavior of the nano-world, but the true nature of the system which we aim to model is shrouded by various complexities including high-order electromagnetic interactions and basic thermodynamic principles. While models are made to illustrate what one ideal system is like, when they are based upon spectroscopic studies, they actually represent a consensus of many systems. Moreover, the signal received by the spectrometer are directly influenced by changes in polarization of the system rather than the electron dynamics of the system itself. Figure 1.9 illustrates how the observed signal is not directly related to the dynamics of an individual, model system.

Nonetheless, controlling factors such as the atomic structure of the molecule, its environment, and proximity to an acceptor or donor remain the basis for spectroscopic observations. In the following subsections will be described briefly the foundational theory of the dynamics of individual molecular and donor-acceptor systems. Though essential to photosynthesis in all organisms, this discussion excludes exciton interactions which occur in reaction centers.[122] It also excludes detrimental or unwanted excitonic and ionization processes which were not observed in this study. The following highlights key

FIGURE 1.9: The observed signal is related to the dynamics of an individual system but not directly.

principles of photophysics which the author has found necessary to both photosynthesis and transient absorption spectroscopy light-harvesting antennae.
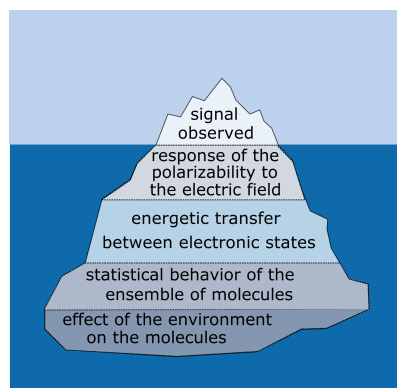
1.2.1 Transitions by Light Absorption and Stimulated Emission

The dynamics observed and the strength of the signal are utterly dependent on the molecules' ability to absorb light considering that molecules must

first be excited, then the excited molecules must be probed at various stages in its transient decay to monitor its dynamics and energy transfer processes. All absorptions occur with the probability of a resonant transition. It is not guaranteed that all molecules in the path of the pump pulse will be excited nor that all excited molecules in the path of the probe will exhibit a transient signal in the desired spectral range. Even the simplest systems are strongly dependent on the molecules' orientation in relation to the polarization of the incident light, although it is not the molecule's orientation itself which is the controlling factor. The probability of the incident light striking a transition in a molecule depends intrinsically on the transition dipole moment μ_{ab} from state a to state b, and its molecular-wide orientation and strength is determined mutually by the electronic wavefunctions in these states. The electronic probabilistic distributions of each, individual state are also dependent on their wavefunctions.

In its most basic sense, the probability of a particular transition between two states a and b due to absorption is related to the transition dipole moment by

$$
\begin{aligned}
\boldsymbol{\mu}_{ab} &= e\langle \Psi_b | \mathbf{r} | \Psi_a \rangle \\
&= e \int \Psi_b^* \mathbf{r} \Psi_a d\sigma
\end{aligned}
\tag{1.1}
$$

Here, Ψ_a and Ψ_b are the wavefunctions describing the initial and final states in which electrons are superimposed in an optical transition. Therefore, to eventually obtain the probability of such a transition, a superposition of states is expressed

$$
\Psi = C_a(t)\Psi_a + C_b(t)\Psi_b + \cdots
\tag{1.2}
$$

where the coefficients as functions of time determine which state the electron will be as the system evolves. Absorption of sunlight, as for the carotenoid, in its most basic sense may be represented by a time-dependent perturbation to an otherwise, steady-state Hamiltonian:

$$
\tilde{H} = \tilde{H}_0 + \tilde{H}'(t).
\tag{1.3}
$$

Here, at the scale of the molecular system, the interaction of light would need to be expressed as a periodically fluctuating electric field

$$\tilde{H}'(t) = -\mathbf{E}(\nu, t) \cdot \tilde{\mu}_{ab} \tag{1.4}$$

Therefore, it is clear that the interaction of these molecules is highly dependent on the polarization of the irradiation. The transition dipole moment's dependence on the probability of striking a transition is elucidated when a time-dependent solution is sought with this perturbating Hamiltonian and the linearly combined wavefunction. When placced in the time-dependent Sch odinger equation, an expression for the rate of final state b's evolution can be isolated as

$$
\begin{aligned}
\frac{\partial C_b}{\partial t} &= -\frac{i}{\hbar} \langle \Psi_b | \tilde{H}' | \Psi_a \rangle \\
&= \frac{i}{\hbar} \left[e^{i(E_g + h\nu)t/\hbar} + e^{i(E_g - h\nu)t/\hbar} \right] \mathbf{E}_0 \cdot \langle \psi_b | \tilde{\mu}_{ab} | \psi_a \rangle
\end{aligned} \tag{1.5}
$$

where the energy gap $E_g = E_b - E_a$ marks the standard for absorption of light with frequency ν and intensity $I = |E_0|^2$. To obtain an expression for the probability of the population being in the second state b after a short time τ, the expression is first integrated over the time the system has been excited:

$$
\begin{aligned}
C_b(\tau) &= \int_0^\tau \frac{\partial C_b}{\partial t} dt \\
&= \left[\frac{e^{i(E_g + h\nu)t/\hbar} - 1}{E_g + h\nu} + \frac{e^{i(E_g - h\nu)t/\hbar} - 1}{E_g - h\nu} \right] \mathbf{E}_0 \cdot \langle \psi_b | \tilde{\mu} | \psi_a \rangle.
\end{aligned} \tag{1.6}
$$

The terms in the brackets indicate two possible transitions between the two states: absorption for the case when the energy is expressed $E_g = h\nu$ and stimulated emission for when $E_g = -h\nu$. Nevertheless, neither absorption nor stimulated emission is not guaranteed as the expression indicates a dependency on the transition dipole expression at the end and its dot product with the light field.

The relation between the probability of populating state b is obtained by

integrating C_b at time τ over all frequencies, the modes of oscillation between ν and $\nu + d\nu$:

$$|C_b(\tau)|^2 = \int_0^\infty C_b^*(\tau,\nu)C_b(\tau,\nu)\rho_\nu d\nu$$

$$|C_b(\tau)|^2 = (\mathbf{E}_0 \cdot \boldsymbol{\mu}_{ab})^2 \rho_\nu(\nu_0)\tau/\hbar^2. \tag{1.7}$$

The variable ρ is the energy density for which $|E_g| = h\nu_0$. This relationship demonstrates that the probability of a transition between states by stimulation of light is dependent not only upon the polarization of the light in relation to the dipole but also the symmetries of the states as $\boldsymbol{\mu}_{ab} = \int \mathbf{r}_{ab}\Psi_b^*\Psi_a d\sigma$.

Take, for example, an excitation exactly along the transition dipole, the z direction:

$$\boldsymbol{\mu}_{ab} = \int_{-\infty}^\infty z\Psi_b^*(x,y,z)\Psi_a(x,y,z)dz. \tag{1.8}$$

If the states are of the same symmetry in z, the integrand will be odd; therefore, the integration will give zero, making the probability zero. This implies a forbidden transition. If, however, the states are of differing symmetry, the transition between the states is allowed. This is the reason why the first excited state of carotenoids is one-photon forbidden; thus, being considered a dark state. Under low irradiation intensities, carotenoids absorb from the ground S_0 state to a second excited state S_2, yet the $S_0 \rightarrow S_1$ transition is not allowed due to their even symmetries.[102] Whereas, S_0 and S_2 differ in symmetry, and the $S_0 \rightarrow S_2$ transition has a strong dipole strength defined as

$$D_{ab} = |\boldsymbol{\mu}_{ab}|^2. \tag{1.9}$$

Therefore, the transition is very probable.[90]

1.2.2 Transitions by Internal Conversion: The Energy Gap Law and Conical Intersections

The Born-Oppenheimer approximation applies only for non-adiabatic transitions, as the nuclei are considered non-moving. There is no accounting

for kinetic energy of nuclei. In the weak coupling limit,* the rate of radiation-less internal conversion between states is related to the energy gap between the states by

$$k \propto exp\left(-\gamma\frac{\Delta E}{\hbar\omega_M}\right) \tag{1.10}$$

where $\gamma = \gamma(\omega_M, \Delta_M, \Delta E)$, ω_M being the frequency of a vibrational mode and Δ_M the reduced reaction coordinate displacement among the potential minima of the states. This is famously known as the Energy Gap Law (EGL).[123] Though the EGL has been described in the strong coupling limit, by this approximation, however, internal conversions are treated only non-adiabatically, which is certainly not the case for all internal conversion processes (See Fig. 1.10). Internal conversion between states, however, can occur for when an correction is added to the approximation in the form of an interaction term in the hamiltonian. This essentially is an adiabatic correction to the non-adiabatic wavefunction expressions of the excitation states of a molecule. Their coefficients express that the probability of transition between states is largest where the potential energy surfaces of states with offset reaction coordinates intersect. As the geometry of a state's potential energy surface affect the dynamics of a molecule, these intersecting points of internal conversion are called conical intersections.

This formalism expresses why certain states, like the S_2 state of carotenoids, do not follow the Energy Gap Law, which is restricted to adiabatic transitions. Additionally, such transitions can account for observed adiabatic processes such as vibrational decay which is observed after $S_2 \rightarrow S_1^*$ internal conversion in carotenoids. In carotenoids, the S_2 and S_1 electronic states are coupled to nuclear vibrations. Therefore, energy accepted into a hot excited state, such as the S_1^* state, must vibrationally relax to the minimum potential energy configuration in that state, that is the minimum nuclear vibration, before a non-adiabatic transition may occur from that state.[124]

In summary, for the carotenoid the interaction between the highly absorbing S_2 and first excited states follows an adiabatic process as described by

---

*In the weak coupling limit, the reaction coordinates of the energy donating and accepting states are only slightly offset.[123]

conical intersections, and the S_1 state, which closely follows the Energy Gap Law, represents, ideally, a non-adiabatic internal conversion process.[123,124]

1.2.3 Donor-Acceptor Transitions
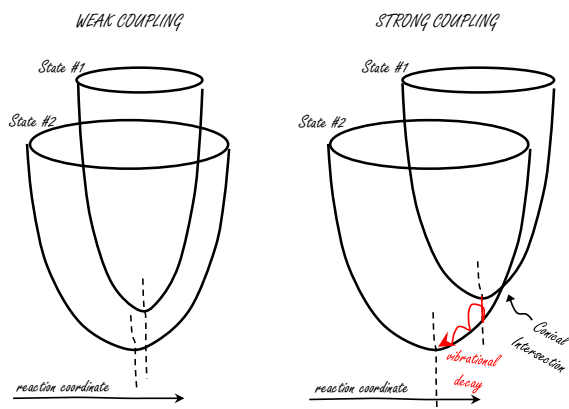
FIGURE 1.10: A sketch of potential energy surfaces in the weak coupling and strong coupling limits. Adapted from Ref. [123]

When considering the total migration of captured sunlight energy in plants, most energy transfer within light harvesting systems is a result of weak intermolecular interactions.* The first process discovered to occur among light-harvesting pigments upon excitation was Förster Resonance Energy Transfer (FRET), the hallmark of Chl-to-Chl and Chl-to-RC energy transfer.[125] This fast and efficient energy transfer relies upon weak dipole-dipole coupling and strong overlap of donor molecule emission and acceptor molecule absorption spectra. In purple bacteria, FRET is the dominant process by which energy is sequentially funneled by resonating chromophores to the reaction center.[126] In any light harvesting system where (B)Chl-(B)Chl resonant energy transfer is involved, transfer across several (B)Chls is possible due to the fact that the FRET process is faster than the (B)Chl's nanosecond total excited state lifetime of the molecule. However, the theory requires a fairly distant 10-100 Å interaction such that the transitions can be treated as point dipoles, and it does not account for the interactions which would occur in close proximity such as the 4 Å Car-to-Chl energy transfer.[90,127] FRET, among other electronic interactions occurring at distances greater than 5 Å, are classified as Coulomb or direct interactions.[128]

---

*that is: not by slow and lossy carrier diffusion!

When energy is transferred in this way, each electron remains in its original molecule and their spin configurations remain the same.

When in closer proximity, intermolecular energy transfers have low dipole strength (Eq. 1.9) and thus low probability (Eq. 1.7) of occuring only if spin is not accounted for. However, in close proximity (<5 Å), the electron orbitals of a donor and acceptor molecule may overlap, allowing Dexter electron exchange coupling as well as charge transfer interactions. When the electrons in both molecules are treated as distinguishable, the electronic interaction matrix element may be written as a contribution of both Coulomb and Dexter interactions in linear combination: linear combination:

$$H_{21(el)} = H_{21}^{Coulomb} + H_{21}^{Dexter}. \qquad (1.11)$$

In short, the resulting $H_{21}^{Coulomb}$ contribution potrays energy being transferred from one molecule to the other by de-excitation of electron 1 from the state b to a in the donor molecule and a corresponding excitation in the acceptor molecule electron from state $a\prime$ to $b\prime$. Whereas, H_{21}^{Dexter} signifies a spin exchange between the molecules: electron 1 changes spin from the donor molecule's excited state b to the acceptor molecule's $b\prime$ spin state while electron 2 originates from lower a spin state of the acceptor molecule to the state a of the donor molecule. This exchange term intrinsically includes a strong dependence on orbital overlap, thus implying the requirement of close proximity.[90] In fact, this rapid Dexter exchange mechanism accounts for not only singlet-singlet electron transfer but triplet electron transfer.

Yet another exchange occurs between molecules when they are in contact with each other, that is, within 3.5 Å. The orbitals of molecules in such proximity can overlap, alowing electrons in the Highest occupied molecular orbital (HOMO) of one molecule to translocate to the lowest unoccupied molecular orbital (LUMO) of another molecule. This process is simply understood to be charge transfer (CT) (intermolecular). The interaction matrix element H_{21}^{CT} must account for transfer of a HOMO electron from the donor molecule to the LUMO of the acceptor molecule. Transitions from one CT state to another also have low dipole strength, but the interaction, nontheless, may occur as

TABLE 1.1: Summary of the primary means of intermolecular
energy transfer among donor and acceptor molecules

energy transfer method	primary means of interaction	approx. range of interaction (Å)	duration of interaction
Coulomb	charge distribution	≥ 5	2 as
Förster	dipole coupling	10-100	100 fs
Dexter	orbital overlap	≤ 5	4 fs
charge transfer	orbital overlap	≤ 3.5	10 as

long as the acceptor is not already reduced. In the chain of photosynthesis, charge transfer occurs in photosynthetic reaction centers between specialized chlorophylls and phytoene.[126]

1.3   Experimental Method

The endeavor to capture the energetic dynamics of carotenoids in solution and in light harvesting antennae is much akin to Eadweard Muybridge's challenge in the 1870s to capture the motion of a horse trotting. With a set of shutter tripwires, a dozen cameras, and a fast shutter he invented, he captured the trotting horse, proving that at some time in the horse's stride, all four of its hooves are off the ground. From then he continued to study animal locomotion of over 700 subjects, including various human subjects.[129]

The goal of transient spectroscopies is similar: to catch the subject "midstride." For carotenoids, this means observing decay and energy transfer pathways (Figure 1.3) by fluorescence[130] or transient absorption through resonant energetic transitions. Ultrafast transient spectroscopies began with the subject of sodium iodide[131] for which Zewail won the Nobel prize for introducing the world to femtochemistry during his pioneering work at Caltech.[132, 133] Later on, they performed the first experiments in stimulated emission pumping, or dumping, by which laser pulses, resonant with an emitting transition, prematurely depopulate an excited state.[131, 134, 135]

Since then, multipulse spectroscopy, including repumping, have been applied to photosynthetic systems, of which are devoted to the study of carotenoids. Such achievements which demonstrate the power of multipulse methods include

- uncovering the existence of a dark intermediate states and conformations in carotenoids[136, 137] and testing the controversial hypothesis of intermediate state coupling in carbonyl carotenoids;[137]
- skipping or short-circuiting certain protein conformational species in a cycle which normally overshadow the spectra of subsequent species;[138, 139]
- various manipulations of light harvesting proteins which lead to the discovery of several intermediate conformations;[40, 111, 140] and
- other applications and variations including relaxation dynamics of retinal and solvation studies.[141–143]
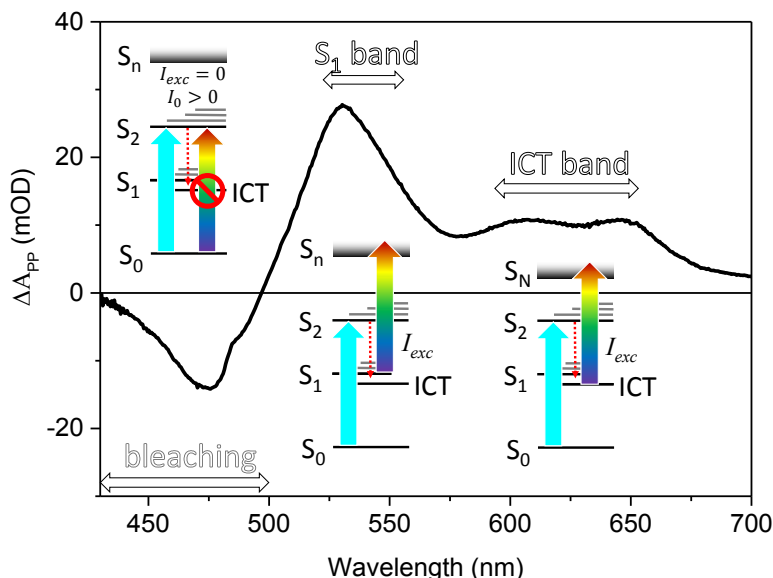
FIGURE 1.11: Transient absorption spectrum of fucoxanthin in methanol at 2.5 ps after excitation in the visible spectral window represents an imprint of the S_1- and ICT-associated bands by transition to a higher energy level. Bleaching is due to the absence of excitable population upon probing

For transient absorption, the system first absorbs an excitation pulse, resonant with an energetic transition, placing it transiently in an excited state. As the system decays, probe pulses are repeatedly sent to the sample at consecutive delay times, and where the probe wavelength is resonant with an energetic transition from an excited state to yet another, higher excitation state, some absorption occurs and the difference spectrum indicates a positive signal. Therefore, much of the spectra of such absorptions are imprints, or in nautical terms, soundings, of the initial states in these transitions (see Figure 1.11). A negative signal occurs when the probe induces stimulated emission or when the probe (I_{exc}) of the excited system encounters the absence of excitable population, called bleaching. The strength of the absorption signal depends in part on the dipole strength, but relative dynamics are observed as states depopulate over time. With a 12 ns delay line and 100 fs pulse width, we are able to distinguish processes from 100 fs to a few nanoseconds. This allows us to observe all processes involving the carotenoid except for ultrafast

internal conversion processes such as $S_2 \rightarrow hot\ S_1$ decay, which occurs on the sub-100 fs timescale in some carotenoids. (Table 1.2).

TABLE 1.2: The typical timescale of some major processes regarding a carotenoid's interaction with a light harvesting system

ms	μs	ns	ps	fs	as
10^{-3}	10^{-6}	10^{-9}	10^{-12}	10^{-15}	10^{-18}
protein folding	Car triplet decay	Chl Q_y decay	Car S_1 decay	Car S_2 decay	electron movement

An example of the internal conversion processes in a carbonyl carotenoid with a scheme various multipulse manipulations of the S_1 and ICT state populations are shown on the lower right in Figure 1.12. This simplified energetic diagram, inspired by Ref. [56], summarizes all the transitions which may be expected to occur in a carbonyl carotenoid. After the S_2 state is excited, or pumped, a carbonyl carotenoid decays through the vibrational levels of a hot S_1 and what is considered to be a separate, hot ICT state. Eventually, the S_1 and ICT states decay to the ground state; albeit, in this diagram the ICT state decays through a ground state intermediate (GSI). Throughout the entire decay process, a broad, supercontinuous probe pulse affects all permitted transitions, mostly those to some higher states, labeled S_N and S_n.

This thesis features an experimental configuration using a probe beam passing through the sample and a reference beam split from the probe before the sample by a neutral density filter, as in Figure 1.12. From the signal received by the double-diode array in the grating spectrometer is computed the absorption difference spectra, which portray the difference of the probe signal when the sample is excited as compared to when it is not excited. For this configuration, the data is calculated as a difference of absorption

$$\Delta A(\lambda, t) = \log\left(\frac{I_{reference}(\lambda, t)}{I_{probe}(\lambda, t)}\right)_{pump} - \log\left(\frac{I_{reference}(\lambda, t)}{I_{probe}(\lambda, t)}\right)_{nopump} \quad (1.12)$$

where I represents intensity of the signal when excited, and *nopump* represents the situation when the sample is not excited. The measurement regime
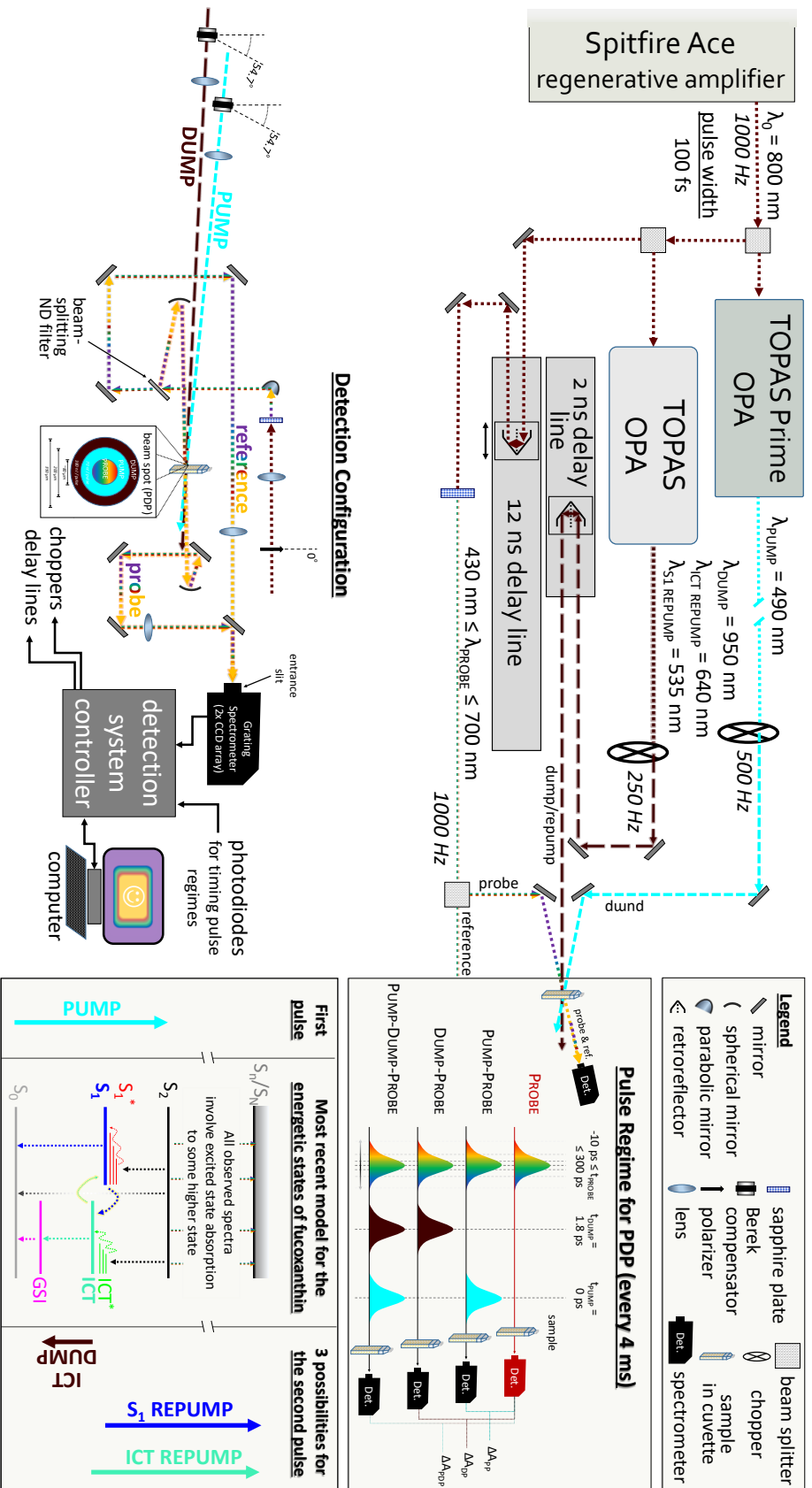
FIGURE 1.12: An illustration of the versatile multi-pulse setup (top) suitable for pump-probe, pump-dump-probe, and pump-repump-probe measurements. The detection configuration illustration (below) is an explicit representation of the optics and beam properties in the immediate sample space. The pulse regime for multi-pulse experiments and the affected carbonyl carotenoid transitions from the coupled S_1 and ICT states are summarized in the boxes on the right. The energy level diagram has been adapted from Ref. [56].

can be simply probe (P), pump-probe (PP), dump-probe (DP), where the sample's reaction to only the dump pulse is observed, or pump-dump-probe (PDP). In a full multipulse experiment, all of these regimes are measured at every probe delay. With a stable laser, the detection system receives 1000 pulses per second, which is the repetition rate of the source, synchronized choppers can block the pump and dump pulses alternatively. Therefore, as seen in the schematic in Figure 1.12, the detector observes four pulse regimes every 4 ms from which three difference of absorption signals are obtained: ΔA_{PP}, ΔA_{DP}, and ΔA_{PDP}.

The laser source is a Spitfire Ace (Spectra Physics) regenerative amplifier seeded by a low intensity, high-repetition rate Ti:Sapphire mode-locked laser. During the process of regenerative amplification, developed by Piskarkas et. al. in 1986,[144] the seed pulses are first "stretched" in wavelength and time, lowering the peak energy of the pulses. The pulses are then selectively amplified several times by pulses from a diode-pumped, green laser while passing through a Ti:Sapphire crystal rod within in a strong electromagnetic field. These broad, amplified pulses are then compressed, providing an output of 4 mJ, 100 fs pulses, centered at 800 nm at a repetition rate of 1000 Hz. In order to tune these pulses to other wavelengths, the source beam was divided in three by beam splitters and these separate beams were directed to optical parametric amplifiers (TOPAS and TOPAS Prime, Light Conversion), for pump and dump beams, and a 2 mm sapphire crystal to produce a broad probe spectrum.

These beams were then focused in the sample space with the probe spot size the smallest so as to detect the signal of the maximum population of excited molecules. The dump/repump pulse was more weakly focused than the pump to have the maximum effect as well. The mutual polarizations of the pump and probe were set to the magic angle of 54.7^o to mitigate the effect of solvation dynamics. In multipulse experiments, the dump/repump beam was set to the same polarization as the pump beam in order to affect the maximum population of molecules pumped a few picoseconds before.

1.4   Analysis of Time-Resolved Spectra

When analyzing transient spectra, it is important to remember that the signal observed is not a direct observation of excited state dynamics, as discussed in section 1.2. In fact, the signal is a result of an ensemble of observed molecules within a volume V which may undergo conformational change, ionization, or a myriad of other possible processes besides excited state decay. Therefore, the term "species" is used to describe some evolving feature in the transient data which may represent any of the above processes. The formalism for chemical reactions can be used to quantify the transience of these species in terms of concentrations and rates, though not directly. For, the difference of absorption signal for species ℓ is actually proportional to the concentration in accordance with Beer's Law:

$$\Delta A_\ell(\lambda, t) = \frac{\varepsilon_\ell L}{V} \left(C_{\ell,exc}(\lambda, t) - C_{\ell,0}(\lambda) \right) \tag{1.13}$$

where L is the beam path length through the sample, $C_{\ell,exc}$ and $C_{\ell,0}$ represent the concentrations of species ℓ when the molecules are excited and not excited, and ε_ℓ is the extinction coefficient of that species. Since the extinction coefficients are often difficult to obtain, ΔA is represented in arbitrary units (a.u.); whereas, the signal strength may be, in any case, represented in terms of optical density (OD).

The difference of absorption spectra retrieved from global and target analyses of time-resolved data do not always represent all the species in the sample. More often than not, when exploring new systems, the correct model is not known. However, these analyses are used as a tool to simplify our understanding of the dynamics, specifically to see trends in the data which are otherwise observable by simply looking at large sets of data.

1.4.1   Global Analysis

When performing global analysis, the system dynamics over all time and a broad spectrum of wavelengths are considered; whereby parameters, such

as lifetime, can be shared across a spectral band. For all time-resolved measurements presented in this thesis, the entire set of data for a pump-probe experiment is represented as a set of difference of absorption measurements $\{\Delta a_i \lambda, \}$ across a spectral range $[\lambda_0, \lambda_n]$ at consecutive times $\{t_i\}$. Overall, the empirical sample response is described in time and wavelength as $\Delta A(\lambda, t)$. However, for global analysis a set of m measurements is best presented as a matrix whose rows make up the set of the individual difference spectra measured at precise delay times

$$\{\Delta a_0(\lambda_0, ..., \lambda_n; t_1), ..., \Delta a_m(\lambda_0, ..., \lambda_n; t_m)\} \rightarrow \mathbb{A}_{mn}. \tag{1.14}$$

Matrix $\mathbb{A}$ represented in Figure 1.13, therefore, represents the full data set of $\Delta A(t)$, as in Equation 1.12, for all times. This signal, however, is comprised not only of the desired time evolution of the sample response after excitation, as well as any other intentional time-dependent manipulations upon the sample, but noise, scattering, chirp, and undesirable non-linear effects such as cross-phase modulation.[145]

    Plotting the kinetic traces (rows of $\mathbb{A}$) and spectra (columns of $\mathbb{A}$) give some information about local trends in the data; however, it is difficult to determine connections between certain trends and deduce what species are present from the raw data. Results from global analysis over the entire data set provide a snapshot of these spectro-temporal trends. The intention is to get a simplified picture which represents the whole data set—the various evolution or decay trends in the system. This is achieved by fitting to $\mathbb{A}$ a global spectrum $\psi(t, \lambda)$ according to some model to observe trends in the data: either sequential or parallel.

    For simplicity, the global spectrum $\psi(t, \lambda)$ can be treated as a first-order representation of decay kinetics. The amplitude of the difference spectra $\alpha_\ell(\lambda)$ representing a component indicated by the symbol ℓ, can be weighted by concentration $C_\ell(t)$ which, in turn, signifies the time evolution of that component. Thus, the separable representation of this total ideal data set can be represented as

$$\psi(\lambda, t) = \sum_{\ell=1}^{S_n} C_\ell(t)\alpha_\ell(\lambda) \tag{1.15}$$
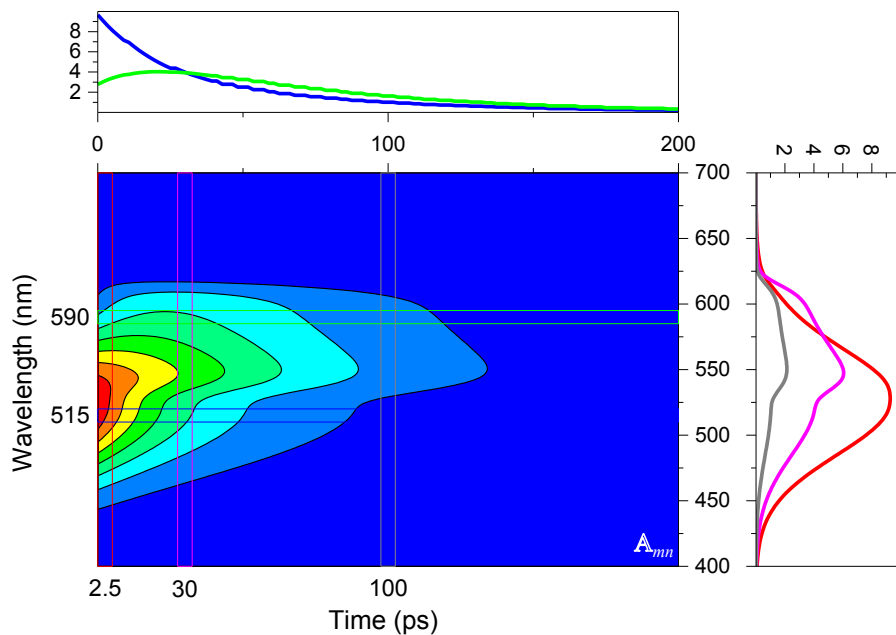
FIGURE 1.13: A 2D map of a synthesized data set.

where S_n is the number of components, in the model.[146] The most simple trends would be observed if each concentration were to decay independently, and the concentration would evolve as

$$C_\ell(t) = e^{-k_\ell t} \tag{1.16}$$

where k_ℓ represents the decay rate of component ℓ and is related to its lifetime $\tau = k_\ell^{-1}$.

A more general representation for these trends, however, may be represented in terms of the amount of a species, n_ℓ, which is proportional to concentration as $C_\ell = n_\ell / V$. The global kinetics for species, in the general case, are comprised of solutions of a set of rate equations

$$\left\{ \frac{dn_\ell}{dt} = \sum_{i}^{S_n} K_{\ell i} n_i \right\} \tag{1.17}$$

where n represents the population of species ℓ and $K_{\ell i}$ is the matrix of population transfer rates between that species and other species i. In a multipulse experiment, this general expression of the rate equation would include a brief excitation pulse $I_p(t)$, usually defined by a Gaussian profile, and a second pulse, $I_m(t)$:

$$\frac{dn_\ell}{dt} = \sum_i^{S_n} \left(A_{\ell i} I_p(t) + K_{\ell i} + B_{\ell i} I_m(t) \right) n_i. \tag{1.18}$$

The coefficients $A_{\ell i}$ and $B_{\ell i}$ reflect the magnitude of an affected transition by the pump and second pulses, respectively.

When the observed system is considered to be an homogeneous ensemble, this general expression offers global analysis a set of discrete, mathematical parameters to describe the system. Consider the synthesized data set in Figure 1.13. Two types of global fits were performed on this set: a sequential scheme and a parallel scheme from time 0 ps. These schemes do not necessarily represent species within the sample, but may highlight transient trends in the data.

The progression of the system over all time is best represented by the Evolution-Associated Difference Spectra (EADS), as in Figure 1.14 (top). This analysis uses a sequential scheme as its model to summarize the evolution of the system in time. The word "difference" implies that the data is obtained from a difference of absorption measurement, ΔA. EADS are most useful for revealing changes in the systems like carotenoids whose excited states decay through sequential excited state and vibrational levels. For light harvesting systems, EADS may reveal energy transfer if a loss in one spectral band coincides with a gain in another region of the spectrum. In the synthetic data set, the EADS reveal one spectral form morphing into another over time.

The parallel scheme also is depicted in Figure 1.14 (bottom). These spectra are called the Decay-Associated Difference Spectra (DADS), and they represent non-interacting components, and generally are less informative than EADS. Nonetheless, they are especially useful for describing processes induced by abrupt changes such as a dump pulse. The analysis of the synthetic data reveals a picture of only the abrupt initial stage in the data, and overemphasizes the magnitude of the concentrations because the scheme assumes the

parallel decay applies for the whole data set.

1.4.2 Target Analysis
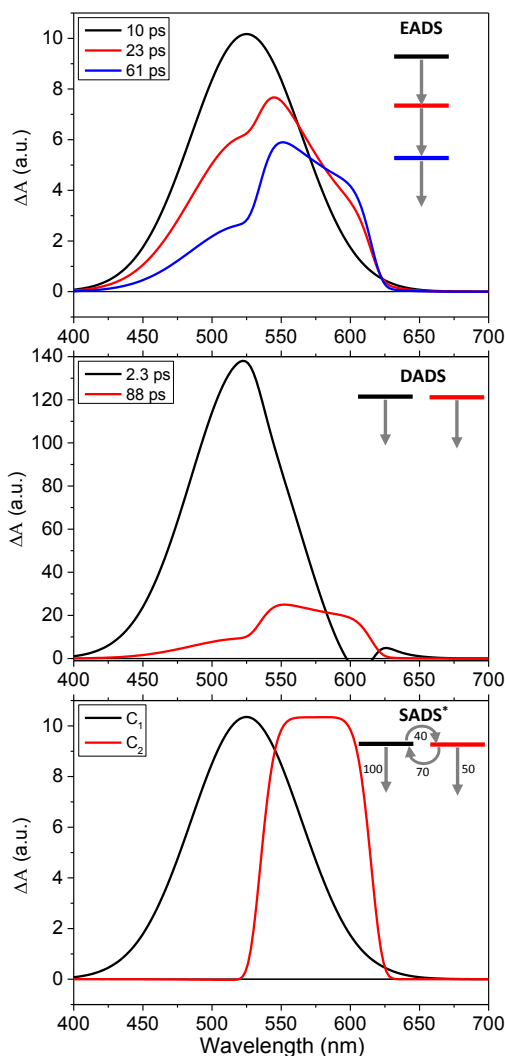
FIGURE 1.14: Sequential (EADS), parallel (DADS), and target (SADS) analyses of the synthetic data set in Fig. 1.13

Though informative, these global analyses rarely are accurate representations of the species' true spectra because the analysis is applied across the whole spectrum; whereas, the spectra of species often overlap. The attempt to apply a connection scheme among the species in the sample is called target analysis, and if the model is accurate, the resulting spectra are called the Species-Associated Decay Spectra (SADS). The SADS in Figure 1.14 (bottom) reveal the components which form the data set. In this fit, the mathematical parameters very closely follow the actual physical parameters. With actual data sets, target analysis is challenging in that increasing the number of mathematical parameters in the connectivity scheme allows for greater freedom when fitting. This results in a greater possible number of solutions which are physically inaccurate.

When multiple models produce the same fitting results, the system is considered structurally unidentifiable and target analysis cannot contribute useful information about the system. Therefore, the goal, or target, of

the analysis is to produce a model with reasonable spectral and kinetic qualities which are structurally identifiable. Identifiability has to do with whether the experiment, for which the data is analyzed, allows for the number of parameters to be determined or distinguish between models.[147,148] For a pump-probe experiment, target analysis may be sufficient for uncoupled species, but pump-probe experiments will not be able to distinguish coupled systems such as fucoxanthin, whose S_1 and ICT states are coupled. For this reason, the pump-dump-probe method was selected in the studies of fucoxanthin in this thesis to perturb these coupled states, to obtain information regarding their coupling, and apply target analysis to a model with distinct states.

1.4.3 Accounting for Chirp and IRF

The short pulses used in this experiment induce chirp and various non-linear effects within the sample which must be accounted for. The term "non-linear" is derived from the fact that high intensity light interacting with a material causes a non-linear dependence in the index of refraction and, thus, polarization density. Due to non-linear effects, various aberrations in the sample response signal comprising $\mathbb{A}_{mn}$ can be observed. Artifacts due to coherent light interactions, such as cross-phase modulation, will contribute to discrepancies in data analysis if not corrected.

FIGURE 1.15: A downchirped 100 fs pulse.

In time-resolved spectroscopy, frequency modulation, simply called chirp, is unavoidable. Light pulses with any spectral bandwidth are affected by the optics with which it interacts simply based upon the fact that the speed of light is varies with wavelength. The chirp of a narrow-banded excitation pulse is not much concern for the experiments presented; however, the probe pulse, consisting of a supercontinuum of wavelengths, greatly affects the data.
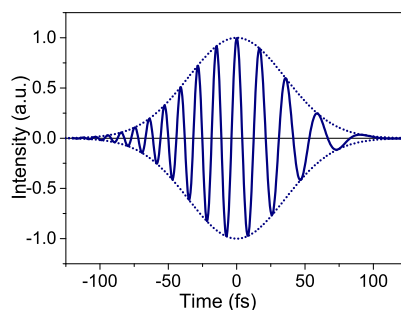
Upon supercontiuum generation, a pulse, or traveling packet of photons, is dispersed according to wavelength with the high energy photons toward the front as in Figure 1.15. In pump-probe measurements, as the probe is scanned past the time of excitation, the events in the blue appear to be measured before events at longer wavelengths. Therefore, before analyzing the difference of absorption signal, the data is corrected according to what time the excitation is observed. The shape of this dispersion curve $\mu(\lambda)$ is typically fit to a higher order polynomial centered about some central wavelength λ_c. Thus, all points on this curve are reassigned to $t = 0$, and the following time points are adjusted accordingly by interpolation.

FIGURE 1.16: IRF applied across the observed spectral bandwidth at time $t = 0$. The non-linear μ is due to chirp.

One must also consider how the excited system interacts with the probe pulse. Due to the probe pulse width and the delay profile of the sample's excitation response, the true signal is convoluted into the Instrument Response Function (IRF). In other words, the IRF is a convolution of the excitation pulse and the observed system's response which is itself partly dependent upon the probe pulse width. For simplicity, it can be expressed as a Gaussian centered about $\mu(\lambda)$:

$$f(t) \sim \exp(-\log(2)(2(t - \mu(\lambda))/2\sigma)^2) \tag{1.19}$$

where 2σ is the full width at half maximum (FWHM) of the Gaussian.[146] Therefore, in the analysis, the IRF is applied to all times by the convolution $\oplus$. Using the separable representation in Equation 1.15, the true signal convoluted with the chirped IRF would be

$$\psi(\lambda, t) = \sum_{\ell=1}^{L} C_\ell(t) \alpha_\ell(\lambda) \oplus f(t). \tag{1.20}$$

Not only is it necessary that the chirped IRF be considered when analyzing; when transient data are compared, they must by chirp-corrected with the IRF

in mind. For the data presented in this thesis, the IRF is assumed to be Gaussian and FWHM lies typically between 110 and 150 fs.[149]

References

1. George Britton, Synnove Liaaen-Jensen, and Hanspeter Pfander. *Carotenoids: A Colorful History*. CaroteNature, Norway, 1st edition, 2017.

2. S. W. Russell and B. C. L. Weedon. The allenic ketone from grasshoppers. *Journal of the Chemical Society D: Chemical Communications*, 0(3):85, jan 1969.

3. Jocelyn Hudon and Alan H Brush. Identification of carotenoid pigments in birds. In Lester Packer B T Methods in Enzymology, editor, *Carotenoids Part A: Chemistry, Separation, Quantitation, and Antioxidation*, volume Volume 213, pages 312–321. Academic Press, 1992.

4. M. A. Lián-Cabello, J. Paniagua-Michel, and P. M. Hopkins. Bioactive roles of carotenoids and retinoids in crustaceans. *Aquaculture Nutrition*, 8(4):299–309, 2002.

5. Helena H Billsten, Prakash Bhosale, Alexander Yemelyanov, Paul S. Bernstein, and Tomás Polívka. Photophysical properties of xanthophylls in carotenoproteins from human retinas. *Photochemistry and photobiology*, 2003.

6. R Hemley and B E Kohler. Electronic structure of polyenes related to the visual chromophore. A simple model for the observed band shapes. *Biophysical journal*, 20(3):377–82, dec 1977.

7. G. J. Handelman, E. A. Dratz, C. C. Reay, and F. J G M Van Kuijk. Carotenoids in the human macula and whole retina. *Investigative Ophthalmology and Visual Science*, 29(6):850–855, 1988.

8. Ramamoorthy Siva. Plant dyes. In *Industrial Crops and Uses*, pages 349–357. 2010.

9. Ramamoorthy Siva. Status of natural dyes and dye-yielding plants in India. *Current Science*, 92(7):916–925, 2015.

10. Saunders. Lipochrome. In *Dorland's Medical Dictionary for Health Consumers*. Elsevier, 2007.

11. Richard Willstätter and Walter Mieg. Untersuchungen über Chlorophyll; IV. Ueber die gelben Begleiter des Chlorophylls. *Justus Liebig's Annalen der Chemie*, 355(1):1–28, 1907.

12. Paul Karrer. The Chemistry of Vitamins A and C. *Chemical Reviews*, 14:17–30, 1933.

13. Richard Willstätter and Harold J. Page. Untersuchungen über Chlorophyll. XXIV. Über die Pigmente der Braunalgen. *Justus Liebig's Annalen der Chemie*, 404(3):237–271, 1914.

14. R. Bonnett, A. K. Mallams, A. A. Spark, J. L. Tee, B. C. L. Weedon, and A. McCormick. Carotenoids and related compounds. Part XX. Structure and reactions of fucoxanthin. *Journal of the Chemical Society C: Organic*, 0(3):429, jan 1969.

15. T. W. Goodwin. *The Comparative Biochemistry of the Carotenoids*. Chemical Publishing Co., Inc., New York, fiurst ame edition, 1934.

16. Harsha M Vaswani, Chao-Ping Hsu, Martin Head-Gordon, and Graham R Fleming. Quantum Chemical Evidence for an Intramolecular Charge-Transfer State in the Carotenoid Peridinin of PeridininChlorophyllProtein. *The Journal of Physical Chemistry B*, 107(31):7940–7946, jul 2003.

17. Tomáš Polívka, Donatas Zigmantas, Villy Sundström, Elena Formaggio, Gianfelice Cinque, and Roberto Bassi. Carotenoid S1 State in a Recombinant Light-Harvesting Complex of Photosystem II. *Biochemistry*, 41(2):439–450, dec 2002.

18. Robert J Thrash, Howard L B Fang, and George E Leroi. The Raman Excitation Profile Spectrum of Beta-Carotene in the Preresonance region: Evidence for a Low-Lying State. *The Journal of Chemical Physics*, 67(12), 1977.

19. Dariusz M Niedzwiedzki, James O Sullivan, Tomás Polívka, Robert R
    Birge, and Harry a Frank. Femtosecond time-resolved transient absorp-
    tion spectroscopy of xanthophylls. *The journal of physical chemistry. B*,
    110(45):22872–22885, 2006.

20. Robert E Blankenship. *Molecular mechanisms of photosynthesis*. John Wiley
    & Sons, 1st edition, 2008.

21. David L. Spector, editor. *Dinoflagellates*. Academic Press, Inc., Orlando,
    1984.

22. Tomas Polivka and Villy Sundstrom. Ultrafast dynamics of carotenoid
    excited States-from solution to natural and artificial systems. *Chemical
    reviews*, 104(4):2021–71, apr 2004.

23. C J Gobler, D J Lonsdale, and G L Boyer. Aureococcus anophagefferens.
    Estuaries, 28(5):726–749, 2005.

24. Radek Kaňa, Eva Kotabová, Roman Sobotka, and Ondřej Prášil. Non-
    photochemical quenching in cryptophyte alga Rhodomonas salina is lo-
    cated in chlorophyll a/c antennae. *PLoS ONE*, 7(1), 2012.

25. A V Rao and S Agarwal. Role of Lycopene as antioxidant carotenoid
    in the prevention of chronic diseases: a Review. *Nutrition Research*,
    19(2):305–323, 1999.

26. E. Giovannucci, E Rimm, Y Liu, M Stampfer, and W Willett. A Prospec-
    tive Study of Tomato Products, Lycopene, and Prostate Cancer Risk.
    Journal of the national Cancer Institute, 94(5):391–398, 2002.

27. Shan Lu and Li Li. Carotenoid metabolism: Biosynthesis, regulation,
    and beyond. *Journal of Integrative Plant Biology*, 50(7):778–785, 2008.

28. Michael Dambek, Ulrike Eilers, Jürgen Breitenbach, Sabine Steiger,
    Claudia Büchel, and Gerhard Sandmann. Biosynthesis of fucoxanthin
    and diadinoxanthin and function of initial pathway genes in Phaeo-
    dactylum tricornutum. *Journal of Experimental Botany*, 63(15):5607–5612,
    2012.

29. Miguel Olaizola, Julie La Roche, Zbigniew Kolber, and Paul G. Falkowski. Non-photochemical fluorescence quenching and the diadinoxanthin cycle in a marine diatom. *Photosynthesis Research*, 41(2):357–370, 1994.

30. Luca Dall'Osto, Chiara Lico, Jean Alric, Giovanni Giuliano, Michel Havaux, and Roberto Bassi. Lutein is needed for efficient chlorophyll triplet quenching in the major LHCII antenna complex of higher plants and effective photoprotection in vivo under strong light. *BMC plant biology*, 6(1):32, jan 2006.

31. James A Bautista, Robert E Connors, B Bangar Raju, Roger G Hiller, Frank P Sharples, David Gosztola, Michael R Wasielewski, and Harry A Frank. Excited State Properties of Peridinin: Observation of a Solvent Dependence of the Lowest Excited Singlet State Lifetime and Spectral Behavior Unique among Carotenoids. *The Journal of Physical Chemistry B*, 103(41):8751–8758, sep 1999.

32. Roberta Croce and Herbert van Amerongen. Natural strategies for photosynthetic light harvesting. *Nature chemical biology*, 10(7):492–501, jun 2014.

33. Herbert J. Dutton, Winston M. Manning, and B. M. Duggar. Chlorophyll Fluorescence and energy Transfer in the Diatom Nitzschia Closterium. 308(4):308–313, 1942.

34. Harry A. Frank and Richard J. Cogdell. Carotenoids in Photosynthesis. *Photochemistry and Photobiology*, 63(3):257–264, mar 1996.

35. Václav Šlouf, Valentyna Kuznetsova, Marcel Fuciman, Céline Bourcier de Carbon, Adjélé Wilson, Diana Kirilovsky, and Tomáš Polívka. Ultrafast spectroscopy tracks carotenoid configurations in the orange and red carotenoid proteins from cyanobacteria. *Photosynthesis Research*, 131(1):105–117, 2017.

36. Marcel Fuciman, Gürkan Keşan, Amy M. LaFountain, Harry A. Frank, and Tomáš Polívka. Tuning the Spectroscopic Properties of Aryl

Carotenoids by Slight Changes in Structure. *The Journal of Physical Chemistry B*, 119(4):1457–1467, jan 2015.

37. Hristina Staleva, Josef Komenda, Mahendra K Shukla, Václav Šlouf, Radek Kaňa, Tomáš Polívka, and Roman Sobotka. Mechanism of photoprotection in the cyanobacterial ancestor of plant antenna proteins. *Nature Chemical Biology*, in press:1–5, 2015.

38. Leszek Fiedor, Heriyanto, Joanna Fiedor, and Mariusz Pilch. Effects of Molecular Symmetry on the Electronic Transitions in Carotenoids. *The Journal of Physical Chemistry Letters*, (May):1821–1829, 2016.

39. Paul Tavan and Klaus Schulten. Electronic excitations in finite and infinite polyenes. *Physical Review B*, 36(8):4337–4358, 1987.

40. Donatella Carbonera, Marilena Di Valentin, Riccardo Spezia, and Alberto Mezzetti. The Unique Photophysical Properties of the Peridinin-Chlorophyll-a-Protein. *Current Protein and Peptide Science*, 15:332–350, 2014.

41. Harry A Frank, James A Bautista, Jesusa Josue, Zeus Pendon, Roger G Hiller, Frank P Sharples, David Gosztola, and Michael R Wasielewski. Effect of the Solvent Environment on the Spectroscopic Properties and Dynamics of the Lowest Excited States of Carotenoids. *The Journal of Physical Chemistry B*, 104(18):4569–4577, apr 2000.

42. Donatas Zigmantas, Tomáš Polívka, Roger G Hiller, Arkady Yartsev, and Villy Sundström. Spectroscopic and Dynamic Properties of the Peridinin Lowest Singlet Excited States. *The Journal of Physical Chemistry A*, 105(45):10296–10306, jun 2001.

43. Tomáš Polívka and Harry A. Frank. Molecular Factors Controlling Photosynthetic Light Harvesting by Carotenoids. 2010.

44. Rudolph Pariser. Theory of the Electronic Spectra and Structure of the Polyacenes and of Alternant Hydrocarbons. *The Journal of Chemical Physics*, 24(2):250–268, feb 1956.

45. Roberta Croce, Rienk van Grondelle, Herbert van Amerongen, and Ivo H. M. van Stokkum, editors. *Light Harvesting in Photosynthesis*. CRC Press, 1st edition, 2018.

46. Yasushi Koyama, Yoshinori Kakitani, Takeshi Miki, Rebecca Christiana, and Hiroyoshi Nagae. Excited-state dynamics of overlapped optically-allowed 1Bu+ and optically-forbidden 1Bu- or 3Ag- vibronic levels of carotenoids: Possible roles in the light-harvesting function. *Int. J. Mol. Sci.*, 59(11):1888–1929, 2010.

47. Ronald L Christensen, Mary Grace I Galinato, Emily F Chu, Jason N Howard, Richard D Broene, and Harry A Frank. Energies of Low-Lying Excited States of Linear Polyenes. *The Journal of Physical Chemistry A*, 112(49):12629–12636, dec 2008.

48. Rudi Berera, Ivo H M Van Stokkum, Gerdenis Kodis, Amy E. Keirstead, Smitha Pillai, Christian Herrero, Rodrigo E. Palacios, Mikas Vengris, Rienk Van Grondelle, Devens Gust, Thomas a. Moore, Ana L. Moore, and John T M Kennis. Energy transfer, excited-state deactivation, and exciplex formation in artificial caroteno-phthalocyanine light-harvesting antennas. *Journal of Physical Chemistry B*, 111:6868–6877, 2007.

49. Jian-Ping Zhang, Toru Inaba, Yasutaka Watanabe, and Yasushi Koyama. Partition of carotenoid-to-bacteriochlorophyll singlet-energy transfer through two channels in the LH2 complex from Rhodobacter sphaeroides G1C. *Chemical Physics Letters*, 340(5-6):484–492, jun 2001.

50. T Buckup, T Miki, M L Marek, and Marcus Motzkus. Direct observation of short-lived excited electronic states and their vibrational dynamics. In M Motzkus, editor, *Light Harvesting Processes*, number March, pages 8–12, Banz, Germany, 2015.

51. S L Bondarev and V N Knyukshto. Fluorescence from the S1(2 1Ag) state of all-trans-β-carotene. *Chemical Physics Letters*, 225(4–6):346–350, aug 1994.

52. Tomáš Polívka and Villy Sundström. Dark excited states of carotenoids: Consensus and controversy. *Chemical Physics Letters*, 477(1-3):1–11, jul 2009.

53. Hiroyoshi Nagae and Yasushi Koyama. Mechanism enabling the observation of the formally optically-forbidden and states in resonance-Raman excitation profiles of spheroidene in KBr disc. *Chemical Physics*, 373(1-2):145–152, jul 2010.

54. J a Bautista, R E Connors, B B Raju, R G Hiller, F P Sharples, D Gosztola, M R Wasielewski, and H. A. Frank. Excited state properties of peridinin: Observation of a solvent dependence of the lowest excited singlet state lifetime and spectral behavior unique among carotenoids. *Journal of Physical Chemistry B*, 103(41):8751–8758, 1999.

55. Hideki Hashimoto. Ultrafast Excited State Dynamics of Marine Carotenoid Fucoxanthin and its Homologues. In *Light Harvesting Processes*, Banz, Germany, 2015.

56. Kipras Redeckas, Vladislava Voiciuk, and Mikas Vengris. Investigation of the S1/ICT equilibrium in fucoxanthin by ultrafast pump–dump–probe and femtosecond stimulated Raman scattering spectroscopy. *Photosynthesis Research*, 2016.

57. Daniele Bovi, Alberto Mezzetti, Rodolphe Vuilleumier, Marie-Pierre Gaigeot, Bertrand Chazallon, Riccardo Spezia, and Leonardo Guidoni. Environmental effects on vibrational properties of carotenoids: experiments and calculations on peridinin. *Physical Chemistry Chemical Physics*, 13:20954, 2011.

58. Miriam M. Enriquez, Amy M. Lafountain, James Budarz, Marcel Fuciman, George N. Gibson, and Harry A. Frank. Direct determination of the excited state energies of the xanthophylls diadinoxanthin and diatoxanthin from Phaeodactylum tricornutum. *Chemical Physics Letters*, 493(4-6):353–357, 2010.

59. Donatas Zigmantas, Roger G Hiller, Arkady Yartsev, and Villy Sundstro. Dynamics of Excited States of the Carotenoid Peridinin in Polar Solvents : Dependence on Excitation Wavelength , Viscosity , and Temperature. *The Journal of Physical Chemistry B*, 107:5339–5348, 2003.

60. Miriam M Enriquez, Marcel Fuciman, Amy M Lafountain, Nicole L Wagner, R Robert, and Harry A Frank. The Intramolecular Charge Transfer State in Carbonyl- Containing Polyenes and Carotenoids. *Journal of physical Chemistry B*, 114(38):12416–12426, 2011.

61. Sumie Shima, Robielyn P Ilagan, Nathan Gillespie, Brandi J Sommer, Roger G Hiller, Frank P Sharples, Harry A Frank, and Robert R Birge. Two-Photon and Fluorescence Spectroscopy and the Effect of Environment on the Photochemical Properties of Peridinin in Solution and in the Peridinin-Chlorophyll-Protein from Amphidinium carterae. *The Journal of Physical Chemistry A*, 107(40):8052–8066, may 2003.

62. Patricia A Linden, Jörg Zimmermann, Tobias Brixner, Nancy E Holt, Harsha M Vaswani, Roger G Hiller, and Graham R Fleming. Transient Absorption Study of Peridinin and PeridininChlorophyll aProtein after Two-Photon Excitation. *The Journal of Physical Chemistry B*, 108(29):10340–10345, may 2004.

63. Lavanya Premvardhan, Daniel J. Sandberg, Holger Fey, Robert Birge, Claudia Büchel, and Rienk van Grondelle. The Charge-Transfer Properties of the S2 State of Fucoxanthin in Solution and in Fucoxanthin Chlorophyll-a/c2 Protein (FCP) Based on Stark Spectroscopy and Molecular-Orbital Theory. *J. Phys Chem B*, 112(37):11838–11853, 2008.

64. Emmanouil Papagiannakis, Delmar S Larsen, Ivo H M van Stokkum, Mikas Vengris, Roger G Hiller, and Rienk van Grondelle. Resolving the Excited State Equilibrium of Peridinin in Solution. *Biochemistry*, 43(49):15303–15309, nov 2004.

65. Daisuke Kosumi, Toshiyuki Kusumoto, Ritsuko Fujii, Mitsuru Sugisaki, Yoshiro Iinuma, Naohiro Oka, Yuki Takaesu, Tomonori Taira, Masahiko

Iha, Harry A. Frank, and Hideki Hashimoto. One- and two-photon pump-probe optical spectroscopic measurements reveal the S1 and intramolecular charge transfer states are distinct in fucoxanthin. *Chemical Physics Letters*, 483(1-3):95–100, 2009.

66. Donatas Zigmantas, Roger G. Hiller, Frank P. Sharples, Harry a. Frank, Villy Sundström, and Tomaš Polívka. Effect of a conjugated carbonyl group on the photophysical properties of carotenoids. *Physical Chemistry Chemical Physics*, 6(11):3009, 2004.

67. Roberto Bassi and Stefano Caffarri. Lhc proteins and the regulation of photosynthetic light harvesting function by xanthophylls. *Photosynthesis Research*, 64:243–256, 2000.

68. Massimo Crimi, Dieter Dorra, Carola S. Bösinger, Elisabetta Giuffra, Alfred R. Holzwarth, and Roberto Bassi. Time-resolved fluorescence analysis of the recombinant photosystem II antenna complex CP29: Effects of zeaxanthin, pH and phosphorylation. *European Journal of Biochemistry*, 268(2):260–267, 2001.

69. Krishna K. Niyogi and Thuy B. Truong. Evolution of flexible non-photochemical quenching mechanisms that regulate light harvesting in oxygenic photosynthesis. *Current Opinion in Plant Biology*, 16(3):307–314, 2013.

70. B P Krueger, S S Lampoura, I H van Stokkum, E Papagiannakis, J M Salverda, C C Gradinaru, D Rutkauskas, R G Hiller, and R van Grondelle. Energy transfer in the peridinin chlorophyll-a protein of Amphidinium carterae studied by polarized transient absorption and target analysis. *Biophysical journal*, 80(6):2843–2855, 2001.

71. Donatas Zigmantas, Roger G Hiller, Villy Sundstrom, and Tomas Polivka. Carotenoid to chlorophyll energy transfer in the peridinin-chlorophyll-a-protein complex involves an intramolecular charge transfer state. *Proceedings of the National Academy of Sciences of the United States of America*, 99(26):16760–16765, 2002.

72. Kipras Redeckas, Vladislava Voiciuk, Donatas Zigmantas, Roger G. Hiller, and Mikas Vengris. Unveiling the excited state energy transfer pathways in peridinin-chlorophyll a-protein by ultrafast multi-pulse transient absorption spectroscopy. *Biochimica et Biophysica Acta - Bioenergetics*, 1858(4):297–307, 2017.

73. Marilena Di Valentin, Elena Meneghin, Laura Orian, Antonino Polimeno, Claudia Büchel, Enrico Salvadori, Christopher W.M. Kay, and Donatella Carbonera. Triplet-triplet energy transfer in fucoxanthin-chlorophyll protein from diatom Cyclotella meneghiniana: Insights into the structure of the complex. *Biochimica et Biophysica Acta - Bioenergetics*, 1827(10):1226–1234, 2013.

74. Emmanouil Papagiannakis, Ivo H M Van Stokkum, Holger Fey, Claudia Büchel, and Rienk Van Grondelle. Spectroscopic characterization of the excitation energy transfer in the fucoxanthin-chlorophyll protein of diatoms. *Photosynthesis Research*, 86(1-2):241–250, 2005.

75. Nina Gildenhoff, Sergiu Amarie, Kathi Gundermann, Anja Beer, Claudia Büchel, and Josef Wachtveitl. Oligomerization and pigmentation dependent excitation energy transfer in fucoxanthin-chlorophyll proteins. *Biochimica et Biophysica Acta - Bioenergetics*, 1797(5):543–549, 2010.

76. Andrius Gelzinis, Vytautas Butkus, Egidijus Songaila, Ramūnas Augulis, Andrew Gall, Claudia Büchel, Bruno Robert, Darius Abramavicius, Donatas Zigmantas, and Leonas Valkunas. Mapping energy transfer channels in fucoxanthin-chlorophyll protein complex. *Biochimica et biophysica acta*, 1847(2):241–7, 2015.

77. D Kosumi, M Kita, R Fujii, M Sugisaki, N Oka, Y Takaesu, T Taira, M Iha, and H Hashimoto. Excitation Energy-Transfer Dynamics of Brown Algal Photosynthetic Antennas. *The journal of physical chemistry letters*, 3(18):2659–64, sep 2012.

78. Andrius Gelzinis, Vytautas Butkus, Egidijus Songaila, Ramunas Augulis, Andrew Gall, Claudia Büchel, Bruno Robert, Darius Abramavicius, Donatas Zigmantas, and Leonas Valkunas. Mapping energy transfer channels in fucoxanthin-chlorophyll protein complex. *Biochimica et Biophysica Acta - Bioenergetics*, 1847(2):241–247, 2015.

79. Robert G. West, David Bína, Marcel Fuciman, Valentyna Kuznetsova, Radek Litvín, and Tomáš Polívka. Ultrafast multi-pulse transient absorption spectroscopy of fucoxanthin chlorophyll a protein from Phaeodactylum tricornutum. *Biochimica et Biophysica Acta (BBA) - Bioenergetics*, 1859(5):357–365, 2018.

80. Y Koyama and H Hashimoto. Spectroscopic studies of carotenoids in photosynthetic systems. In AndrewJ. Young and George Britton, editors, *Carotenoids in Photosynthesis SE - 9*, pages 327–408. Springer Netherlands, 1993.

81. Timothy H. Goldsmith, James S. Collins, and Sherry Licht. The cone oil droplets of avian retinas. *Vision Research*, 24(11):1661–1671, 1984.

82. Ronald L. Christensen, Michelle Goyette, Laurie Gallagher, Joanna Duncan, Beverly DeCoster, Johan Lugtenburg, Frans Jos Jansen, and Ineke van der Hoef. S 1 and S 2 States of Apo- and Diapocarotenes. *The Journal of Physical Chemistry A*, 103(14):2399–2407, apr 1999.

83. Ronald L Christensen and Bryan E Kohler. LOW RESOLUTION OPTICAL SPECTROSCOPY OF RETINYL POLYENES: LOW LYING ELECTRONIC LEVELS AND SPECTRAL BROADNESS*. *Photochemistry and Photobiology*, 18(4):293–301, oct 1973.

84. Per Ola Andersson, Sergei M. Bachilo, Rong-Liang Chen, and Tomas Gillbro. Solvent and Temperature Effects on Dual Fluorescence in a Series of Carotenes. Energy Gap Dependence of the Internal Conversion Rate. *The Journal of Physical Chemistry*, 99(44):16199–16209, nov 1995.

85. Harry A. Frank, Ruel Z. B. Desamero, Veeradej Chynwat, Ronald Gebhard, Ineke van der Hoef, Frans Jos Jansen, Johan Lugtenburg, David

Gosztola, and Michael R. Wasielewski. Spectroscopic Properties of Spheroidene Analogs Having Different Extents of π-Electron Conjugation. *The Journal of Physical Chemistry A*, 101(2):149–157, jan 1997.

86. Harry A. Frank, Jesusa S. Josue, James A. Bautista, Ineke van der Hoef, Frans Jos Jansen, Johan Lugtenburg, Gary Wiederrecht, and Ronald L. Christensen. Spectroscopic and Photochemical Properties of Open-Chain Carotenoids. *The Journal of Physical Chemistry B*, 106(8):2083–2092, feb 2002.

87. Michael Kasha. Characterization of electronic transitions in complex molecules. *Discussions of the Faraday Society*, 9:14, jan 1950.

88. Ritsuko Fujii, Tatsuya Ishikawa, Yasushi Koyama, Miwa Taguchi, Yoshie Isobe, Hiroyoshi Nagae, and Yasutaka Watanabe. Fluorescence Spectroscopy of All- trans -anhydrorhodovibrin and Spirilloxanthin: Detection of the 1B u - Fluorescence. *The Journal of Physical Chemistry A*, 105(22):5348–5355, jun 2001.

89. Kengo Onaka, Ritsuko Fujii, Hiroyoshi Nagae, Michitaka Kuki, Yasushi Koyama, and Yasutaka Watanabe. The state energy and the displacements of the potential minima of the 2Ag state in all-trans-β-carotene as determined by fluorescence spectroscopy. *Chemical Physics Letters*, 315(1-2):75–81, dec 1999.

90. William W Parson. *Modern Optical Spectroscopy*. Springer-Verlag, 1st studen edition, 2009.

91. Seiji Akimoto, Iwao Yamazaki, Takahiro Sakawa, and Mamoru Mimuro. Temperature Effects on Excitation Relaxation Dynamics of the Carotenoid β-Carotene and Its Analogue β-Apo-8'-carotenal, Probed by Femtosecond Fluorescence Spectroscopy. *The Journal of Physical Chemistry A*, 106(10):2237–2243, mar 2002.

92. Seiji Akimoto, Tomoko Yamazaki, Iwao Yamazaki, and Atsuhiro Osuka. Excitation relaxation of zinc and free-base porphyrin probed by femtosecond fluorescence spectroscopy. *Chemical Physics Letters*, 309(3-4):177–182, aug 1999.

93. Alisdair N Macpherson and Tomas Gillbro. Solvent Dependence of the Ultrafast S2 - S1 Internal Conversion Rate of Beta-Carotene. *J. Phys. Chem. A*, 5639(98):5049–5058, 1998.

94. Marilena Ricci, Stephen E. Bradforth, Ralph Jimenez, and Graham R. Fleming. Internal conversion and energy transfer dynamics of spheroidene in solution and in the LH-1 and LH-2 light-harvesting complexes. *Chemical Physics Letters*, 259(3-4):381–390, sep 1996.

95. Mamoru Mimuro, Umpei Nagashima, Shinichi Takaichi, Yoshinobu Nishimura, Iwao Yamazaki, and Tetzuya Katoh. Molecular structure and optical properties of carotenoids for the in vivo energy transfer function in the algal photosynthetic pigment system. *Biochimica et Biophysica Acta (BBA) - Bioenergetics*, 1098(2):271–274, jan 1992.

96. Mamoru Mimuro, Yoshinobu Nishimura, Shinichi Takaichi, Yumiko Yamano, Masayoshi Ito, Shin-ichi Nagaoka, Iwao Yamazaki, Tetzuya Katoh, and Umpei Nagashima. The effect of molecular structure on the relaxation processes of carotenoids containing a carbonyl group. *Chemical Physics Letters*, 213(5-6):576–580, oct 1993.

97. Nicole L. Wagner, Jordan A. Greco, Miriam M. Enriquez, Harry A. Frank, and Robert R. Birge. The nature of the intramolecular charge transfer state in Peridinin. *Biophysical Journal*, 104(6):1314–1325, 2013.

98. Jörg Zimmermann, Patricia a. Linden, Harsha M. Vaswani, Roger G. Hiller, and Graham R. Fleming. Two-photon excitation study of peridinin in benzene and in the peridinin chlorophyll a-protein (PCP). *Journal of Physical Chemistry B*, 106(Figure 1):9418–9423, 2002.

99. Hideki Hashimoto, Yuko Sugai, Chiasa Uragami, Alastair T. Gardiner, and Richard J. Cogdell. Natural and Artificial Light-Harvesting Systems Utilizing the Functions of Carotenoids. *Journal of Photochemistry and Photobiology C: Photochemistry Reviews*, 2015.

100. Emmanouil Papagiannakis, John T M Kennis, Ivo H M van Stokkum, Richard J Cogdell, and Rienk van Grondelle. An alternative carotenoid-to-bacteriochlorophyll energy transfer pathway in photosynthetic light harvesting. *Proceedings of the National Academy of Sciences of the United States of America*, 99(9):6017–22, apr 2002.

101. Warren F. Beck, Michael M. Bishop, Jerome D. Roscioli, Soumen Ghosh, and Harry A. Frank. Excited state conformational dynamics in carotenoids: Dark intermediates and excitation energy transfer. *Archives of Biochemistry and Biophysics*, 572:175–183, 2015.

102. C C Gradinaru, J T Kennis, E Papagiannakis, I H van Stokkum, R J Cogdell, G R Fleming, R a Niederman, and R van Grondelle. An unusual pathway of excitation energy deactivation in carotenoids: singlet-to-triplet conversion on an ultrafast timescale in a photosynthetic antenna. *Proceedings of the National Academy of Sciences of the United States of America*, 98(5):2364–9, feb 2001.

103. Wendel Wohlleben, Tiago Buckup, Hideki Hashimoto, Richard J. Cogdell, Jennifer L. Herek, and Marcus Motzkus. PumpDepleteProbe Spectroscopy and the Puzzle of Carotenoid Dark States. *The Journal of Physical Chemistry B*, 108(10):3320–3325, mar 2004.

104. Wendel Wohlleben, Tiago Buckup, Jennifer L Herek, Richard J Cogdell, and Marcus Motzkus. Multichannel carotenoid deactivation in photosynthetic light harvesting as identified by an evolutionary target analysis. *Biophysical journal*, 85(1):442–450, 2003.

105. Emmanouil Papagiannakis, Somes Kumar Das, Andrew Gall, Ivo H M van Stokkum, Bruno Robert, Rienk van Grondelle, Harry A Frank, and John T M Kennis. Light Harvesting by Carotenoids Incorporated into

the B850 Light-Harvesting Complex from Rhodobacter sphaeroides R-26.1: Excited-State Relaxation, Ultrafast Triplet Formation, and Energy Transfer to Bacteriochlorophyll. *The Journal of Physical Chemistry B*, 107(23):5642–5649, jun 2003.

106. Hong Cong, Dariusz M Niedzwiedzki, George N Gibson, and Harry A Frank. Ultrafast Time-Resolved Spectroscopy of Xanthophylls at Low Temperature. *The Journal of Physical Chemistry B*, 112(11):3558–3567, mar 2008.

107. Dariusz Niedzwiedzki, Jeremy F Koscielecki, Hong Cong, James O Sullivan, George N Gibson, Robert R Birge, and Harry A Frank. Ultrafast Dynamics and Excited State Spectra of Open-Chain Carotenoids at Room and Low Temperatures. *The Journal of Physical Chemistry B*, 111(21):5984–5998, may 2007.

108. Vytautas Jr. Balevičius, Darius Abramavicius, Tomáš Polívka, Arpa Galestian Pour, and Jürgen Hauer. A Unified Picture of S * in Carotenoids. *Journal of Physical chemistry Letters*, 7(August):3347–3352, 2016.

109. Tokutake Sashima, Hiroyoshi Nagae, Michitaka Kuki, and Yasushi Koyama. A new singlet-excited state of all-trans-spheroidene as detected by resonance-Raman excitation profiles. *Chemical Physics Letters*, 299(2):187–194, jan 1999.

110. Kentaro Furuichi, Tokutake Sashima, and Yasushi Koyama. The first detection of the 3Ag state in carotenoids using resonance-Raman excitation profiles. *Chemical Physics Letters*, 356(5-6):547–555, apr 2002.

111. G. Cerullo. Photosynthetic Light Harvesting by Carotenoids: Detection of an Intermediate Excited State. *Science*, 298(5602):2395–2398, 2002.

112. Ritsuko Fujii, Tatsuya Fujino, Toru Inaba, Hiroyoshi Nagae, and Yasushi Koyama. Internal conversion of 1Bu+ → 1Bu → 2Ag and fluorescence from the 1Bu state in all-trans-neurosporene as probed by

up-conversion spectroscopy. *Chemical Physics Letters*, 384(1-3):9–15, jan 2004.

113. Ferdy S Rondonuwu, Yasutaka Watanabe, Ritsuko Fujii, and Yasushi Koyama. A first detection of singlet to triplet conversion from the 11Bu to the 13Ag state and triplet internal conversion from the 13Ag to the 13Bu state in carotenoids: dependence on the conjugation length. *Chemical Physics Letters*, 376(3-4):292–301, jul 2003.

114. D. L. Dexter. A Theory of Sensitized Luminescence in Solids. *The Journal of Chemical Physics*, 21(5):836, 1953.

115. Pavel Chabera, Marcel Fuciman, Petr Hribek, and Tomas Polivka. Effect of carotenoid structure on excited-state dynamics of carbonyl carotenoids. *Physical Chemistry Chemical Physics*, 11(39):8795–8803, 2009.

116. Jörg Zimmermann, Patricia A. Linden, Harsha M. Vaswani, Roger G. Hiller, and Graham R. Fleming. Two-photon excitation study of peridinin in benzene and in the peridinin chlorophyll a-protein (PCP). *Journal of Physical Chemistry B*, 106(36):9418–9423, 2002.

117. Martin Kleinschmidt, Christel M Marian, Mirko Waletzke, and Stefan Grimme. Parallel multireference configuration interaction calculations on mini-beta-carotenes and beta-carotene. *The Journal of chemical physics*, 130(4):044708, jan 2009.

118. Marcel Fuciman, Pavel Chábera, Anita Zupcanová, Petr Hríbek, Juan B Arellano, Frantisek Vácha, Jakub Psencík, and Tomás Polívka. Excited state properties of aryl carotenoids. *Physical chemistry chemical physics : PCCP*, 12:3112–3120, 2010.

119. Gürkan Keşan, Milan Durchan, Josef Tichý, Babak Minofar, Valentyna Kuznetsova, Marcel Fuciman, Václav Šlouf, Cemal Parlak, and Tomáš Polívka. Different Response of Carbonyl Carotenoids to Solvent Proticity Helps to Estimate Structure of the Unknown Carotenoid from Chromera velia. *Journal of Physical Chemistry B*, 119(39):12653–12663, 2015.

120. Miriam M. Enriquez, Shohei Hananoki, Shinji Hasegawa, Takayuki Kajikawa, Shigeo Katsumura, Nicole L. Wagner, Robert R. Birge, and Harry A. Frank. Effect of molecular symmetry on the spectra and dynamics of the intramolecular charge transfer (ICT) state of peridinin. *Journal of Physical Chemistry B*, 116(35):10748–10756, 2012.

121. M J Rosker, M Dantus, and A H Zewail. Femtosecond Clocking of the Chemical-Bond. *Science*, 241(4870):1200–1202, 1988.

122. Leonas Valkunas, Darius Abramavicius, and Tomas Mancal. *Molecular Excitation Dynamics and Relaxation*. Wiley-VCH, Weinheim, 2013.

123. Veeradej Chynwat and Harry A. Frank. The application of the energy gap law to the S1 energies and dynamics of carotenoids. *Chemical Physics*, 194(2-3):237–244, 1995.

124. W. Fuß, Y. Haas, and S. Zilberg. Twin states and conical intersections in linear polyenes. *Chemical Physics*, 259(2-3):273–295, 2000.

125. Theodore Förster and O Sinanoglu. Modern quantum chemistry. In *Modern Quantum Chemistry*, page 93. Academic Press, New York, 1965.

126. Tihana Mirkovic, Evgeny E. Ostroumov, Jessica M. Anna, Rienk Van Grondelle, Gregory D. Scholes, Rienk Van Grondelle, Govindjee, and Gregory D. Scholes. Light Absorption and Energy Transfer in the Antenna Complexes of Photosynthetic Organisms. *Chemical Reviews*, 117:249–293, 2017.

127. R. M. Clegg. Fluorescence resonance energy transfer. *Current opinion in biotechnology*, 6(1):103–10, feb 1995.

128. Gregory D Scholes. Long-range resonance energy transfer in molecular systems. *Annual review of physical chemistry*, 54(18):57–87, jan 2003.

129. The Royal Borough of Kingston upon Thames. Eadweard Muybridge, 2018.

130. J R Lakowicz. *Principles of Fluorescence Spectroscopy*. Kluwer Academic/Plenum, 1999.

131. H-L Dai and R. W. Field. *Molecular Dynamics and Spectroscopy by Stimulated Emission Pumping*, volume 4 of *Advanced Series in Physical Chemistry*. World Scientific, jun 1995.

132. Ahmed H Zewail. *Femtochemistry: Ultrafast Dynamics of the Chemical Bond*, volume 3 of *World Scientific Series in 20th Century Chemistry*. World Scientific Publishing Company, sep 1994.

133. Douglas L. Smith. Coherent Thinking. *Journal of Chemical Information and Modeling*, LXII(4):5–17, 1999.

134. Martin Gruebele and Ahmed H. Zewail. Ultrafast Reaction Dynamics. *Physics Today*, 43(5):24–33, may 1990.

135. J. H. Glownia, J. A. Misewich, and P. P. Sorokin. Femtosecond transition-state absorption spectroscopy of Bi atoms produced by photodissociation of gaseous Bi2 molecules. *The Journal of Chemical Physics*, 92(6):3335–3339, mar 1990.

136. Delmar S. Larsen, Emmanouil Papagiannakis, Ivo H.M. van Stokkum, Mikas Vengris, John T.M. Kennis, and Rienk van Grondelle. Excited state dynamics of β-carotene explored with dispersed multi-pulse transient absorption. *Chemical Physics Letters*, 381(5-6):733–742, nov 2003.

137. Emmanouil Papagiannakis, Mikas Vengris, Delmar S Larsen, Ivo H M van Stokkum, Roger G Hiller, and Rienk van Grondelle. Use of ultrafast dispersed pump-dump-probe and pump-repump-probe spectroscopies to explore the light-induced dynamics of peridinin in solution. *The journal of physical chemistry. B*, 110(1):512–21, jan 2006.

138. John T M Kennis, Delmar S Larsen, Ivo H M van Stokkum, Mikas Vengris, Jasper J van Thor, and Rienk van Grondelle. Uncovering the hidden ground state of green fluorescent protein. *Proceedings of the National Academy of Sciences of the United States of America*, 101(52):17988–93, 2004.

139. Delmar S Larsen, Ivo H M van Stokkum, Mikas Vengris, Michael a van Der Horst, Frank L de Weerd, Klaas J Hellingwerf, and Rienk van Grondelle. Incoherent manipulation of the photoactive yellow protein photocycle with dispersed pump-dump-probe spectroscopy. *Biophysical journal*, 87(3):1858–72, sep 2004.

140. Tiago Buckup and Marcus Motzkus. Multidimensional time-resolved spectroscopy of vibrational coherence in biopolyenes. *Annual review of physical chemistry*, 65:39–57, 2014.

141. S L Logunov, V V Volkov, M Braun, and M a El-Sayed. The relaxation dynamics of the excited electronic states of retinal in bacteriorhodopsin by two-pump-probe femtosecond studies. *Proceedings of the National Academy of Sciences of the United States of America*, 98(15):8475–8479, 2001.

142. Pascale Changenet-Barret, Christin T. Choma, Edward F. Gooding, William F. DeGrado, and Robin M. Hochstrasser. Ultrafast Dielectric Response of Proteins from Dynamics Stokes Shifting of Coumarin in Calmodulin. *The Journal of Physical Chemistry B*, 104(39):9322–9329, 2000.

143. G. Cerullo, C.J. Bardeen, Q. Wang, and C.V. Shank. High-power femtosecond chirped pulse excitation of molecules in solution. *Chemical Physics Letters*, 262(3-4):362–368, 1996.

144. A. Piskarkas, A. Stabinis, and A. Yankauskas. Phase phenomena in parametric generators and amplifiers of ultrashort light pulses. *In its USSR Report: Physics and Mathematics p 13 (SEE N88-15575 07-70) Transl. into ENGLISH from Uspekhi Fizicheskikh Nauk (Moscow, USSR), v. 150, no. 1, Sep. 1986 p 127-143*, 1987.

145. Bahaa E A Saleh and Malvin Carl Teich. Fundamentals of Photonics , 2nd Edition, 2007.

146. Ivo H.M. van Stokkum. Global and target analysis of time-resolved spectra, 2005.

147. S. Vajda and H. Rabitz. Identifiability and distinguishability of first-order reaction systems. *The Journal of Physical Chemistry*, 92(3):701–707, feb 1988.

148. Sandor Vajda and Herschel Rabitz. Identifiability and Distinguishability of General Reaction Systems. *The Journal of Physical Chemistry*, 98(20):5265–5271, may 1994.

149. Rudi Berera, Rienk van Grondelle, and John T M Kennis. Ultrafast transient absorption spectroscopy: principles and application to photosynthetic systems. *Photosynthesis research*, 101(2-3):105–18, 2009.

2 Research Chapter

2.1 Equilibrium Dynamics of S_1 and ICT States of Fucoxanthin in Solution as revealed by Multi-Pulse Spectroscopy: Dependence on Polarity, Proticity, and Temperature

This chapter is based on PAPER I:

West, R. G. et al. Equilibrium Dynamics of S_1 and ICT States of Fucoxanthin in Solution as revealed by Multi-Pulse Spectroscopy: Dependence on Polarity, Proticity, and Temperature. Submitted: May 2018.

Abstract

To demonstrate the value of the multi-pulse method in revealing the nature of coupling between excited states and explore the environmental dependencies of S_1 and ICT state equilibration, we performed ultrafast transient absorption pump-dump-probe and pump-repump-probe spectroscopies on fucoxanthin in various solvent conditions. The effects of polarity, proticity, and temperature were tested in solvents methanol at 293 and 190 K, acetonitrile, and isopropanol. We show that manipulation of the kinetic traces can produce one trace reflecting the equilibration kinetics of the states which reveals that lower polarity, proticity, and temperature delays S_1/ICT equilibration. Based upon a two-state model representing the S_1 and ICT states on the same S_1/ICT potential energy surface, we were able to show that the kinetics are strictly dependent on the initial relative populations of the states as well as the decay of the ICT state to the ground state. Informed by global analysis, a systematic method for target analysis based upon this model allowed us to quantify the population transfer rates throughout the life of the S_1/ICT state as well as separate the S_1 and ICT spectral signatures. The results are consistent with the concept that the S_1 and ICT states are part of one potential energy surface.

2.1.1 Introduction

The carotenoids' various roles in the scheme of photosynthesis are well understood, but the diverse methods and mechanisms by which they perform their duty in host organisms, especially in light-harvesting[1-3] and photoprotection,[4,5] still provide a flourishing field of study. All carotenoids share a conjugated polyene backbone scheme, and their spectroscopic properties that are directly related to diverse functions. These functions are determined, in part, by the number of conjugate C=C bonds,[6] N, which is well understood by the theory of the electronic energetic structure for polyenes.[7] Specifically, carotenoid photophysics has attracted much attention particularly due to its dark excited states. Due to strong correlations among the conjugated π-electrons, the lowest excited state has a significant doubly-excited character, rendering the transition between the ground (S_0) and the lowest excited singlet state (S_1) forbidden for single-photon processes[7] Nonetheless, the S_1 state has been shown to play the key role both in light-harvesting, serving as energy donor in a number of antenna proteins,[1] and in photoprotection, where it acts as a quencher of excited chlorophyll in some systems.[8-11]

The spectroscopic properties of both the strongly absorbing (S_2) state and the dark S_1 state are primarily determined by N, but significant tuning can be achieved by structural groups attached to the conjugated backbone as well as the environment which interacts with these groups. Such tuning is especially pronounced for carotenoids containing a conjugated keto group which are often referred to as carbonyl carotenoids.[12,13] Spectroscopic properties of carbonyl carotenoids depend on solvent polarity, which is related to an intramolecular charge transfer (ICT) state induced by the conjugated keto group.[13,14] With increasing polarity the typical signatures of the ICT state become more pronounced: the broad stimulated ICT emission found in the near-IR region (900-100 nm) and a corresponding ICT excited state absorption in the 600-750 nm spectral region appear in transient absorption spectra. The appearance of these features correlates with shortening of the S_1 lifetime.[13,14]

Interestingly, however, the lifetimes of the S_1 and ICT bands in transient absorption spectra are typically indistinguishable in global analysis schemes, leading to the concept of a coupled S_1/ICT state[14,15]. Since the first reported

polarity-dependent behavior in peridinin[12], the coupled behavior has been reported for a number of carbonyl carotenoids.[13,14,16−18] Although the conditions for which the ICT characteristics arise are known,[19−22] the observed behavior of the alleged ICT state has led to various, if not, incongruent conclusions about its nature and relation to the S_1 state[23−27]. In recent years, the ICT state has been considered to be 1) strongly coupled to the S_1 state and visualized as a potential minimum at S_1/ICT potential energy surface whereby the states are coherently mixed,[15,28] 2) a distinct electronic state,[12,24,25,29] or 3) even the S_1 state itself, albeit with enhanced charge transfer character.[30]

Due to its abundance in nature and the functional role of its ICT state in energy transfer within photosynthetic antenna proteins,[18,31,32] research has often centered on the characteristics of the carbonyl carotenoid fucoxanthin (Fx). In solution, fucoxanthin has well-resolved S_1-associated ($\sim$525 nm) and ICT-associated (600 and 640 nm) spectral bands in transient absorption spectra,[13] and the S_1/ICT lifetime spans the 20-60 ps range in various solvents,[13,19,23] making it a suitable candidate for systematic studies of polarity-dependent behavior. Moreover, contrary to other carbonyl carotenoids, fucoxanthin's properties also significantly depend on solvent proticity as evidenced by the S_1/ICT lifetimes in methanol (20 ps) and acetonitrile (30 ps). Yet, despite numerous studies on polarity-dependent excited-state dynamics of fucoxanthin in solut[33]ion,[33−38] the precise relation between the S_1 and ICT states has remained unclear. Even though a small difference between kinetics measured at the maxima of the S_1-associated and ICT-associated transitions were reported,[34,38] they are likely due to different fucoxanthin conformers whose ICT states have slightly different degrees of charge transfer character.[38]

A significant step forward in understanding the relation between the S_1 and ICT states was reported in a recent study by Redeckas, et. al.[39], who employed pump-dump-probe spectroscopy to fucoxanthin in methanol. In this experiment, adding a second excitation pulse to the standard pump-probe scheme allows selective manipulation of excited-state populations, making it possible to monitor excited-state dynamics hidden in the standard pump-probe experiment (PP).[15,25,39−42] The second excitation pulse was tuned to 960 nm, matching the maximum of the ICT stimulated emission, therefore,

selectively dumping a fraction of ICT population back to the ground state. This manipulation of the ICT population of fucoxanthin in methanol, demonstrated that prematurely removing some of the population of the ICT state does not instantaneously, nor equally, affect the population of the S_1 state. Instead, the ICT dumping leads to distortion of equilibrium between the S_1 and ICT states which is restored in less than 5 ps.[39] Thus, the S_1 and ICT states are two strongly-interacting states in equilibrium. It must be noted that similar experiment was carried out more than a decade ago by Papagiannakis et al.[15] for peridinin in methanol, but fixed wavelength of the dump pulse (800 nm) limited selectivity of the ICT dumping in that experiment.

The study presented here seeks to explore further this interaction between the S_1 and ICT states of fucoxanthin. We expand the experiments to other solvents and temperatures to explore polarity, proticity, and temperature dependence of the S_1/ICT state equilibration. By fitting and modeling the pump-dump-probe data, we show that the equilibration between the S_1 and ICT states is the key process leading to the identical lifetimes of the S_1-associated and ICT-associated bands measured in pump-probe experiments. In addition, we find that equilibration is the controlling factor for the observed polarity, proticity, and temperature dependence of the S_1/ICT lifetime of fucoxanthin in pump-probe experiments. In addition to experiments using the dumping of the ICT state, for fucoxanthin in methanol we also apply repumping of the ICT and S_1 states by tuning the second excitation pulse into the S_1-like or ICT-like excited state absorption bands.

2.1.2 Materials and Methods

Sample preparation – Analytical standard, all-trans fucoxanthin was obtained from Sigma-Aldrich and dissolved in methanol, acetonitrile, and isopropanol to 0.4 OD for 2 mm path length at 490 nm, the pump wavelength. This allowed for fucoxanthin to be tested in various environments: polar aprotic and two protic solvents of different polarity. The samples were maintained at room temperature during the measurements and stirred with a magnetic stir bar within a 2 mm path length quartz cuvette. Fucoxanthin in methanol, however, was also measured at 190 K in a plastic cuvette. Insignificant changes in

the steady-state spectra before and after the measurement affirmed the invari-
ability of the sample throughout the experiments.

Spectroscopy – The source of ultrafast pulses for time-resolved measurements
was a chirped-pulse regenerative amplification system (Spectra Physics,
Spitfire Ace) seeded by a mode-locked Ti:sapphire oscillator (MaiTai) and
pumped by a Nd-YLF Q-switched laser (Empower). The system was con-
figured to produce 100 fs, 4.2 mJ pulses centered at 800 nm at a repetition rate
of 1 kHz. Beam splitters directed the pulses through optical parametric ampli-
fiers (TOPAS Prime and TOPAS, Light Conversion) for tuning the pump and
dump/repump pulses, respectively, as well as a 3 mm sapphire plate for pro-
ducing a broadband, supercontinuum probe pulse which was then focused to
a 100 μm spot size at the sample space.

For room temperature measurements, pump pulses were tuned to a cen-
tral wavelength of 490 nm, resonant with the 0-0 transition to the S_2 state,
and focused to an approximately 200 μm spot size with a 70 nJ/pulse. The
dump pulse was tuned to 950 nm and focused to an approximately 350 μm
spot size at 380 nJ/pulse. With a delay line, the dump pulse was set to ar-
rive at the sample space about 1.7 seconds after the excitation pulse. Repump
pulses had similar focusing and timing as the dump pulse configuration and
were tuned to 535 nm and 640 nm for respective S_1 and ICT repumping. For
the repump measurements, pump power was about 25 nJ/pulse and repump
power was adjusted to no greater than 200 nJ/pulse. For the measurement
at 190 K, the focusing of all pulses remained the same as above though the
pump wavelength was set to 510 nm and the dump wavelength remained at
950 nm; their respective energies were about 30 nJ/pulse and 360 nJ/pulse.

The supercontinuum produced by the sapphire plate was divided by a
50/50 beam splitter into a reference and probe beams which passed through
the sample space; both were simultaneously directed onto the entrance slit of
a 600-groove grating spectrograph equipped with a double linear CCD de-
tection system (Pascher Instruments). To ensure the accuracy and quality of
the difference in absorption measurements (ΔA) the pump, dump, and probe
pulses incident in the sample space were selectively staggered by choppers
placed in the pump and dump beam paths, set at 500 Hz (pump) and 250 Hz

2.1. Equilibrium Dynamics of S_1 and ICT States of Fucoxanthin in Solution as revealed by Multi-Pulse Spectroscopy: Dependence on Polarity, Proticity, and Temperature

73

(dump, repump), respectively. The configuration allowed for observation of the pulses' influence on the sample within three regimes: pump-probe (PP), dump-probe (DP), and pump-dump-probe (PDP).

Data analysis – The data-collection system produces one data set for each pulse regime mentioned above, including a fourth data set with the dump-probe (DP) data subtracted from pump-dump-probe data (PDP = PDP' – DP). This pump-dump-probe (PDP) data set is the data set featured in the graphs and analysis below. All global and target analyses were performed in data analysis software (CarpetView, Light Conversion) which allows simultaneous fitting of PP and PDP data sets.

For evaluation of PP data, a sequential scheme was considered for the global analysis to obtain the Evolution-Associated Difference Spectra (EADS). Global analysis using a parallel scheme was also performed on the double-difference data set (PP-PDP) to obtain the Decay-Associated Difference Spectra (DADS) to elucidate the immediate effect of the dump pulse on the system. To explore the equilibrium dynamics of the system perturbed by the dump pulse, both PP and PDP data were chirp-corrected and truncated from 1.0 ps after excitation for target analysis, and a simple two-state connectivity scheme was applied.

For a more rigorous analysis of S_1 and ICT state kinetics, as described in the discussion section, a simple, two-state model was analytically defined and applied to the target analyses of S1-associated and ICT-associated species, informed by global analyses.

Absorption spectra of fucoxanthin in the three solvents used in this study are shown in Fig. 2.1. At room temperature (Fig. 2.1a), negligible shift in the vibronic bands was observed among the three solvents, and the typical broadening of the vibronic spectral structure in more polar solvents is apparent. Upon lowering temperature to 190 K (Fig. 2.1b), the absorption spectrum of fucoxanthin in methanol broadens, indicating that polarity-related features are enhanced at low temperature. The excitation wavelength was chosen such that mostly the 0-0 transition to the S_2 state was excited in order that any dynamics within the vibrational manifold of the S_2 state would not complicate the dynamics.

2.1.3   Results

Transient absorption spectra measured after excitation of fucoxanthin in acetonitrile at 490 nm in both PP and PDP regime are shown in Fig. 2.2a. Further, Fig. 2.2b demonstrates the effect of the dump pulse by showing the PP-PDP double difference spectra at selected times after applying the dump pulse. The transient absorption spectra of fucoxanthin in polar acetonitrile exhibit two positive features corresponding to the S_1-S_n transition, peaking at 535 nm and ICT-S_N transition in the 600-670 nm spectral region. When comparing the PP data set with the PDP data set, it is clear that within less than 1 ps after the dump, the dumping of the ICT state (640 nm band) appears to cause a comparable population drop

FIGURE 2.1: (a) Steady-state absorption spectra of Fx in various solvents, normalized to the pump peak maximum which was tuned to select only the 0-0 vibrational transition. (b) Steady-state absorption spectra of Fx in methanol at room temperature and 190 K.

also in the S_1 state (535 nm band), from which it does not recover throughout the decay lifetime (Fig. 2.2a). However, within picoseconds after the dump, the true nature of the relative effect on both states is clarified when the PDP spectra are subtracted from the PP spectra as in the double-difference spectra in Fig. 2.2b. These spectra more clearly reveal the equilibrium process
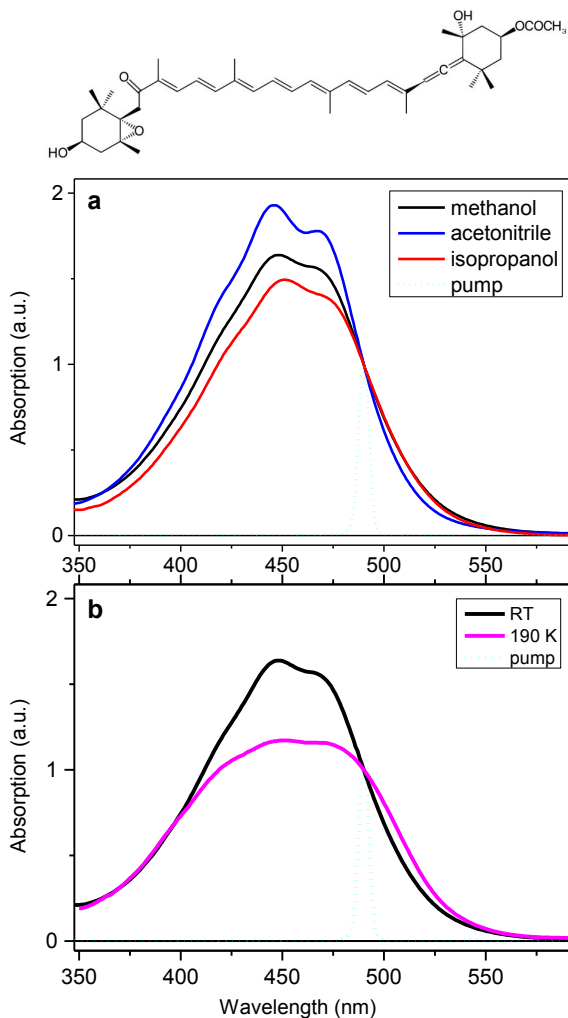
2.1. Equilibrium Dynamics of S_1 and ICT States of Fucoxanthin in Solution as revealed by Multi-Pulse Spectroscopy: Dependence on Polarity, Proticity, and Temperature

75

between the two states. In the first moments after dumping, the ICT band indicates a greater population displacement in proportion to the S_1 state as indicated by the double-difference spectrum at 0.7 ps after the dump. Over time, however, the ratio of the effect of the dump in the ICT band in relation to the S_1 band is decreased as shown by double-difference spectra at later times.

Fig. 2.3 compares the PP and PDP data sets of fucoxanthin in methanol, but also includes the effect of temperature on the transient spectra. At room temperature, the overall behavior is comparable to that observed in acetonitrile. At low temperature (190 K), however, there is a red shift of the entire spectrum: the S_1-S_n band has a maximum at 543 nm at 190 K and the same shift from room temperature of $\sim$8 nm occurs also for the ICT bands. As for the absorption spectrum in Fig. 2.1, no narrowing of the transient spectral bands is observed upon cooling to 190 K. Evidence of S_1/ICT coupling by ICT state dumping is still evident at 190 K. This is shown by the reduction of the S_1 state signal at 2.5 ps after excitation in Fig. 2.3a, and an equilibration process simi-

FIGURE 2.2: (a) PP (solid) and PDP (dotted) spectra of Fx in acetonitrile at various times after excitation. (b) The double-difference spectrum (PP–PDP) of Fx in acetonitrile. The underlined values indicate delay after the dump pulse.

lar to the room temperature measurement is also observed in the double-difference spectrum in Fig. 2.3b implying that an equilibration process is still present even at low temperature. The PP and PDP data sets measured for fucoxanthin in 2-propanol again give qualitatively similar behavior, as observed in acetonitrile and methanol, shown in the Supporting Information (Fig. 2.12).
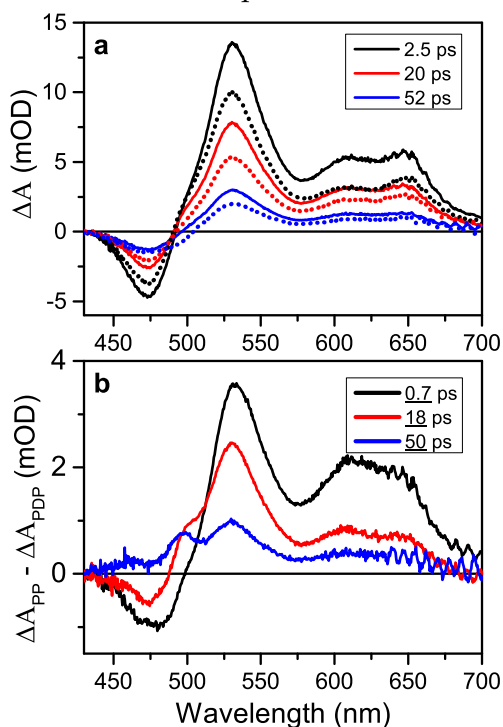
Despite a number of reports on excited-state dynamics of fucoxanthin,[21,22,34,37,38,43] it has never been measured at low temperature. Therefore, we show the results of global fitting the PP data on fucoxanthin in methanol at 190 K in Fig. 2.4 to provide basic characterization of excited-state processes at low temperature. As for the room temperature data (Fig. 2.13), four decay components are needed for a reasonable fit. Besides the first EADS which characterizes the decay of the initially excited S_2 state, all other decay components are slower at 190 K. Vibrational decay of the S_1/ICT state is about twice slower (470 fs) at 190 K, and the same is observed for the two components characterizing the decay of the S_1/ICT state that yield 13 and 47 ps at 190 K. This is again slower than 8 and 20 ps obtained at room temperature. We note that two S_1/ICT decay components are needed to fit transient data of

FIGURE 2.3: (a) Excited state spectra at 2.5 ps after excitation comparing Fx in methanol at room temperature (RT) and 190 K. The spectra of the pump-dump-probe regime is indicated by the dotted lines. (b) The double difference spectra (PP – PDP) demonstrating only the effect of the dump on Fx in methanol at three different times after the dump (underline indicates time after dump). The underlined values indicate delay after the dump pulse.

fucoxanthin exclusively in methanol, most likely due to multiple fucoxanthin conformations occurring in this solvent.[33,34,38,44] Interestingly, at 190 K the slow, 47 ps S_1/ICT decay component has significantly reduced ICT bands and blue-shifted bleaching (Fig. 2.4), suggesting that cooling the sample separates the different conformations better than at room temperature. The presence of different conformations is also the reason why there is no narrowing of
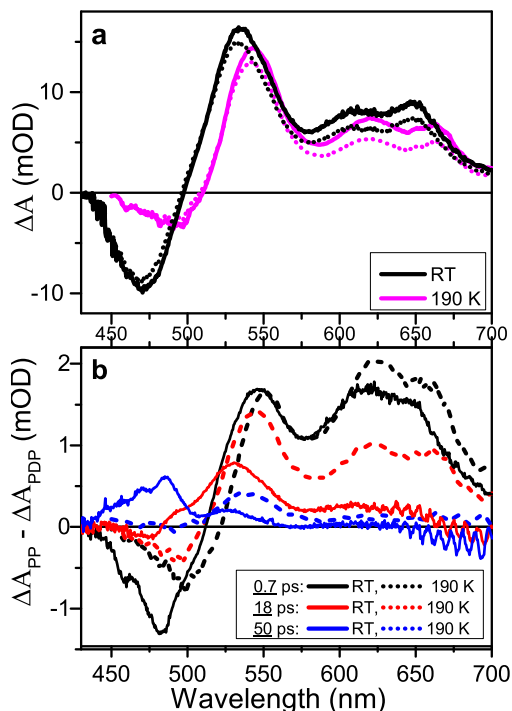
2.1. Equilibrium Dynamics of S_1 and ICT States of Fucoxanthin in
Solution as revealed by Multi-Pulse Spectroscopy: Dependence   77
on Polarity, Proticity, and Temperature

the spectral bands upon cooling. EADS resulting from global fitting the data measured at room temperature in all three solvents are shown in Supporting Information (Fig. 2.13). All time constants obtained from global fitting are summarized in Table 2.1.

TABLE 2.1: The decay rates for fucoxanthin in all solvent environments obtained from the EADS in order of appearance in the decay dynamics.

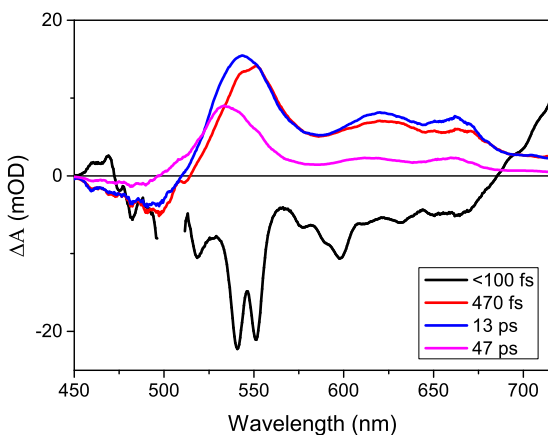| Rates^{-1} (ps)	methanol		acetonitrile	isopropanol
	RT	190 K		
EADS				
k_1^{-1}	0.10	<0.10	0.10	0.12
k_2^{-1}	0.19	0.47	0.34	0.28
k_3^{-1}	7.8	13	33	51
k_4^{-1}	19	47	--	--

FIGURE 2.4: EADS of fucoxanthin in methanol at 190 K.

Kinetics about the minimum of the bleaching (Fig. 2.5a) and in the S_1 (Fig. 2.5b) and ICT (Fig. 2.5c) band maxima for all solvents demonstrate the different lifetimes of the S_1/ICT state in different solvents: 19 ps, 33 ps and 51 ps in methanol, acetonitrile and 2-propanol (Table 2.1) as reported earlier.[13,19,33] Application of the dump immediately removes some of the ICT state population, subsequently decreases the S_1 band, and returns a certain population to the ground state as indicated by the reduction of ground state bleaching. However, by comparison of the PDP traces in Figs. 2.5b and 2.5c, different dynamics within the S_1 and ICT bands following the dump pulse are obvious. This difference reflects the equilibration between the S_1 and ICT states after selectively perturbing the ICT population by the 950
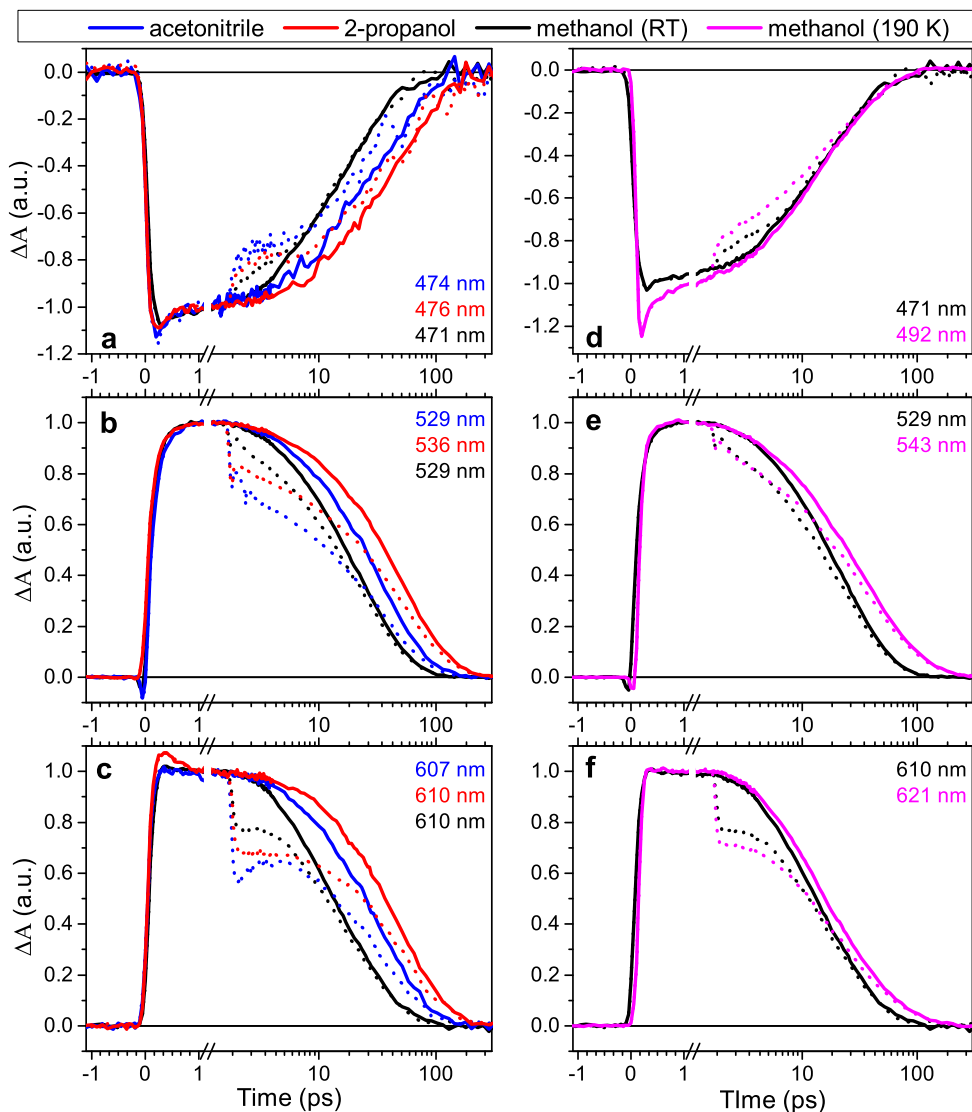
FIGURE 2.5: Kinetic traces of ground state bleaching minimum (a,d), S1 state maximum (b,d), and ICT state maximum (c,f) bands of fucoxanthin in three solvents: methanol at room temperature (black) and methanol at 190 K (magenta), acetonitrile (blue), and 2-propanol (red). Pump-probe traces are indicated by the solid lines and the pump-dump-probe traces are dotted. The numbers indicate the wavelength of the traces, ordered according to the legend. All traces are normalized to the signal magnitude just before the dump.

2.1. Equilibrium Dynamics of S_1 and ICT States of Fucoxanthin in
Solution as revealed by Multi-Pulse Spectroscopy: Dependence
on Polarity, Proticity, and Temperature   79

nm pulse.[39] The dump pulse also repumps a very small S_1 population, most
likely through the S_1-S_2 transition,[19] similar to that seen in our PDP study
of fucoxanthin in FCP,[45] indicated by the notch in the S_1-associated dump
traces in Fig. 2.5b. Oddly, the decay of the bleach of fucoxanthin at 490 nm
in methanol seems unaffected by temperature. However, the EADS shown in
Fig. 2.4 explain this, because the bleaching band associated with the longer,
47 ps component has negligible amplitude at 490 nm. The effect of the lower
temperature on dynamics of fucoxanthin in methanol is clearly seen by com-
paring the kinetic traces to those at room temperature as in Fig. 2.5e-f. Nor-
malized to the time just before dumping, the traces show how decay at 190 K
is slower for the S_1 and ICT bands, but the effect of the dump is comparable.

   To gain further insight into the excited-state dynamics, we have also car-
ried out experiments with repumping the S_1 and ICT transition by tuning
the second excitation (repump) pulse to 535 and 640 nm. The repump pulse
was applied at 1.7 and 2 ps for repumping the S_1 and ICT population, respec-
tively.The effect of selective repumping on the S_1 and ICT bands of fucoxan-
thin in acetonitrile at room temperature is shown in Fig. 2.6. Regardless of
which state is selected for repumping, the effect of a loss of population in the
coupled state is immediately seen. The population recovers quickly and dy-
namics of this fast recovery monitors return of the repumped population back
to its initial state. Interestingly, while the repumped S_1 population returns al-
most immediately, the slower component of the recovery is observed after ICT
repumping (Fig. 2.6). The same behavior is seen in methanol (Fig. 2.14).

   When simply looking at the traces of populations affected by the dump or
repump pulse it is clear that the perturbation does affect the S_1 and ICT bands
of the spectrum individually, and the system tends to return, or equilibrate,
to the condition of an unperturbed system, regardless of the environment.
However, the exact characteristics of the equilibration after perturbation are
more easily examined when the kinetics of the S_1 and ICT traces are com-
pared with respect to one another. One way to do this is to observe how
the kinetic of the ratio of the S_1-associated ESA band to the ICT-associated
band behaves.[38,45] In this way, the perturbation is seen clearly affecting the
S_1:ICT ratio, setting the system into an imbalanced condition from which the

system equilibrates toward the usually unperturbed trajectory (Fig. 2.7a).
Further still, in order to clearly
see how much the perturbation
specifically affects the equilibra-
tion among these two states,
the kinetic of the S_1:ICT ra-
tio itself may be compared in
the unperturbed and perturbed
conditions—that is, for exam-
ple, taking the ratio of the per-
turbed S_1:ICT ratio to that of
the unperturbed S_1:ICT ratio, de-
noted here as $(S_1 : ICT)_{PDP}$:
$(S_1 : ICT)_{PP}$. The traces of this
ratio of ratios, as seen in Fig.
2.7b, elucidate the pure dynam-
ics of equilibration of fucoxan-
thin in various environments.
The value of this manipulation
of the kinetic traces is substanti-
ated by the opposite effect of re-
pumping the S_1 state where the
imbalance is deviated in the op-

FIGURE 2.6: Kinetic traces of S_1 and ICT band
repumping compared to pump-probe traces
in the (a) S_1-associated band and the (b) ICT-
associated band of fucoxanthin in acetonitrile
(see Fig. 2.14 for methanol).

posite direction of the ICT dump or repump as in Fig. 2.7c (Fig. 2.15 for
methanol).

The pure equilibration dynamics shown in Fig. 2.7 reveal an inter-
esting behavior. Clearly, though polarity of the environment is a fac-
tor determining the rate of the $S_1 \rightleftharpoons ICT$ equilibration, in that the less po-
lar isopropanol takes longer to equilibrate than methanol by a certain de-
gree, it is not the only controlling factor. As for the S_1/ICT lifetime
of fucoxanthin, the equilibration is also affected by solvent proticity be-
cause in aprotic acetonitrile, the equilibration rate is notably faster than
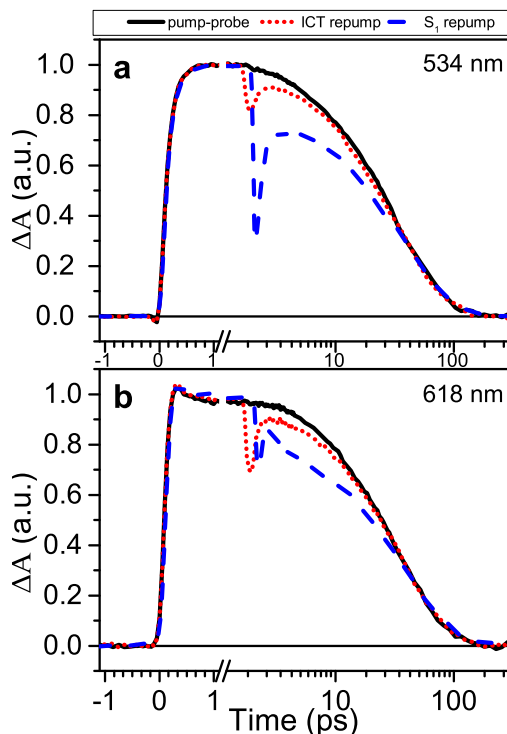in protic methanol even though both solvents have comparable polarity.

Interestingly, however, the effect of proticity on equilibration dynamics is opposite than on the S_1/ICT lifetime: while equilibration is faster in aprotic acetonitrile, the S_1/ICT lifetime is slower in acetonitrile than in methanol (Table 2.1). Lowering the temperature of the methanol, as generally expected, slows the rate of equilibration, similar to the behavior of Fucoxanthin-Chlorophyll *a* Protein (FCP) at 77 K, as reported in our previous study.[45]

As the ratio of perturbed and unperturbed S_1:ICT ratios reveals the nature of the equilibration in time, the Decay Associated Difference Spectra (DADS) of the data from unperturbed minus the perturbed systems reveal the spectrum of the equilibration. DADS provide valuable information regarding immediate, parallel processes induced by the dump such as the equilibration rate k_{eq}. Therefore, we fit globally the double-difference data (PP – PDP) obtained from experiments with dumping of

FIGURE 2.7: (a) The S_1 to ICT -associated band traces (S_1:ICT) in the PDP and PP regimes (PDP:PP). (b) The ratio of the S_1 to ICT -associated band traces (S_1:ICT) in the PDP regime to that of the PP regime (PDP:PP)—that is $(S_1:ICT)_{PDP}:(S_1:ICT)_{PP}$. (c) The same manipulation of the traces for the S_1 repump and the ICT repump in acetonitrile, compared to PDP (same graph for methanol in Fig. 2.15). Magnitude of all traces normalized to maximum.

the ICT state at 950 nm. These data contain solely information about the dynamics induced by the dump pulse, therefore fully and uniquely describing
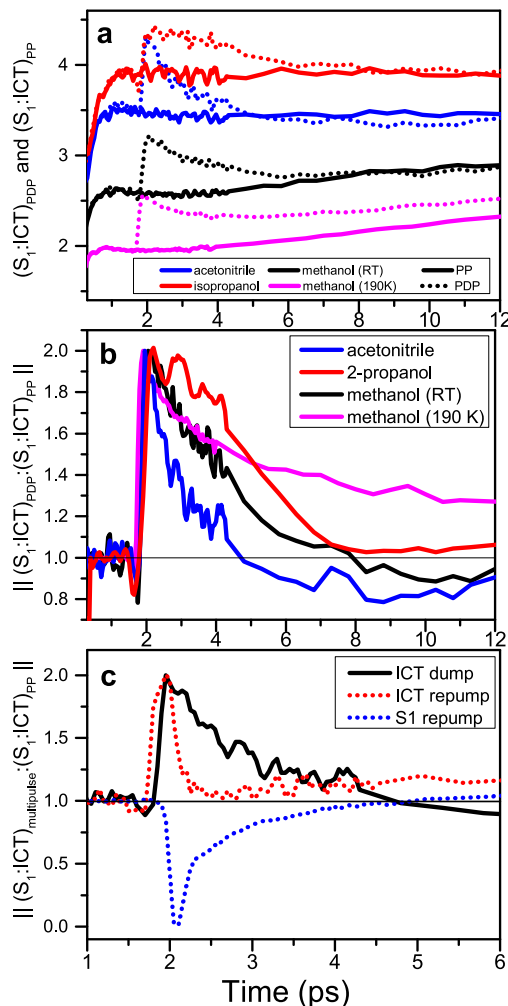
the equilibrium rate as well as the S_1/ICT decay rate. The S_1/ICT decay rate must appear in the double difference data because the 950 nm dump pulse sends a fraction of excited state population to the ground state. This missing fraction appears in the PP-PDP dataset as a kinetic process with the S_1/ICT decay lifetime.

The DADS obtained from the global fitting of the PP-PDP dataset of fucoxanthin in acetonitrile are shown in Fig. 2.8 (Fig. 2.16 for remaining solvents). The first DADS has a lifetime of 120 fs and is most likely associated with a fraction of the S_1 population that is repumped by the 950 nm pulse via the S_1-S_2 transition. Its lifetime thus reflects the S_2 relaxation. The second DADS has a lifetime of 1.3 ps and clearly reflects the equilibration component as it demonstrates the imbalance between the S_1 and ICT bands, which is recovered at rate k_{eq}. More importantly, the last component takes the same shape and has the same lifetime of 33 ps as the PP EADS, corresponding to the S_1/ICT lifetime. This decay rate we will further denote as the common decay rate k_{com}.
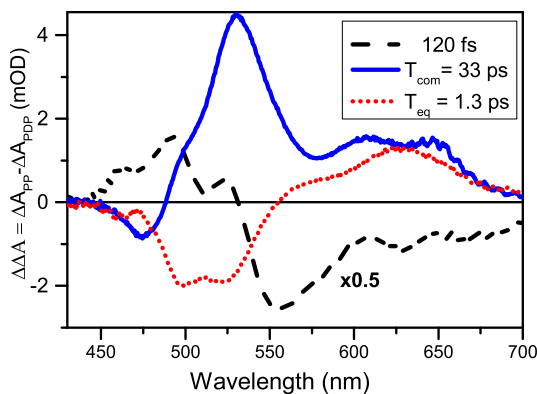

FIGURE 2.8: DADS of the double-difference spectrum (PP-PDP) of fucoxanthin in acetonitrile (results for other solvents in Fig. S5). The amplitude of the fast component was reduced by half.

2.1. *Equilibrium Dynamics of S_1 and ICT States of Fucoxanthin in Solution as revealed by Multi-Pulse Spectroscopy: Dependence on Polarity, Proticity, and Temperature*

83

TABLE 2.2: Rates and initial S_1 to ICT initial population ratios determined by global and target analysis of data sets truncated from 1 ps. Common and equilibrium rates for the target analyses, k_{com} and k_{eq}, were calculated using the four rates below the break.

Rates^{-1} (ps)	methanol		acetonitrile	isopropanol
	RT	190 K		
global analysis				
k_{com}^{-1}	19	41	33	51
k_{eq}^{-1}	3.5	12	1.3	8.3
target analysis				
k_{com}^{-1}	18	49	33	53
k_{eq}^{-1}	3.2	13	1	11
$k_{S_1 \rightarrow ICT}^{-1}$	6	60	2.0	33
$k_{ICT \rightarrow S_1}^{-1}$	10	40	2.0	25
$k_{S_1 \rightarrow S_0}^{-1}$	60	84	60	60
$k_{ICT \rightarrow S_0}^{-1}$	12	22	22	45
$\left(n_{S_1} / n_{ICT} \right)_0$	0.8	1.0	1.0	0.6

The general shape of the DADS is maintained for isopropanol, with, as expected, longer rates of 8.3 ps (equilibration) and 51 ps (common rate) (Fig. 2.16). In methanol at both 293 and 190K, the components have similar trends but appear much more complex. The intermediate EADS components of 7.8 ps (293 K) and 13 ps (190 K), respectively, cannot be obtained in DADS of PP - PDP. This underlines the complexity of the excited-state dynamics of fucoxanthin in methanol and identifies limits of using EADS for such systems, as discussed recently.[38] The absence of the intermediate decay component in the double-difference DADS also suggests that the 'true' common S_1/ICT lifetime of fucoxanthin in methanol is rather associated with the slowest EADS having time constants of 19 ps (293 K) and 41 ps (190 K). The common and equilibration rates from global analyses are summarized in the first two lines of Table 2.2.

2.1.4 Discussion

The data presented in the previous section demonstrate that the S_1 and ICT states can be selectively affected by the dump or repump pulse. As reported earlier for fucoxanthin in methanol,[39] the selective perturbation of the ICT population results in an imbalance of the equilibration between the ICT and S_1 states which eventually restores the original distribution of excited state population between the S_1 and ICT parts of the S_1/ICT potential energy surface. We also showed that by appropriate data treatment we can extract not only the common lifetime of the coupled S_1/ICT state, which is readily obtained from standard PP experiment, but also the $S_1 \rightleftharpoons ICT$ equilibration time from the DADS of the double-difference data set (PP – PDP). Both these rates, k_{com} and k_{eq}, exhibit dependence on solvent polarity and proticity as well as the temperature.
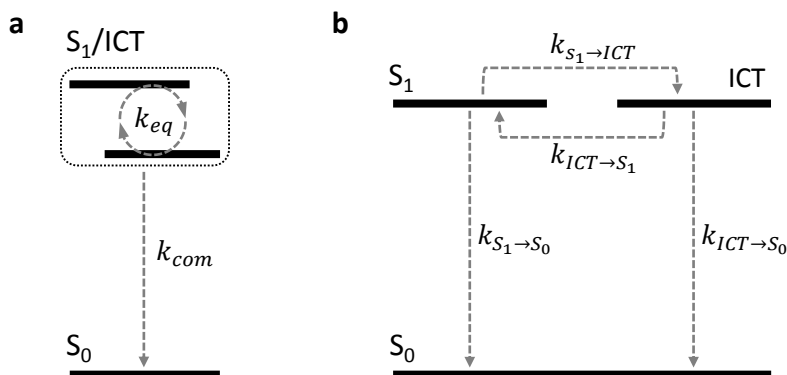

FIGURE 2.9: Diagram related to global and target analyses models of a two-state system of an excited carbonyl carotenoids from 1 ps after the dump, after all dynamics of higher states have taken place.

Since direct application of global and/or target analyses to the collected datasets did not provide a unique solution, we make use of the knowledge of k_{com} and k_{eq} obtained from the fitting and focus first on modeling the equilibrium kinetics of the S_1/ICT state in terms of population dynamics of a two-state system to reveal the properties of this elusive state in the simplest

2.1. Equilibrium Dynamics of S_1 and ICT States of Fucoxanthin in Solution as revealed by Multi-Pulse Spectroscopy: Dependence on Polarity, Proticity, and Temperature

85

way. By this basic two-state model, depicted in Fig. 2.9, we have also simplified our inquiry of the nature of the ICT state and have gained insight into what are reasonable rate parameters related to the S_1/ICT relaxation dynamics. Since the relaxation processes preceding the population of the $S_1 \rightleftharpoons ICT$ state are mostly over within the first picosecond after excitation (the S_2 decay, vibrational cooling of hot S_1 and ICT states),[15,34,46] we begin our analyses at a time when a two-state model would be the most relevant: less than a picosecond before the dump pulse, 1.0 ps after excitation of fucoxanthin into the S_2 state. We note that the ground state intermediate (GSI) seen in some other studies,[14,39,42] upon dumping the ICT state, is ignored in this model. Its spectral influence has been seen as a relatively small peak shifted to the blue of the maximum $S_1 S_N$ peak absorption wavelength. Nonetheless, we have found the two-state model to be fully sufficient to match the $S_1 \rightleftharpoons ICT$ equilibration kinetics without consideration of the GSI. Also, our model does not account for repumping due to any resonance with the $S_1 S_2$ transition caused by the 950 nm pulse, which is seen in the S_1-associated band. Nonetheless, such transitions are quickly recovered as the dynamics targeted in our modeling are an order of magnitude slower. It is also important to note that though we have named these two states "S_1" and "ICT" in our model, we only imply their associations with the S_1 and ICT parts of one potential energy surface and how they appear to be equilibrating. By monitoring the absorption response, they represent individual concentrations, or species, of the sample undergoing disparate, yet interrelated, dynamics.

Global analyses of pump-probe studies cannot resolve the equilibration rate k_{eq} of the S_1/ICT coupled state; therefore, S_1 and ICT are seen as a single, common, decaying state at a rate k_{com} as depicted in Fig. 9. The imbalance caused by prematurely dumping the ICT state allows for the S_1 and ICT states to be observed acting separately, requiring four rates: the rates of transfer between the equilibrating states $k_{S1 \rightarrow ICT}$ and $k_{ICT \rightarrow S1}$ as well as the decay of these individual states to a lower state, the "S_0" state, $k_{S1 \rightarrow S0}$ and $k_{ICT \rightarrow S0}$ (Fig. 2.9b). All four of these rates affect the common decay and equilibrium dynamics. However, as the following paragraphs describe, if the rate $k_{S1 \rightarrow S0}$ is considered constant, regardless of solvent polarity at room temperature, only

$k_{ICT \to S0}$ is required as the unknown rate parameter to describe the two-state system's evolution beyond 1 *ps*.

In this model, we treat the S_1, ICT, and S_0 states as separate species represented by a set of populations, or concentrations, $\{n_\ell\}$ of the sample undergoing interconversion processes determined by a set of real, positive rates, or decay parameters, $\{k_{i \to j} > 0 \mid i, j \epsilon \ell\}$. The model of unperturbed relaxation, therefore, is described by these rate equations:

$$
\begin{aligned}
\frac{dn_{S1}}{dt} &= k_{ICT \to S1} n_{ICT} - k_{S1 \to ICT} n_{S1} - k_{S1 \to S0} n_{S1} \qquad (2.1) \\
\frac{dn_{ICT}}{dt} &= k_{S1 \to ICT} n_{S1} - k_{ICT \to S1} n_{ICT} - k_{ICT \to S0} n_{ICT}.
\end{aligned}
$$

If the system is briefly perturbed by a dump, the second rate equation can be modified with the addition of a transient Gaussian-shaped dump term $-\exp\left\{-2.77[(t - t_D)/\Delta\lambda]^2\right\} k_D n_{ICT}$ where t_D is the timing of the arrival of the dump pulse, $\Delta\lambda$ is the pulse width, and k_D is the rate at which the dump transfers population from the ICT to the S_0 state.[47,48]

Nonetheless, Eqns. 2.1 represent the intrinsic behavior of the S_1 and ICT -associated populations in some decay trajectory, and they have analytical solutions which are the common decay and equilibration rates:

$$
k_{eq,com} = \frac{1}{2}\left\{ K_{sum} \pm \sqrt{K_{sum}^2 - 4\left[K_{S1}K_{ICT} - k_{S1 \to ICT}k_{ICT \to S1}\right]} \right\} \qquad (2.2)
$$

where

$$
K_{sum} = k_{S1 \to ICT} + k_{ICT \to S1} + k_{S1 \to S0} + k_{ICT \to S0} = k_{com} + k_{eq},
$$

the total S_1-associated species decay rate $K_{S1} = k_{S1 \to ICT} + k_{S1 \to S0}$ and the total ICT-associated species decay rate $K_{ICT} = k_{ICT \to S1} + k_{ICT \to S0}$. The common decay rate k_{com} takes the negative sign, and the equilibration rate k_{eq} takes the positive sign of discriminant in Eqn. 2.2. Already, it is clear there exists a range of reasonable decay rates among the states restricted by the common decay rate k_{com} which can be determined by sequential global analysis (EADS)

2.1. Equilibrium Dynamics of S_1 and ICT States of Fucoxanthin in
Solution as revealed by Multi-Pulse Spectroscopy: Dependence   87
on Polarity, Proticity, and Temperature

of the S_1/ICT state in the pump-probe (PP) regime. In the PDP regime, the dump pulse removes populations previously destined to decay to the ground state and induces an imbalance to be naturally recovered, revealing the equilibration rate. These parallel processes are best analyzed globally by the Decay-Associate Difference Spectra (DADS) of the double-difference (PP - PDP) data set. The DADS, as seen in Fig. 2.8 for acetonitrile (Fig. 2.16 for other solvents), gives k_{eq} in addition to k_{com}, when k_{com} is fixed to the singlet state decay value found in the EADS (Fig. 2.13).

Therefore, if k_{eq} and k_{com} are known from global analyses, then the rates of transfer between the states may be expressed as dependent parameters

$$k_{S1 \to ICT} = \frac{k_{ICT \to S0}^2 - K_{sum}k_{ICT \to S0} + k_{com}k_{eq}}{(k_{S1 \to S0} - k_{ICT \to S0})} \qquad (2.3)$$

and

$$k_{ICT \to S1} = \frac{k_{S1 \to S0}^2 - K_{sum}k_{S1 \to S0} + k_{com}k_{eq}}{(k_{ICT \to S0} - k_{S1 \to S0})} \qquad (2.4)$$

In many studies on the effect of solvent polarity on carbonyl carotenoids, it has been found that the ICT character becomes more pronounced in polar solvents;[13,14] whereas, in non-polar n-hexane, the ICT character of fucoxanthin is almost non-existent, and the lowest single excited state has been found to decay at a rate of $(60 \text{ ps})^{-1}$.[19] Therefore, if this is assumed to be the intrinsic rate $k_{S1 \to S0}$ at room temperature, regardless of solvent polarity, the only independent rate parameter in the model would be $k_{ICT \to S0}$, and its range of possible values is limited by the model.

Other factors limiting the range of possible decay parameters are the initial conditions to Eqns. 2.1: the initial concentrations of the S_1 and ICT states. Although an estimate of initial populations of the S_1 and ICT states are indeterminable without knowledge of their extinction coefficients, the ratio of their initial populations at the moment of dumping, $(n_{S1}/n_{ICT})_0$, is determinable by the model. Further still, the relative magnitude between $k_{S1 \to ICT}$ and $k_{ICT \to S1}$ is also dependent on whether this ratio is greater or less than unity. Because it is not intrinsically known which rate is faster, target analyses

of a two-state system may reveal more than one reasonable solution where $(n_{S1}/n_{ICT})_0$ is either equal to or greater than or less than unity. To gain insight into which solution is proper, the fit traces should, by use of a scaling factor $(\varepsilon_{S1}/\varepsilon_{ICT})$, match closely the population ratio $n_{S1}/n_{ICT}(t)$ at all times. In other words, the ratio of the S_1-associated band to the ICT-associated band of the model $(S_1{:}ICT)_{model}$ should, with a scaling coefficient, match the data $(S_1{:}ICT)_{data}$ in both pump probe and pump-dump-probe regimes shown in Fig. 2.7a. Certainly, special care should be taken as the spectral bands usually associated with the S_1 and ICT states contain dynamics of a mixture of populations. Therefore, the fitting algorithm for the model must include considerations for a mixture of signatures in these bands to properly match the data.
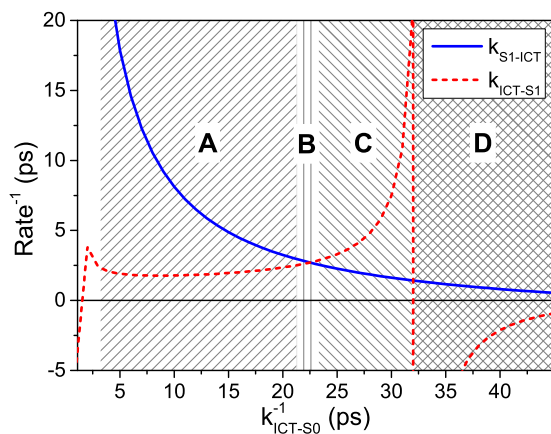

FIGURE 2.10: The possible values for the inter-S_1 ↔ICT energy transfer rates $k_{S1 \rightarrow ICT}$ and $k_{ICT \rightarrow S1}$ as a function of ICT-ground state transfer rate $k_{ICT \rightarrow S0}$ under the two-state model according to the common and equilibrium rates of fucoxanthin in acetonitrile (results for other solvents in Fig. S6). A, B, C, and D demarcate regions of non-convergence or convergence to different results in target analysis.

Before determining the remaining individual rates in the scheme in Fig. 2.9b, we must understand what limits the model intrinsically implies regarding these rates so that we may direct our fitting. As described above, according to the model and rates made available by global analyses, there are basically only two unknowns in the model: the ICTground-state decay rate, $k_{ICT \rightarrow S0}$, and the initial population ratio, $(n_{S1}/n_{ICT})_0$. There is a limitation to the possible values of $k_{ICT \rightarrow S0}$. In acetonitrile, for example, according to the model it must be that $k_{ICT \rightarrow S_0} < (32\ ps)^{-1}$ since $k_{ICT \rightarrow S1}$ is negative for all $k_{ICT \rightarrow S0} > (32\ ps)^{-1}$.

2.1. Equilibrium Dynamics of S_1 and ICT States of Fucoxanthin in
Solution as revealed by Multi-Pulse Spectroscopy: Dependence   89
on Polarity, Proticity, and Temperature

This requirement is clearly seen when considering both $S_1 \leftrightarrow$ICT rates, described by Eqns. 2.3 and 2.4, as a function of $k_{ICT \rightarrow S0}$. The possible values are presented in Fig. 2.10 for acetonitrile (Fig. 2.17 for the remaining solvents). If we assume, as in earlier reports[24,38] $k_{S_1 \rightarrow ICT}$ be faster than $k_{ICT \rightarrow S_1}$, then the possible values are limited $(21 ps)^{-1} < k_{ICT \rightarrow S_0} < (32\ ps)^{-1}$. Beyond this restriction, convergences may be found in all three allowed regions labeled A, B, and C; whereby, these regions differ in the relative magnitudes of the S1$\leftrightarrow$ICT transfer rates $k_{S1 \rightarrow ICT}$ and $k_{ICT \rightarrow S1}$. Therefore, we sought a "reasonable convergence" in one of these regions where the solutions of target analysis (1) produced rates in close agreement with global analyses, (2) the ratio $(S_1:ICT)_{model}$ of the fit traces more closely matched the empirical ratio $(S_1:ICT)_{data}$, and (3) the resulting S_1-related and ICT-related spectra are clearly separated.

When applying these requirements to fucoxanthin in acetonitrile, the solution converges such that the ICT decay rate to the ground state is close to the lower limit of the range mentioned above: near 21 ps. Therefore, as seen in Fig. 2.10, the rates of $S_1 \leftrightarrow$ICT population transfer converges to very similar rates as in region B. If the rate $k_{ICT \rightarrow S0}$ is applied as an initial condition in region D, that is $k_{ICT \rightarrow S0} > (32\ ps)^{-1}$, target analysis gives nonsensical solutions with rates in several s^{-1} or even negative rates. This analysis provides the upper bound for $k_{ICT \rightarrow S_0}$ in all solvents, and according to Eqns. 2.3 and 2.4 this boundary remains even though $k_{S1 \rightarrow S0}$ may change, as long as k_{com} and k_{eq} are described. For isopropanol, the limit for $k_{ICT \rightarrow S_0}$ is $(50\ ps)^{-1}$, and for methanol $(20\ ps)^{-1}$ and $(40\ ps)^{-1}$ for 293 and 190 K, respectively (Fig. 2.17). These limits coincide with the common decay rates in these solvents.

In regard to the initial ratio of S_1 and ICT state populations, in acetonitrile, for example, the target analysis converges to reasonable results where $(n_{S1}/n_{ICT})_0 = 1$ and the $S_1 \leftrightarrow$ICT rates are found in region B (see Fig. 10). As for the other solvents, however, a solutions did not even converge to region B. The model shows that if the condition $k_{S1 \rightarrow ICT} > k_{ICT \rightarrow S1}$ is expected, then it must be that $(n_{S1}/n_{ICT})_0 < 1$ in order for the solution to converge and produce distinct S_1 and ICT spectral amplitudes. This places reasonable convergence in region C for isopropanol and methanol at both temperatures.

Nonetheless, we found that often target analyses can converge in region A for the opposite case that $(n_{S1}/n_{ICT})_0 > 1$ as long as the associated condition $k_{S1 \to ICT} > k_{ICT \to S1}$ is held. In fact, the spectra of the species in both condi-
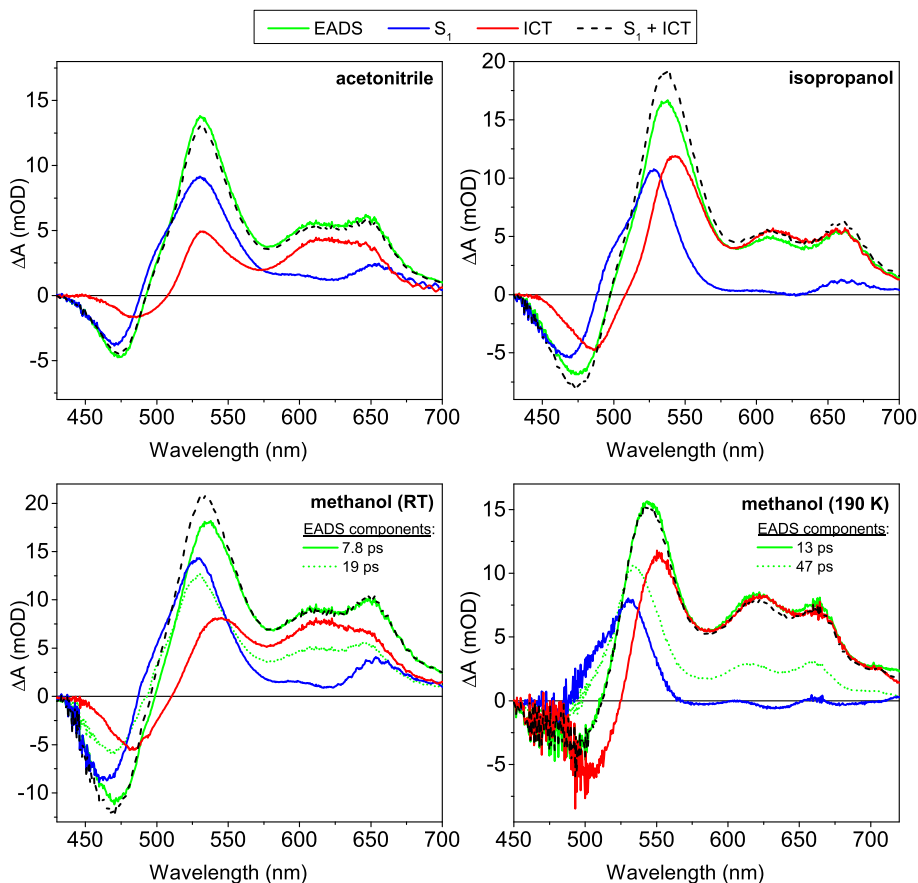

FIGURE 2.11: Comparison between a global sequential decay model (EADS, gray) and a two-compartment model (target analysis) representing the S1 (blue) and ICT (red) related species, with their sum (dashed line), in all solvents and methanol at room temperature and 190 K.

tions may be practically indistinguishable. However, when the ratio of the S_1-associated and ICT-associated bands (S1:ICT) is considered (Fig.2.7a; Fig. 2.18b) the model clearly fits better the conditions of region C. This implies that if it is desired that $k_{S1 \to ICT} > k_{ICT \to S1}$, since the ICT state is generally considered to be lower in energy than the S_1 state due to its low energy stimulated

2.1. Equilibrium Dynamics of S_1 and ICT States of Fucoxanthin in Solution as revealed by Multi-Pulse Spectroscopy: Dependence on Polarity, Proticity, and Temperature

91

emission[19], the absolute rate from the S_2 state to ICT must be faster than to S_1.

Having knowledge of which values are more acceptable, we applied them as initial parameters in our target analyses, fixing $k_{S1 \to S0}$ for all room temperature studies. For methanol at 190 K, we investigated also likely values for the rate $k_{S1 \to S0}$ as an independent parameter because this rate should slow upon cooling.[23] The data sets for target analysis were chirp-corrected and truncated at 1 *ps*, just less than a picosecond before the dump. The parameter values and spectra resulting from target analyses are shown compared to results from global analyses in Fig. 2.11 and Table 2.2. This figure represents the individual components of the coupled S_1/ICT state underlying the common decay observed in transient absorption studies of carbonyl carotenoids as their sums closely match the spectral forms of the global analyses. Generally, values for the common decay rates reverse-calculated with the analysis results closely matched the values obtained by global analysis, again confirming the functionality of the two-state model. The equilibration rate values are less accurate, yet they follow the same general order already observed in Fig. 2.7b: acetonitrile equilibrates the fastest, and methanol at 190 K is the slowest; whereby, the 190 K model converged such that the rate from S_1 to ICT was faster than the reverse path. Thus a reasonable convergence was found in region A.

Therefore, our approach allowed to discriminate feasible fitting solutions from a landscape of many possible models. The population transfer rates (Table 2.2) we have obtained for fucoxanthin in methanol qualitatively matches those reported by Redeckas et al.[39] Even the actual values differ slightly, the overall trend (e.g. $k_{S1 \to ICT} > k_{ICT \to S1}$) is reproduced. Also, the S_1-like peak in the ICT spectra (Fig. 2.11) is somehow stronger in our target analysis compared to Redeckas et. al.[39] This high-energy, ICT-related peak is found shifting to the red as the equilibration rate decreases and the polarity of the solvent increases (Fig. 2.11). This strong mixing of the S_1 characteristics into the ICT spectrum could be related to absence of hot states in our model which can still have some influence at the time of dumping, 1.7 ps after excitation. Also

it must be noted that fucoxanthin in methanol displays more complicated dynamics compared to the other two solvents, an observation most likely resulting from existence of multiple species having different degree of charge transfer character.[38,44]

Our extension of the PDP study of fucoxanthin to other solvents provided some new, interesting observations. First, the $k_{S1 \rightarrow ICT}$ and $k_{ICT \rightarrow S1}$ rates characterizing the S_1-ICT equilibration become slower upon cooling the sample to 190 K, suggesting a presence of a barrier separating the S_1 and ICT parts of the S_1/ICT potential surface. Second, both these equilibration rates become faster with increasing polarity, which translates into decreasing the barrier between the S_1 and ICT parts of the S_1/ICT potential surface, confirming the hypothesis proposed a more than a decade ago[23]. Third, it is obvious that the difference in common S_1/ICT lifetimes measured in two solvents with nearly identical polarity, methanol and acetonitrile, results from different ICT-S_0 coupling as the ICT-S_0 rate is about twice slower in acetonitrile. On the other hand, the S_1-ICT equilibration rates are notably faster in acetonitrile, indicating that hydrogen bonding available in protic methanol likely increases the barrier between the S_1 and ICT parts of the S_1/ICT potential surface.

Further information about excited state dynamics is provided by experiments using repumping of either S_1 or ICT populations. The effect of repumping, shown in Fig. 7c for fucoxanthin in acetonitrile and in Fig. S4 for fucoxanthin in methanol, reveals differences between behavior of S_1 and ICT populations. Repumping the ICT state results in return of the re-excited molecules back to equilibrium within less than ~300 fs (Fig. 2.7c), as the dynamics return to a fairly unperturbed trajectory, signaling that essentially all repumped ICT population returns back to its original location, the ICT part of the S_1/ICT potential surface. Repumping the S_1 population, however, results in more complicated population dynamics (Fig. 7c): it contains a fast recovery, which accounts for about half of the magnitude, again signaling a quick return of the re-excited population back to the S_1 potential minimum, but there is also a slower part. This slower part matches the S_1-ICT equilibration dynamics, implying that the re-excited S_1 population returns to both S_1 and ICT states. Qualitatively, the same behavior is observed for repumping the fucoxanthin

2.1. Equilibrium Dynamics of S_1 and ICT States of Fucoxanthin in Solution as revealed by Multi-Pulse Spectroscopy: Dependence on Polarity, Proticity, and Temperature

93

in methanol (Fig. S4) though the effect of the repump subsides to a different equilibrium ratio, suggesting some loss of the repumped population, most likely due to formation of fucoxanthin radical from the upper excited state as reported earlier.[15,40]

Finally, we can hypothesize how the observed excited state behavior may relate to function of fucoxanthin (and possible other carbonyl carotenoids) in light-harvesting antenna. We showed that hydrogen bonding with the polar methanol slows fucoxanthin's equilibration rate and the $S_1\leftrightarrow$ICT rates as a result. Thus, hydrogen bonding in the polar environment of light-harvesting antennae would be conceivably more advantageous for energy transfer to chlorophyll. If indeed this is the case, the advantage of using keto carotenoids in light harvesting antennae could also be the possibility of tuning the S_1/ICT equilibration by hydrogen bonding.

In our study of FCP,[45] we claimed to observe fast and slow-decaying fucoxanthin species and that only the S_1 part of the S_1/ICT potential energy surface of the slow species transfers energy to chlorophyll with a lifetime of 1.9 ps. How the preferred donor states are selected we cannot hypothesize; however, it is certain that if one state is a donor to chlorophyll, the advantage of having equilibrating states is that the other state may support the donor state by population transfer. Longer equilibration would generally be more advantageous such that energy transfer to the acceptor is preferred. With exception of acetonitrile, this study indicates the $S_1\leftrightarrow$ICT transfer rates are slower than energy transfer rates determined for PCP and FCP. Though fucoxanthin in the less polar isopropanol demonstrates the longest equilibration time, its ICT character is slightly mitigated compared to that in methanol, as is its dipole strength. In this less polar hydrogen bonding condition, energy transfer via the S_1 state may be conceivably preferred in FCP.

2.1.5   Conclusions

The systematic analysis in this ultrafast multi-pulse study, aimed at the equilibration of the S_1/ICT state in fucoxanthin in solution, utilized the results of global analysis (EADS of PP data and DADS of PP-PDP data) to properly inform target analysis of the S_1 and ICT states as separate species. Truncated at the time where S_1-ICT coupling and decay is most relevant, target analysis of pump-dump probe data reveals a tight restriction on the possible parameters for target analysis. Building a simple, two-state model with decay to the ground state allows that the description of population transfer solely depends upon the ICT state decay rate $k_{ICT \rightarrow S0}$ and initial S_1 and ICT state population ratio $(n_{S1}/n_{ICT})_0$. In addition to this analysis we manipulated the modeled kinetic traces to achieve an effective equilibrium trace $(S_1 : ICT)_{PDP} : (S_1 : ICT)_{PP}$ which reveals the dependence of the equilibration on polarity, proticity, and temperature.

When comparing the two protic solvents, methanol and isopropanol, the highly polar methanol exhibits a relative shortening of the S_1/ICT equilibration in fucoxanthin at room temperature but similar dynamics at 190 K. If the S_1 and ICT states are considered to be two parts of one potential energy surface separated by a barrier and measured by their equilibration lifetime, lower polarity, proticity, and temperature increases this barrier. Target analysis affirms this trend and quantifies the relative rates population transfer between the S_1 and ICT states such that population transfer from S_1 to ICT is preferred in polar environments and with hydrogen bonding. This conclusion is congruent with previous studies indicating that the S_1 and ICT states are best modeled as parts of the same potential energy surface.[23,24,26]

The results demonstrate a strong dependence on hydrogen bonding; whereby, the rate of equilibration among the S_1 and ICT states is prolonged. This implies a possible advantage in hydrogen bonding for antenna-bound carotenoids in that energy transfer to chlorophyll may be preferred to internal conversion such as equilibration. If this is the case, a primary donating state, S_1 for example, may be supported by the secondary or non-donating state in equilibrium. Hydrogen bonding in a highly polar environment creates a distinct advantage in that the charge transfer character will be enhanced.

2.1. Equilibrium Dynamics of S$_1$ and ICT States of Fucoxanthin in Solution as revealed by Multi-Pulse Spectroscopy: Dependence on Polarity, Proticity, and Temperature
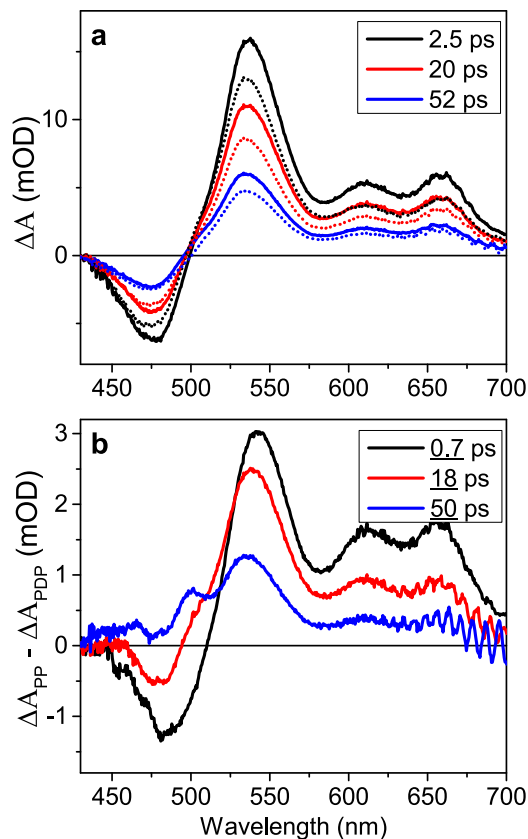
95

Supplementary Information

FIGURE 2.12: PP (solid) and PDP (dotted) spectra of fucoxanthin in isopropanol (a) at various times after excitation. The double-difference spectrum (PP – PDP) of fucoxanthin in isopropanol (b). The underlined values indicate the delay time after the dump pulse.
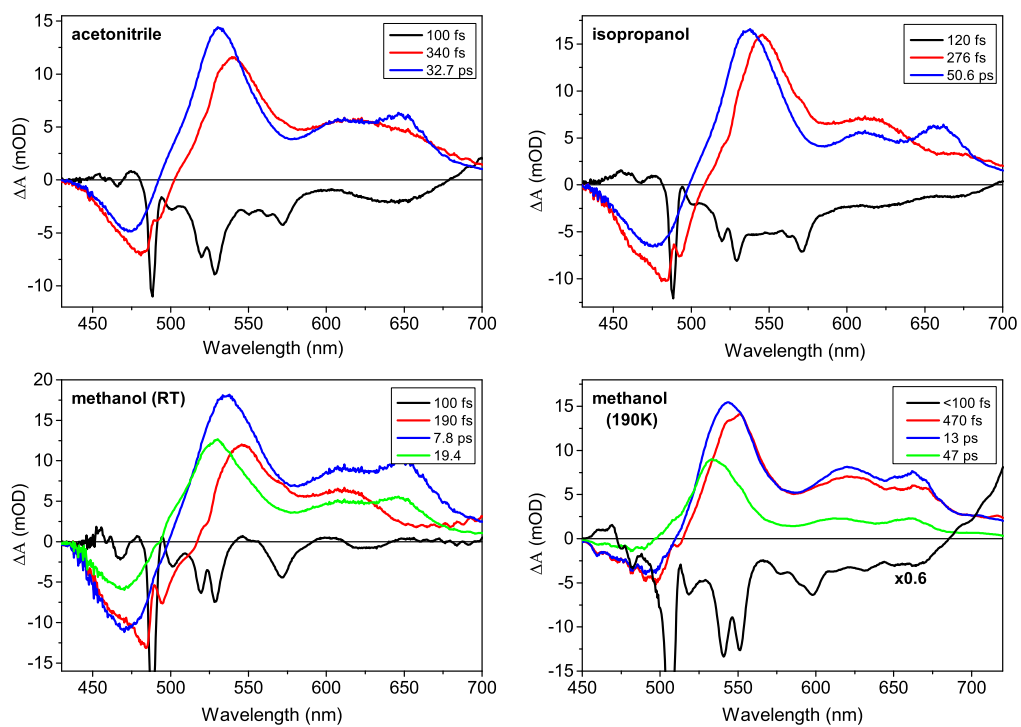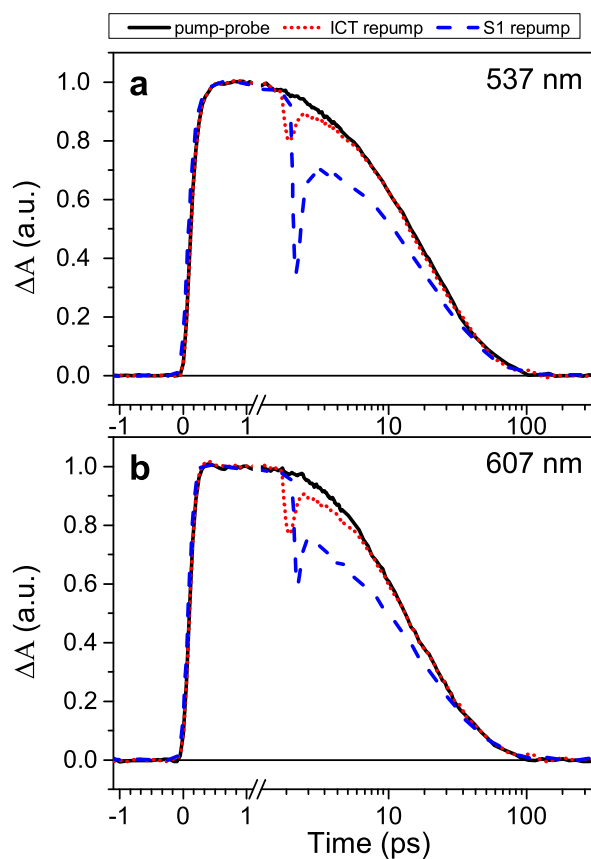
FIGURE 2.13: EADS of fucoxanthin in all solvents.

2.1. Equilibrium Dynamics of S₁ and ICT States of Fucoxanthin in Solution as revealed by Multi-Pulse Spectroscopy: Dependence on Polarity, Proticity, and Temperature

97

FIGURE 2.14: Kinetic traces of S_1 and ICT band after repumping compared to pump-probe traces in the (a) S1-associated band and the (b) ICT-associated band of fucoxanthin in methanol.
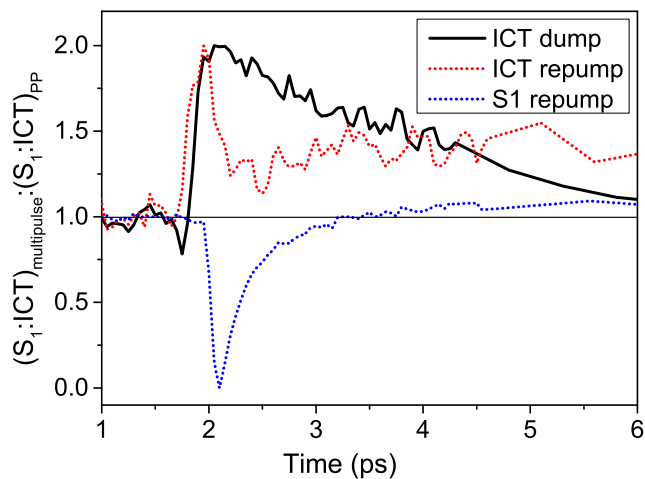
FIGURE 2.15:   The   ratio   of   the S_1-associated   to   ICT-associated band traces (S_1:ICT) in the pump-repump-probe (PrPP) regime to that of the PP regime (PrPP:PP)—that is (S_1:ICT)PrPP:(S_1:ICT)PP). Compared to the same manipulation of the PDP data.

2.1. Equilibrium Dynamics of S_1 and ICT States of Fucoxanthin in Solution as revealed by Multi-Pulse Spectroscopy: Dependence on Polarity, Proticity, and Temperature
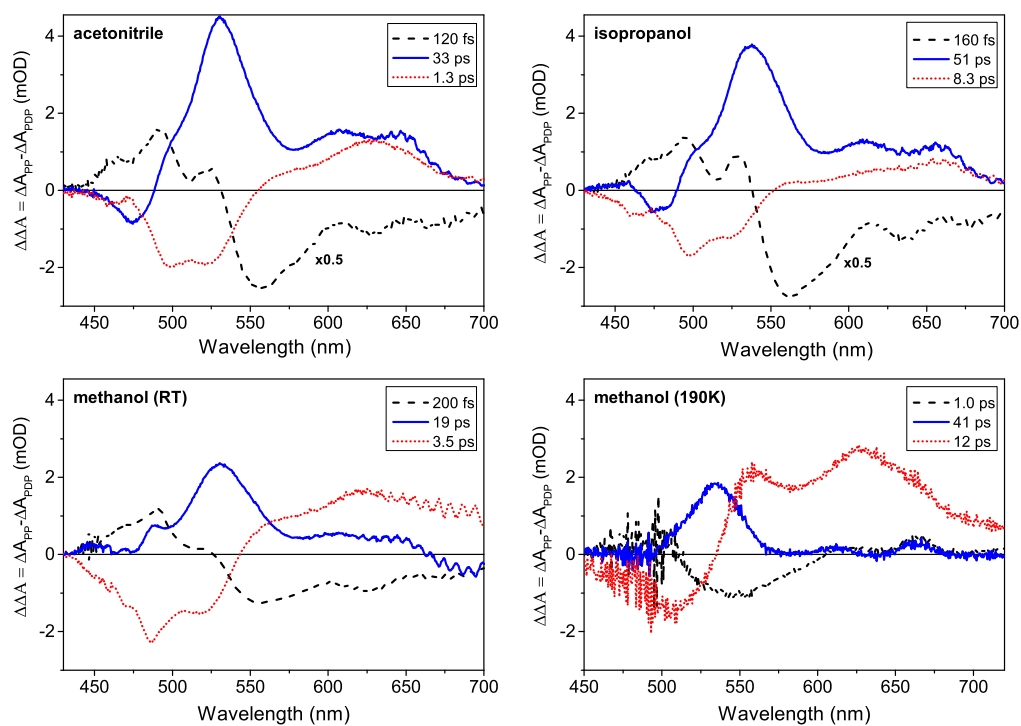
99

FIGURE 2.16: DADS of the double-difference spectrum (PP-PDP) of fucoxanthin in all solvents. The amplitude of the fastest component was reduced by half in each case.
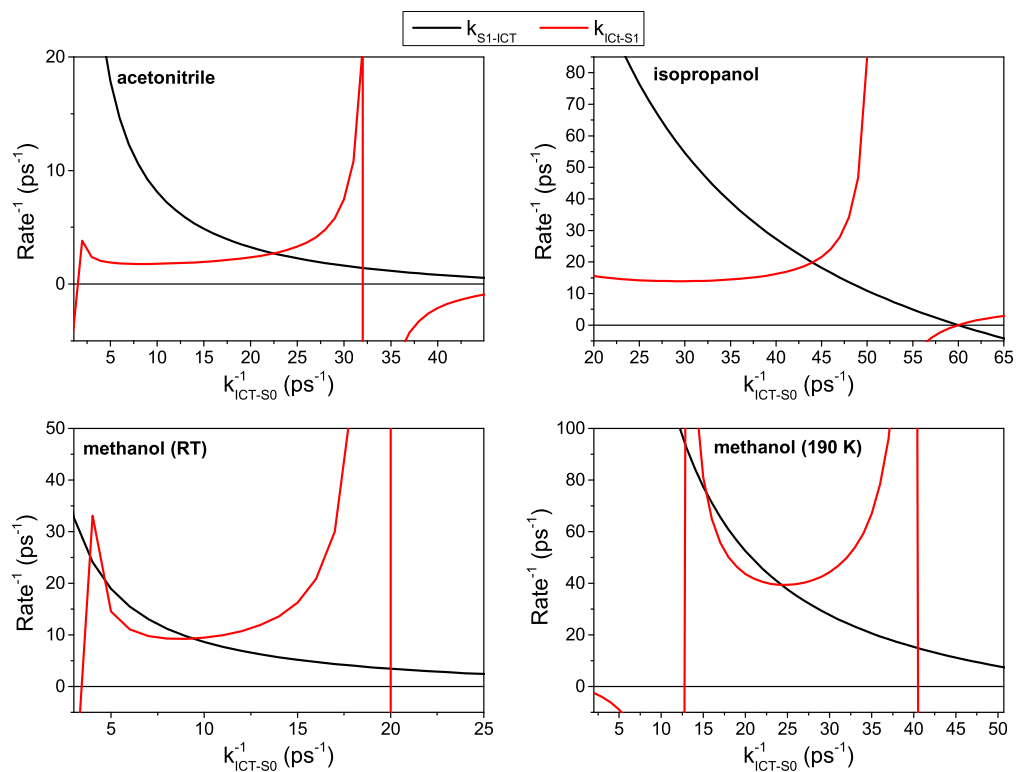
FIGURE 2.17: The possible values for the inter-S1-ICT energy transfer rates $k_{S1 \rightarrow ICT}$ and $k_{ICT \rightarrow S1}$ as a function of ICT-ground state transfer rate $k_{ICT \rightarrow S0}$ under the two-state model according to the common and equilibrium rates of fucoxanthin in all solvent environments. Curves in methanol at both temperatures are associated with the longer common decay components as found in the EADS.
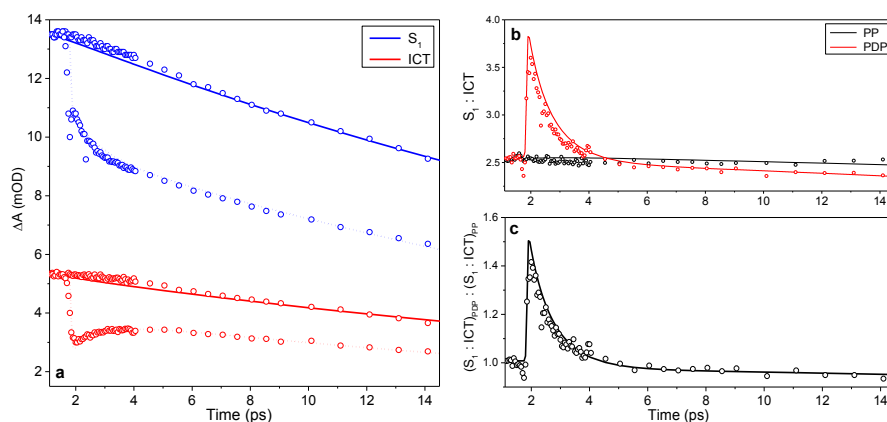
*2.1.   Equilibrium Dynamics of S_1 and ICT States of Fucoxanthin in
Solution as revealed by Multi-Pulse Spectroscopy: Dependence
on Polarity, Proticity, and Temperature*   101

FIGURE 2.18: Fits resulting from the two-level model of the coupled S_1 and ICT states for Fx in acetonitrile. As kinetic signatures of these states and the ground state overlap, the proper amount of S_0 bleaching and excite state absorption (ESA) signal had to be determined in order to match the contributions at 535 nm (61% S_1 ESA, 13% S_0 bleaching, 26% ICT ESA) and 610 nm (91% ICT ESA, 9% S_1 ESA). The dump pulse width is 70 fs, and the rate of dumping is $(120\ fs)^{-1}$. (a) Fits associated with undumped (solid) and dumped (dotted) populations of the S_1 (535 nm) and ICT (610 nm) states. (b) The ratio of the S_1 band to the ICT band (535:610 nm) for undumped (black) and dumped (red) populations. (c) The effect of the dump demonstrated in the ratio of the dumped S_1:ICT ratio (red line in b) to the undumped S_1:ICT ratio (black line in b).

References (Paper I)

1. Polivka, T.; Frank, H. A. Molecular Factors Controlling Photosynthetic Light Harvesting by Carotenoids. *Acc. Chem. Res.* **2010,** *43*, 1125-1134.

2. Croce, R.; van Amerongen, H. Natural Strategies for Photosynthetic Light Harvesting. *Nat. Chem. Biol.* **2014**, *10*, 492–501.

3. Mirkovic, T.; Ostroumov, E. E.; Anna, J. M.; van Grondelle, R.; Govind- jee; Scholes, G. D. Light Absorption and Energy Transfer in the Antenna Complexes of Photosynthetic Organisms. *Chem. Rev.* **2017,** *117*, 249-293.

4. Jahns, P.; Holzwarth, A. R. The Role of the Xanthophyll Cycle and of Lutein in Photoprotection of Photosystem II. *Biochim. Biophys. Acta - Bioenerg.* **2012**, *1817*, 182–193.

5. Duffy, C. D. P.; Ruban, A. V. Dissipative Pathways in the Photosystem-II Antenna in Plants. *J. Photochem. Photobiol. B Biol.* **2015**, *152*, 215–226.

6. Polivka, T.; Sundstrom, V. Ultrafast Dynamics of Carotenoid Excited States-from Solution to Natural and Artificial Systems. *Chem. Rev.* **2004**, *104*, 2021–2071.

7. Tavan, P.; Schulten, K. Electronic Excitations in Finite and Infinite Polyenes. *Phys. Rev. B* **1987**, *36*, 4337–4358.

8. Holt, N. E.; Zigmantas, D.; Valkunas, L.; Li, X. P.; Niyogi, K. K.; Fleming, G. R. Carotenoid cation formation and the regulation of photosynthetic light harvesting. *Science* **2005,** *307*, 433-436.

9. Ruban, A. V; Berera, R.; Ilioaia, C.; van Stokkum, I. H. M.; Kennis, J. T. M.; Pascal, A. A.; van Amerongen, H.; Robert, B.; Horton, P.; van Grondelle, R. Identification of a Mechanism of Photoprotective Energy Dissipation in Higher Plants. *Nature* **2007**, *450*, 575–578.

10. Bode, S.; Quentmeier, C. C.; Liao, P. N.; Hafi, N.; Barros, T.; Wilk, L.; Bittner, F.; Walla, P. J. On the regulation of photosynthesis by excitonic interactions between carotenoids and chlorophylls. *Proc. Natl. Acad. Sci. USA* **2009,** *106*, 12311-12316.

2.1. Equilibrium Dynamics of S_1 and ICT States of Fucoxanthin in Solution as revealed by Multi-Pulse Spectroscopy: Dependence on Polarity, Proticity, and Temperature

103

11. Staleva, H.; Komenda, J.; Shukla, M. K.; Šlouf, V.; Kaňa, R.; Polívka, T.; Sobotka, R. Mechanism of Photoprotection in the Cyanobacterial Ancestor of Plant Antenna Proteins. *Nat. Chem. Biol.* **2015**, *11*, 287.

12. Bautista, J. A.; Connors, R. E.; Raju, B. B.; Hiller, R. G.; Sharples, F. P.; Gosztola, D.; Wasielewski, M. R.; Frank, H. A. Excited State Properties of Peridinin: Observation of a Solvent Dependence of the Lowest Excited Singlet State Lifetime and Spectral Behavior Unique among Carotenoids. *J. Phys. Chem. B* **1999**, *103*, 8751–8758.

13. Frank, H. A.; Bautista, J. A.; Josue, J.; Pendon, Z.; Hiller, R. G.; Sharples, F. P.; Gosztola, D.; Wasielewski, M. R. Effect of the Solvent Environment on the Spectroscopic Properties and Dynamics of the Lowest Excited States of Carotenoids. *J. Phys. Chem. B* **2000**, *104*, 4569–4577.

14. Zigmantas, D.; Polivka, T.; Hiller, R. G.; Yartsev, A.; Sundstrom, V. Spectroscopic and dynamic properties of the peridinin lowest singlet excited states. *J. Phys. Chem. A* **2001,** *105*, 10296-10306.

15. Papagiannakis, E.; Vengris, M.; Larsen, D. S.; van Stokkum, I. H. M.; Hiller, R. G.; van Grondelle, R. Use of Ultrafast Dispersed Pump-Dump-Probe and Pump-Repump-Probe Spectroscopies to Explore the Light-Induced Dynamics of Peridinin in Solution. *J. Phys. Chem. B* **2006**, *110*, 512–521.

16. Stalke, S.; Wild, D. a; Lenzer, T.; Kopczynski, M.; Lohse, P. W.; Oum, K. Solvent-Dependent Ultrafast Internal Conversion Dynamics of N'-apo-Beta-Carotenoic-N'-acids (N = 8, 10, 12). *Phys. Chem. Chem. Phys.* **2008**, *10*, 2180–2188.

17. Niedzwiedzki, D. M.; Chatterjee, N.; Enriquez, M. M.; Kajikawa, T.; Hasegawa, S.; Katsumura, S.; Frank, H. A. Spectroscopic Investigation of Peridinin Analogues Having Different-Electron Conjugated Chain Lengths: Exploring the Nature of the Intramolecular Charge Transfer State. *J. Phys. Chem. B* **2009**, *113*, 13604–13612.

18. Kosumi, D.; Kita, M.; Fujii, R.; Sugisaki, M.; Oka, N.; Takaesu, Y.; Taira, T.; Iha, M.; Hashimoto, H. Excitation Energy-Transfer Dynamics of Brown Algal Photosynthetic Antennas. *J. Phys. Chem. Lett.* **2012,** *3*, 2659-2664.

19. Zigmantas, D.; Hiller, R. G.; Sharples, F. P.; Frank, H. A.; Sundström, V.; Polívka, T. Effect of a Conjugated Carbonyl Group on the Photophysical Properties of Carotenoids. *Phys. Chem. Chem. Phys.* **2004**, *6*, 3009–3016.

20. Enriquez, M. M.; Hananoki, S.; Hasegawa, S.; Kajikawa, T.; Katsumura, S.; Wagner, N. L.; Birge, R. R.; Frank, H. A. Effect of Molecular Symmetry on the Spectra and Dynamics of the Intramolecular Charge Transfer (ICT) State of Peridinin. *J. Phys. Chem. B* **2012**, *116*, 10748–10756.

21. Kosumi, D.; Kajikawa, T.; Okumura, S.; Sugisaki, M.; Sakaguchi, K.; Katsumura, S.; Hashimoto, H. Elucidation and Control of an Intramolecular Charge Transfer Property of Fucoxanthin by a Modification of Its Polyene Chain Length. *J. Phys. Chem. Lett.* **2014**, *5*, 792–797.

22. Staleva-Musto, H.; Kuznetsova, V.; West, R. G.; Keşan, G.; Minofar, B.; Fuciman, M.; Bína, D.; Litvín, R.; Polívka, T. Nonconjugated Acyloxy Group Deactivates the Intramolecular Charge-Transfer State in the Carotenoid Fucoxanthin. *J. Phys. Chem. B* **2018**, *122*, 2922–2930.

23. Zigmantas, D.; Hiller, R. G.; Yartsev, A.; Sundström, V. Dynamics of Excited States of the Carotenoid Peridinin in Polar Solvents: Dependence on Excitation Wavelength, Viscosity, and Temperature. *J. Phys. Chem. B* **2003**, *107*, 5339–5348.

24. Vaswani, H. M.; Hsu, C.-P.; Head-Gordon, M.; Fleming, G. R. Quantum Chemical Evidence for an Intramolecular Charge-Transfer State in the Carotenoid Peridinin of Peridinin−Chlorophyll−Protein. *J. Phys. Chem. B* **2003**, *107*, 7940–7946.

25. Papagiannakis, E.; Larsen, D. S.; van Stokkum, I. H. M.; Vengris, M.; Hiller, R. G.; van Grondelle, R. Resolving the Excited State Equilibrium of Peridinin in Solution. *Biochemistry* **2004**, *43*, 15303–15309.

26. Wagner, N. L.; Greco, J. A.; Enriquez, M. M.; Frank, H. A.; Birge, R. R. The Nature of the Intramolecular Charge Transfer State in Peridinin. *Biophys. J.* **2013**, *104*, 1314–1325.

27. Carbonera, D.; Valentin, M. Di; Spezia, R.; Mezzetti, A. The Unique Photophysical Properties of the Peridinin-Chlorophyll- a -Protein. *Curr. Protein Pept. Sci.* **2014**, *15*, 332–350.

28. Linden, P. A.; Zimmermann, J.; Brixner, T.; Holt, N. E.; Vaswani, H. M.; Hiller, R. G.; Fleming, G. R. Transient Absorption Study of Peridinin and Peridinin−Chlorophyll a−Protein after Two-Photon Excitation. *J. Phys. Chem. B* **2004**, *108*, 10340–10345.

29. Bonetti, C.; Alexandre, M. T. A.; van Stokkum, I. H. M.; Hiller, R. G.; Groot, M. L.; van Grondelle, R.; Kennis, J. T. M. Identification of Excited-State Energy Transfer and Relaxation Pathways in the Peridinin-Chlorophyll Complex: An Ultrafast Mid-Infrared Study. *Phys. Chem. Chem. Phys.* **2010**, *12*, 9256–9266.

30. Shima, S.; Ilagan, R. P.; Gillespie, N.; Sommer, B. J.; Hiller, R. G.; Sharples, F. P.; Frank, H. A.; Birge, R. R. Two-Photon and Fluorescence Spectroscopy and the Effect of Environment on the Photochemical Properties of Peridinin in Solution and in the Peridinin-Chlorophyll-Protein from Amphidinium Carterae. *J. Phys. Chem. A* **2003**, *107*, 8052–8066.

31. Papagiannakis, E.; Van Stokkum, I. H. M.; Fey, H.; Büchel, C.; Van Grondelle, R. Spectroscopic Characterization of the Excitation Energy Transfer in the Fucoxanthin-Chlorophyll Protein of Diatoms. *Photosynth. Res.* **2005**, *86*, 241–250.

32. Gildenhoff, N.; Amarie, S.; Gundermann, K.; Beer, A.; Büchel, C.; Wachtveitl, J. Oligomerization and Pigmentation Dependent Excitation Energy Transfer in Fucoxanthin-Chlorophyll Proteins. *Biochim. Biophys. Acta - Bioenerg.* **2010**, *1797*, 543–549.

33. Keşan, G.; Durchan, M.; Tichý, J.; Minofar, B.; Kuznetsova, V.; Fuciman, M.; Šlouf, V.; Parlak, C.; Polívka, T. Different Response of Carbonyl

Carotenoids to Solvent Proticity Helps to Estimate Structure of the Unknown Carotenoid from Chromera Velia. *J. Phys. Chem. B* **2015**, *119*, 12653–12663.

34. Kosumi, D.; Kusumoto, T.; Fujii, R.; Sugisaki, M.; Iinuma, Y.; Oka, N.; Takaesu, Y.; Taira, T.; Iha, M.; Frank, H. A. Ultrafast Excited State Dynamics of Fucoxanthin: Excitation Energy Dependent Intramolecular Charge Transfer Dynamics. *Phys. Chem. Chem. Phys.* **2011**, *13*, 10762.

35. Kosumi, D.; Fujii, R.; Sugisaki, M.; Oka, N.; Iha, M.; Hashimoto, H. Characterization of the Intramolecular Transfer State of Marine Carotenoid Fucoxanthin by Femtosecond Pump-Probe Spectroscopy. *Photosynth. Res.* **2014**, *121*, 61–68.

36. Kosumi, D.; Kajikawa, T.; Okumura, S.; Sugisaki, M.; Sakaguchi, K.; Katsumura, S.; Hashimoto, H. Elucidation and Control of an Intramolecular Charge Transfer Property of Fucoxanthin by a Modi Fi Cation of Its Polyene Chain Length. *J. Phys. Chem. Lett.* **2014**.

37. Kosumi, D.; Kajikawa, T.; Yano, K.; Okumura, S.; Sugisaki, M.; Sakaguchi, K.; Katsumura, S.; Hashimoto, H. Roles of Allene-Group in an Intramolecular Charge Transfer Character of a Short Fucoxanthin Homolog as Revealed by Femtosecond Pump-Probe Spectroscopy. *Chem. Phys. Lett.* **2014**, *602*.

38. Kuznetsova, V.; Chábera, P.; Litvín, R.; Polívka, T.; Fuciman, M. Effect of Isomerization on Excited-State Dynamics of Carotenoid Fucoxanthin. *J. Phys. Chem. B* **2017**, *121*, 4438–4447.

39. Redeckas, K.; Voiciuk, V.; Vengris, M. Investigation of the S1/ICT Equilibrium in Fucoxanthin by Ultrafast Pump–dump–probe and Femtosecond Stimulated Raman Scattering Spectroscopy. *Photosynth. Res.* **2016**, *128*, 169-181.

40. Larsen, D. S.; Papagiannakis, E.; van Stokkum, I. H. M.; Vengris, M.; Kennis, J. T. M.; van Grondelle, R. Excited State Dynamics of -Carotene

2.1. Equilibrium Dynamics of S_1 and ICT States of Fucoxanthin in Solution as revealed by Multi-Pulse Spectroscopy: Dependence on Polarity, Proticity, and Temperature

107

Explored with Dispersed Multi-Pulse Transient Absorption. *Chem. Phys. Lett.* **2003**, *381*, 733–742.

41. Vengris, M.; van Stokkum, I. H. M.; He, X.; Bell, A. F.; Tonge, P. J.; van Grondelle, R.; Larsen, D. S. Ultrafast Excited and Ground-State Dynamics of the Green Fluorescent Protein Chromophore in Solution. *J. Phys. Chem. A* **2004**, *108*, 4587–4598.

42. Redeckas, K.; Voiciuk, V.; Zigmantas, D.; Hiller, R. G.; Vengris, M. Unveiling the Excited State Energy Transfer Pathways in Peridinin-Chlorophyll a-Protein by Ultrafast Multi-Pulse Transient Absorption Spectroscopy. *Biochim. Biophys. Acta - Bioenerg.* **2017**, *1858*, 297–307.

43. Kosumi, D.; Kusumoto, T.; Fujii, R.; Sugisaki, M.; Iinuma, Y.; Oka, N.; Takaesu, Y.; Taira, T.; Iha, M.; Frank, H. A. One- and Two-Photon Pump-Probe Optical Spectroscopic Measurements Reveal the S1 and Intramolecular Charge Transfer States Are Distinct in Fucoxanthin. *Chem. Phys. Lett.* **2009**, *483*, 95–100.

44. Kosumi, D.; Fujii, R.; Sugisaki, M.; Oka, N.; Iha, M.; Hashimoto, H. Characterization of the Intramolecular Transfer State of Marine Carotenoid Fucoxanthin by Femtosecond Pump-Probe Spectroscopy. *Photosynth. Res.* **2014**, *121*, 61–68.

45. West, R. G.; Bína, D.; Fuciman, M.; Kuznetsova, V.; Litvín, R.; Polívka, T. Ultrafast Multi-Pulse Transient Absorption Spectroscopy of Fucoxanthin Chlorophyll a Protein from Phaeodactylum Tricornutum. *Biochim. Biophys. Acta - Bioenerg.* **2018**, *1859*, 357–365.

46. Zigmantas, D.; Hiller, R. G.; Sundstrom, V.; Polivka, T. Carotenoid to Chlorophyll Energy Transfer in the Peridinin-Chlorophyll-a-Protein Complex Involves an Intramolecular Charge Transfer State. *Proc. Natl. Acad. Sci. U. S. A.* **2002**, *99*, 16760–16765.

47. Changenet-Barret, P.; Choma, C. T.; Gooding, E. F.; DeGrado, W. F.; Hochstrasser, R. M. Ultrafast Dielectric Response of Proteins from Dynamics Stokes Shifting of Coumarin in Calmodulin. *J. Phys. Chem. B* **2000**, *104*, 9322–9329.

48. Logunov, S. L.; Volkov, V. V; Braun, M.; El-Sayed, M. A. The Relaxation Dynamics of the Excited Electronic States of Retinal in Bacteriorhodopsin by Two-Pump-Probe Femtosecond Studies. *Proc. Natl. Acad. Sci. U. S. A.* **2001**, *98*, 8475–8479.

2.2. Ultrafast multi-pulse transient absorption spectroscopy of fucoxanthin chlorophyll a protein from Phaeodactylum tricornutum

109

2.2 Ultrafast multi-pulse transient absorption spectroscopy of fucoxanthin chlorophyll a protein from *Phaeodactylum tricornutum*

Abstract

We have applied femtosecond transient absorption spectroscopy in pump-probe and pump-dump-probe regimes to study energy transfer between fucoxanthin and Chl *a* in fucoxanthin-Chl *a* complex from the pennate diatom *Phaeodactylum tricornutum*. Experiments were carried out at room temperature and 77 K to reveal temperature dependence of energy transfer. At both temperatures, the ultrafast (<100 fs) energy transfer channel from the fucoxanthin S_2 state is active and is complemented by the second pathway via the combined S_1/ICT state. The S_1/ICT-Chl *a* pathway has two channels, the fast one characterized by sub-picosecond energy transfer, and slow having time constants of 4.5 ps at room temperature and 6.6 ps at 77 K. The overall energy transfer via the S_1/ICT is faster at 77 K, because the fast component gains amplitude upon lowering the temperature. Pump-dump-probe regime with the dump pulse centered in the spectral region of ICT stimulated emission at 950 nm and applied at 2 ps after excitation proved that the S_1 and ICT states of fucoxanthin in FCP are individual, yet coupled entities. Analysis of the pump-dump-probe data suggested that the main energy donor in the slow S_1/ICT-Chl *a* route is the S_1 part of the S_1/ICT potential surface.

2.2.1   Introduction

All photosynthetic organisms rely on efficient light harvesting systems containing arrays of pigments which absorb sunlight and transfer excitation energy to the reaction centers. While the structure and function of reaction centers are conserved throughout various types of photosynthetic organisms, light harvesting systems exhibit large variability in structure, pigment composition and energy transfer efficiency.[1−3] The large diversity of photosynthetic antenna proteins reflects the large variability of light conditions in various ecological niches in which photosynthetic organisms live. Depending on the light conditions, robust and very efficient light harvesting systems, such as the chlorosomes of green sulfur bacteria which contain thousands of pigments, have evolved in low light environments.[4] Light harvesting proteins of plants and algae are much smaller and less efficient than chlorosomes, but they have a built-in, sophisticated photoprotective machinery that is able to regulate energy flow to the reaction centers, thereby coping with variable light conditions typical for the environments in which these organisms live.[5] There are even examples of light-harvesting proteins that are locked in a quenched state; thus, their only role is to block energy flow and convert the absorbed energy into heat.[6]

An important factor responsible for the large variability of light-harvesting systems, especially their ability to switch between light-harvesting and photoprotection, is the presence of carotenoids. Carotenoids are present in nearly all photosynthetic antennas and serve as accessory pigments that either collect light in the spectral regions not accessible to (bacterio)chlorophylls[2,7,8] or regulate energy flow by quenching of excited (bacterio)chlorophylls.[6,8−11] The ability of this multi-functionality of carotenoids is closely related to their spectroscopic properties. They absorb light predominantly in the 450-550 nm region via a strong transition from the ground (S_0) state to second excited state (S_2). The lowest excited state (S_1) is forbidden for one-photon processes such as direct absorption of sunlight.[7] Therefore, the S_1 state can only be populated via internal conversion (typically in less than 200 fs) from the S_2 state.[7] The internal conversion most likely involves a conical intersection,[12,13] but other dark states might be also involved

2.2. Ultrafast multi-pulse transient absorption spectroscopy of fucoxanthin chlorophyll a protein from Phaeodactylum tricornutum

111

in the S_2-S_1 transition.[14,15] The S_1 state has a lifetime of several picoseconds, depending on the conjugation length of the carotenoid.[7]

While the S_2 and S_1 lifetimes are only mildly affected by the carotenoid-protein interaction, except for keto-carotenoids (see below), the energies of both carotenoid excited states can be significantly tuned by the protein binding pocket, which is crucial for optimizing the efficiency of carotenoid-(B)Chl energy transfer from both S_1 and S_2 states. Keto-carotenoids, which have a conjugated keto group in their structure, exhibit greater tunability of their spectroscopic properties. These carotenoids exhibit polarity-dependent spectroscopic properties, and this behavior is related to the presence of an intramolecular charge transfer (ICT) state. Since the discovery of the ICT state in keto-carotenoids in 1999,[16] it has been assumed that the ICT state couples to the S_1 state, forming a "collective" S_1/ICT state whose lifetime depends on solvent polarity.[17−19] Recently, however, Redeckas et al., using pump-dump-probe spectroscopy, unequivocally proved that the S_1 and ICT states can be affected separately.[20] Since the interaction between the S_1 and ICT states depends on polarity, tuning the local environment of the conjugated keto-group may significantly affect the spectroscopic properties of keto-carotenoids bound to light-harvesting proteins.

The light-harvesting properties of keto-carotenoids have been studied, for example, in the membrane antenna protein of diatoms, fucoxanthin chlorophyll-a protein (FCP). Although the high resolution structure of FCP remains unresolved, the high sequence homology with LHCII antenna from plants suggests similar structural elements among FCP and LHCII.[21] The most studied FCP antenna are derived from *Cyclotella meneghiniana* in which are found two FCP forms, denoted FCPa and FCPb, differing in the number of subunits. While FCPa forms trimers, a highly oligomeric state is typically found for FCPb.[22−24] FCP binds carotenoid fucoxanthin along with Chl *a* and Chl *c* in a stoichiometric ratio approximately 4:4:1.[25,26] Further, the carotenoid diadinoxanthin is also found in FCP, accounting for less than 20% of total carotenoid content.[26,27] Earlier studies of FCP from *C. meneghiniana* demonstrated efficient fucoxanthin-Chl *a* energy transfer achieved through three pathways: the S_2 pathway with <150 fs energy transfer time, and two S_1/ICT

routes with energy transfer times in 0.6-0.9 ps and 2.5-3.5 ps range.[25,28−30] Within the chlorophyll pool, excited Chl *c* transfers energy efficiently to Chl *a* on sub-100 fs time scale.[30,31] Essentially the same energy transfer parameters were reported for the FCP complex from the brown alga *Cladosiphon okamuranus*.[32]

Recently, it has been shown that further insight into excited-state dynamics of keto-carotenoids may be obtained from a pump-dump-probe experiment, which can selectively dump the ICT state by tuning the second excitation pulse (dump) to the spectral region of the ICT stimulated emission which occurs within 900-1000 nm.[33] This approach has been successfully used to monitor S_1-ICT equilibration of keto-carotenoids in solution[20,34] as well as to follow excited state processes of another keto-carotenoid, peridinin, bound to peridinin-chlorophyll-a protein (PCP).[35] These studies showed that the S_1 and ICT states are separate states in equilibrium, whether in solution or in the PCP complex. The S_1 and ICT states can be viewed as two minima on the S_1/ICT potential surface; thus we will refer to a coupled S_1/ICT state if we refer to the whole potential surface, while S_1 and ICT states will be used when addressing the two minima individually.

Since pump-dump-probe spectroscopy helps to resolve complex dynamics involving the S_1 and ICT states, we have applied it here to study fucoxanthin-Chl *a* energy transfer in the FCP complex from the pennate diatom *Phaeodactylum tricornutum*. FCP from this organism exhibits a slightly different structure as it consists predominantly of FCP trimers.[36] We compare excited-state processes in FCP from *P. tricornutum* at room temperature and at 77 K in both pump-probe and pump-dump-probe regimes to explore temperature dependence and pathways of fucoxanthin-Chl *a* energy transfer.

2.2.2   Materials and Methods

Trimeric FCP complexes were purified from *P. tricornutum* strain SAG 1090-1a. Cells were grown in batch culture in artificial sea water medium with f/2+Si nutrient addition[37] in 5L Erlenmeyer flasks and illuminated by a metal halide lamp at an intensity of 30 mol photons m^{-2} s^{-1} (15h light/9h

2.2. *Ultrafast multi-pulse transient absorption spectroscopy of fucoxanthin chlorophyll a protein from Phaeodactylum tricornutum*

113

dark). Cells were pelleted by centrifugation at 8000× g and stored at -80°C until further use.

The FCP antenna was isolated as described previously [36]. Briefly, thylakoid membranes were solubilized by 2% n-dodecyl -D-maltoside and pre-purified using linear sucrose gradient ultracentrifugation. The major antenna zone was collected from the gradient and further purified using anion exchange chromatography on a 2 mL column packed with DEAE Sepharose CL-6B (Sigma-Aldrich, St. Louis, USA) using a linear NaCl gradient of 5-400 mM (elution buffer: 50 mM HEPES pH 7.5, 2 mM KCl, and 0.03% n-dodecyl -D-maltoside). The fractions eluted at 180-220 mM NaCl were selected for spectroscopic measurements based on the simultaneous criteria of lowest protein/Chl a (A270/A674) and highest carotenoid/Chl a (A480/A674) ratios. The collected fractions were desalted and stored at -80°C. Prior to experiments, the isolated FCP was dissolved in a buffer (50 mM HEPES pH 7.5, 2 mM KCl, and 0.03% n-dodecyl -D-maltoside) to yield optical density ∼0.5 at the maximum of Q_y band of Chl a. Pigment composition was analyzed by HPLC as described in [38].

For room temperature measurements, the sample was placed in a 2 mm path length quartz cuvette resulting in ∼0.35 OD at excitation wavelength. For all measurements at 77 K, the sample buffer was modified with 60% glycerol to ensure homogeneity upon freezing. Low temperature measurements were carried out in a 2 mm pathlength spectroscopic-grade plastic cuvette, mounted in an Optistat DN2 nitrogen bath cryostat (Oxford Instruments), and subsequently cooled to 77 K. For all transient absorption measurements at room temperature, the sample was continuously agitated with a magnetic stir bar.

Ultrafast TA measurements were performed with a regenerative chirped pulse amplification system (Spectra-Physics) producing 100 fs pulse width, 800 nm central wavelength pulses at a repetition rate of 1 kHz at 4 W average power. Beam splitters directed pulses to two optical parametric amplifiers, TOPAS and TOPAS Prime (Light Conversion), which generated pump pulses at 510 nm and dump pulses at 950 nm. A third beam path led to a 3 mm sapphire plate which produced a supercontinuum for probing at the repetition

rate of the source. Additionally, this supercontinuum beam was split into a reference beam which passed outside the sample and probe beam which over-lapped the pump beam in the sample. Choppers in the pump and dump paths set at 500 Hz and 250 Hz ensured that every 4 ms, four pulse regimes reached the sample space: probe without pump excitation, pump-probe (PP), dump pulse with probing or dump-probe (DP), and pump-dump-probe (PDP). The timing of the dump pulses relative to the pump pulses were fixed at 2 ps and probe times were varied with a delay line.

Near the sample space, pump and dump beams were focused with 350 and 600 mm focal length fused silica convex lenses. The resulting spot sizes where the beams overlapped in the sample space in air were approximately 220, 370, and 120 μm for pump, dump, and probe, respectively. Therefore, the photon flux at the sample space for 293 K measurements for pump and dump were 2.8 x 10^{14} photons pulse^{-1} cm^{-2} and 1.9 x 10^{15} photons pulse^{-1} cm^{-2}, respectively. For 77 K measurements, due to loss of intensity and de-focusing through the cryostat glass, we may only estimate the intensity to have been 5 x 10^{14} photons pulse^{-1} cm^{-2} and 2 x 10^{15} photons pulse^{-1} cm^{-2}, respectively, for pump and dump. Two Berek compensators placed into the pump and dump beams set the pump beam polarization to 54.7 degrees to the probe beam and the dump beam polarization parallel to the pump beam. Time-resolved spectra obtained from reference and probe signals were de-tected with a double CCD array system (Pascher Instruments) which synchro-nized the choppers and controlled the delay line. Fitting results for global analysis for sequential decay models (evolution associated difference spectra, EADS) were obtained with Glotaran software for time-resolved spectroscopy (VU Amsterdam).[39] Monte-Carlo simulations, fitting and modelling the PDP data described in the discussion section were performed in Matlab.

2.2.3 Results

Absorption spectra of the FCP complex from *P. tricornutum* at room tem-perature and at 77 K are shown in Fig. 2.19. The absorption of fucoxan-thin dominates in the 480-550 nm spectral region. At 77 K there are fucox-anthin bands are evident at 545 and 515 nm, with a weak additional band

2.2. Ultrafast multi-pulse transient absorption spectroscopy of
fucoxanthin chlorophyll a protein from Phaeodactylum tricornutum

115

around 495 nm. The energy gap between these bands does not match the characteristic vibrational spacing of the vibronic bands of the S_2 state, indicating that these bands correspond to different fucoxanthins in FCP from *P. tricornutum*, in agreement with earlier analyses of FCP from *Cyclotella meneghiniana*.[25,28,40] The weak band around 495 nm is likely due to 0-0 band of diadinoxanthin. At room temperature, the individual fucoxanthin bands merge to a nearly featureless, broad absorption band extending from 470 to 550 nm. Cooling of the FCP down to 77 K induces a slight (3-4 nm) red shift of the carotenoid absorption bands. In contrast, the Q_y band of Chl *a* peaks at 672 nm at room temperature, but it is blue-shifted to 669 nm at 77 K. The blue shift of Q_y band of Chl *a* is typical for FCP,[40] though it has been also reported for the peridinin-containing acpPC complexes from *Symbiodinium*[41] or *Amphidinium carterae*.[42] The Soret bands of Chl *a* (440 nm) and Chl *c* (460 nm) are less sensitive to the decreased temperature.

Pump-probe transient absorption
The FCP complexes were excited at 510 nm, a wavelength at which fucoxanthin will be nearly exclusively excited. Comparison of transient absorption spectra of the FCP complex measured at 1 ps after excitation at 293 and 77 K are shown in Fig. 2.20. Excitation of fucoxanthin induces energy transfer to Chl *a* as indicated by the presence of Q_y bleaching around 670 nm. The

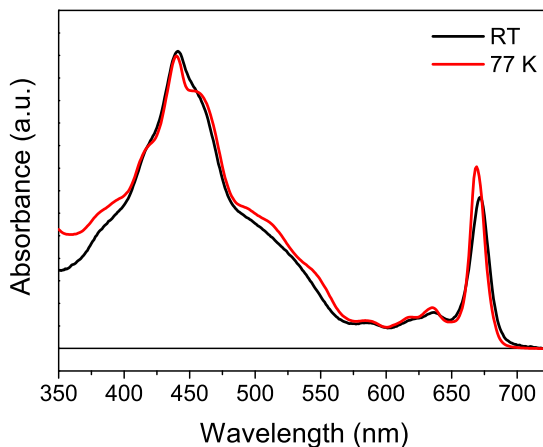

FIGURE 2.19: Absorption spectra of FCP complex from P. tricornutum measured at room temperature (black) and at 77 K (red). Spectra are normalized to unit area of the Q_y band.

positive signal is associated with both the primarily S_1-S_n and the primarily ICT-S_N excited state absorption (ESA) bands of fucoxanthin. Though there is some overlap between S_1 and ICT state signatures, these bands have been shown to be distinct in numerous studies by direct correlation of the ESA amplitude to the polarity dependence of the ICT-S_N band.[17,33]

Additionally, pump-dump-probe studies demonstrate how the signatures in these bands are readily differentiated by prematurely dumping the ICT state population.[20,35] The S_1-S_n band has a maximum at 560 nm at room temperature, and it is shifted to 565 nm upon cooling to 77 K. The ICT state of fucoxanthin generates a broad, positive signal above 600 nm and overlaps with Q_y bleaching of Chl *a*. It is worth noting that the magnitude of the ICT-S_N band in relation to the S_1-S_n band is affected by temperature. At 77 K, the ICT signal above 625 nm is stronger in respect to the magnitude of the S_1-S_n excited state absorption and ground state bleaching, as previously reported, suggesting that the ICT character increases at low temperature.[43]

While no significant temperature-induced changes except the red shift of the S_1-S_n band are observed in transient absorption spectra, clear differences are observed in kinetics depicted in Fig. 2.21. Normalized kinetics measured in the spectral region of fucoxanthin bleaching (490 nm), fucoxanthin ICT-S_N band (645 nm), and Chl *a* Q_y bleaching (670 nm) clearly show that the dynamics are faster at 77 K. Since the simultaneous fucoxanthin decay and
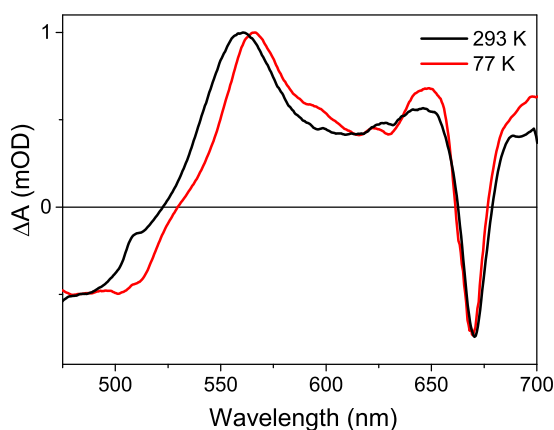

FIGURE 2.20: Transient absorption spectra of FCP measured at 1 ps after excitation at 510 nm at room temperature (black) and 77 K (red). Spectra are normalized to maximum of the S_1-S_n band.

Chl *a* rise are faster at 77 K, in contrast to a number of other light harvesting systems, cooling FCP down to 77 K makes the carot-enoid-Chl *a* energy transfer faster.

The dynamics can be better analyzed by fitting the data globally. Fig. 2.22 shows the EADS obtained from the data measured at 293 and 77 K. It is obvious that the first three EADS, corresponding to the S_2 state of fucoxanthin (black) and two different S_1/ICT states (red and blue EADS) indicate that these states have comparable lifetimes at both temperatures. This

2.2. Ultrafast multi-pulse transient absorption spectroscopy of
fucoxanthin chlorophyll a protein from Phaeodactylum tricornutum

117

seemingly contradicts the kinetics shown in Fig. 2.21, but a closer look reveals that the amplitudes of these components differ at different temperatures.

All three components are associated with energy transfer from fucoxanthin to Chl *a*. The first, black EADS has a lifetime shorter than 90 fs and a precise time constant cannot be reliably obtained due to limits of the time resolution of our system. Yet, it is clear that while at 293 K this initial EADS does not contain Q_y bleaching, at 77 K the Chl *a* contribution is significant, suggesting faster S_2-mediated energy transfer at 77 K. At 77 K, the Q_y bleaching in the second EADS (red) accounts for about half of the total Q_y amplitude, while at 293 K it is less than 30%. This comparison demonstrates that the S_2 pathway is more efficient at 77 K.

The dynamics associated with the second and third EADS corresponds to energy transfer from the coupled S_1/ICT state of fucoxanthin. The faster S_1/ICT-Chl *a* channel (800 fs at RT and 930 fs at 77 K) has significant amplitude at both temperatures, but the slower channel (4.5 ps at RT and 6.6 ps at 77 K) contributes significantly to energy transfer only at 293 K. Thus, while at 77 K the energy transfer occurs predominantly via the ultrafast (<90 fs) S_2-mediated pathway and the fast (930
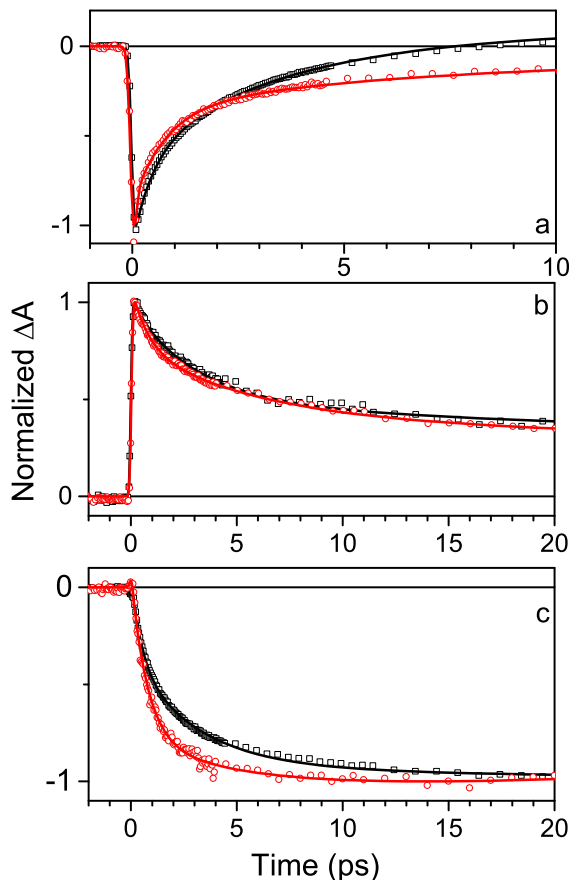

FIGURE 2.21: Comparison of room temperature (black) and 77 K (red) kinetics at wavelengths corresponding to (a) fucoxanthin bleaching at 490 nm, (b) fucoxanthin ICT band at 645 nm, and (c) bleaching of Chl *a* at 671 nm. Solid lines are fits from global fitting. Kinetics are normalized to maximum. The FCP complex was excited at 510 nm.

fs) S_1/ICT pathway, at 293 K there is a significant contribution from the slow (4.5 ps) S_1/ICT-Chl *a* channel, which makes the overall fucoxanthin-Chl *a* energy transfer slower at 293 K as indicated by the kinetics in Fig. 2.21.

The slower components (magenta and green EADS) corresponds to decays of individual pigments and they are not related to energy transfer. Magenta EADS have a shape characteristic of the coupled S_1/ICT state of fucoxanthin, but since there is no increase in Chl *a* bleaching, it must be due to the S_1/ICT state that does not transfer energy to Chl *a*. The lifetime of this non-transferring S_1/ICT state is 38 ps at 293 K and is markedly prolonged to 74 ps at 77 K. The green EADS with time constant of 3.9 ns are the lifetime of Chl *a* in FCP. These green EADS are transformed into non-decaying EADS which, especially at 293 K, contains a pronounced band at 550 nm that is due to the fucoxanthin triplet, which has a lifetime of several microseconds.
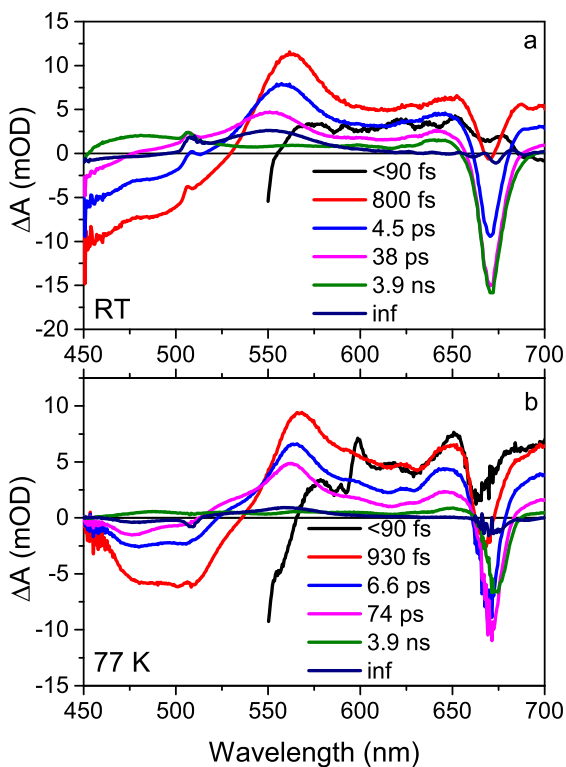
FIGURE 2.22: EADS obtained from global fitting the data measured after excitation of FCP at 510 nm at (a) room temperature and (b) 77 K.

Pump-dump-probe

To provide further insight into the excited state processes of the FCP complex, we have applied a dump pulse centered at 950 nm. This wavelength is around the maximum of the ICT stimulated emission which occurs in the 900-1000 nm spectral region for most keto-carotenoids in solution[20,33] and bound

2.2. Ultrafast multi-pulse transient absorption spectroscopy of fucoxanthin chlorophyll a protein from Phaeodactylum tricornutum

119

to proteins.[35,44] Since recent reports using pump-dump-probe spectroscopy clearly demonstrated that the S_1 and ICT states are separate entities,[20,35] the dump pulse tuned to the maximum of the ICT stimulated emission selectively depletes a fraction of the ICT population of fucoxanthin in FCP by transferring it to the ground state. We have applied the dump pulse at 2 ps after excitation. At this delay time the relaxation processes associated with the S_2-S_1 internal conversion and vibrational cooling within the S_1 and ICT states are mostly over, and the S_1/ICT coupled state population dominates.

The effect of the 950 nm dump pulse on transient absorption spectra is shown in Fig. 2.23. The effect of the dump pulse, shown as the grey spectrum, representing the difference between the pump-probe and pump-dump-probe data, is captured at 1 ps after the dump pulse. The effect is stronger in the spectral region of the ICT state, confirming that the ICT and S_1 bands are affected differently, and this difference is more pronounced at 77 K. The negative signal in the bleaching region reflects the decrease of the bleaching signal due to repopulation of the ground state by the ICT-S_0 transition facilitated by the dump. Interestingly, at the maximum of Chl a Q_y bleaching at 670 nm, the net effect of the dump at 1 ps is nearly
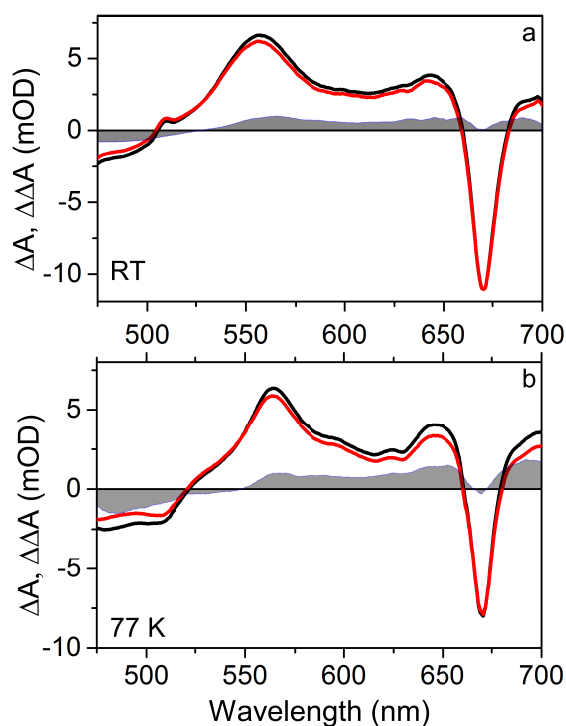

FIGURE 2.23: Transient absorption spectra measured at 3 ps after excitation at 510 nm in the pump-probe (PP, black) and pump-dump-probe (PDP, red) regime. In the PDP experiment, dump at 950 nm was applied 2 ps after excitation. The grey area is the double difference spectrum obtained by PDP-PP subtraction and monitors spectral response of the system to the dump pulse. The data were measured at room temperature (top) and 77 K (bottom).

zero at both temperatures.

The excited state dynamics induced by the dump pulse are visualized in kinetics shown in Fig. 2.24 (room temperature) and Fig. 2.25 (77 K). The effect of the dump is similar at both temperatures, though the magnitude of some signals differs between 293 and 77 K. At 560 nm, the maximum of the S_1-S_n band, there is an initial spike in the double difference kinetics (shown in blue) indicating that even the S_1 state population is instantaneously affected by the dump. The initial depopulation of the S_1 state, however, recovers within 200 fs, suggesting the dump is also in resonance with some excited-state absorption of the S_1 state, which is most likely the S_1-S_2 transition.[33] The initial signal at 560 nm is, therefore, the result of transferring a fraction of the S_1 population to some higher state (possibly higher vibrational levels of
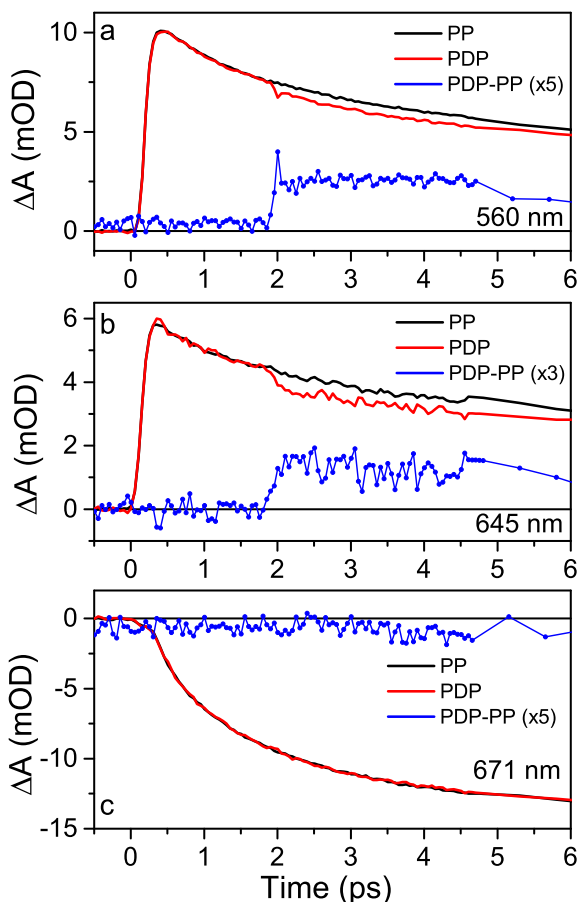

FIGURE 2.24: PP (black) and PDP (red) kinetics of FCP excited at 510 nm at room temperature. Depicted kinetics monitor the S1-Sn transition at 560 nm (a), ICT state at 645 nm (b) and Qy band of Chl a at 671 nm (c). The 960 nm dump pulse was applied 2 ps after excitation.

the S_2 state) which returns back to the S_1 state in less than 200 fs. After these initial dynamics, the double difference signal in the S_1 region slowly rises, reflecting equilibration between the S_1 and ICT states.[20] No such dynamics (initial spike and slow rise) is observed at 645 nm; the

2.2. *Ultrafast multi-pulse transient absorption spectroscopy of*
fucoxanthin chlorophyll a protein from Phaeodactylum tricornutum

121

ICT state is depleted immediately and the disturbance of the ICT popula-
tion slowly decreases in magnitude, again due to the S_1-ICT equilibration.

In the Chl a Q_y region, the
dump has very little influence
on the kinetics, as already in-
dicated by the transient absorp-
tion spectra after dump shown
in Fig. 2.23. An initial spike,
similar to that observed in the
S_1 spectral region, occurs espe-
cially in the 77 K kinetics. Since
it is known that there is a rather
flat excited state absorption of
Chl a in the 800-1200 nm spec-
tral region,[44] this spike is also
likely associated with transfer-
ring a fraction of the Q_y popu-
lation to some higher state, fol-
lowed by fast return back to the
Q_y state. The spike is stronger
in the 77 K kinetics, because
fucoxanthin-Chl a energy trans-
fer is faster at 77 K (Fig. 2.21);
thus the population of excited
Chl a when the dump pulse is
applied at 2 ps is larger at 77 K.
Besides this initial spike, there is
almost no effect of the dump on
the Q_y bleaching kinetics within
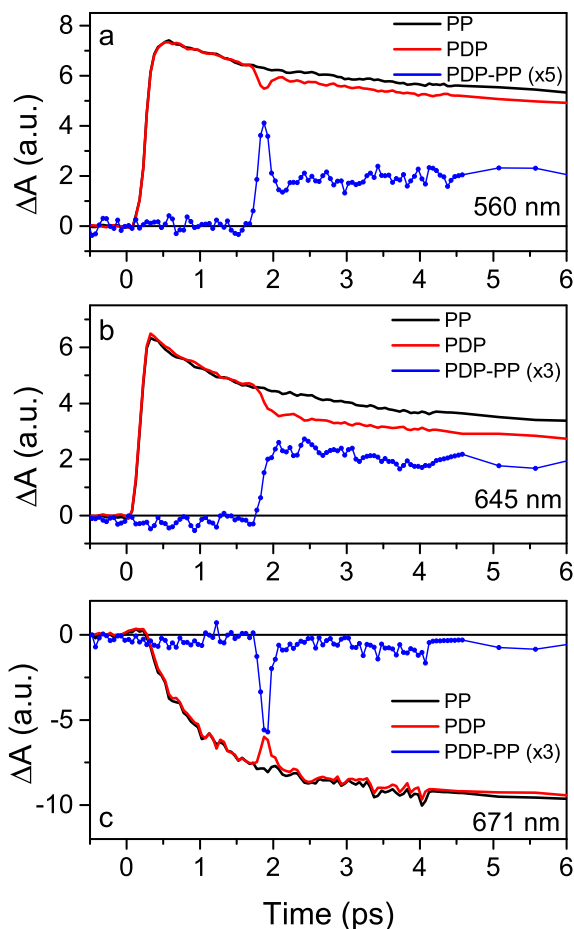the first 6 ps (Figs. 2.24c and
2.25c).

FIGURE 2.25: PP (black) and PDP (red) kinetics
of FCP excited at 510 nm at 77 K. The kinetics
monitor the S1-Sn transition at 560 nm (a), ICT
state at 645 nm (b) and Qy band of Chl a at 671
nm (c). The 960 nm dump pulse was applied 2
ps after excitation.

2.2.4   Discussion

Our transient absorption data demonstrate efficient energy transfer from fucoxanthin to Chl *a* in FCP from *P. tricornutum*, corroborating earlier ultrafast spectroscopy data on FCP from *C. meneghiniana*[25,28,29] and *Cladosiphon okamuranus*.[32] Some differences in time constants might be related to different excitation wavelengths used in various studies as it is known that fucoxanthin-Chl *a* pathways are excitation wavelength dependent.[28] Qualitatively, however, the energy transfer routes are comparable in all FCP's studied so far: they consist of the sub-100 fs S_2-pathway and two S_1/ICT pathways characterized by time constants of 700-900 fs and 3-7 ps.

Effect of temperature on excited-state processes in FCP

Since no transient absorption data on FCP at cryogenic temperatures were reported so far, we will first discuss the effect of temperature on excited state processes in FCP. The comparison of kinetics at the key wavelengths shown in Fig. 2.21 provides clear evidence that fucoxanthin-Chl *a* energy transfer is faster at 77 K. Although this may sound surprising, similar result was reported for PCP, in which the peridinin-Chl *a* energy transfer was, compared to room temperature, markedly faster at the even lower temperature of 10 K.[43,45] Yet, the PCP structure is strikingly different from that of FCP, suggesting that the effect of speeding up the energy transfer could be related to the ICT state of keto-carotenoids.

Looking at the EADS in Fig. 2.22, however, we see that the situation is a bit more complicated. In fact, both time constants associated with the S_1/ICT pathway are actually slightly slower at 77 K. We note, however, that the standard deviation of all time constants is about 10%; thus the differences are indeed rather marginal. Yet, it is obvious from EADS in Fig. 2.22 that the reason for the overall faster energy transfer at 77 K is the difference in magnitudes of the fast ($\sim$800 fs) and slow ($\sim$5 ps) S_1/ICT-Chl *a* pathways. While at room temperature these two routes contribute almost equally to the overall S_1/ICT-Chl *a* energy transfer, at 77 K the faster route dominates, and the slow one contributes only marginally. Further, the Chl *a* contribution in the first EADS (the fucoxanthin S_2 state) is much larger at 77 K. Thus, even the S_2 route is

2.2. Ultrafast multi-pulse transient absorption spectroscopy of
fucoxanthin chlorophyll a protein from Phaeodactylum tricornutum

123

more efficient at 77 K.

In searching for an explanation for this unexpected temperature dependence, it is also worth noting that the Q_y band of Chl *a* is blue-shifted by $\sim$3 nm upon lowering the temperature (Fig. 2.19). Such a blue shift could, in principle, improve the spectral overlap between donor emission and acceptor absorption, but since the ICT emission is very broad, extending far beyond 700 nm,[16] such a scenario is very unlikely. Moreover, for PCP, which also has faster carotenoid-Chl *a* energy transfer and blue-shifted Q_y at cryogenic temperatures, it has been shown by pigment reconstitution that a blue shift of the Q_y band decreases the energy transfer efficiency.[46] The dependence of energy transfer on the Q_y blue shift can be also ruled out on the basis of comparison with acpPC, for which the energy transfer is slower at 77 K even though the Q_y blue shift is present.[41,42]

The origin of the faster energy transfer at 77 K should, rather, be traced to the properties of fucoxanthin. Because this effect has been so far observed only for PCP[43,45] and FCP (data shown in this manuscript), it is likely that the specific properties of keto-carotenoids will play a role. It is known that the ICT state of keto-carotenoids is important for tuning the energy transfer efficiency in light-harvesting complexes binding these carotenoids,[2,25,35,44] although details of the mechanisms by which the ICT state facilitates carotenoid-Chl *a* energy transfer remain unclear (see also discussion below). There are only a few studies of keto-carotenoids at 77 K. For example, Niedzwiedzki et al[47] compared excited-state properties of peridinin analogs at room temperature in THF and at 77 K in 2-MTHF. The data show that the ICT state of all peridinin analogs is more pronounced at 77 K. Thus, it is likely that lowering the temperature shifts the equilibrium towards the ICT part of the potential surface of the coupled S_1/ICT state, which in turn may facilitate the energy transfer efficiency via the S_1/ICT-Chl *a* route.

Indeed, comparison of transient absorption spectra of FCP at 293 and 77 K shown in Fig. 2.20 supports this suggestion. The magnitude of the ICT signal is best visualized as the magnitude ratio of the S_1-S_n and ICT-S_N bands. The transient absorption spectra in Fig. 2.20 are normalized to the S_1-S_n maximum; and the magnitude of the ICT band, which occurs in the 630-700 nm

spectral region and overlapping with the Q_y bleaching, is clearly larger at 77 K. This enhancement indicates an increased ICT character of the donor state at 77 K, which could be the reason for more efficient fucoxanthin-Chl *a* energy transfer at 77 K. The relation between the ICT magnitude and energy transfer is further manifested by the EADS corresponding to a non-transferring fucoxanthin (magenta EADS in Fig. 2.22). This spectrum has only weak ICT signal in the 630-700 nm region underlining the importance of the ICT state for fucoxanthin-Chl *a* energy transfer. Interestingly, however, while the S_1/ICT lifetime of the non-transferring fucoxanthin is significantly slower at 77 K (74 ps) compared to room temperature (38 ps), the fucoxanthin-Chl *a* energy transfer rate via the S_1/ICT-Chl *a* route is only marginally affected by temperature.

The S_1 and ICT states of fucoxanthin are separable in FCP

Further insight into the excited state processes is provided by PDP spectroscopy. Recently. Redeckas et al. provided clear evidence that the S_1 and ICT states of fucoxanthin in solution are separate entities: dumping the fucoxanthin stimulated emission at 950 nm selectively affected the ICT state, while the influence on the S_1 state was delayed due to equilibration between the S_1 and ICT states.[20] A comparable situation occurs for fucoxanthin in FCP as evidenced by the data shown here. The effect of dumping the ICT population via the stimulated emission at 950 nm is shown by the grey curve in Fig. 2.23. It is obvious that the net effect of the dump pulse does not match the pump-probe spectrum. If the S_1 and ICT states were one entity, all features in the pump-probe spectrum should be affected in the same way, resulting in the double difference (PDP-PP) spectrum with the same shape as the PP spectrum. Instead, the double difference spectrum has its amplitude shifted towards the 600-700 nm spectral region, clearly showing that the ICT state is selectively affected by the dumping.

2.2. Ultrafast multi-pulse transient absorption spectroscopy of
fucoxanthin chlorophyll a protein from Phaeodactylum tricornutum

125

Thus, even in FCP the S_1 and ICT states are separate states in equilibrium. The distortion of equilibrium by the dump pulse reveals the S_1-ICT equilibration dynamics that is manifested by the slow rise of the double difference kinetics in the S_1 region (Fig. 2.24 and 2.25). Since the effect is more pronounced at 77 K (another evidence that the ICT character is enhanced at 77 K), we will focus here on the low temperature data.

The S_1-ICT equilibration dynamics can be visualized by monitoring the time dependence of the amplitude ratio of the S_1-like (565 nm) and ICT-like (645 nm) transitions shown in Fig. 2.26a. For fucoxanthin in acetonitrile, this ratio is constant in PP spectra, because the S_1 and ICT states decays with the same lifetime.[48] In FCP, the S_1/ICT amplitude ratio in PP spectra is slanted due to presence of a non-transferring fucoxanthin, which has a stronger signal in the S_1 region and decays much slower ($\sim$70 ps) than fucoxanthins transferring energy to Chl *a*. This results in the S_1/ICT amplitude ratio increasing with time as shown by the black curve in Fig. 2.26a.

Application of the 950 nm dump pulse at 2 ps after excitation immediately affects the S_1/ICT amplitude ratio: the ICT band is disturbed more, thus the S_1/ICT ratio increases suddenly. Then, due
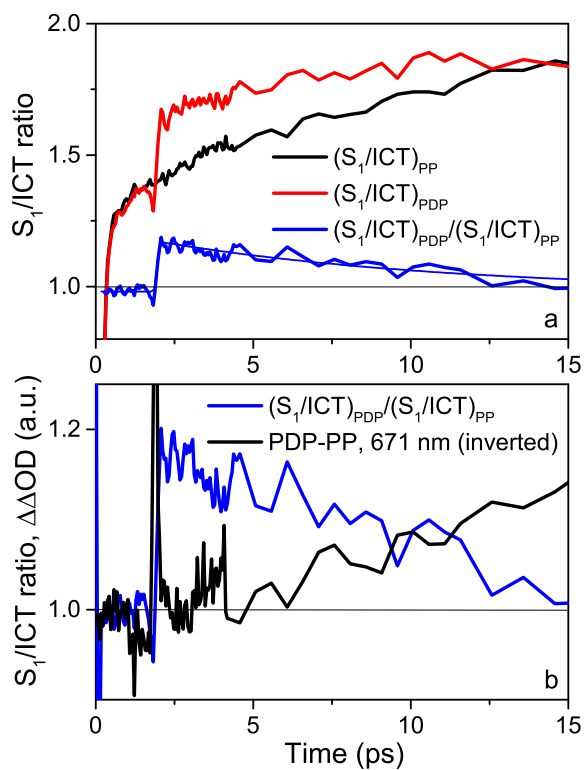
FIGURE 2.26: (a) Time dependence of the magnitude ratio of the S1 and ICT bands extracted from data measured in the PP (black) and PDP (red) regimes. The blue curve is the ratio of the red and black curves and shows recovery of the distortion caused by the dump pulse. (b) Comparison of the recovery of the dump-induced distortion of the S1/ICT ratio (blue) and effect of the dump pulse on Qy bleaching (black). All data were measured at 77 K.

to the S_1-ICT equilibration, the S_1/ICT ratio returns to its original value. The equilibration dynamics is better visualized by normalizing the S_1/ICT amplitude ratio of this PDP regime to its value in the PP regime (blue curve in Fig. 2.26a). This normalized ratio purely monitors the equilibration dynamics between the S_1 and ICT states. Thus, the data in Fig. 2.26a shows that the S_1-ICT equilibrium distorted by the dump pulse is fully restored within a few picoseconds. Fitting the time-dependence of the normalized ICT ratio gives a net equilibration lifetime of ~ 7 ps. Therefore, our data corroborate recent PDP experiments on fucoxanthin in methanol,[20] or peridinin in PCP,[35] demonstrating that the coupled S_1/ICT state can be viewed as a single potential surface with two minima corresponding to the S_1 and ICT states.

Finally, other evidence for the S_1 and ICT states being separate entities comes from the initial spike in the double difference kinetics in the S_1 spectral region (Fig. 2.24a and Fig. 2.25a). This sudden drop in the S_1 population caused by the 950 nm dump pulse results from the presence of excited state absorption from the S_1 part of the potential surface that overlaps with ICT stimulated emission. The presence of such excited state absorption may be inferred from the near-IR probe targeting the S_1-S_2 transition [33, 44]. Then a fraction of the 950 nm light is used to re-pump the higher vibrational levels of the S_2 state via the S_1-S_2 transition. Clearly, only the S_1 state is affected as no such signal is detected in the ICT kinetics measured at 645 nm (Fig 2.24c and Fig. 2.25c) This provides further evidence that the S_1 and ICT states can be independently affected.

The S_1/ICT energy transfer pathway in FCP

Having established that fucoxanthin S_1 and ICT states in FCP are two separate states that equilibrates on ~ 7 ps time scale at 77 K, we will discuss the identity of the energy donor in the S_1/ICT-Chl *a* pathway. This energy transfer channel to Chl *a* is very efficient in essentially all light-harvesting complexes binding keto-carotenoids, regardless their structure. So far, the "collective" S_1/ICT state has usually been considered the donor state, as no distinction between the S_1 and ICT states were possible in standard pump-probe spectroscopy, used almost exclusively to follow the energy transfer in these

2.2. Ultrafast multi-pulse transient absorption spectroscopy of fucoxanthin chlorophyll a protein from Phaeodactylum tricornutum

127

complexes. Also, theoretical studies, which focused on PCP as the only keto-carotenoid binding light harvesting protein with known structure, assumed only one state as the energy donor, albeit some of these studies were able to reproduce the experimental transfer rates quite accurately.[49,50] Recently, even other schemes pointing to a distorted S_2 state of peridinin as the energy donor in PCP have been suggested.[51]

Here, however, we show that the S_1/ICT state consists of two individual states in equilibrium. Therefore, it is natural to ask which of these two states is the primary energy donor in the S_1/ICT route. This question has been recently addressed by Redeckas et al[35] for the PCP complex. Based on PDP data they concluded that the ICT part of the S_1/ICT potential surface is the key donor in the S_1/ICT route.[35] The energy transfer routes in FCP are more complex than in PCP as there are clearly two fucoxanthin donors, representing the fast and slow S_1/ICT channel. Since we have applied the dump pulse at 2 ps after excitation, we predominantly affect the 'slow' ones, because the 'fast' fucoxanthins have already transferred energy to Chl *a*.

Even though the absence of any significant effect of the dump pulse on kinetics measured in the maximum of Q_y bleaching (Fig. 2.25c) may indicate that the dump-induced processes could be just due to the non-transferring fucoxanthin, expanding the time scale beyond 6 ps proves opposite. In Fig. 2.26b, the double-difference PDP-PP kinetic measured at 671 nm is shown at a longer time scale. Clearly, the dump pulse at 950 nm disturbs the Q_y kinetic, but the effect is visible only after a few picoseconds. The reason for this slow onset is explained here. The dump pulse removes a fraction of excited fucoxanthin molecules and those excitations are lost from the system thus they cannot transfer energy to Chl *a*. However, because the energy transfer from fucoxanthin to Chl *a* takes some time, the loss of Chl *a* population must appear with the expected fucoxanthin-Chl *a* energy transfer rate. Thus, the slow appearance of Chl *a* disturbance shown in Fig. 2.26b confirms our assumption that the dump pulse at 2 ps hits predominantly the slow-transferring fucoxanthins in FCP, which at 77 K transfer energy to Chl *a* with a ~6 ps time constant. A comparable situation, albeit with different time constants, has been reported for PCP.[35]

The observed behavior may suggest that the ICT state is the primary donor in the S_1/ICT route: the selective dumping of a fraction of fucoxanthin ICT population 'propagates' to Chl *a* with a time constant corresponding to the fucoxanthin-Chl *a* energy transfer rate, pointing to the ICT state as energy donor. However, the slow fucoxanthins transfer energy to Chl *a* at 77 K with ∼6 ps time constant (Fig. 2.22b); therefore, the S_1-ICT equilibration occurs with roughly the same time constant as energy transfer. Thus, the involvement of the S_1 part of the S_1/ICT potential surface in donating energy to Chl *a* in FCP must also be considered. In fact, assigning the ICT state as the sole energy donor in the S_1/ICT-Chl *a* route in FCP brings some serious complications. One major complication is the spectral overlap between the donor emission and acceptor absorption. Even though mechanisms other than Förster energy transfer have been suggested for the S_1/ICT-Chl *a* route,[35] the spectral overlap is a direct manifestation of the energy conservation law, thus must be obeyed regardless the mechanism. The energy of the donor state must be larger than the acceptor state. This is not easy to fulfill assuming the ICT state as the energy donor since its emission extends beyond 1000 nm,[16,33] while the lowest energy acceptor states are around 680 nm. Even though the emission spectrum of the ICT may reach below 680 nm, it is nearly impossible to reconcile high (∼90%) efficiency of the S_1/ICT-Chl *a* pathway, because a large fraction of the excited states emits at energies not sufficient to excite a Chl *a* molecule.

In order to achieve a more quantitative insight, we used a simplified model of the excited state dynamics of fucoxanthin in FCP (Fig. 2.27) to fit the double difference (PP-PDP) kinetics (blue traces in Fig. 72.25. In this simplified model we assume the following properties: 1) the excitation energy flow was initiated from an initially excited state decaying within 100 fs into S_1 and ICT states; 2) the population transfer between the S_1 and ICT states is reversible, characterized by the respective rate constants k_{S1ICT} and k_{ICTS1}; 3) both S_1 and ICT states decay independently into a common ground state. We have incorporated fucoxanthin-Chl *a* energy transfer testing two transfer pathways: either from S_1 or from the ICT state. Based on the results of the analysis of the excitation energy flow (Fig. 2.22b), the model

2.2. Ultrafast multi-pulse transient absorption spectroscopy of
fucoxanthin chlorophyll a protein from Phaeodactylum tricornutum

129

was also required to fit the observed ∼6.6 ps lifetime of the energy donor.

The dynamics of the states within the model were treated as a simulation of population transfer and decay and whose rates were determined as an eigenvalue problem of the first order from the time of the dump, the time at which the model would be relevant. The simulation was run for both control (pump-probe, PP) and dumped conditions (PDP), and the simulated PP – PDP kinetics were then used to concurrently fit the experimental PP – PDP kinetics of fucoxanthin and Chl a (Fig. 2.27). This yielded the rate constants and three scaling factors converting concentrations into absorbances (∼extinction coefficients). No bounds were applied to the fitted parameters during the optimization. In the first step

FIGURE 2.27: (top) Simplified model used for fitting the PDP data. Each process is labeled by the corresponding time constant in picoseconds. (bottom) Fitting results obtained from the model. The fitted data are the PDP-PP double difference kinetics shown also in Fig. 2.25.

of the analysis, the effect of initial conditions was tested by running the fit ∼200 times with different randomized initial parameter sets covering a wide range of values (e.g. 0-100 ps for the rate constants). Rather surprisingly, for the ICTChl a energy transfer scheme, all the tested initial parameter sets caused the procedure to converge to physically meaningless results, such as negative scaling factors or negative values for the branching ratios from the S_2 state. On the contrary, for the S_1Chl a energy transfer, plausible best fit values of the time constants were found: $S_1 \rightarrow$ICT 11.7 ps, ICT$\rightarrow S_1$ 6.9 ps, $S_1 \rightarrow$Chl a

1.9 ps, $S_1 \rightarrow So$ 40 ps, ICT$\rightarrow S_0$ 30 ps. The yield of the S_2 decay into S_1 was below 10%. The apparent ratio of the extinction coefficients of the S_1-like and ICT-like transitions yielded value of $\sim$2.7. Confidence intervals for these best fit parameters were obtained using the Monte-Carlo (MC) approach as described in [52] by fitting 10000 simulated datasets generated using the best fit parameters and standard deviation of fit residuals (root mean square). Each fit of an MC dataset started from a random initial estimate of parameters (varied within $\pm$10 % of the value used to obtain the best fit parameters). The resulting distributions of the fit parameters obtained by MC analysis runs can be found in the Supplementary material.

Thus, our model favors the S_1 part of the S_1/ICT potential surface as the main energy donor. Yet, it is important to stress that this assignment applies only to the slow, $\sim$6 ps, fucoxanthin-Chl *a* energy transfer channel. The fast, sub-picosecond energy transfer channel that actually dominates at 77 K has not been affected by the dump pulse at 2 ps employed in this study. For the fast channel, the whole dynamics will be more complicated as it is likely that unrelaxed, hot S_1 and/or ICT states will be involved in energy transfer; thus the ICT state may be significantly involved in this channel as suggested by Redeckas et al. for PCP.[35]

2.2.5   Conclusions

Ultrafast transient absorption spectroscopy shows that FCP antenna is a robust light-harvesting system that effectively collects light. Our results on FCP from *P. tricornutum* does not differ much from the earlier results reported on FCP from other organisms,[25,28−30,32,53] showing that small differences in FCP structure and organization of subunits do not significantly affect light harvesting efficiency. Moreover, other light-harvesting systems closely related to FCP, such as acpPC from *Amphidinium carterae* binding peridinin,[41,42] or the CLH complex from *Chromera velia*,[54] exhibit energy transfer efficiencies, routes, and energy transfer times comparable to that in FCP, indicating that major structural features represent the key factor determining efficiency and routes of energy transfer between carotenoids and Chl *a*.

2.2. Ultrafast multi-pulse transient absorption spectroscopy of fucoxanthin chlorophyll a protein from Phaeodactylum tricornutum

131

In FCP from *P. tricornutum*, three major energy transfer pathways are active. The first utilizes the route via the S_2 state of fucoxanthin and, as for many other systems, operates on sub-100 fs time scale. The other two pathways go via the coupled S_1/ICT state which can be viewed as a potential surface with two minima corresponding to the S_1 and ICT states in equilibrium. PDP experiments show that these two states can be affected individually by distorting the equilibrium via dumping the ICT population to the ground state. Analysis of PDP data suggests that the slow S_1/ICT-Chl *a* channel, which is more pronounced at room temperature, utilizes the S_1 part of the potential surface as the energy donor. The fast, subpicosecond S_1/ICT-Chl *a* channel becomes dominant at 77 K, making the overall S_1/ICT-Chl *a* transfer faster at 77 K. Whether the S_1 or ICT state is the major energy donor in this route remains unclear and will be a subject of subsequent studies.

Supplementary Information
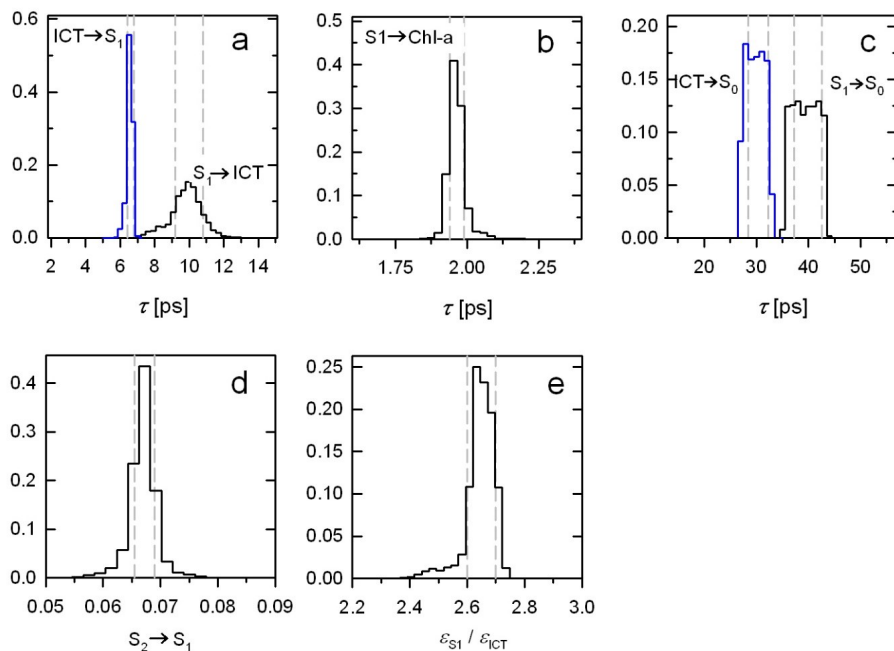
FIGURE 2.28: Distribution of the time constants (a-c), fraction of the S_1 population going to the S_1 part of the S_1/ICT potential surface (d) and ratio of S_1-S_n and ICT-S_N extinction coefficients (e) resulting from Monte-Carlo approach used for fitting the pump-dump-probe data. Dashed lines denote the confidence intervals.

References (Paper II)

1. T. Mirkovic, E.E. Ostroumov, J.M. Anna, R. van Grondelle, Govindjee, G.D. Scholes, Light absorption and energy transfer in the antenna complexes of photosynthetic organisms, Chem. Rev. 117 **2017** 249-293.

2. T. Polívka, H.A. Frank, Molecular factors controlling photosynthetic light harvesting by carotenoids, *Acc. Chem. Res. 43* **2010** 1125-1134.

3. R. Croce, H. van Amerongen, Natural strategies for photosynthetic light harvesting, *Nat. Chem. Biol. 10* **2014** 492-501.

2.2. Ultrafast multi-pulse transient absorption spectroscopy of fuchoxanthin chlorophyll a protein from Phaeodactylum tricornutum

133

4. G.T. Oostergetel, H. van Amerongen, E.J. Boekema, The chlorosome: a prototype for efficient light harvesting in photosynthesis, *Photosynth. Res. 104* **2010** 245-255.

5. C.D.P. Duffy, A.V. Ruban, Dissipative pathways in the photosystem-II antenna in plants, *J. Photochem. Photobiol. B 152* **2015** 215-226.

6. H. Staleva, J. Komenda, M.K. Shukla, V. Šlouf, R. Kaňa, T. Polívka, R. Sobotka, Mechanism of photoprotection in the cyanobacterial ancestor of plant antenna proteins, *Nat. Chem. Biol. 11* **2015** 287-291.

7. T. Polívka, V. Sundström, Ultrafast dynamics of carotenoid excited states - From solution to natural and artificial systems, *Chem. Rev. 104* **2004** 2021-2071.

8. H. Hashimoto, Y. Sugai, C. Uragami, A.T. Gardiner, R.J. Cogdell, Natural and artificial light-harvesting systems utilizing the functions of carotenoids, *J Photochem. Photobiol. C 25* **2015** 46-70.

9. A.V. Ruban, R. Berera, C. Ilioaia, I.H.M. van Stokkum, J.T.M. Kennis, A.A. Pascal, H. van Amerongen, B. Robert, P. Horton, R. van Grondelle, Identification of a mechanism of photoprotective energy dissipation in higher plants, *Nature 450* **2007** 575-U522.

10. N.E. Holt, D. Zigmantas, L. Valkunas, X.P. Li, K.K. Niyogi, G.R. Fleming, Carotenoid cation formation and the regulation of photosynthetic light harvesting, *Science 307* **2005** 433-436.

11. S. Bode, C.C. Quentmeier, P.N. Liao, N. Hafi, T. Barros, L. Wilk, F. Bittner, P.J. Walla, On the regulation of photosynthesis by excitonic interactions between carotenoids and chlorophylls, Proc. Natl. Acad. Sci. U.S.A. 106 **2009** 12311-12316.

12. T. Buckup, M. Motzkus, Multidimensional time-resolved spectroscopy of vibrational coherence in iopolyenes, *Annu. Rev. Phys. Chem. 65* **2014** 39-57.

13. W. Fuss, Y. Haas, S. Zilberg, Twin states and conical intersections in linear polyenes, *Chem. Phys. 259* **2000** 273-295.

14. M. Maiuri, D. Polli, D. Brida, L. Luer, A.M. LaFountain, M. Fuciman, R.J. Cogdell, H.A. Frank, G. Cerullo, Solvent-dependent activation of intermediate excited states in the energy relaxation pathways of spheroidene, *Phys. Chem. Chem. Phys. 14* **2012** 6312-6319.

15. T. Polívka, V. Sundström, Dark excited states of carotenoids: Consensus and controversy, *Chem. Phys. Lett. 477* **2009** 1-11.

16. J.A. Bautista, R.E. Connors, B.B. Raju, R.G. Hiller, F.P. Sharples, D. Gosztola, M.R. Wasielewski, H.A. Frank, Excited state properties of peridinin: Observation of a solvent dependence of the lowest excited singlet state lifetime and spectral behavior unique among carotenoids, *J. Phys. Chem. B 103* **1999** 8751-8758.

17. H.A. Frank, J.A. Bautista, J. Josue, Z. Pendon, R.G. Hiller, F.P. Sharples, D. Gosztola, M.R. Wasielewski, Effect of the solvent environment on the spectroscopic properties and dynamics of the lowest excited states of carotenoids, *J. Phys. Chem. B 104* **2000** 4569-4577.

18. D. Zigmantas, T. Polívka, R.G. Hiller, A. Yartsev, V. Sundström, Spectroscopic and dynamic properties of the peridinin lowest singlet excited states, *J. Phys. Chem. A 105* **2001** 10296-10306.

19. D. Kosumi, T. Kajikawa, S. Okumura, M. Sugisaki, K. Sakaguchi, S. Katsumura, H. Hashimoto, Elucidation and control of an intramolecular charge transfer property of fucoxanthin by a modification of its polyene chain length, *J. Phys. Chem. Lett. 5* **2014** 792-797.

20. K. Redeckas, V. Voiciuk, M. Vengris, Investigation of the S1/ICT equilibrium in fucoxanthin by ultrafast pump-dump-probe and femtosecond stimulated Raman scattering spectroscopy, *Photosynth. Res. 128* **2016** 169-181.

2.2. Ultrafast multi-pulse transient absorption spectroscopy of fucoxanthin chlorophyll a protein from Phaeodactylum tricornutum

135

21. M. Di Valentin, E. Meneghin, L. Orian, A. Polimeno, C. Buchel, E. Salvadori, C.W.M. Kay, D. Carbonera, Triplet-triplet energy transfer in fucoxanthin-chlorophyll protein from diatom Cyclotella meneghiniana: Insights into the structure of the complex, *BBA-Bioenergetics 1827* **2013** 1226-1234.

22. L. Premvardhan, L. Bordes, A. Beer, C. Buchel, B. Robert, Carotenoid structures and environments in trimeric and oligomeric fucoxanthin chlorophyll a/c_2 proteins from resonance Raman spectroscopy, *J. Phys. Chem. B 113* **2009** 12565-12574.

23. C. Büchel, Fucoxanthin-chlorophyll proteins in diatoms: 18 and 19 kDa subunits assemble into different oligomeric states, *Biochemistry 42* **2003** 13027-13034.

24. A. Röding, E. Boekema, C. Büchel, The structure of FCPb, a light-harvesting complex in the diatom Cyclotella meneghiniana, *Photosynth. Res. 135* **2016** 203-211.

25. E. Papagiannakis, I.H.M. van Stokkum, H. Fey, C. Büchel, R. van Grondelle, Spectroscopic characterization of the excitation energy transfer in the fucoxanthin-chlorophyll protein of diatoms, *Photosynth. Res. 86* **2005** 241-250.

26. B. Lepetit, D. Volke, M. Szabo, R. Hoffmann, G.Z. Garab, C. Wilhelm, R. Goss, Spectroscopic and molecular characterization of the oligomeric antenna of the diatom Phaeodactylum tricornutum, *Biochemistry 46* **2007** 9813-9822.

27. M. Herbstová, D. Bína, R. Kaňa, F. Vácha, R. Litvín, Red-light phenotype in a marine diatom involves a specialized oligomeric red-shifted antenna and altered cell morphology, *Sci. Rep. 7* **2017**.

28. N. Gildenhoff, S. Amarie, K. Gundermann, A. Beer, C. Büchel, J. Wachtveitl, Oligomerization and pigmentation dependent excitation energy transfer in fucoxanthin-chlorophyll proteins, *BBA-Bioenergetics 1797* **2010** 543-549

29. N. Gildenhoff, J. Herz, K. Gundermann, C. Büchel, J. Wachtveitl, The excitation energy transfer in the trimeric fucoxanthin-chlorophyll protein from Cyclotella meneghiniana analyzed by polarized transient absorption spectroscopy, *Chem. Phys. 373* **2010** 104-109.

30. A. Gelzinis, V. Butkus, E. Songaila, R. Augulis, A. Gall, C. Büchel, B. Robert, D. Abramavicius, D. Zigmantas, L. Valkunas, Mapping energy transfer channels in fucoxanthin-chlorophyll protein complex, *BBA-Bioenergetics 1847* **2015** 241-247.

31. E. Songaila, R. Augulis, A. Gelzinis, V. Butkus, A. Gall, C. Büchel, B. Robert, D. Zigmantas, D. Abramavicius, L. Valkunas, Ultrafast energy transfer from chlorophyll c_2 to chlorophyll a in fucoxanthin-chlorophyll protein complex, *J. Phys. Chem. Lett. 4* **2013** 3590-3595.

32. D. Kosumi, M. Kita, R. Fujii, M. Sugisaki, N. Oka, Y. Takaesu, T. Taira, M. Iha, H. Hashimoto, Excitation energy transfer dynamics of brown algal photosynthetic antennas, *J. Phys. Chem. Lett. 3* **2012** 2659-2664.

33. D. Zigmantas, R.G. Hiller, F.P. Sharples, H.A. Frank, V. Sundström, T. Polívka, Effect of a conjugated carbonyl group on the photophysical properties of carotenoids, *Phys. Chem. Chem. Phys. 6* **2004** 3009-3016.

34. E. Papagiannakis, M. Vengris, D.S. Larsen, I.H.M. van Stokkum, R.G. Hiller, R. van Grondelle, Use of ultrafast dispersed pump-dump-probe and pump-repump-probe spectroscopies to explore the light-induced dynamics of peridinin in solution, *J. Phys. Chem. B 110* **2006** 512-521.

35. K. Redeckas, V. Voiciuk, D. Zigmantas, R.G. Hiller, M. Vengris, Unveiling the excited state energy transfer pathways in peridinin-chlorophyll a-protein by ultrafast multi-pulse transient absorption spectroscopy, *BBA-Bioenergetics 1858* **2017** 297-307.

36. Z. Gardian, R. Litvín, D. Bína, F. Vácha, Supramolecular organization of fucoxanthin-chlorophyll proteins in centric and pennate diatoms, *Photosynth. Res. 121* **2014** 79-86.

2.2. Ultrafast multi-pulse transient absorption spectroscopy of fucoxanthin chlorophyll a protein from Phaeodactylum tricornutum

137

37. R.R. Guillard, J.H. Ryther, Studies of Marine Planktonic Diatoms .1. Cyclotella Nana Hustedt, and Detonula Confervacea (Cleve) Gran, *Can. J. Microbiol. 8* **1962** 229-239.

38. M. Herbstová, D. Bína, P. Koník, Z. Gardian, F. Vácha, R. Litvín, Molecular basis of chromatic adaptation in pennate diatom Phaeodactylum tricornutum, *BBA-Bioenergetics 1847* **2015** 534-543.

39. I.H.M. van Stokkum, D.S. Larsen, R. van Grondelle, Global and target analysis of time-resolved spectra, *Biochimica et Biophysica Acta-Bioenergetics 1657* **2004** 82-104.

40. L. Premvardhan, B. Robert, A. Beer, C. Büchel, Pigment organization in fucoxanthin chlorophyll a/c_2 proteins (FCP) based on resonance Raman spectroscopy and sequence analysis, *BBA-Bioenergetics 1797* **2010** 1647-1656.

41. D.M. Niedzwiedzki, J. Jiang, C.S. Lo, R.E. Blankenship, Spectroscopic properties of the Chlorophyll a-Chlorophyll c_2-Peridinin-Protein-Complex (acpPC) from the coral symbiotic dinoflagellate Symbiodinium, *Photosynth. Res. 120* **2014** 125-139.

42. V. Šlouf, M. Fuciman, S. Johanning, E. Hofmann, H.A. Frank, T. Polívka, Low-temperature time-resolved spectroscopic study of the major light-harvesting complex of Amphidinium carterae, *Photosynth. Res. 117* **2013** 257-265.

43. R.P. Ilagan, J.F. Koscielecki, R.G. Hiller, F.P. Sharples, G.N. Gibson, R.R. Birge, H.A. Frank, Femtosecond time-resolved absorption spectroscopy of main-form and high-salt peridinin-chlorophyll a-proteins at low temperatures, *Biochemistry 45* **2006** 14052-14063.

44. D. Zigmantas, R.G. Hiller, V. Sundström, T. Polívka, Carotenoid to chlorophyll energy transfer in the peridinin-chlorophyll-a-protein complex involves an intramolecular charge transfer state, *Proc. Natl. Acad. Sci. U.S.A. 99* **2002** 16760-16765.

45. T. Schulte, D.M. Niedzwiedzki, R.R. Birge, R.G. Hiller, T. Polívka, E. Hofmann, H.A. Frank, Identification of a single peridinin sensing Chl-a excitation in reconstituted PCP by crystallography and spectroscopy, *Proc. Natl. Acad. Sci. U.S.A. 106* **2009** 20764-20769.

46. T. Polívka, T. Pascher, V. Sundström, R.G. Hiller, Tuning energy transfer in the peridinin-chlorophyll complex by reconstitution with different chlorophylls, *Photosynth. Res. 86* **2005** 217-227.

47. D.M. Niedzwiedzki, T. Kajikawa, K. Aoki, S. Katsumura, H.A. Frank, Excited states energies and dynamics of peridinin analogues and the nature of the intramolecular charge transfer state in carbonyl-containing carotenoids, *J. Phys. Chem. B 117* **2013** 6874-6887.

48. V. Kuznetsova, P. Chábera, R. Litvín, T.G. Polívka, M. Fuciman, Effect of isomerization on excited-state dynamics of carotenoid fucoxanthin, *J. Phys. Chem. B 121* **2017** 4438-4447.

49. W.P. Bricker, C.S. Lo, Efficient pathways of excitation energy transfer from delocalized S2 excitons in the Peridinin-chlorophyll a-protein complex, *J. Phys. Chem. B 119* **2015** 5755-5764.

50. W.P. Bricker, C.S. Lo, Excitation energy transfer in the Peridinin-chlorophyll a-protein complex modeled using configuration interaction, *J. Phys. Chem. B 118* **2014** 9141-9154.

51. J.D. Roscioli, S. Ghosh, A.M. LaFountain, H.A. Frank, W.F. Beck, Quantum coherent excitation energy transfer by carotenoids in photosynthetic light harvesting, *J. Phys. Chem. Lett. 8* **2017** 5141-5147.

52. A.C. H. J. Motulsky, A Practical Guide to Curve Fitting, GraphPad Software, San Diego, 2003.

53. V. Butkus, A. Gelzinis, R. Augulis, A. Gall, C. Büchel, B. Robert, D. Zigmantas, L. Valkunas, D. Abramavicius, Coherence and population dynamics of chlorophyll excitations in FCP complex: Two-dimensional spectroscopy study, *J. Chem. Phys. 142* **2015** 212414.

2.2. Ultrafast multi-pulse transient absorption spectroscopy of
fucoxanthin chlorophyll a protein from Phaeodactylum tricornutum

139

54. M. Durchan, G. Keşan, V. Šlouf, M. Fuciman, H. Staleva, J. Tichý, R. Litvín, D. Bína, F. Vácha, T. Polívka, Highly efficient energy transfer from a carbonyl carotenoid to chlorophyll a in the main light harvesting complex of Chromera velia, *BBA-Bioenergetics 1837* **2014** 1748-1755.

2.3 Non-Conjugated Acyloxy Group Deactivates the Intramolecular Charge Transfer State in the Carotenoid Fucoxanthin

This chapter is based on PAPER III:

Abstract

We used ultrafast transient absorption spectroscopy to study excited-state dynamics of the keto-carotenoid fucoxanthin (Fx) and its two derivatives: 19'-butanoyloxyfucoxanthin (bFx) and 19'-hexanoyloxyfucoxanthin (hFx). These derivatives occur in some light-harvesting systems of photosynthetic microorganisms and their presence is typically related to stress conditions. Even though the hexanoyl (butanoyl) moiety is not a part of the conjugated system of bFx and hFx, their absorption spectra in polar solvents exhibit more pronounced vibrational bands of the S_2 state than for Fx. The effect of the non-conjugated acyloxy moiety is further observed in transient absorption spectra which for Fx exhibits characteristic features of an intramolecular charge transfer (ICT) state in all polar solvents. For bFx and hFx, however, much weaker ICT features are detected in methanol, and the spectral markers of the ICT state disappear completely in polar, but aprotic acetonitrile. The presence of the acyloxy moiety also alters the lifetimes of the S_1/ICT state. For Fx, the lifetimes are 60, 30, and 20 ps in n-hexane, acetonitrile, and methanol; whereas for bFx and hFx, these lifetimes yield 60, 60, and 40 ps. Testing the S_1/ICT state lifetimes of hFx in other solvents revealed that some ICT features can be induced only in polar, protic solvents (methanol, ethanol, and ethylene glycol). Thus, bFx and hFx represent a rather rare example of a system in which a non-conjugated functional group significantly alters excited-state dynamics.

By comparison with other carotenoids, we show that a keto group at the acyloxy tail, even though it is not in conjugation, affects the electron distribution along the conjugated backbone, resulting in the observed decrease of the ICT character of the S_1/ICT state of bFx and hFx.

2.3.1   Introduction

Carotenoids have attracted much attention for their specific spectroscopic properties that significantly differ from those of other pigments found in nature. Carotenoids have extremely low fluorescence quantum yields even though they are strong colorants with molar extinction coefficients around 10^5 M^{-1} cm^{-1}.[1,2] This unusual property of carotenoids has its origin in the one-photon forbidden transition between the ground (S_0) and the first excited (S_1) states, resulting in absence of fluorescence from the S_1 state. The characteristic absorption band of carotenoids in the blue-green part of the visible spectrum is then due to the S_0-S_2 transition which has large oscillator strength providing the large extinction coefficients.[3]

Studies of excited-state dynamics flourished with the development of ultrafast spectroscopic techniques because excited state lifetimes of carotenoids, abundant in nature, usually do not exceed 100 ps.[4] The absorbing S_2 state relaxes to form a vibrationally hot S_1 state in less than 300 fs,[5,6] though the pathways of the S_2-S_1 internal conversion remain a matter of debate as the process may involve additional dark excited states.[7−10] The unrelaxed S_1 state cools down in less than 1 ps,[11] and the S_1 state then decays back to the ground state on a picosecond time scale. The actual S_1 lifetime depends on the conjugation length (N, number of conjugated C=C bonds in the chromophore), spanning the range from $\sim$1 ps (N = 13) to $\sim$150 ps (N = 7).[4]

For a long time it has been believed that the S_1 lifetime is essentially independent of solvent properties. This paradigm was, however, altered at the turn of the millennium for keto-carotenoids. These carotenoids have their conjugation extended to one or more C=O groups which introduce significant asymmetry in the conjugated backbone. As shown for the first time in 1998 for the carotenoid peridinin,[12] the conjugated keto group introduces an intramolecular charge transfer (ICT) state that makes the spectroscopic properties, especially the S_1 lifetime, polarity-dependent. Since then, it has been established that any carotenoid with an asymmetrically positioned keto group in conjugation will exhibit polarity-dependent behavior, and the shorter the conjugation length is, the more pronounced the polarity-induced changes are.[13−17]

*2.3. Non-Conjugated Acyloxy Group Deactivates the Intramolecu-
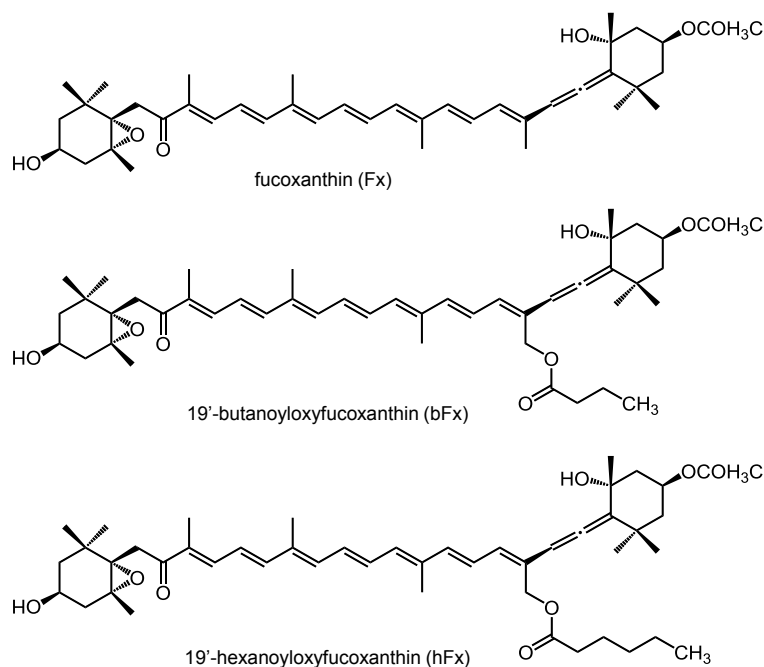lar Charge Transfer State in the Carotenoid Fucoxanthin*

143

FIGURE 2.29: Molecular structures of fucoxanthin and its two
derivatives.

The carotenoid fucoxanthin (Fig. 2.29) is a typical representative of the keto-carotenoid family. It is one of the most abundant carotenoids in nature as it is an integral part of the photosynthetic apparatus of marine algae and diatoms, usually bound to the fucoxanthin-chlorophyll protein (FCP). FCP is a light-harvesting protein in which fucoxanthin is the key antenna pigment absorbing light in the 450-550 nm region. Fucoxanthin transfers energy to chlorophyll with an efficiency approaching 100%, and most of the energy is transferred via the S_1 state which is coupled to the ICT state.[18,19] Since it is believed that this coupling is the key factor allowing such highly efficient energy transfer, the polarity-dependent effects of fucoxanthin have been a subject of numerous studies.

The ICT state can be readily monitored through its typical markers in the

transient absorption spectra. As the basic properties of the S_1 state can be extracted from the S_1-S_n excited state absorption band in transient absorption spectra, the ICT state can be traced either via the ICT-S_N transition, which is usually red-shifted from the S_1-S_n band, or via the ICT stimulated emission in the near-IR spectral region.[20] The ICT-related features occur solely for keto-carotenoids and are largely enhanced in polar solvents. For fucoxanthin, the S_1 and ICT features in transient absorption spectra are well-separated, making it an ideal system for study. The appearance of the ICT bands is also closely associated with shortening of the S_1 lifetime. The more pronounced the ICT bands are in transient absorption spectra, the shorter the S_1 lifetime. Interestingly, regardless of the solvent polarity, the S_1 and ICT bands decay with the same lifetime. This property that has been puzzling for a long time and has led to various interpretations of the concept of the S_1/ICT state, interpreted either as two strongly-coupled states[13,4,20] or as one state with varying degree of charge-transfer character.[21] Only recently, using pump-dump-probe spectroscopy on fucoxanthin, Redeckas et al. unequivocally showed that the S_1 and ICT states are indeed two individual, though coupled, states; and the identical lifetimes of the S_1 and ICT features in transient absorption spectra result from fast S_1-ICT equilibration.[22]

Besides the dependence of spectroscopic properties on solvent polarity, fucoxanthin is also strongly affected by the solvent proticity. The S_1/ICT lifetime yields 20 ps in the protic solvent methanol, but it is prolonged to 30 ps in aprotic acetonitrile, which is more polar than methanol.[23] This clearly demonstrates that factors other than polarity affect the spectroscopic properties of keto-carotenoids. The solvent proticity dependence has so far been identified only in a few keto-carotenoids, and although its origin remains unexplained, it must be related to the position of the keto group in the conjugated chain and/or presence of other groups such as an allene or a lactone in the conjugated system.[23]

The proticity dependence of fucoxanthin is an example of a phenomenon whereby specific structural features affect the spectroscopic properties. While the presence of an asymmetrically positioned keto group is enough to induce polarity-dependent behavior in keto-carotenoids, only some subtle structural

details may lead to the proticity dependence.[23] This raises the question of how the presence or absence of other functional groups in the carotenoid structure affect the spectroscopic properties. It was demonstrated using synthetic derivatives of peridinin that the position of the keto group at the lactone ring enhances the polarity-induced effects,[24] while the presence/absence of an allene group has a rather minor effect.[25] For very short conjugation lengths however, the presence of the allene group enhances the polarity-induced effects as reported for a short derivative of fucoxanthin.[26]

Both the lactone group of peridinin and the allene group of peridinin and fucoxanthin are part of the conjugated system of the carotenoids; therefore, some influence of the spectroscopic properties can be expected. However, can structural modifications which are not in the conjugation have any effect on spectroscopic properties? A vast amount of data reported on carotenoids during the past twenty years suggest that the answer is no. Number of examples can be found in the literature where non-conjugated structural modifications do not change the spectroscopic behavior of the carotenoids. For example, β-carotene and zeaxanthin, which differ by the presence of hydroxyl groups at the terminal rings, are spectroscopically identical.[4]

Nonetheless, a recent study of psittacofulvins, polyenes known as colorants of parrot feathers, demonstrated that in some specific cases even the groups that are not in conjugation may affect spectroscopic properties. The psittacofulvin studied by Adamec et al.[27] has a molecular structure comparable to the keto-carotenoid 8,8′-diapocarotene-8′-ol-8-al,[16] except that psittacofulvin lacks methyl groups—it is just a polyene chain with 8 conjugated C=C bonds terminated by a C=O group in conjugation. While the keto-carotenoid reported in Ref. 16 has comparable S_1/ICT lifetimes in methanol (18 ps) and acetonitrile (21 ps), for psittacofulvin the lifetimes in these two solvents differ substantially, yielding 15 ps and 35 ps, respectively.[27] Therefore, even groups which are not in conjugation may affect the spectroscopic properties, namely, the response to solvent polarity and proticity.

Here we compare excited state dynamics of fucoxanthin (Fx) with two fucoxanthin derivatives, 19'-butanoyloxyfucoxanthin (bFx) and 19'-hexanoyloxyfucoxanthin (hFx). These two derivatives, depicted along with

Fx in Fig. 2.29, contain a non-conjugated acyloxy moiety attached to C19'. These two derivatives occur naturally in some classes of Chromophyta.[28] They were identified in the photosynthetic apparatus of the coccolithophore *Emiliana huxleyi* (hFx) or in the heterokont alga *Aureococcus anophagefferens* (bFx),[28, 29] always along with Fx. Interestingly, the Fx/hFx(bFx) ratio is related to stress conditions. Under high light, high CO_2 or nutrient starvation conditions, the amount of hFx (bFx) increases at the expense of Fx,[30,31] suggesting that the acyloxy moiety provides some advantage for protection. In order to explore the possible influence of the acyloxy moiety on spectroscopic properties, we applied femtosecond transient absorption spectroscopy to study excited state dynamics of Fx, bFx, and hFx in different solvents. We show that, in contrast to Fx, the acyl moiety switches off the polarity-dependent behavior almost completely. Instead, the solvent proticity is the major factor affecting the excited state dynamics, demonstrating that the acyloxy moiety, though non-conjugated, significantly alters the spectroscopic properties.

2.3.2   Methods

Sample preparation

Fucoxanthin and its derivatives were obtained from cells of marine algae. Fucoxanthin was purified from cells of diatom *Phaeodactylum tricornutum* strain SAG 1090-1a. hFx was purified from coccolitophore alga *Emiliania huxleyi* strain CCMP1516, and bFx was purified from pelagophyte alga *Aureococcus anophagefferens* strain CCMP1984. All species were grown in a batch culture in an artificial sea water medium with a f/2 nutrient addition[32] in 5L Erlenmeyer flasks, illuminated with an intensity of 300 μmol photons.m^{-2}.s^{-1} by a metal-halide lamp (15h light/9h dark).

All pigment extraction and purification steps were carried out in the dark on ice; HPLC quality solvents were used. Pigments were extracted from harvested cells by several methanol extractions with brief (1.5 min) sonication. Crude pigment extracts were pooled, dried under vacuum, and dissolved in methanol for HPLC purification. Pigments were purified by an HPLC system consisting of a Pump Controller Delta 600, a manual

injection system, and a PDA 2996 detector (Waters, USA). Pigments were separated on a reverse-phase Zorbax SB-C18 column (4.6 x 150 mm, 5m, silica-based, non-endcapped; Agilent).[33] A ternary solvent system was used for elution with solvent A (80:20 methanol:0.5 M ammonium acetate (aq., pH 7.2 v/v), solvent B (90:10 acetonitrile:water), and solvent C (100 % ethyl acetate).[34] Pigments were identified on the basis of their absorption spectra and retention times. Collected fractions were dried under vacuum and stored at -20°C until further use. All samples were analyzed by HPLC before use to eliminate possible contamination or degradation artifacts.

Ultrafast spectroscopy

The femtosecond spectrometer used for collecting transient absorption spectra is based on an amplified Ti:Sapphire laser system. The femtosecond pulses were generated by a modular laser system consisting of an ultrafast Ti:sapphire regenerative amplifier (Spitfire Ace-100F, Spectra-Physics, USA) seeded with a Ti:sapphire oscillator (MaiTai SP, Spectra-Physics), and pumped by Nd:YLF laser (Empower 30, Spectra-Physics). The laser system produces ~100 fs pulses centered at 800 nm with a 1-kHz repetition rate. The produced pulses were divided into excitation and probe beams by a beam splitter. Tunable excitation pulses were generated by an optical parametric amplifier (TOPAS-C, Light Conversion, Lithuania). The probe pulses were generated by focusing a fraction of the 800 nm beam to a 2-mm sapphire plate to generate a broadband (450-750 nm), white-light pulse. In order to minimize chirp, the white-light beam was collimated by an off-axis parabolic mirror and split by a broadband, 50/50 beam splitter to a reference and probe beam. The probe beam was focused by a 150 mm spherical mirror to the sample where it overlapped with the excitation beam. Probe and reference beams were then focused to the entrance slit of a spectrograph where the beams were dispersed onto a double CCD array allowing measurements of transient spectra in a ~250 nm spectral window. The time delay between the excitation and probe pulses was introduced by a computer-controlled delay line. The mutual polarization of the excitation and probe beams was set to the magic angle (54.7°) by placing a polarization rotator in the excitation beam. For all measurements,

a 2-mm path length quartz cuvette was used. To avoid sample degradation, we employed a micro stirrer that continuously mixed the sample during the measurements. For all excitation wavelengths, neutral density filters were used to keep the excitation intensity at $\approx 10^{14}$ photons pulse^{-1} cm^{-2}. All measurements were realized at room temperature.

The spectro-temporal datasets were fitted globally using either DAFit software (Pascher Instruments) or the Glotaran package (glotaran.org). Both software packages fit the data to a sum of exponentials, including the numerical deconvolution of the response function, and a polynomial describing the chirp. The fitting procedure used either general linear regression (DAFit) or singular-value decomposition (Glotaran) to fit the data. To visualize the excited-state dynamics, we assumed that the excited system evolves according to a sequential, irreversible scheme. Each component in the sequential scheme represent individual excited-state species, and the spectral profile of each species is called evolution-associated difference spectrum (EADS).[35]

Calculations

To perform molecular dynamics (MD) simulations for solvation dynamics of carotenoids in different molecular solvents, general amber force field (GAFF) has been employed for carotenoids and molecular solvents.[36] The Restrained Electrostatic Potential[37] fitting procedure was used to calculate partial charges from geometric optimization molecules by Gaussian 09 package[38] by employing the Density Functional Theory (DFT) with the B3LYP/cc-pVDZ level. All simulated systems were energy-minimized by steepest descent minimization then equilibrated by 100 ps with restrained NVT (canonical ensemble), followed by 100 ps restrained NPT (isothermal–isobaric ensemble) molecular dynamics simulations. The linear constraint solver algorithm[39] was used for bonds involving hydrogen atoms. The short-range non-bonded interactions were truncated to zero with a cut-off at 1.2 nm, and the long-range, electrostatic interaction was calculated with the Particle Mesh Ewald method.[40] The V-rescale coupling algorithm[41] was used with time constant of 0.1 ps for temperature and pressure of all systems. All production runs were done in NPT

ensemble for 50 ns at 300 K with a time step of 2 fs. Simulations were performed by Gromacs 4.5.5 program package,[42] and the Visual Molecular Dynamics (VMD) program was used for visualizations of the trajectories and preparation of snapshots.[43]

2.3.3 Results

In this section we compare data measured for bFx and hFx with those of Fx. Since the two derivatives, bFx and hFx, exhibit essentially identical spectroscopic properties, we focus on comparison of hFx and Fx. All data measured for bFx can be found in the Supporting Information where they are compared to hFx to demonstrate the nearly identical spectroscopic properties of these two fucoxanthin derivatives.

Absorption spectra of hFx are compared to those of Fx in three solvents in Fig. 2.30. In n-hexane, both molecules exhibit the well-resolved vibrational bands of the S_2 state as expected for Fx in nonpolar solvent.[13,14] The hexanoyloxy moiety of hFx does not alter the resolution of vibrational bands, though the absorption spectra of Fx and hFx
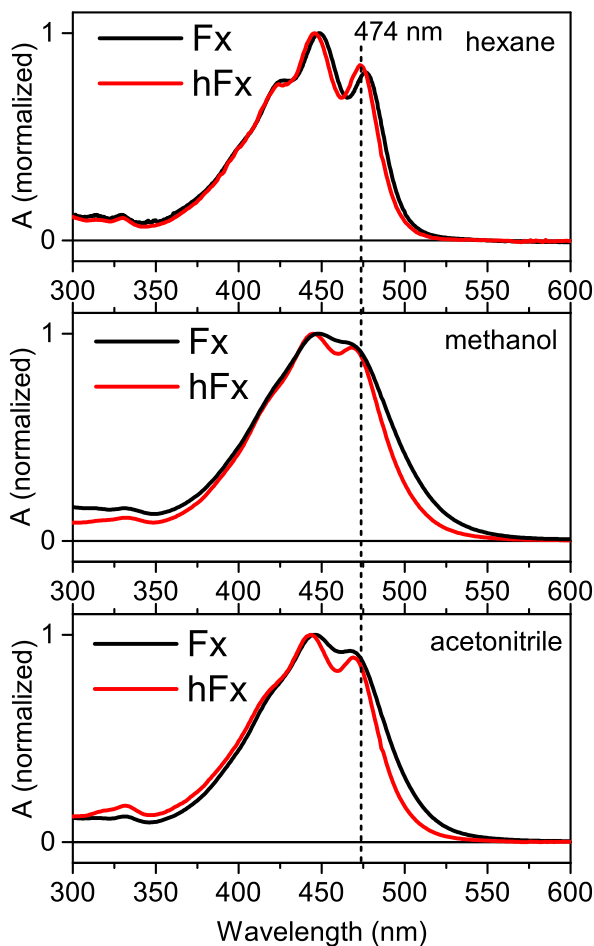
FIGURE 2.30: Absorption spectra of Fx (black) and hFx (red) in *n*-hexane, methanol, and acetonitrile. The 0-0 peak of hFx in *n*-hexane at 474 nm is marked as a refernce point.

in n-hexane are not identical. This is confirmed by a small blue-shift of the 0-0 band observed for hFx, which has a maximum at 474 nm, Fx peaks at 477 nm. The same 0-0 maximum of 474 nm is observed also for bFx (Fig. S2.36).

Moving the samples to polar solvents reveals a clear difference between the absorption spectra of Fx and hFx. In both molecules, the resolution of vibrational bands is diminished, but hFx, in contrast to Fx, still retains clearly distinct 0-0 and 0-1 vibrational bands. Also, the second typical polarity-induced effect reported for keto carotenoids, the asymmetric broadening of absorption spectrum towards lower energies,[13,14] is more pronounced in Fx than in hFx. Thus, although the hexanoyloxy moiety of hFx is not in conjugation, its effect on the response of the molecule to change of solvent polarity is clearly visible. It is worth mentioning that the proticity of the solvent also plays a role as the vibrational bands are more resolved in the aprotic acetonitrile than in protic methanol (Fig. 2.30). The energy of the S_0-S_2 transition, however, is not affected by polarity.
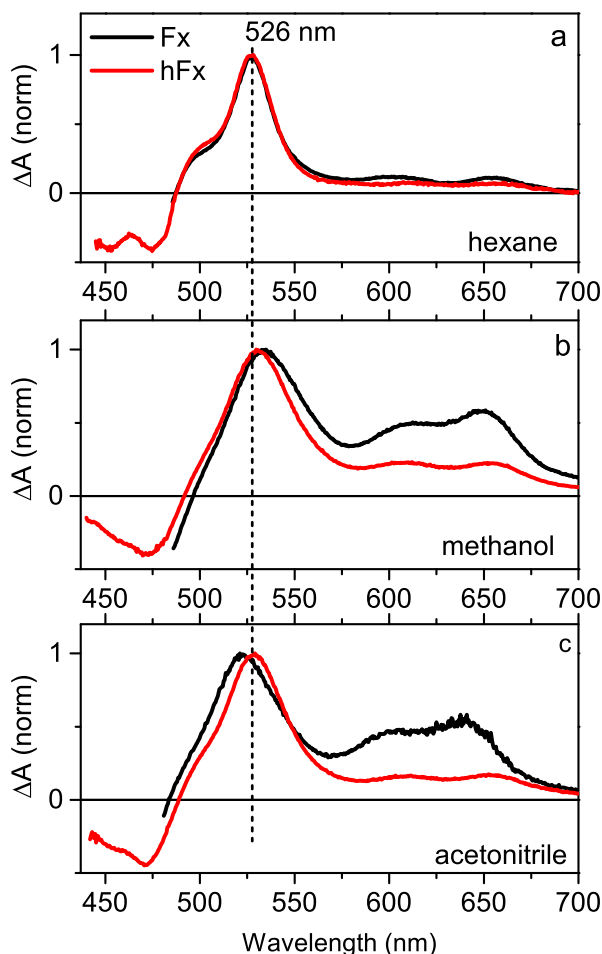
FIGURE 2.31: Transient absorption spectra of Fx (black) and hFx (red) in *n*-hexane (a), methanol (b), and acetonitrile (c) measured at 4 ps after excitation at 490 nm. The S_1-S_n maximum in *n*-hexane at 526 nm is marked as a reference point. Spectra are normalized to the S_1-S_n maximum.

The influence of the hexanoyloxy tail on the spectroscopic properties of hFx is further magnified in the transient absorption spectra shown in Fig. 2.31.

In n-hexane, the transient absorption spectra of hFx and Fx are very similar, reflecting the properties of the absorption spectra. The main spectral feature, the S_1-S_n excited state absorption band, has a maximum at 526 nm for both Fx and hFx, matching the value reported for Fx earlier.[13,14,23] Yet, even in n-hexane some small differences can be traced. The two weak bands in the 600-700 nm spectral region, observed exclusively in keto carotenoids, are barely visible in hFx. Since these bands are related to the presence of the ICT state and become significantly more pronounced in polar solvents, the near absence of these bands for hFx in n-hexane suggests that the presence of the hexanoyloxy moiety affects the ICT state. This assumption is confirmed when the transient absorption spectra of Fx and hFx are measured in polar solvents

FIGURE 2.32: Kinetics measured at the maximum of the S_1-S_n band for Fx (black) and hFx (red) in *n*-hexane (a), methanol (b), and acetonitrile (c). Corresponding lifetimes are indicated in each panel. The excitation wavelength was 490 nm, kinetics are normalized to maximum.

methanol (Fig. 2.31b) and acetonitrile (Fig. 2.31c). While for Fx the characteristic ICT bands peaking at 610 and 650 nm reach amplitude of about 50% of the S_1-S_n band, in hFx these bands remain at low amplitude. In methanol, the

amplitude of the ICT bands of hFx is only 20% of the S_1-S_n band; in acetonitrile it is even less: ∼15%. Essentially the same values are observed for bFx (Fig. 2.37).

Another characteristic polarity-induced effect reported for fucoxanthin and other keto-carotenoids having conjugation length $N<9$ is shortening of the S_1/ICT lifetime with increasing solvent polarity.[13,14,16,23] To demonstrate this behavior, we show kinetics measured at the S_1-S_n maximum for Fx and hFx in n-hexane, methanol, and acetonitrile (Fig. 2.32). The decay profiles of Fx and hFx are identical in n-hexane, yielding the S_1/ICT lifetime of 60 ps, the value reported earlier for Fx in nonpolar solvents.[13,14,23] Surprisingly, however, the same S_1/ICT lifetime of 60 ps is obtained for hFx in
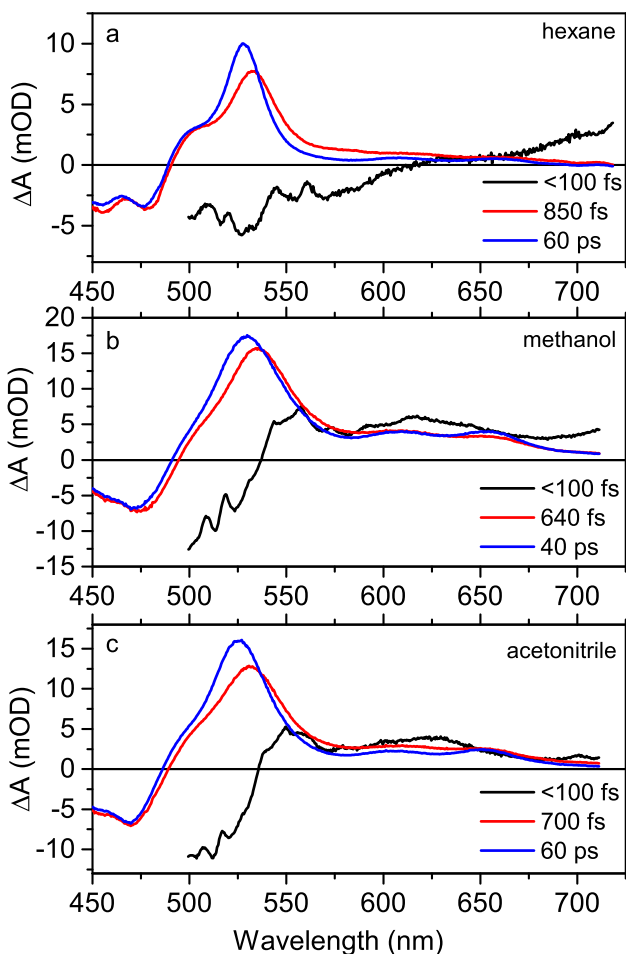
FIGURE 2.33: EADS obtained from global fitting of the data measured for hFx in *n*-hexane (a), methanol (b), and acetonitrile (c) after excitation at 490 nm.

the highly polar acetonitrile, suggesting that solvent polarity has no effect on the S_1/ICT lifetime. This is in sharp contrast to Fx, for which the polar acetonitrile shortens the S_1/ICT lifetime to 30 ps (Fig. 2.32c). In methanol the S_1/ICT lifetime of hFx is 40 ps, significantly shorter than 60 ps in n-hexane

and acetonitrile but still longer than the 20 ps reported for Fx in methanol (Fig. 2.32b).

Since hFx has never been explored by ultrafast spectroscopies, in Fig. 2.33 we show the results of the global fitting the data measured for hFx in n-hexane, acetonitrile, and methanol. In all three solvents, reasonable fits were obtained using a sequential model with three decay components: the S_2 state (black EADS), hot S_1/ICT state (red), and relaxed S_1/ICT state (blue). We do not observe any significant deviation from the three-exponential decay even in methanol, in which Fx exhibits a more complicated decay pattern caused by the presence of (at least) two Fx configurations.[44,45] Precise determination of the S_2 lifetime of hFx in either solvent is beyond the limits of our time resolution; thus, we can only conclude that the S_2 lifetime is shorter than 100 fs. On the basis of the spectral profile of the S_2 EADS in Fig. 2.33, it is likely that the hFx S_2 lifetime in polar solvents is slightly shorter than in n-hexane as the black EADS in polar solvents contain some features attributable to the S_1/ICT state (the positive features in the 550-700 nm spectral region). This mixing is not present in EADS corresponding to the S_2 state of hFx in n-hexane (Fig. 2.33a). The relaxation of the hot S_1/ICT state shows similar trend: it is longer in the non-polar n-hexane (850 fs) than in polar methanol or acetonitrile where the corresponding time constants are 640 and 700 fs, respectively. A comparable trend was reported for Fx, though the actual values were faster: 430 fs in n-hexane and 270 fs in methanol.[45] The time constant associated with the last EADS in Fig. 2.33 corresponds to the S_1/ICT lifetime of hFx in each solvent, yielding values of 60 ps in n-hexane and acetonitrile and 40 ps in methanol. The global fitting of the data measured for bFx yields essentially the same results as for hFx (Fig. 2.39).

TABLE 2.3: S_1/ICT Lifetimes of Fx and hFx in Various Solvents

solvent	S_1/ICT lifetime		$P(\varepsilon)$[a]
	hFx	Fx	
n-hexane	60	60	0.229
acetonitrile	60	30	0.921
DMSO	60		0.940
ethanol	50	40[b]	0.886
ethylene glycol	42		0.923
methanol	40	20	0.913

[a]Polarity factor calculated from the dielectric constant using the expression $P(\varepsilon = (\varepsilon - 1)/(\varepsilon + 2)$. [b]From ref [13]
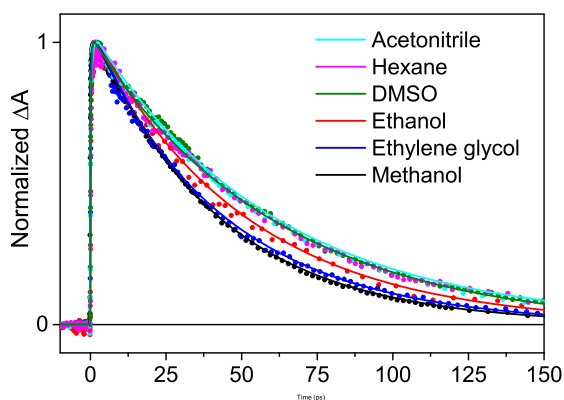
FIGURE 2.34: Kinetics measured at the maximum of the S_1-S_n band for hFx in various solvents. The excitation wavelength was 490 nm, kinetics are normalized to maximum. See Table 2.3 for the corresponding lifetimes.

To explore the effect of solvent further, we have measured excited state dynamics of hFx also in other solvents: dimethyl sulfoxide (DMSO), ethanol, and ethylene glycol. While DMSO is very polar, yet aprotic, ethylene glycol has similar polarity as acetonitrile can readily form hydrogen bonds. The decays of the S_1 band of hFx in all solvents are shown in Fig. 2.34 and the S_1/ICT lifetimes summarized in Table 2.3. It is obvious that polarity does not alter excited state dynamics of hFx. In the three aprotic solvents, hexane, acetonitrile, and DMSO, the S_1 lifetime of hFx is the same, underlining the absence of any effects induced solely by the solvent polarity. The S_1/ICT lifetime shortening is induced only in polar, protic solvents: methanol, ethanol, and ethylene glycol. The difference in S_1 lifetimes in methanol and ethanol shows that polarity also plays a role, but it is only

secondary to solvent proticity. Yet, even in polar, protic solvents the effect on excited-state properties of hFx is much smaller than for Fx.

2.3.4 Discussion

The data presented in the previous section demonstrate that a non-conjugated, acyloxy moiety can significantly alter excited-state properties of fucoxanthin: namely, the features related to the presence of the ICT state. The polarity-induced shortening of the S_1/ICT lifetime and the magnitude of the ICT bands in transient absorption spectra are affected by the presence of the acyloxy moiety. All these effects, reported for a number of keto-carotenoids, are diminished by the presence of the hexanoyl or butanoyl tail. It is obvious that the acyloxy moiety at the C19' carbon has a notable effect on the excited-state properties of fucoxanthin, even though it is not a part of the conjugated backbone. Moreover, the influence of the acyloxy moiety is controlled by hydrogen bonding as the characteristic, polarity-induced behavior is observed exclusively in protic solvents, while in aprotic solvents these effects are nearly absent regardless of the polarity of the aprotic solvent.
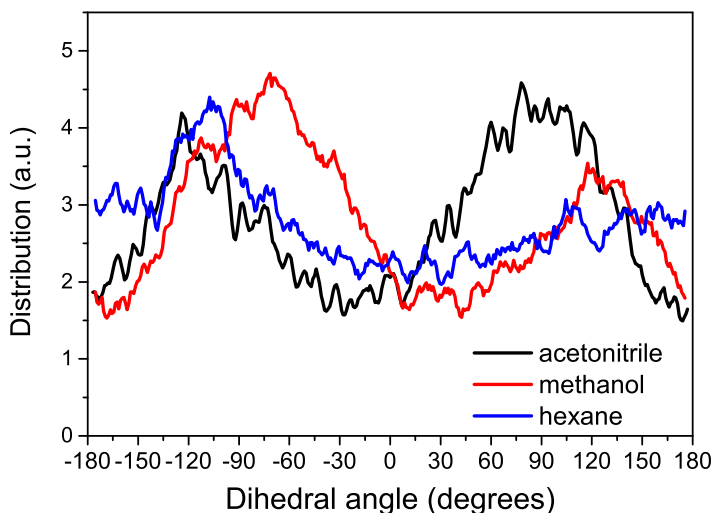
FIGURE 2.35: Distribution of dihedral angles determining the orientation of the hexanoyl tail in hFx in various solvents.

The data measured in the non-polar n-hexane provide information about possible effects of the acyloxy moiety on properties that are not related to

polarity or proticity such as effective conjugation length, N_{eff}. The characteristic markers of N_{eff}, the spectral position of the S_1-S_n band and the S_1/ICT lifetime, remain the same for Fx, hFx, and bFx in n-hexane, showing that the acyloxy moiety does not alter N_{eff}. This observation is in line with a recent report on the non-carbonyl carotenoid vaucheriaxanthin (19'-OH neoxanthin), whose 19'-OH group is often esterified. Both vaucheriaxanthin and vaucheriaxanthin ester are spectroscopically identical.[46]

Although the non-conjugated acyloxy moiety of bFx and hFx does not alter N_{eff}, it diminishes the effects related to the ICT state induced by the presence of the conjugated keto group of fucoxanthin. To explore the possible influence of the acyloxy moiety, we have first carried out a molecular modeling simulation to reveal the most likely position of the acyloxy moiety of hFx in different solvents. We have monitored the C29-C44-C46-C48 dihedral angle (see Fig. 2.40 for examples of a few characteristic dihedral angles), and the results are shown in Fig. 2.35. In both polar solvents, protic methanol and aprotic acetonitrile, the distribution of dihedral angles shows that the most represented configurations are those with the hexanoyl moiety bent by 90-120°. In hexane, the distribution of possible configurations is flatter, with only one weak maximum around -120°. It shows that while polar solvents preferentially stabilize certain configurations, no such preference exists in n-hexane.

Molecular dynamics simulations provided further information about hFx conformations, but they do not offer explanation of the observed spectroscopic behavior. Interestingly, differences in the solvent-dependent behavior between Fx and hFx are reminiscent of those reported for a different pair of carotenoids: 8,8'-diapocarotene-8'-ol-8-al and crocetindial.[16] In that study, 8,8'-diapocarotene-8'-ol-8-al exhibits strong polarity dependence, having an S_1/ICT lifetime of 300 ps in n-hexane shortened to 21 and 18 ps in acetonitrile and methanol. Crocetindial, on the other hand, has a 127 ps S_1/ICT lifetime in hexane which remains essentially the same in acetonitrile (135 ps) and is slightly shortened to 97 ps in methanol.[16] Even though these are completely different carotenoids than Fx and hFx, the observed trend is comparable: switching from 8,8*I*-diapocarotene-8*I*-ol-8-al to crocetindial somehow

mimics the change we observe when going from Fx to hFx.

The structural difference between 8,8′-diapocarotene-8′-ol-8-al and crocetindial is key for the explanation of the data we have measured for Fx and hFx. The difference is in the symmetry of the conjugated keto groups (see Fig. 2.41 for structures). While 8,8′-diapocarotene-8′-ol-8-al has one conjugated carbonyl group and one hydroxyl group, making the whole conjugated system strongly asymmetric, crocetindial has two symmetric conjugated keto groups located at the opposite ends of the conjugated chain. The symmetry of the keto-groups in crocetindial nearly completely blocks the polarity-dependent behavior, resulting in absence of the characteristic ICT bands in transient absorption spectra and identical lifetimes of the S_1/ICT states in hexane and acetonitrile.[16] Hydrogen bonding in protic methanol slightly shortens the S_1/ICT lifetime, but the ICT bands are absent for crocetindial even in methanol.[16]

On the basis of the obvious similarity of our results with those reported for 8,8′-diapocarotene-8′-ol-8-al and crocetindial,[16] we assume that the mechanism for switching off the polarity-dependent effects is the same for both pairs of carotenoids. The strongly asymmetric conjugated chain of Fx (a conjugated keto group at C8 position, Fig. 2.29) is symmetrized in hFx, resulting in the absence of polarity-dependent behavior. This implies that in hFx the symmetrization must be achieved by the acyloxy moiety that contains a keto group that is non-conjugated (Fig. 2.29). The two oxygens of the acyloxy moiety have significant electron-withdrawing character, counteracting the effect of the conjugated keto group at C8.

The results demonstrate that non-conjugated groups significantly alter the polarity-dependent spectroscopic properties of keto-carotenoids. We have reported earlier a similar case for psittacofulvin, in which the absence of methyl groups modified the polarity-dependent effects compared to the carotenoid counterpart with methyl groups.[27] Here, the acyloxy moiety of hFx or bFx switches off the characteristic polarity-dependent behavior of the parent carotenoid, Fx. In contrast to psittacofulvins, which are colorants in bird feathers,[27] the significant differences between the excited-state properties of

Fx and hFx (bFx) are likely related to the function they play in the photo-synthetic apparatus in a number of microorganisms. The Fx/hFx(bFx) ratio in the light harvesting antenna varies depending on the stress conditions, as when the hFx(bFx) fraction increases upon high light and nutrient limited conditions.[29−31] Since the ICT character of the S_1/ICT state is important for maintaining the high energy transfer efficiency,[47] and considering that the ICT part of the S_1/ICT potential surface has even been suggested to be the primary energy donor in the S_1/ICT energy transfer pathway,[48] it is possible that the conversion of Fx to hFx (bFx) leads to less efficient energy transfer from the antennae to the reaction centers and serves as a simple photoprotective mechanism when the organisms are under stress. Because ICT states have a strong ionic/single-electron character, their presence will have a large impact on the transition density associated with this state and consequently also on the carotenoid-Chl coupling. The absence of the ICT state in the acyloxy fucoxanthin derivatives will thus likely affect the energy transfer between carotenoid and Chl. Alternatively, the acyloxy moiety can cause small structural changes in the protein leading to an induction of a quenched state. Recently, Krueger et al.[49] showed using single-molecule spectroscopy that FCP can switch between two distinct states. Presence of the acyloxy moiety could shift the equilibrium between these two states, resulting in a possible regulatory role not be related to the ICT state.

Supporting Information Available: Absorption and transient absorption data measured for bFx in various solvents, examples of orientations of the hexanoyl tail obtained from MD simulations, and structures of crocetindial and 8,8′-diapocarotene-8′-ol-8-al. This material is available free of charge via the Internet at http://pubs.acs.org.
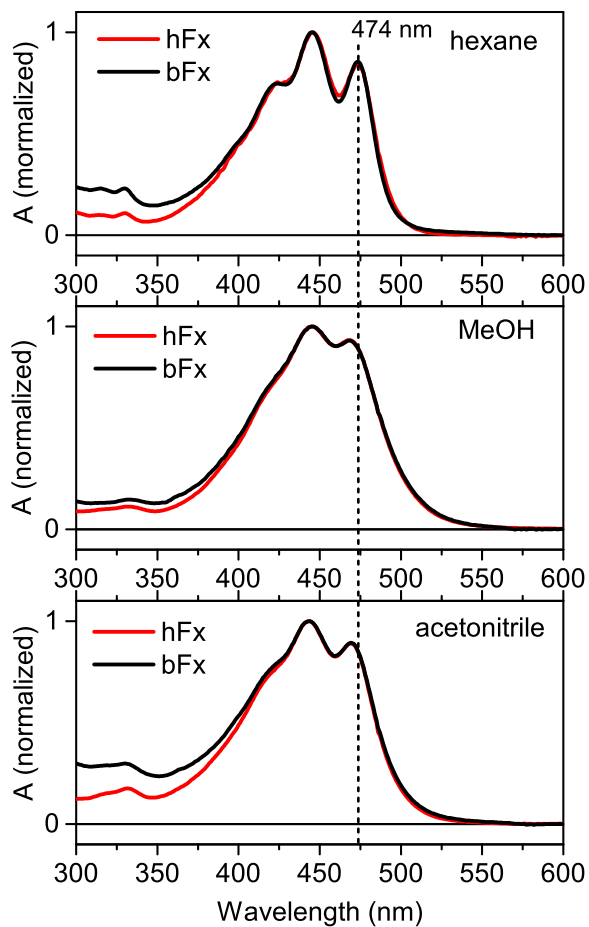
Supporting Information

FIGURE 2.36: Comparison of absorption spectra of bFx (black)
and hFx (red) in n-hexane, methanol and acetonitrile.

*2.3. Non-Conjugated Acyloxy Group Deactivates the Intramolecu-
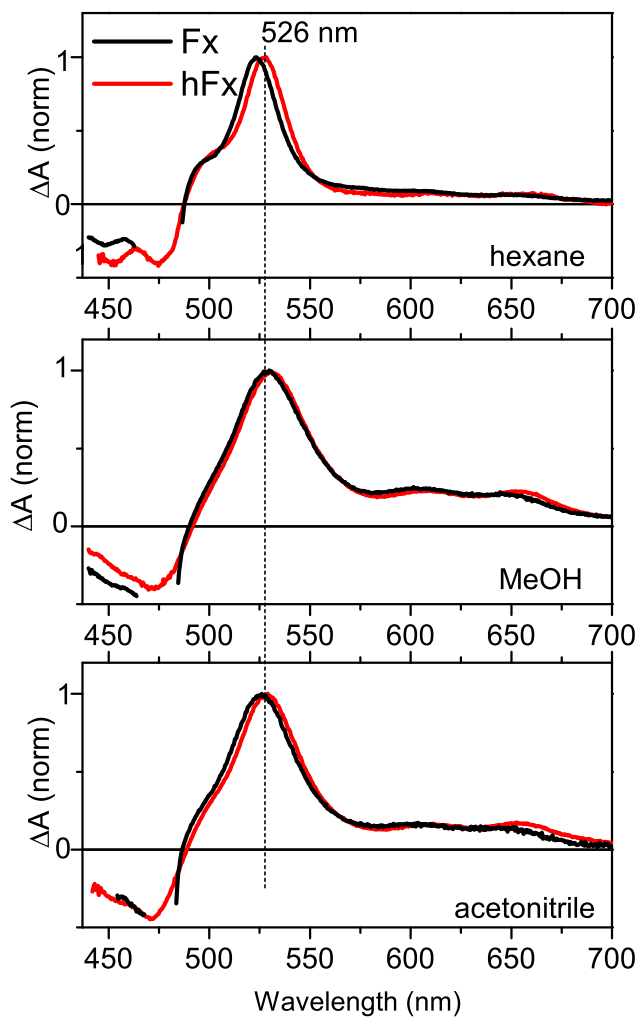lar Charge Transfer State in the Carotenoid Fucoxanthin*

161

FIGURE 2.37: Transient absorption spectra of bFx (black) and hFx (red) in n-hexane, methanol and acetonitrile measured at 4 ps after excitation at 490 nm. The S1-Sn maximum of hFx in n-hexane at 526 nm is marked as a reference point. Spectra are normalized to the S1-Sn maximum.
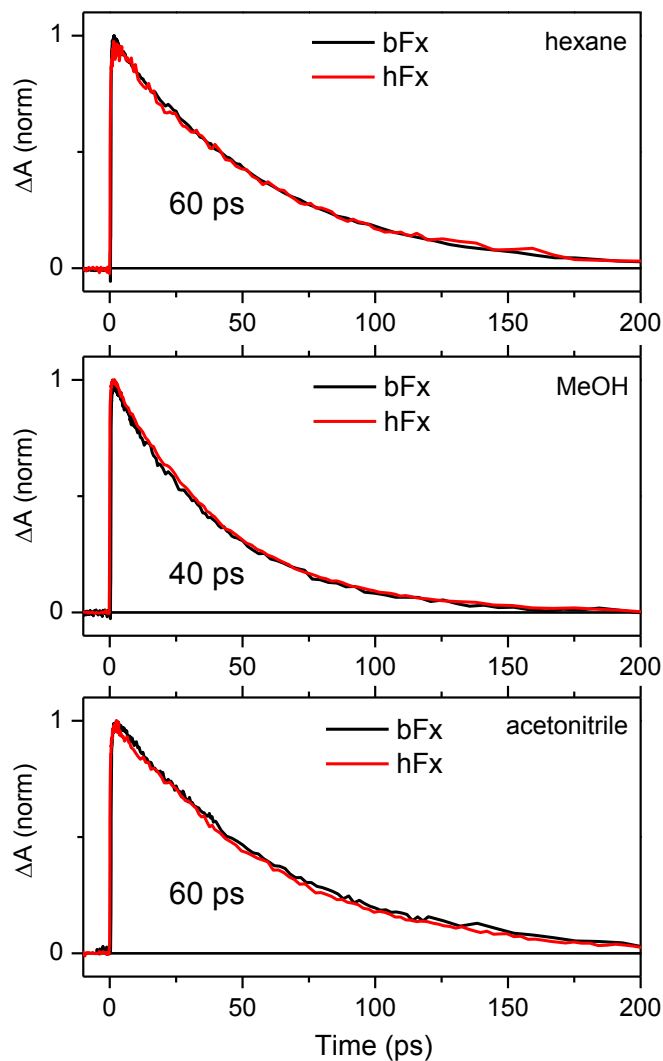
FIGURE 2.38: Kinetics measured at the maximum of the S_1-S_n band for bFx (black) and hFx (red) in n-hexane, methanol and acetonitrile. Corresponding lifetimes are indicated in each panel. Excitation wavelength was 490 nm, kinetics are normalized to maximum.
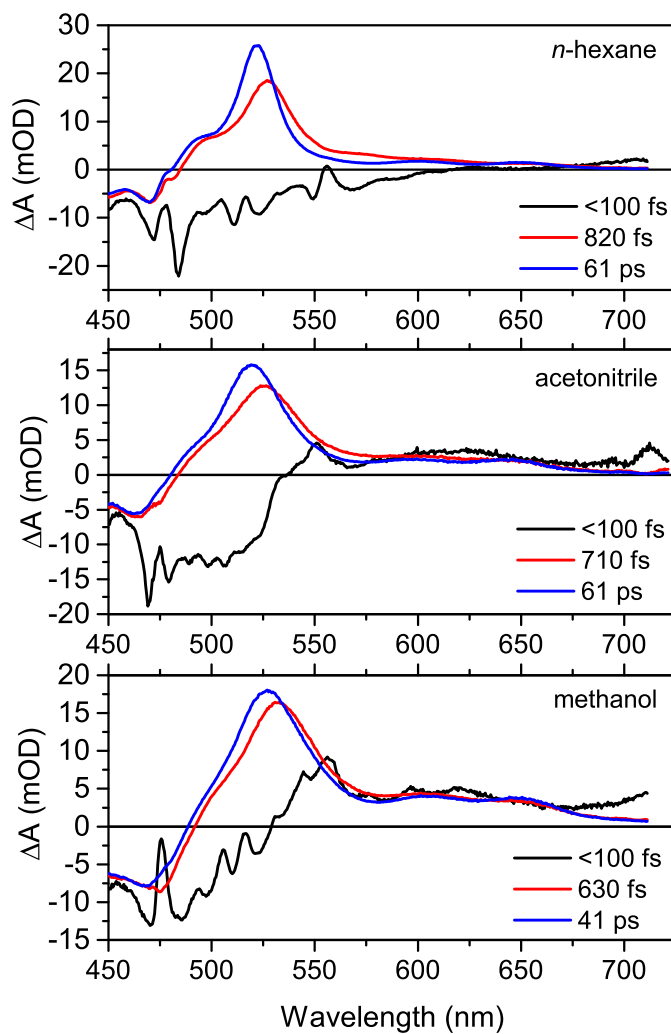
FIGURE 2.39: EADS obtained from global fitting the data measured for bFx in *n*-hexane, methanol and acetonitrile after excitation at 490 nm.
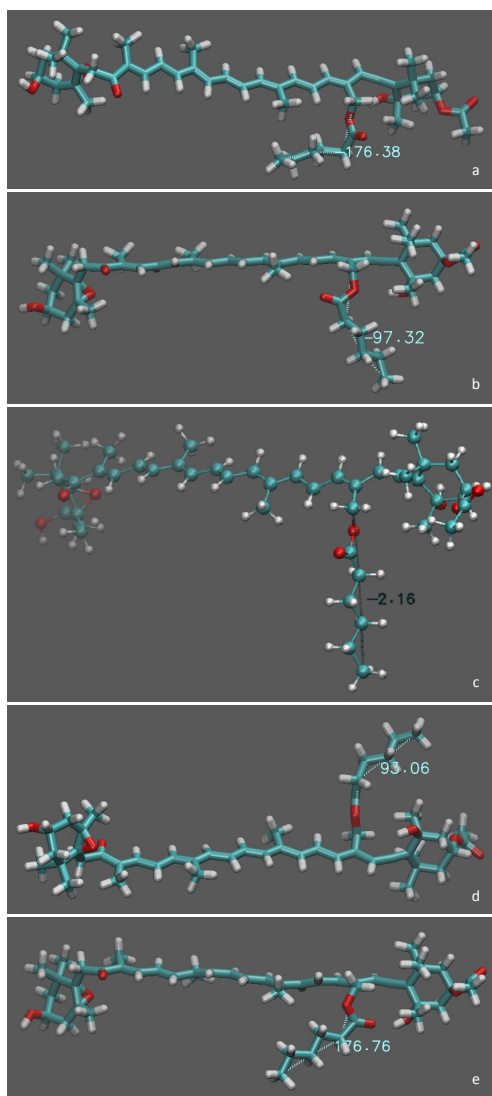
FIGURE 2.40: Five different orientations of the hexanoyl tail of hFx obtained from molecular dynamic simulations showing the dihedral angle close to (a) -180°, (b) -90°, (c) 0°, (d) 90°, and (e) 180°.

crocetindial

8,8'-diapocarotene-8'-ol-8-al
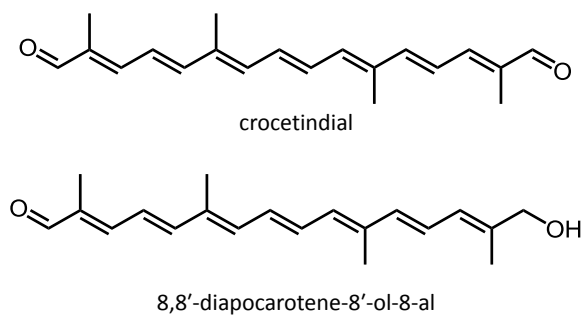
FIGURE 2.41: Structures of 8,8'-diapocarotene-8'-ol-8-al and crocetindial.

References (Paper III)

1. Frank, H. A.; Desamero, R. Z. B.; Chynwat, V.; Gebhard, R.; vanderHoef, I.; Jansen, F. J.; Lugtenburg, J.; Gosztola, D.; Wasielewski, M. R., Spectroscopic properties of spheroidene analogs having different extents of π-electron conjugation. *J. Phys. Chem. A* **1997,** *101*, 149-157.

2. Mimuro, M.; Nagashima, U.; Takaichi, S.; Nishimura, Y.; Yamazaki, I.; Katoh, T., Molecular structure and optical properties of carotenoids for the *in vivo* energy transfer function in the algal photosynthetic pigment system. *BBA-Bioenergetics* **1992,** *1098*, 271-274.

3. Carotenoids, Britton, G.; Liaaen-Jensen, S.; Pfander, H; Eds. Vol. 1B Spectroscopy. Birkhauser 1995.

4. Polívka, T.; Sundström, V. Ultrafast dynamics of carotenoid excited states – from solution to natural and artificial systems. *Chem. Rev.* **2004,** *104*, 2021-2071.

5. Macpherson, A. N.; Gillbro, T., Solvent dependence of the ultrafast S_2-S_1 internal conversion rate of β-carotene. *J. Phys. Chem. A* **1998,** *102*, 5049-5058.

6. Kosumi, D.; Fujiwara, M.; Fujii, R.; Cogdell, R. J.; Hashimoto, H.; Yoshizawa, M., The dependence of the ultrafast relaxation kinetics of the S_2 and S_1 states in β-carotene homologs and lycopene on conjugation length studied by femtosecond time-resolved absorption and Kerr-gate fluorescence spectroscopies. *J. Chem. Phys.* **2009,** *130*, 214506.

7. Polívka, T.; Sundström, V., Dark excited states of carotenoids: Consensus and controversy. *Chem. Phys. Lett.* **2009,** *477*, 1-11.

8. Ostroumov, E. E.; Mulvaney, R. M.; Cogdell, R. J.; Scholes, G. D., Broadband 2D electronic spectroscopy reveals a carotenoid dark state in purple bacteria. *Science* **2013,** *340*, 52-56.

9. Beck, W. F.; Bishop, M. M.; Roscioli, J. D.; Ghosh, S.; Frank, H. A., Excited state conformational dynamics in carotenoids: Dark intermediates and excitation energy transfer. *Arch. Biochem. Biophys.* **2015,** *572*, 175-183.

10. Feng, J.; Tseng, C. W.; Chen, T. W.; Leng, X.; Yin, H. B.; Cheng, Y. C.; Rohlfing, M.; Ma, Y. C., A new energy transfer channel from carotenoids to chlorophylls in purple bacteria. *Nature Communications* **2017,** *8*, 71.

11. Kuznetsova, V.; Southall, J.; Cogdell, R. J.; Fuciman, M.; Polívka, T., Spectroscopic properties of the S_1 state of linear carotenoids after excess energy excitation. *Chem. Phys. Lett.* **2017,** *683*, 448-453.

12. Bautista, J. A.; Connors, R. E.; Raju, B. B.; Hiller, R. G.; Sharples, F. P.; Gosztola, D.; Wasielewski, M. R.; Frank, H. A., Excited state properties of peridinin: Observation of a solvent dependence of the lowest excited singlet state lifetime and spectral behavior unique among carotenoids. *J. Phys. Chem. B* **1999,** *103*, 8751-8758.

13. Frank, H. A.; Bautista, J. A.; Josue, J.; Pendon, Z.; Hiller, R. G.; Sharples, F. P.; Gosztola, D.; Wasielewski, M. R., Effect of the solvent environment on the spectroscopic properties and dynamics of the lowest excited states of carotenoids. *J. Phys. Chem. B* **2000,** *104*, 4569-4577.

14. Zigmantas, D.; Hiller, R. G.; Sharples, F. P.; Frank, H. A.; Sundström, V.; Polívka, T., Effect of a conjugated carbonyl group on the photophysical properties of carotenoids. *Phys. Chem. Chem. Phys.* **2004,** *6*, 3009-3016.

15. Stalke, S.; Wild, D. A.; Lenzer, T.; Kopczynski, M.; Lohse, P. W.; Oum, K., Solvent-dependent ultrafast internal conversion dynamics of n '-apo-β-carotenoic-n '-acids (n=8, 10, 12). *Phys. Chem. Chem. Phys.* **2008,** *10*, 2180-2188.

() Enriquez, M. M.; Fuciman, M.; LaFountain, A. M.; Wagner, N. L.; Birge, R. R.; Frank, H. A., The intramolecular charge transfer state in carbonyl-containing polyenes and carotenoids. *J. Phys. Chem. B* **2010,** *114*, 12416-12426

16. Niedzwiedzki, D. M.; Chatterjee, N.; Enriquez, M. M.; Kajikawa, T.; Hasegawa, S.; Katsumura, S.; Frank, H. A., Spectroscopic investigation of peridinin analogues having different π-electron conjugated chain lengths: Exploring the nature of the intramolecular charge transfer state. *J. Phys. Chem. B* **2009**, *113*, 13604-13612.

17. Papagiannakis, E.; van Stokkum, I. H. M.; Fey, H.; Büchel, C.; van Grondelle, R., Spectroscopic characterization of the excitation energy transfer in the fucoxanthin-chlorophyll protein of diatoms. *Photosynth. Res.* **2005,** *86*, 241-250.

18. Gildenhoff, N.; Herz, J.; Gundermann, K.; Büchel, C.; Wachtveitl, J., The excitation energy transfer in the trimeric fucoxanthin-chlorophyll protein from *Cyclotella meneghiniana* analyzed by polarized transient absorption spectroscopy. *Chem. Phys.* **2010,** *373*, 104-109.

19. Zigmantas, D.; Polívka, T.; Hiller, R. G.; Yartsev, A.; Sundström, V., Spectroscopic and dynamic properties of the peridinin lowest singlet excited states. *J. Phys. Chem. A* **2001,** *105*, 10296-10306.

20. Durchan, M.; Fuciman, M.; Šlouf, V.; Keşan, G.; Polívka, T., Excited-state dynamics of monomeric and aggregated carotenoid 8'-apo-β-carotenal. *J. Phys. Chem. A* **2012,** *116*, 12330-12338.

21. Redeckas, K.; Voiciuk, V.; Vengris, M., Investigation of the S_1/ICT equilibrium in fucoxanthin by ultrafast pump-dump-probe and femtosecond stimulated Raman scattering spectroscopy. *Photosynth. Res.* **2016,** *128*, 169-181.

22. Keşan, G.; Durchan, M.; Tichý, J.; Minofar, B.; Kuznetsova, V.; Fuciman, M.; Šlouf, V.; Parlak, C.; Polívka, T., Different response of carbonyl carotenoids to solvent proticity helps to estimate structure of the unknown carotenoid from *Chromera velia*. *J. Phys. Chem. B* **2015,** *119*, 12653-12663.

23. Chatterjee, N.; Niedzwiedzki, D. M.; Aoki, K.; Kajikawa, T.; Katsumura, S.; Hashimoto, H.; Frank, H. A., Effect of structural modifications on the

spectroscopic properties and dynamics of the excited states of peridinin. *Arch. Biochem. Biophys.* **2009,** *483*, 146-155.

24. Fuciman, M.; Enriquez, M. M.; Kaligotla, S.; Niedzwiedzki, D. M.; Kajikawa, T.; Aoki, K.; Katsumura, S.; Frank, H. A., Singlet and triplet state spectra and dynamics of structurally modified peridinins. *J. Phys. Chem. B* **2011,** *115*, 4436-4445.

25. Kosumi, D.; Kajikawa, T.; Yano, K.; Okumura, S.; Sugisaki, M.; Sakaguchi, K.; Katsumura, S.; Hashimoto, H., Roles of allene-group in an intramolecular charge transfer character of a short fucoxanthin homolog as revealed by femtosecond pump-probe spectroscopy. *Chem. Phys. Lett.* **2014,** *602*, 75-79.

26. Adamec, F.; Greco, J. A.; LaFountain, A. M.; Magdaong, N. M.; Fuciman, M.; Birge, R. R.; Polívka, T.; Frank, H. A., Spectroscopic investigation of a brightly colored psittacofulvin pigment from parrot feathers. *Chem. Phys. Lett.* **2016,** *648*, 195–199.

27. Wright, S. W.; Jeffrey, S. W., Fucoxanthin pigment markers of marine phytoplankton analyzed by Hplc and Hptlc. *Mar. Ecol. Prog. Ser.* **1987,** *38*, 259-266.

28. Alami, M.; Lazar, D.; Green, B. R., The harmful alga *Aureococcus anophagefferens* utilizes 19 '-butanoyloxyfucoxanthin as well as xanthophyll cycle carotenoids in acclimating to higher light intensities. *BBA-Bioenergetics* **2012,** *1817*, 1557-1564.

29. Liu, X.; Li, Y.; Wu, Y.; Huang, B.; Dai, M.; Fu, F.; Hutchings, D.A.; Gao, K. Effects of elevated CO_2 on phytoplankton during a mesocosm experiment in the southern eutrophicated coastal water of China. *Sci. Rep.* **2017**, *7*, 6868.

30. Garrido, J.L.; Brunet, C.; Rodriguez, F., Pigment variations in *Emiliania huxleyi* (CCMP370) as a response to changes in light intensity or quality. Environmental Microbiology, **2016**, *18*, 4412-4425.

31. Guillard, R. R.; Ryther, J. H., Studies of marine planktonic diatoms .1. *Cyclotella Nana* Hustedt, and *Detonula Confervacea* (Cleve) Gran. *Can J Microbiol* **1962,** *8*, 229-239.

32. Litvín, R.; Bína, D.; Herbstová, M.; Gardian, Z., Architecture of the light-harvesting apparatus of the eustigmatophyte alga Nannochloropsis oceanica. *Photosynth. Res.* **2016,** *130*, 137-150.

33. Jeffrey, S.W.; Mantoura, R.F.C.; Wright, S.W., Phytoplankton pigments in oceanography: guidelines to modern methods, 2nd edition, Monographs on Oceanographic Methodology, 10, UNESCO Publishing, Paris, 2005.

34. van Stokkum, I.H.M.; Larsen, D.S.; van Grondelle, R., Global and target analysis of time-resolved spectra. *BBA – Bioenegetics* **2004**, *1657*, 82-104.

35. Wang, J.; Wolf, R. M.; Caldwell, J. W.; Kollman, P. A.; Case, D. A., Development and testing of a general AMBER force field. *J. Comput. Chem.* **2004**, *25*, 1157-1174.

36. Bayly, C.I.; Cieplak, P.; Cornell, W.; Kollman, P.A. A well behaved electrostatic potential based method using charge restraints for deriving atomic charges: the RESP model. *J. Phys. Chem.* **1993**, *97*, 10269–10280.

37. Frisch, M. J. et al. Gaussian 03 (Revision D.01), Gaussian, Inc., Wallingford CT, 2004.

38. Hess, B.; Bekker, H.; Berendsen, H.J.; Fraaije, J.G. LINCS: a linear constraint solver for molecular simulations. *J. Comput. Chem.* **1997**, *18*, 1463-1472.

39. Darden, T.; York, D.; Pedersen, L. Particle mesh Ewald: An N log (N) method for Ewald sums in large systems. *J. Chem. Phys.* **1993**, *98*, 10089-10092.

40. Bussi, G.; Donadio, D.; Parrinello, M. Canonical sampling through velocity rescaling. *J. Chem. Phys.* **2007**, *126*, 014101.

41. Van der Spoel, D.; Lindahl, E.; Hess, B.; Groenhof, G.; Mark, A.E.; H. J. C. Berendsen. GROMACS: Fast, flexible and free. *J. Comput. Chem.* **2005**, *26*, 1701-1719.

42. Humphrey, W.; Dalke, A.; Schulten, K. VMD: Visual molecular dynamics. *J. Mol. Graph.* **1996**, *14*, 33–38.

43. Kosumi, D.; Kusumoto, T.; Fujii, R.; Sugisaki, M.; Iinuma, Y.; Oka, N.; Takaesu, Y.; Taira, T.; Iha, M.; Frank, H. A.; Hashimoto, H., Ultrafast excited state dynamics of fucoxanthin: excitation energy dependent intramolecular charge transfer dynamics. *Phys. Chem. Chem. Phys.* **2011,** *13*, 10762-10770.

44. Kuznetsova, V.; Chábera, P.; Litvín, R.; Polívka, T. G.; Fuciman, M., Effect of isomerization on excited-state dynamics of carotenoid fucoxanthin. *J. Phys. Chem. B* **2017,** *121*, 4438-4447.

45. KeŞan, G.; Litvín, R.; Bína, D.; Durchan, M.; Šlouf, V.; Polívka, T., Efficient light-harvesting using non-carbonyl carotenoids: Energy transfer dynamics in the VCP complex from *Nannochloropsis oceanica*. *BBA-Bioenergetics* **2016,** *1857*, 370-379.

46. Polívka, T.; Frank, H. A., Molecular factors controlling photosynthetic light harvesting by carotenoids. *Acc. Chem. Res.* **2010,** *43*, 1125-1134.

47. Redeckas, K.; Voiciuk, V.; Zigmantas, D.; Hiller, R. G.; Vengris, M., Unveiling the excited state energy transfer pathways in peridinin-chlorophyll a-protein by ultrafast multi-pulse transient absorption spectroscopy. *BBA-Bioenergetics* **2017,** *1858*, 297-307.

48. Kruger, T. P. J.; Malý, P.; Alexandre, M. T. A.; Manèal, T.; Büchel, C.; van Grondelle, R., How reduced excitonic coupling enhances light harvesting in the main photosynthetic antennae of diatoms. *Proc. Natl. Acad. Sci. U.S.A.* **2017**, *114*, 11063-11071.

2.4 Spectroscopic properties of the triple bond carotenoid alloxanthin

Abstract

Alloxanthin, which has two triple bonds within its backbone, was studied by steady-state and femtosecond transient absorption spectroscopies. Alloxanthin demonstrates an S_2 energy comparable to its non-triple bond homolog, zeaxanthin, while the S_1 lifetime of 19 ps is markedly longer than that of zeaxanthin (9 ps). Along with corroborating quantum chemistry calculations, the results show that the long-lived S_1 state of alloxanthin, which typically corresponds to the dynamic of a shorter carotenoid backbone, implies the triple bond isolates the conjugation of the backbone, increasing the S_1 state energy and diminishing the S_1-S_2 energy gap.

2.4.1   Introduction

Carotenoids are known for their rich excited-state dynamics, the elucidation of which is key to understanding the various functions the molecules perform in many biological systems.[1-3] Basic spectroscopic properties of carotenoids can be explained using a three-state model consisting of the ground state (S_0), and two excited states denoted S_1 and S_2.[4] Assuming carotenoids belong to the idealized C_{2h} symmetry group, the S_0-S_1 transition is symmetry-forbidden for one-photon processes, while the characteristic visible coloration of carotenoids is due the S_0-S_2 transition that gives rise to strong absorption in the blue-green spectral region. Therefore, the symmetry of the carotenoid conjugated backbone is the key property determining the spectroscopic properties.

Another key parameter determining the spectroscopic properties is the conjugation length, N, defined as a number of conjugated C=C bonds in the carotenoid structure. For carotenoids with conjugation extended to various functional groups the effective conjugation length, N_{eff}, is often used. It makes use of the fact that some spectroscopic parameters, such as S_1 lifetime, have a well-defined dependence on $1/N$.[5-7] Therefore, knowing the value of e.g. S_1 lifetime of any carotenoid, and comparing the value to that of a linear carotenoid, allows one to obtain an effective value of N_{eff}.[7] For example, it has been demonstrated that the extension of conjugation to various types of terminal rings decreases N_{eff}, but it also provides opportunity for tuning the spectroscopic properties as the torsional angle of a terminal ring in respect to the main conjugation allows for fine tuning of N_{eff}.[7] Thus, in contrast to linear carotenoids whose properties can be only slightly altered by environment, carotenoids with conjugated terminal rings may have a wide range of spectroscopic properties, depending on their protein binding sites.[8,9]

While there exist many carotenoids with conjugated terminal rings or keto groups, carotenoids having conjugated triple bonds are quite rare. Out of the nearly thousand carotenoids identified so far, only about 50 contain triple bonds[10] and only three triple bond carotenoids are commonly found in nature. Alloxanthin (Fig. 2.42) is a common carotenoid of cryptophytes,[11] and diadinoxanthin and diatoxanthin (Supporting Information, Fig. 2.47) are

found in diatoms and some marine algae.[12] Diadinoxanthin and diatoxanthin have one triple bond in their structure and due to their well-documented role in photoprotection in diatoms,[12−14] their excited-state properties were studied in detail.[15,16]
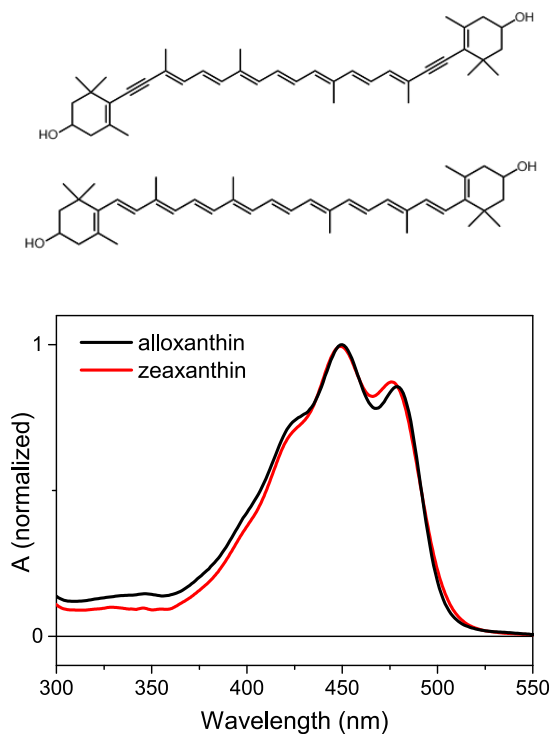

FIGURE 2.42: Molecular structures (top) and absorption spectra (bottom) of alloxanthin and zeaxanthin in methanol.

Alloxanthin is the only carotenoid with two triple bonds found in photosynthetic organisms. The role of carotenoid triple bonds in proper functioning of carotenoids in light-harvesting systems remains unknown. As demonstrated earlier for diadinoxanthin and diatoxanthin, their specific molecular structure with a triple bond may help in tuning the spectroscopic properties when bound to protein.[17] Alloxanthin, whose excited-state properties have not been reported so far, is the major antenna carotenoid in the cryptophyte *Rhodomonas salina*.[18] This organism, despite lack of any xanthophyll cycle, has developed a flexible and effective photoprotective quenching,[18] in which alloxanthin may play a role.

Here we present ultrafast transient absorption study of alloxanthin complemented by quantum chemical calculations. We compare these results with those of zeaxanthin (Fig. 2.42) which has comparable structure but lacks the triple bonds. We show that the presence of triple bonds in the carotenoid

structure has important consequences for excited-state dynamics of alloxanthin.

2.4.2 Materials and Methods

Alloxanthin was purified by an adapted method described previously for violaxanthin.[19] *Rhodomonas salina* cells (strain CCAP 978/27) were grown in an artificial seawater medium supplemented with f/2 nutrient. Irradiation was provided by fluorescence tubes (40 µmol m^{-2} s^{-1}, day-night cycle 12/12 hours) and cells were continuously bubbled by air. Harvested cells were resuspended in 25 mM Hepes buffer, pH 7.8 and broken by glass beads using Mini-Bead-Beater (BioSpec, USA). Thylakoid membrane fraction was separated by centrifugation, resuspended in 1 ml of distilled water, mixed with 9 ml of methanol and incubated for one hour in dark at room temperature. The extract was clarified by centrifugation and the remaining pellet was extracted again by 10 ml of 90% methanol. Both supernatants were pooled and completely evaporated by a vacuum evaporator. Pigments were dissolved in methanol and separated by HPLC (Agilent 1200) on a semi-preparative reverse phase column (Reprosil 250x10 mm C8 5 μm, Watrex, Czech Republic) with 35% methanol and 15% acetonitrile in 0.25M pyridine (solvent A) and 20% methanol and 20% acetone in acetonitrile as solvent B. Pigments were eluted with a linear gradient of solvent B (30 to 95% in 25 min) followed by 95% of solvent B at a flow rate of 0.8 mL min^{-1} at 40 °C.

The sample was maintained at room temperature during transient absorption measurements, constantly stirred with a magnetic stir bar within a 2 mm quartz cuvette. The pump and probe pulses were generated by the Spitfire Ace regenerative amplifier system (Spectra Physics), producing 4.2 mJ pulses about 800 nm wavelength at 1 kHz by chirped pulse amplification of a mode-locked Ti:Sapphire laser (MaiTai, Spectra Physics) pumped by a Nd:YLF pump laser (Empower, Spectra Physics). The excitation wavelength of 490 nm was achieved through parametric amplification (TOPAS, Light Conversion) and reduced to ∼18 nJ per pulse at the sample location (4 x 10^{13} photons / pulse cm^{-2}) for an excitation spot size of approximately 400 µm. The

probe pulse supercontinuum was generated in a 2-mm sapphire plate and fo-
cused to an area smaller than the spot size of the pump beam by a spherical
mirror. The resulting probe absorbance was observed using a double-diode
array detection system (Pascher Instruments) with a 300-groove grating spec-
trometer calibrated by the absorption bands of holmium oxide. Data were fit-
ted globally using Glotaran global fitting analysis software (VU Amsterdam)
under a sequential exponential decay scheme.[20]

Optimized ground state geometries of carotenoids were created using
standard ground-state density functional theory (DFT). All ground state con-
formers for each carotenoids were optimized with the B3LYP level of the-
ory using the 6-31G (d,p) basis set in order to find stable conformers. This
level of theory is suitable for calculations of structure geometry having $C{\equiv}C$
bonds.[21] Stable conformers were re-optimized by means of Becke-Lee-Yang-
Parr (BLYP) with the triple--quality (TZVP) basis set. These optimized struc-
tures were used as an initial guess to determine the equilibrium geometries
of the excited states by means of time-dependent density functional theory
within the Tamm−Dancoff approximation (TD-DFT/TDA) using either the
BLYP functional, which provides the correct energy ordering for the two low-
est excited states of carotenoids,[7,22,23] or the hybrid exchange-correlation func-
tional (Cam- B3LYP) with the TZVP basis set, which gives more reasonable
data for the S_2 state energy.[7] All calculations were completed in the gas phase
and performed with the Gaussian09 package.

2.4.3   Results and Discussion

The absorption spectra of zeaxanthin and alloxanthin displayed in Fig.
2.42 show that adding two triple bonds to the carotenoid structure only
marginally affects the S_0-S_2 transition. The absorption spectra are very simi-
lar, although alloxanthin has the lowest vibrational band slightly red-shifted,
peaking at 479 nm while zeaxanthin's is at 477 nm. The resolution of vibra-
tional bands, reflecting the conformational disorder in the ground state, is also
comparable for both carotenoids. These observations imply that properties of
the S_2 state are not much affected by the presence of triple bonds in alloxan-
thin.

Transient absorption spectra and dynamics monitoring spectroscopic properties of the S_1 state, however, demonstrate a more divergent spectral response among alloxanthin and zeaxanthin. The spectra in Fig. 2.43a represent the transient absorption profiles measured at 4 ps after excitation, corresponding to the S_1-S_n transition after all S_1 vibrational dynamics, which usually takes place at subpicosecond time scale,[24] have subsided. In contrast to the S_0-S_2 transition shown in Fig. 2.42, the spectral profiles of the S_1-S_n transitions are clearly different for alloxanthin and zeaxanthin. Again, the peak wavelength is comparable, yielding 548 nm for alloxanthin and 550 nm for zeaxanthin, but it must be noted that while for the S_0-S_2 transition (Fig. 2.42) zeaxanthin
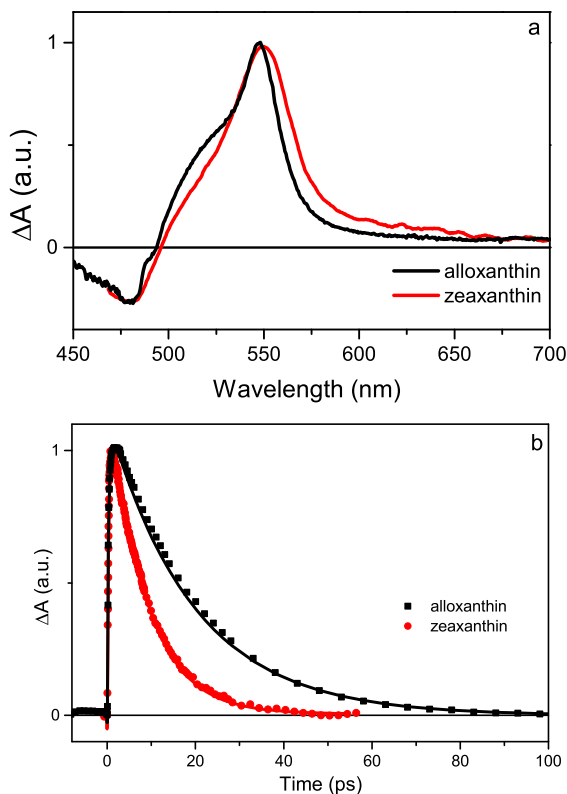
FIGURE 2.43: (a) Transient absorption spectra of alloxanthin and zeaxanthin in methanol measured at 4 ps after excitation at 490 nm. (b) Kinetics measured at the maximum of the S1-Sn transition at 548 nm (alloxanthin) and 550 nm (zeaxanthin).

has the slightly higher energy, it is opposite for the S_1-S_n transition. Further, the S_1-S_n profile of alloxanthin is narrower with a pronounced, blue shoulder, found to decay at the same rate as the peak's maximum (see below). In contrast, the blue shoulder is much less pronounced in zeaxanthin, but its main peak is broader than alloxanthin's and extends more to longer wavelengths (Fig. 2.43a). Further, the kinetics measured at the peak S_1-S_n transition wavelengths in both carotenoids, monitoring the S_1 lifetime, are shown in Fig. 2.43b, demonstrating markedly longer S_1 lifetime of alloxanthin compared to
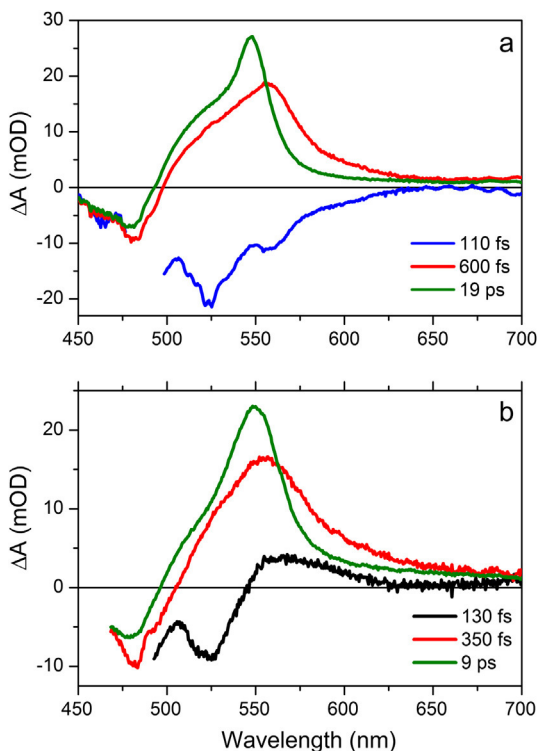
zeaxanthin.

FIGURE 2.44: EADS obtained from global fitting the data measured for (a) alloxanthin and (b) zeaxanthin in methanol excited at 490 nm.

Three sequentially decaying evolution associated difference spectra (EADS), shown in Fig. 2.44, satisfactorily fit the total decay profiles of alloxanthin and zeaxanthin. The bleaching EADS, the fastest and most immediate profile, expresses the 110 fs (alloxanthin) and 130 fs (zeaxanthin) decay of the S_2 state stimulated emission combined with ground state bleaching. The second, broad spectrum, recognized as hot S_1 state,[24,25] decays to the slightly narrower, bluer S_1 signal within 600 fs in alloxanthin. For zeaxanthin, this component is faster, yielding 350 fs. The final EADS, effectively representing the spectrum of the S_1 state, decays by 19 ps in alloxanthin, confirming the difference in the S_1 lifetimes of alloxanthin and zeaxanthin shown in Fig. 2.2b; the S_1 lifetime of zeaxanthin is 9 ps in agreement with a number of previous studies.[26,27]

Considering the spectroscopic findings described above, namely the nearly identical absorption spectra and the markedly longer S_1 lifetime of alloxanthin as compared to zeaxanthin, as well as the different spectral profiles of their S_1-S_n transitions, we must conclude that adding a triple bond into conjugation markedly affects the S_1 state while leaving the S_2 state nearly untouched. The alloxanthin S_1 lifetime of 19 ps is actually comparable to the S_1 lifetimes of carotenoids with N_{eff} = 9 such as neurosporene or violaxanthin
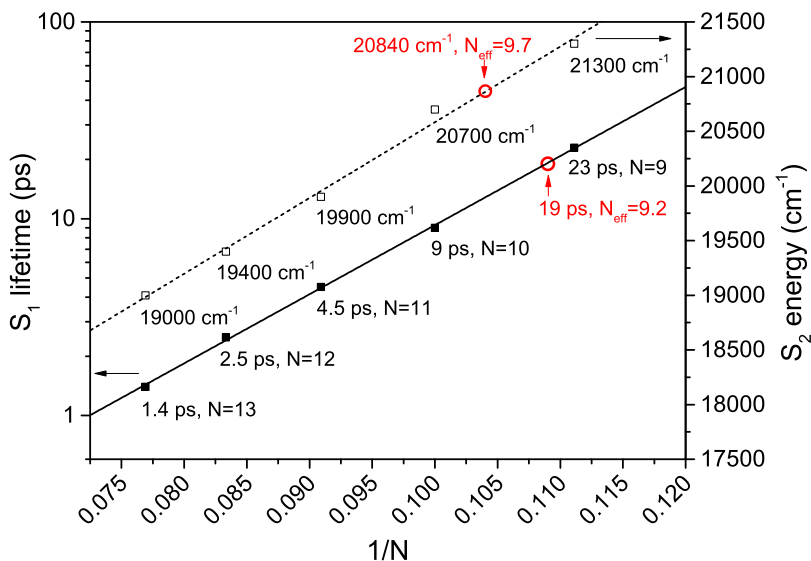
FIGURE 2.45: Dependence of the S_1 lifetimes on conjugation length. Black symbols denotes the S1 lifetimes of linear carotenoids in n-hexane (data taken from Ref. [6]) plotted against $1/N$. The solid line is a linear fit to the S1 lifetimes of linear carotenoids. Red circles show the S1 lifetimes of zeaxanthin and alloxanthin. Placing these lifetimes on the black line allows a determination of the effective conjugation length, N_{eff}, of these carotenoids. Each point is labeled by a corresponding S_1 lifetime and N (or N_{eff}).

whose S_1 lifetimes were reported in the 21-24 ps range.[6,24,26] In contrast, alloxanthin S_2 energy is rather in the range expected for carotenoids with $N_{eff} = 10$. This split effect of the triple bonds of alloxanthin can be visualized by comparing its S_1 lifetime and S_2 energy with those of linear carotenoids. For linear carotenoids with well-defined conjugation length N, these parameters depend linearly on $1/N$ and allow estimation of N_{eff}. As shown in Fig. 2.45, the interpolation based on the S_1 lifetime yields for alloxanthin $N_{eff} = 9.2$, while the interpolation using the S_2 energy gives estimation of $N_{eff} = 9.7$, confirming the different effect of the triple bonds on the S_2 and S_1 states.

It is instructive to compare our results obtained for alloxanthin with those of diatoxanthin, a carotenoid having only one triple bond thus representing an intermediate structure between zeaxanthin and alloxanthin (Supporting

Information, Fig. 2.47). A previous study of diatoxanthin reported a 13 ps S_1 lifetime, thus markedly shorter than for alloxanthin, yet the S_2 energy of diatoxanthin remains the same as for alloxanthin.[16] Therefore, it is obvious that the number of triple bonds in the carotenoid backbone correlates monotonically to the S_1 lifetime, but the S_2 energy is insensitive to the presence or number of triple bonds in the carotenoid structure.

Interestingly, the intensity of the blue shoulder of the S_1-S_n transition also correlates with the number of triple bonds: it is weakest for zeaxanthin, increases slightly in diatoxanthin,[16] and it is strongest in the two triple bond carotenoid alloxanthin. This shoulder is known as the S* signal whose origin is still a matter of considerable debate.[28−30] Yet, it is generally agreed that whatever is the precise origin of the S* signal, it is most likely related to specific conformations,[31−33] and extension of conjugation to the terminal rings allows for larger conformational space thereby enhancing the S* signal.[32] This hypothesis matches our observation and shows that connection of the terminal ring via a triple bond enhances the S* signal, which in alloxanthin decays with the same lifetime as the S_1 state (Fig. 2.44).

TABLE 2.4: Calculated ground states Gibbs free energies and dihedral angles of zeaxanthin and alloxanthin.

	Conformers	Dihedral Angle (Degrees)	Gibbs free energy (Hartree)	Relative ΔG (kcal/mol)
zeaxanthin	*s-cis-s'-cis*	47.9/47.9	-1707.538685	0.0
	s-cis-s'-trans s-trans-s'-cis	46.2/-167.9	-1707.535694	1.88
	s-trans-s'-trans	169.05/169.05	-1707.532556	3.85
alloxanthin	s-cis-s'-cis	3.8/3.8	-1705.111494	0.51
	s-cis-s'-trans s-trans-s'-cis	0.9/175.9	-1705.107567	2.97
	s-trans-s'-trans	175.5/175.5	-1705.112307	0.0

Our observations show that the effect of triple bonds is different for the S_1 and S_2 states. To corroborate this finding, we carried out quantum chemical calculations to obtain equilibrium structures of zeaxanthin and alloxanthin in various energy states and to estimate vertical excited-state energies of the

S_1 and S_2 states. Relative energies of the ground state optimized geometries for s-*cis* and s-*trans* configurations in gas phase of zeaxanthin and alloxanthin calculated with the B3LYP/6-31g(d,p) method are given in Table 2.4. For zeaxanthin, the lowest energy configuration is that with s-*cis* position of both terminal rings that are twisted by ~48° from the plane of the central conjugated chain, matching values reported earlier for zeaxanthin and β-carotene.[7,34] The torsional twist of the terminal ring is caused by repulsion between the methyl group at the ring and the hydrogen atoms near the ends of the conjugated chain.[35]

In alloxanthin, the terminal rings have the same structure as in zeaxanthin but since they are connected via triple bonds, the steric constraints which twist the terminal ring of zeaxanthin are relaxed. This results in terminal rings of alloxanthin being essentially the in plane of the main conjugation for both s-*cis* and s-*trans* configurations (Table 2.4). The s-*trans* configuration has slightly lower energy compared to zeaxanthin, whereby the lowest energy ground state structure of alloxanthin is s-*trans* with terminal rings nearly ideally aligned with the plane of the central conjugated backbone (Supporting Information, Fig. 2.48). This configuration is likely the reason for the slightly lower S_2 energy of alloxanthin compared to zeaxanthin (Fig. 2.42), because torsion of the ring critically determines how much the double bonds at the ring will be involved in conjugation.[7]

But this cannot explain why alloxanthin in the S_1 state behaves as a carotenoid with effective conjugation length clearly shorter than zeaxanthin. Thus, we calculated relaxed geometries in the S_1 and S_2 excited states, and bond lengths, corresponding to each excited state, as depicted in Fig. 2.46. It is evident the S_0 and S_2 states are more congruent in bond length than the S_1 state. While in the S_0 and S_2 states the single and double bond character is retained, partial equilibration of the bond length is characteristic for the S_1 state.[7,34] However, all states nearly coincide for the length of triple bonds, preventing the extension of the bond length equilibration in the S_1 state beyond the triple bonds. Thus, the typical bond length alternation pattern of the S_1 state is disturbed by the triple bonds though it is obvious that the conjugation must extend beyond the triple bonds since $N_{eff} > 9$ (Fig. 2.45). The role
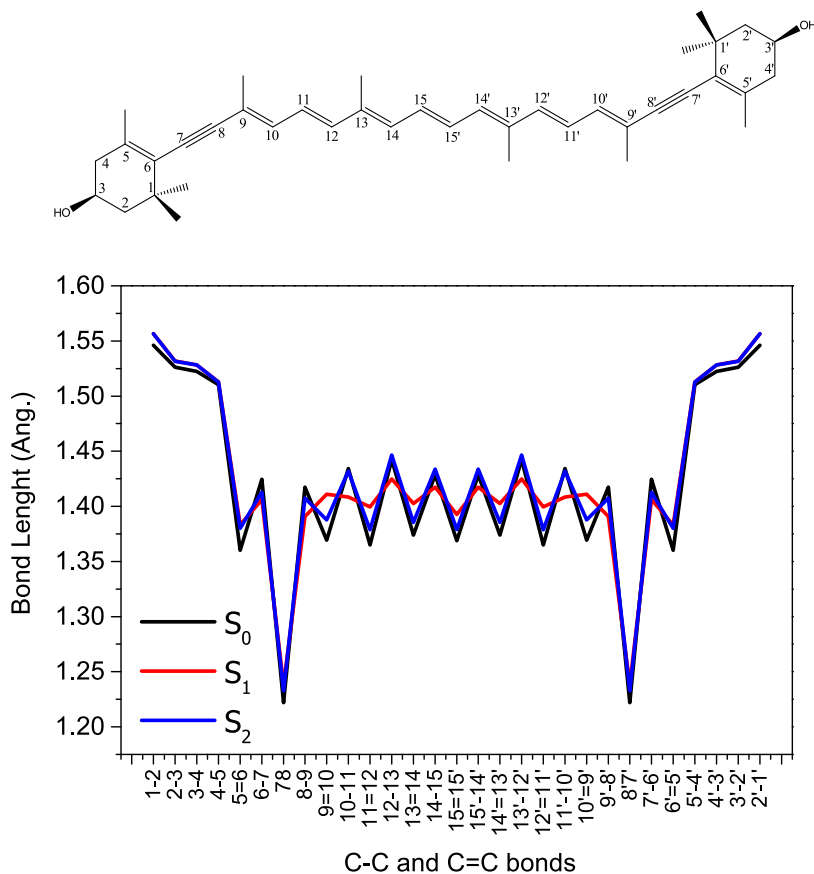
FIGURE 2.46: Calculated bond lengths in the S_0 state (black), S_1 state (red), and S_2 state (blue) of alloxanthin in relaxed s-trans-s'-trans configuration.

of the conjugated triple bonds can be visualized by calculating electron densities of the involved orbitals (Supporting Information, Fig. 2.49): the triple bonds of alloxanthin significantly decrease π-electron densities at the end of the conjugated chain.

Finally, we calculated the S_0-S_2 and S_0-S_1 vertical transition energies for the optimized ground state geometry that are summarized in Table 2.5. Here, different levels of theory were used because, while the Cam-B3LYP and B3LYP functionals reasonably reproduce the S_2 energies, it gives the wrong excited state ordering resulting in the forbidden S_1 state being placed above the S_2

state.[22,23,36] Thus, the TDA Cam-B3LYP/TZVP approach was used to calculate the S_2 energies, but the BLYP functional, which is known to give the proper state ordering, was used to calculate S_1 energies. It is obvious that regardless the method used to calculate S_2 energies, calculations reproduces qualitatively the experimental results.

While the calculated S_2 energy of alloxanthin is lower than that of zeaxanthin, the trend is opposite for the S_1 state, which is higher for alloxanthin than for zeaxanthin (Table 2.5). The S_1 energy correlates with the S_1 lifetime according to the energy gap law in non-carbonyl carotenoids.[37] Thus, the measured alloxanthin S_1 lifetime of 19 ps implies the S_1 energy higher than that of zeaxanthin whose S_1 lifetime is 9 ps, precisely as predicted by calculations. The calculated difference of $\sim$650 cm^{-1} matches reasonably the difference between S_1 energies of carotenoids with N=9 and N=10 observed experimentally.[4] For the S_2 state, the energy difference between alloxanthin and zeaxanthin calculated with the BLYP functional is far too large to match the experimental value, but using TDA Cam-B3LYP/TZVP approach gives the energy difference of $\sim$150 cm^{-1} which is much closer to the observed value (Fig. 2.42).

TABLE 2.5: Calculated ground states Gibbs free energies and dihedral angles of zeaxanthin and alloxanthin.

	Dihedral angle (degrees)			Transition energy (cm^{-1})	
	S_0	S_1	S_2	S_0-S_2	S_0-S_1
zeaxanthin	47.9	32.4	38.2	23 775	15 402
			44.7	*(4.796)*	*(0.000)*
				22 422	
				(5.222)	
alloxanthin	175.5	176.6	176.5	21 551	16 077
				(5.679)	*(0.000)*
				22 271	
				(5.325)	

Note: Calculations were carried out using either the BLYP/TZVP (ground state) or TDA BLYP/TZVP (excited states) level of theory. Calculations involving the S2 state were also carried out by TDA Cam-B3LYP/TZVP (results

shown in italics). Oscillator strengths of the transitions are shown in parentheses.

2.4.4   Conclusions

Comparison of spectroscopic properties of the triple bond carotenoid alloxanthin and its non-triple bond counterpart zeaxanthin revealed that the effect of a triple bond on carotenoid spectroscopic properties differ for the S_2 and S_1 excited states. While the S_2 energy is slightly lowered by introduction of two triple bonds into the carotenoid structure, the S_1 energy of alloxanthin is higher than that of zeaxanthin. This is evidenced by significantly longer S_1 lifetime of alloxanthin (19 ps) compared to zeaxanthin (9 ps). The different effect on the S_1 state is explained by the triple bonds preventing the extension of the typical S_1 state bond length equilibration to the terminal rings. Thus, the triple bonds in alloxanthin shrinks the S_1-S_2 energy gap by decreasing the S_2 energy and increasing the S_1 energy compared to zeaxanthin, which may have significant consequences for alloxanthin function in photosynthetic light-harvesting complexes. This effect, reminiscent of carbonyl carotenoids,[38] allows to extend the light-harvesting capacity to longer wavelengths, while keeping the S_1 energy high enough to transfer energy to Chl-a. Thus, it is likely that alloxanthin is a light-harvesting carotenoid transferring energy efficiently to Chl-a.
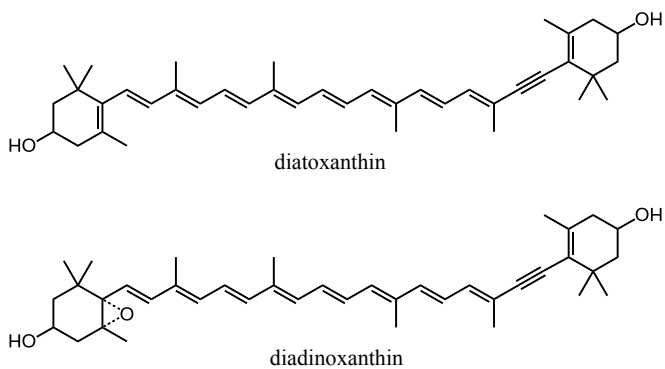
Supporting Information

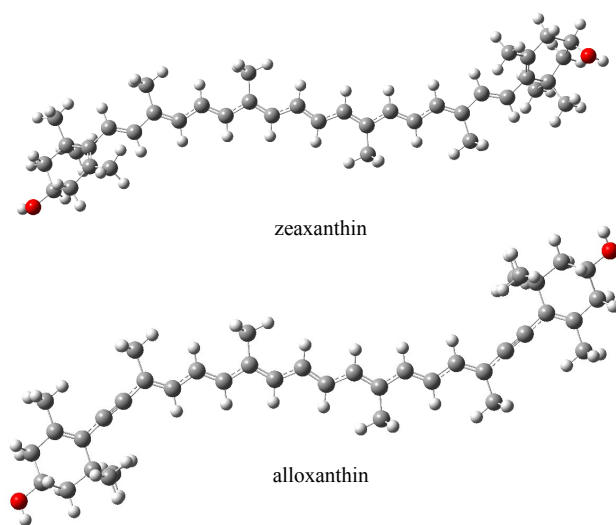FIGURE 2.47: Molecular structures of diatoxanthin and diadi-
noxanthin.

FIGURE 2.48: Relaxed ground state geometries of zeaxanthin
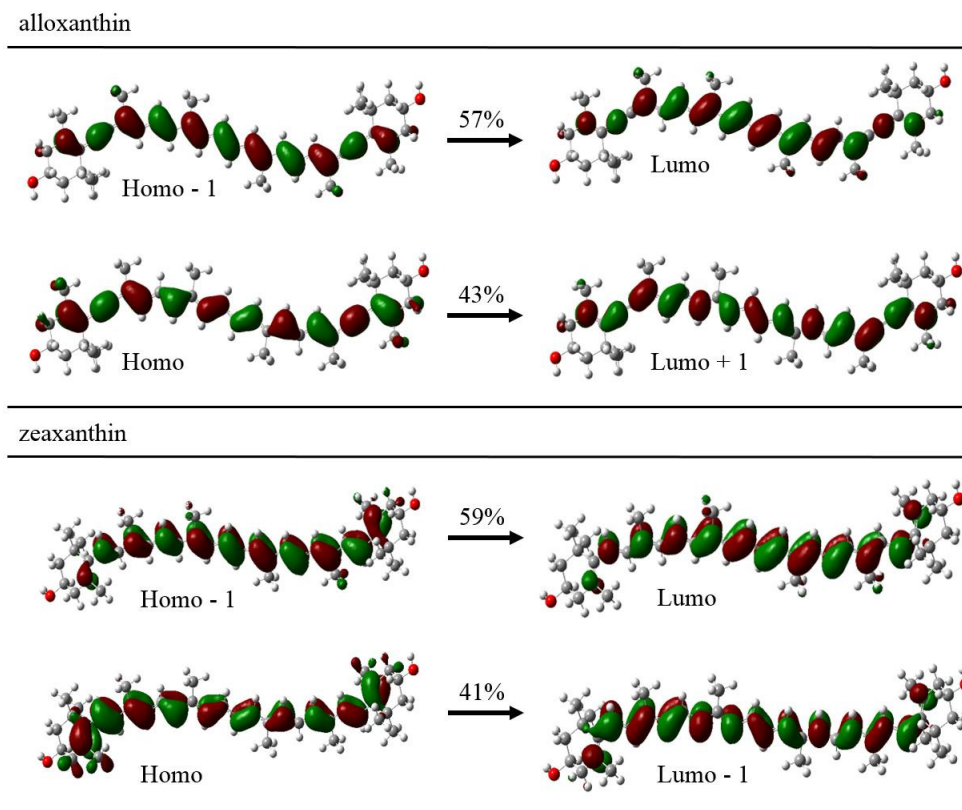and alloxanthin.

FIGURE 2.49: The S_1 state transition densities of alloxanthin and zeaxanthin calculated by using TDDFT/TDA with BLYP method including TZVP basis set. In this level of theory, the S_1 state, which has the A_g^- symmetry, is a doubly-excited state represented as a linear combination of two singly-excited determinants corresponding to HOMO-1 $\rightarrow$ LUMO and HOMO $\rightarrow$ LUMO + 1 transitions [39]. Contribution of each transition to this linear combination is indicated in the figure. The calculations of electron densities show that electron density at the terminal parts of alloxanthin (triple bond and the C=C bond at the terminal ring) is less than the corresponding density in zeaxanthin. This difference implies that the presence of the triple bonds affects the overall electron densities and, consequently, the effective conjugation length.

References (Paper IV)

1. T. Polívka and H. A. Frank, Acc. Chem. Res. 46 (2010) 1125-1134.

2. H. A. Frank and R. J. Cogdell, Photochem. Photobiol. 63 (1996) 257-264.

3. H. Hashimoto, Y. Sugai, C. Uragami, A. T. Gardiner, R. J. Cogdell, J. Photochem. Photobiol. C 25 (2015) 46-70.

4. T. Polívka, V. Sundström, Chem. Rev. 104 (2004) 2021-2071.

5. R. L. Christensen, M. M. Enriquez, N. L. Wagner, A. Y. Peacock-Villada, C. Scriban, R. R. Schrock, T. Polívka, H. A. Frank, R. R. Birge, J. Phys. Chem. A 117 (2013) 1449-1465.

6. R. Fujii, T. Inaba, Y. Watanabe, Y. Koyama, J.-P. Zhang, Chem. Phys. Lett. 369 (2003) 165-172.

7. M. Fuciman, G. Keşan, A. M. LaFountain, H. A. Frank, T. Polívka, J. Phys. Chem. B 119 (2015) 1457-1467.

8. R. L. Leverenz, M. Sutter, A. Wilson, S. Gupta, A. Thurotte, C. Bourcier de Carbon, C. J. Petzold, C. Ralston, F. Perreau, D. Kirilovsky, C. A. Kerfeld, *Science* 348 (2015) 1463-1466.

9. V. Šlouf, P. Chábera, J. D. Olsen, E. C. Martin, P. Qian, C. N. Hunter, T. Polívka, Proc. Natl. Acad. Sci. 109 (2012) 8570-8575.

10. G. Britton, S. Liaaen-Jensen, H. Pfander, Eds., Carotenoids, Handbook, Birkäuser Verlag, 2004.

11. F. C. Pennington, F. T. Haxo, G. Borch, S. Liaaen-Jensen, Biochem. Syst. Ecol. 13 (2015) 215-219.

12. A. N. Macpherson, R. G. Hiller, in Light-Harvesting Antennas in Photosynthesis, Dordrecht 2003, pp. 323-352.

13. P. Horton, A. V. Ruban, J. Exp. Bot. 56 (2005) 365-373.

14. M. Olaizola, J. La Roche, Z. Kolber, P. G. Falkowski, Photosynth. Res. 41 (1994) 357-370.

15. H. A. Frank, A. Cua, V. Chynwat, A. Young, D. Gosztola, M. R. Wasielewski, Biochim. Biophys. Acta 1277 (1996) 243-252.

16. M. M. Enriquez, A. M. LaFountain, J. Budarz, M. Fuciman, G. N. Gibson, H. A. Frank, Chem. Phys. Lett. 493 (2010) 353-357.

17. M. Durchan, J. Tichý, V. Šlouf, Z. Gardian, P. Hříbek, F. Vácha, T. Polívka, J. Phys. Chem. B 116 (2012) 8880-8889.

18. R. Kaňa, E. Kotabová, R. Sobotka, O. Prášil, PLoS One 7 (2012) e29700.

19. R. Kaňa, E. Kotabová, J. Kopečná, E. Trsková, E. Belgio, R. Sobotka, A. V Ruban, *FEBS Lett.* (2016), in press. doi:10.1002/1873-3468.12130.

20. I. H. M. van Stokkum, D. S. Larsen, R. van Grondelle, Biochim. Biophys. Acta 1657 (2004) 82-104.

21. M. N. Ramos, K. C. Lopes, A. M. Tavares, E. Ventura, S. A. do Monte, R. Araujo, J. Mol. Struct. 758 (2006) 253-258.

22. C.-P. Hsu, S. Hirata, M. Head-Gordon, J. Phys. Chem. A 105 (2001) 451-458.

23. J. H. Starcke, M. Wormit, J. Schirmer, A. Dreuw, Chem. Phys. 329 (2006) 39-49.

24. D. Niedzwiedzki, J. F. Koscielecki, H. Cong, J. O. Sullivan, G. N. Gibson, R. R. Birge, H. A. Frank, J. Phys. Chem. B 111 (2007) 5984-5998.

25. H. H. Billsten, D. Zigmantas, V. Sundström, T. Polı´vka, Chem. Phys. Lett. 355 (2002) 465-470.

26. T. Polívka, J. L. Herek, D. Zigmantas, H. E. Ĺkerlund, V. Sundström, Proc. Natl. Acad. Sci. U. S. A. 96 (1999) 4914-4917.

27. H. H. Billsten, J. Pan, S. Sinha, T. Pascher, V. Sundström, T. Polívka, J. Phys. Chem. A 109 (2005) 6852-6859.

28. T. Polívka, V. Sundström, Chem. Phys. Lett. 477 (2009) 1-11.

29. F. Ehlers, M. Scholz, J. Schimpfhauser, J. Bienert, K. Oum, T. Lenzer, Phys. Chem. Chem. Phys. 17 (2015) 10478-10488.

30. V. Balevičius, A. G. Pour, J. Savolainen, C. N. Lincoln, V. Lukeš, E. Riedle, L. Valkunas, D. Abramavicius, J. Hauer, Phys. Chem. Chem. Phys. 17 (2015) 19491-19499.

31. P. Chábera, M. Fuciman, P. Hříbek, T. Polívka, Phys. Chem. Chem. Phys. 11 (2009) 8795-8803.

32. D. M. Niedzwiedzki, J. O. Sullivan, T. Polívka, R. R. Birge, H. A. Frank, J. Phys. Chem. B 110, (2006) 22872-22885.

33. V. Lukeš, N. Christensson, F. Milota, H. F. Kauffmann, J. Hauer, Chem. Phys. Lett. 506 (2011) 122-127.

34. A. Dreuw, J. Phys. Chem. A 110 (2006) 4592-4599.

35. R. L. Christensen, M. Goyette, L. Gallagher, J. Duncan, B. DeCoster, J. Lugtenburg, F. J. Jansen, I. van der Hoef, J. Phys. Chem. A 103 (1999) 2399-2407.

36. A. E. Masunov, I. A. Mikhailov, Eur. J. Chem. 1 (2010) 142-161.

37. V. Chynwat, H. A. Frank, Chem. Phys. 194 (1995) 237-244.

38. D. Zigmantas, R. G. Hiller, F. P. Sharples, H. A. Frank, V. Sundström, T. Polívka, Phys. Chem. Chem. Phys. 6 (2004) 3009-3016.

39. J. H. Starcke, M. Wormit, J. Schirmer, A. Dreuw, Chem. Phys. 329 (2006) 39-49.

3 Summary and Conclusions

There is still much to learn about the function of specific carotenoids in their host light harvesting antennae; to understand the purpose of their precise structure and effect of the binding environment so the host organism may thrive in its environment. Specifically, as only recently the S_1 and intramolecular charge transfer (ICT) states of carotenoids has been clearly acting as separate states, further research must uncover the function of this pervasive light-harvesting strategy for the various antennae with carbonyl carotenoids.

The research in this thesis represents a step toward a more complete understanding of the roles of both carotenoid structure and the debated the ICT state in light harvesting antennae. We present a few new strategies for evaluating the nature of the equilibrium between this state and the S_1 state to gain insight regarding its utility as a sensitizing pigment, and we explore its dependence on various environmental factors which the carotenoid may be subject in the protein environment.

Primarily, this coupled, charge transfer state mechanism in fucoxanthin solute was explored in depth in Section 2.1 where we exploited the multi-pulse method in the pump-ICT-dump (PDP), pump-ICT-repump (PrPP)$_{ICT}$, and pump-S_1-repump (PrPP)$_{S1}$ regimes for solvents of varied polarity (in methanol and isopropanol) and proticity (methanol and acetonitrile) as well as temperature (methanol at 293 and 190 K). For each perturbation, dump or repump, the S_1 and ICT states were individually affected, the dump permanently depopulating the ICT state, but led to recover by equilibration with the S_1 state, and repumping the ICT in methanol rending the system

in an altered equilibration state than before, hinting at multiple fucoxanthin species at both temperatures. For a comparative evaluation of the effect of these various environments on equilibration dynamics, we introduced the following manipulation of the kinetic traces to obtain the equilibrium trace: the ratio of the S_1 band to ICT band ratio under the influence of the dump/repump to the same ratio in a typical, unperturbed dynamic– that is $(S_1 : ICT)_{multipulse} : (S_1/ICT)_{PP}$. Additionally, we were able to quantify population transfer rates among the two states using a simple, two-state equilibrated decay model informed by global analyses of the difference (ΔA_{PP}) and double-difference $(\Delta\Delta A = \Delta A_{PP} - \Delta A_{PDP})$ data sets. These global analyses provide the common S_1/ICT decay lifetime as well as the equilibrium lifetime by which the solvents of the target analysis of combined ΔA_{PP} / ΔA_{PDP} data sets can be checked.

Considering the S_1 and ICT states to be parts of one potential energy surface, assuming that a longer equilibration lifetime implies a greater barrier between the S_1 and ICT potential minima, we conclude that the barrier is increased by lower environment polarity, proticity, and temperature. The results of the target analysis imply that the forward transfer $S_1 \rightarrow ICT$ is preferred for highly polar and highly protic environments. Thus, hydrogen bonding prolongs equilibration. If either one of the states were to donate energy to chlorophyll (Chl) in an antenna, longer equilibration would be preferred for more efficient energy transfer; therefore, greater polarity as well as hydrogen bonding in the protein environment would be advantageous.

In Section 2.2 the pump-dump-probe method is utilized in a temperature-dependent investigation of the trimeric fucoxanthin chlorophyll *a* protein (FCP)* from *Phaeodactylum tricornutum*. This study, aimed at the individual roles of S_1 and ICT states in the protein environment, is the first ultra-fast transient absorption study of FCP at cryogenic temperatures. Global analysis reveals three energy transfer pathways in FCP: $S_2 \rightarrow Chl$, a slow $S_1/ICT \rightarrow Chl$ channel, and a fast $S_1/ICT \rightarrow Chl$ channel. The slow channel

---

*The structure of FCP remains unresolved.

appears more pronounced at room temperature; whereas, at 77 K the fast channel dominates. The energy transfer parameters obtained are similar to those found in studies of FCP from other species; thus, slight differences in the protein structure are not likely to affect the energy transfer characteristics of the antenna. Applying an three-level model (S_1, ICT, Chl Q_y states), with help of a Monte-Carlo algorithm producing distribution of linear regression fits, rendered likely rates and relative extinction coefficients of the S_1 and ICT states. The results indicate that the S_1 state is the primary donor in $S_1/ICT \rightarrow Chl$ energy transfer.

In a separate study of the intrinsic nature and dependencies of the charge transfer character of carbonyl carotenoids, presented in Section 2.3, we investigated fucoxanthin and two naturally occuring derivatives: 19-butanoyloxyfucoxanthin (bFx) and 19- hexanoyloxyfucoxanthin (hFx) in six solvents with varying degrees of polarity and proticity. These moieties are different, in structure, compared to fucoxanthin in that they contain a non-conjugated acyloxy group attached to one end of the backbone. In nature, these moeities can be found in increased concentration in their host organism when there is stress on the system, such as overexposure to light. Therefore, this investigation sought to determine the effect of the added acyloxy group on the ICT state, and if it would be affected, what advantage this effect would imply.

Of the six solvents, only the polar, protic solvents methanol, ethanol, and ethylene glycol exhibited ICT signatures: the broad, red-shifted shoulder of the $S_1/ICT \rightarrow S_{n/N}$ transition and the shortened excited state absorption lifetime. Curiously, the added acyloxy group affected the ICT signatures by reducing them, even though the group is not a part of the conjugation. The associated S_1/ICT lifetime was also extended as if the polarity of the environment were decreased. The results harmonize with other studies; whereby, greater assymmetry in ketone group positioning, the stronger the charge transfer character. This implies that the electron distribution in the

conjugation is affected by the presence of this non-conjugated group, balancing the electron distribution in the conjugation. Beyond these intramolecular implications, the suppression of the ICT character by the addition of these groups would, as a result, suppress energy transfer: a unwanted process for stressed organisms.

The relatively exotic carotenoid alloxanthin, the subject of Section 2.4, is also found in a unique antenna system which performs some form of non-photochemical quenching (NPQ). Whether, the twice triple-bonded alloxanthin performs a NPQ is yet to be determined. Nonetheless, in systems containing the once triple-bonded diadinoxanthin and diatoxanthin are known for their photoprotection role in diatoms. This investigation, however, intended to explore the effect of the triple bond on the carotenoid behavior and imply from the dynamic response, the effect on the conjugation. The coincidence of the alloxanthin and zexanthin speady-state spectra, their S_2 state energies appear to be very much the same. By virtue of the association of first excited state lifetime and conjugation length N, zeaxanthin's conjugation length was determined to be longer than alloxanthin even though the two molecules have the same number of conjugated carbon-carbon multi-bonds on their backbones. As quantum chemical calculations typically show an equilibration of bond length in the alternating single-double carbon-carbon bonds in the backbone for the S_1 state, it was revealed that the triple bonds shunt this congruent bond length behavior. Therefore, the S_1 state energy is higher in alloxanthin as compared to zeaxanthin and using the S_2 and S_1 lifetimes, its effective conjugation length was determined to be shorter than zeaxanthin.